

Durham E-Theses

Electrical Resistivity Method for Water Content Characterisation of Unsaturated Clay Soil

HASSAN, ASEM,AHMED

How to cite:

HASSAN, ASEM,AHMED (2014) *Electrical Resistivity Method for Water Content Characterisation of Unsaturated Clay Soil*, Durham theses, Durham University. Available at Durham E-Theses Online:
<http://etheses.dur.ac.uk/10806/>

Use policy

The full-text may be used and/or reproduced, and given to third parties in any format or medium, without prior permission or charge, for personal research or study, educational, or not-for-profit purposes provided that:

- a full bibliographic reference is made to the original source
- a [link](#) is made to the metadata record in Durham E-Theses
- the full-text is not changed in any way

The full-text must not be sold in any format or medium without the formal permission of the copyright holders.

Please consult the [full Durham E-Theses policy](#) for further details.

Academic Support Office, Durham University, University Office, Old Elvet, Durham DH1 3HP
e-mail: e-theses.admin@dur.ac.uk Tel: +44 0191 334 6107
<http://etheses.dur.ac.uk>

Durham University

**Electrical Resistivity Method for Water Content
Characterisation of Unsaturated Clay Soil**

Asem Ahmed Hassan

Thesis submitted towards the
degree of Doctor of Philosophy in the Faculty of Science



Geotechnical Group
School of Engineering and Computing Sciences
Durham University
United Kingdom

October 2014

Electrical Resistivity Method for Water Content Characterisation of Unsaturated Clay Soil

ABSTRACT

This thesis presents an automated multi-electrode resistivity system which was developed for the water content characterisation of unsaturated clay soil. The system controls 64 electrodes in a fully automated procedure, offering continuous real-time data acquisition, which is one of the recent advances in resistivity instrumentation. The system was tested using a wide range of high precision reference resistors and different soils, and validated using commercial standard instruments. The results indicated a high precision, accuracy and resolution of the outputs, with a measurement error of 0.19% (maximum 0.80%) in a four-electrode method and 0.21% in an automated acquisition mode.

Water content characteristics of mechanically compacted BIONICS clay soil was extensively investigated, with particular focus on the effect of wetting, drying and cracking on soil properties. It was found that the electrical resistivity of soil is sensitive to water content and compaction conditions. Experimental relationships that relate soil resistivity, volumetric water content and degree of saturation were developed. These relationships are useful to estimate the in situ water content. The resistivity behaviour of clay soils subjected to drying and wetting procedures was discussed. Soil water content and microstructure changes are key controlling parameters for resistivity behaviour. Numerical and experimental techniques were used to characterise cracking in clay soils. The results showed that cracks have anomalous high resistivity values that can be distinguished from the background, and changing cracking depth, length, width and orientation causes significant changes in soil resistivity. As the cracks form barriers that disturb the flow of electrical current, the depth and length of the crack have the major influence on soil resistivity.

It was concluded that the degree of saturation or volumetric water content is a more reliable parameter than the gravimetric water content to calibrate in situ resistivity data against water content and soil resistivity can be used as a useful indicator for monitoring water content changes in clay soils subjected to drying and wetting cycles.

DECLARATION

The work in this thesis is based on research carried out in the Geotechnical Group, School of Engineering and Computing Sciences, Durham University. No part of this report has been submitted elsewhere for any other degree or qualification and it is all my own work unless referenced to the contrary in the text. Parts of this work have been published in the following:

Hassan, A. and Toll, D. G. (2013). Electrical resistivity tomography for characterizing cracking of soils. *Geo-Congress 2013: Stability and performance of Slopes and Embankments*, Meehan, C., Pradel, D., Pando, M. and Labuz, J. F. (Eds.), California, American Society of Civil Engineers ASCE, pp. 818-827.

Hassan, A. A. and Toll, D. G. (2014). Investigation of the directional dependence of soil resistivity in cracking clays. *Unsaturated Soils: Research & Applications- Khalili, Russell & Khoshghalb (Eds.)* London: Taylor & Francis Group, pp. 137-142.

Hassan, A. A. and Toll, D. G. (2015). Water content characteristics of mechanically compacted clay soil determined using the electrical resistivity method, the XVI ECSMGE Conference, Edinburgh (*Accepted*).

Toll, D. G. and Hassan, A. (2014). Data acquisition and control software for automated resistivity measurements, 2nd International Conference on Information Technology in Geo-Engineering ICITG, D.G. Toll et al. (Eds.), IOS Press, pp. 170-176.

Toll, D. G., Hassan, A. A., King, J. M. and Asquith, J. D. (2013). New devices for water content measurement. *Proceedings of the 18th International Conference on Soil Mechanics and Geotechnical Engineering*, Paris, France, pp. 1199-1202.

Toll, D., Mendes, J., Hassan, A., Glendinning, S., Hughes, P., Chambers, J., Gunn, D., Dijkstra, T, Hughes, D. and Smethurst, J. (2015). Water content relationships for infrastructure slopes, the XVI ECSMGE Conference, Edinburgh (*Accepted*).

Copyright © 2014 by Asem Ahmed Hassan

“The copyright of this thesis rests with the author. No quotations from it should be published without the author's prior written consent and information derived from it should be acknowledged.”

Acknowledgements

First and foremost, I would like to express my sincere gratitude to my supervisor Prof. David G. Toll for the continuous support of my Ph.D study, for his patience, motivation and immense knowledge. His guidance helped me in all the time of research and writing of this thesis.

My sincere thanks also go to Dr. Mohammed Seaid, my second supervisor, for the continuous support and guidance. I would like to express my gratitude to Dr. Jonathan E. Chambers, from the British Geological Survey, for providing me with the resistivity software and for his invaluable discussions.

I would like to thank Mr. Stephen Richardson and Mr. Kevan Longley for the assistance given in the lab. I would like to thank Mr. Ian Hutchinson for preparing the circuit boards and the assistance with electronic problems.

I thank my fellow PhD students: Salma Hashim, Syazwan MD-Rahim, Jonathan Asquith, and other friends, Amer Mustafa and Piotr Osinski. They each helped make my time more interesting.

I gratefully acknowledge my beloved family for their support, encouragement and love throughout my life. I must acknowledge my wife, Saja, without her encouragement and support; I would not have finished this thesis

Finally, I would like to acknowledge the financial support from the Ministry of Higher Education and Scientific Research (MOHESR) of Iraq.

Asem Ahmed Hassan

Durham, August 2014

CONTENTS

	<u>Page</u>
1 Introduction	1
1.1 Overview	1
1.2 Thesis objectives	4
1.3 Thesis structure	5
2 Soil water content measurement: Background and literature review	7
2.1 Soil water content	7
2.1.1 Background	7
2.1.2 Clay soils: Mineralogy and microstructure	9
2.2 Soil water content measurement methods	11
2.2.1 Direct method: Gravimetric method	11
2.2.2 Indirect methods.....	11
2.3 Soil water content: Scaling issues	18
2.4 Soil water content changes: Climate effects	19
2.5 BIONICS Project	23
2.5.1 The embankment	24
2.6 Electrical resistivity method	27
2.6.1 Basic theory	28
2.6.2 Data acquisition	31
2.7 Resistivity method for water content characterisation	41
2.7.1 Soil resistivity-water content relationship	41
2.8 Resistivity method for characterising drying and wetting of clay soils	45
2.9 Resistivity method for characterising cracking of clay soils	47
2.9.1 Cracking mechanism	47
2.9.2 Application of the resistivity method for characterising cracking of clay soils	47
2.10 Chapter summary	53
3 Design and construction of an automated multi-electrode resistivity system	55
3.1 Introduction	55
3.2 Multi-electrode resistivity system: Main components	59
3.3 Design and construction of the multi-electrode resistivity system	62
3.3.1 Power source	63
3.3.2 Datascan logger	64
3.3.3 Switching system	65
3.3.4 Data acquisition and control software	67
3.4 Laboratory resistivity devices constructed and measurement procedures	70
3.4.1 Miller resistivity box	70
3.4.2 Circular resistivity cell	71
3.4.3 Resistivity devices for local measurements	77
3.5 Chapter summary	81
4 Calibration and validation of the multi-electrode resistivity system	83
4.1 Introduction.....	83
4.1.1 Calibration and validation of resistivity instrument	85

4.1.2 Data quality and error	85
4.2 Calibration: Reference resistors	86
4.2.1 A four electrode method	86
4.2.2 Automated data acquisition	89
4.3 Validation.....	101
4.3.1 Resistivity and conductivity	102
4.3.2 Resist and Terrameter SAS 300 C	104
4.4 Chapter summary	115
5 Water content characteristics of mechanically compacted clay soil	116
5.1 Introduction	116
5.2 Compaction key variables	118
5.3 Experimental setup	121
5.3.1 Specimen preparation	121
5.3.2 Resistivity measurements	122
5.4 Results and discussion	123
5.4.1 Compaction and compaction effort	123
5.4.2 Gravimetric water content	128
5.4.3 Dry density and void ratio	130
5.4.4 Volumetric water content	136
5.4.5 Degree of saturation	138
5.4.6 Compaction mechanism	140
5.5 Chapter summary	142
6 The role of temperature and pore water conductivity on resistivity of clay soil	144
6.1 Introduction.....	145
6.1.1 The temperature correction	146
6.1.2 The influence of pore water conductivity	148
6.2 Experimental setup	150
6.2.1 Sample Preparation	150
6.2.2 Resistivity measurements	151
6.3 The experimental results and discussion	152
6.3.1 The influence of the temperature	152
6.3.2 The influence of salt type and concentration on pore water resistivity	158
6.4 Chapter summary	169
7 Electrical resistivity for characterising drying and wetting of clay soils	170
7.1 Introduction	170
7.2 Experimental setup	172
7.2.1 Specimen preparation	172
7.2.2 Drying and wetting procedures	173
7.2.3 Automated data acquisition: Continuous procedure.....	173
7.3 Results and Discussion	176
7.3.1 Discrete drying and wetting: uncompacted specimens	176
7.3.2 Drying and wetting: Compacted specimens	181
7.3.3 Continuous drying	185
7.4 Chapter summary	193
8 Electrical resistivity for characterising cracking of clay soils	194
8.1 Introduction	194

8.2 Numerical modelling	196
8.2.1 Method	196
8.2.2 Numerical modelling results and discussion	198
8.3 Experimental methods	211
8.3.1 Methods.....	211
8.3.2 Experimental results and discussion	214
8.4 Chapter summery.....	235
9 Conclusions and recommendations for future work.....	236
9.1 Conclusions	236
9.2 Future work	242
References	246
Appendix A	272

LIST OF FIGURES

	<u>Page</u>
Figure 2.1. Schematic representation of soil phases (Budhu, 2011)	8
Figure 2.2. Clay minerals structure (a) Silica tetrahedron (b) Silica sheets (c) Aluminium octahedron and (d) Aluminium sheets (Budhu, 2011)	10
Figure 2.3. Clay minerals structure (a) Kaolinite (b) illite, and (c) montmorillonite (Budhu, 2011)	10
Figure 2.4. Neutron scattering probe (Muñoz-Carpena et al., 2006)	12
Figure 2.5. TDR probes (Muñoz-Carpena et al., 2006)	14
Figure 2.6. FD probes (a) Capacitance (plates) (b) Capacitance (rods) and (c) FDR (rings) (Muñoz-Carpena, 2002)	15
Figure 2.7. ADR probe (Muñoz-Carpena, 2002)	16
Figure 2.8. Schematic diagram showing the GPR working principle (Lunt et al., 2005).....	17
Figure 2.9. Passive (radiometer) and active (radar) sensors	18
Figure 2.10. Soil water retention curve of BIONICS clay (Lourenço, 2008)	21
Figure 2.11. The UK map (a) Swell-shrink potential map (BGS, 2014a), (b) Landslide potential map (BGS, 2014b)	21
Figure 2.12. Rainfall and landslide events in the UK (January 2012 to July 2014)	22
Figure 2.13. The earthwork failures in the UK rail network (2004-2008) (Department of Transport, 2008).....	23
Figure 2.14. Plan view and cross-section of the BIONICS embankment (Toll et al., 2012a) ...	25
Figure 2.15. Particle size distribution of the material (Mendes, 2011)	25
Figure 2.16. 2D ERT profile of the BIONICS embankment (Sellers et al., 2012)	26
Figure 2.17. Ohm's law on simple conductor of length L and cross-sectional area A^2	30
Figure 2.18. The current flow and potential distribution in a homogenous and half-space medium (a) a single current source (b) four-electrode method.....	30
Figure 2.19. General four-electrode arrangement	30
Figure 2.20. Traditional four-electrode resistivity system.....	32
Figure 2.21. Standard four electrode resistivity method (ASTM G57, 2006)	33
Figure 2.22. Typical circular four-electrode resistivity cell (Kalinski and Kelly, 1994).....	35
Figure 2.23. Resistivity probes (a) A probe for geotechnical and geoenvironmental studies (Peixoto et al., 2010) (b) Moisture, Resistivity and Temperature (SMRT) Module (VERTEK, 2013) (C), and Electric Conductivity (Resistivity) Module HT series (VERTEK, 2013).....	36
Figure 2.24. Resistivity probe for local water content monitoring (Muñoz-Castelblanco, 2011)	36
Figure 2.25. 2D data collection using multi-electrode resistivity system (Loke et al., 2013) ..	38
Figure 2.26. The ALERT-ME system developed by BGS (Gunn et al., 2010b)	39
Figure 2.27. Build-up of moisture prior to slope failure, inferred using 2D ERT (Jackson et al. 2002)	40
Figure 2.28. Time-lapse 2D resistivity sections (Chambers et al., 2009)	41
Figure 2.29. A schematic diagram illustrating the approach of water content mapping using ERT (Di Maio and Piegari, 2011)	42
Figure 2.30. Electrical resistivity-volumetric water content relationship of different types of clay (Samouëlian et al., 2005)	42

Figure 2.31. Resistivity-volumetric relationships reported in the literature for different soils (yellow: clay, Red: loam, Black: sand) (Calamita et al., 2012)	45
Figure 2.32. Resistivity-water content relationships of different local and pure clay soils (Russell and Barker, 2010)	46
Figure 2.33. Distortion of current flow lines in (A) high and (B) low conductive anomaly	48
Figure 2.34. Development of cracking in clay soil sampled from flood embankment located near Thorngumbald in England: (a) photographs showing surface cracks development; (b) resistivity section, model layer ($z=0.01$ m) (c), vertical slice at $x\approx 38$ cm (Jones et al., 2014)	49
Figure 2.35. Azimuthal resistivity measurements (a) Parallel fractures (b) Polar diagram using square array (Busby and Jackson, 2006)	50
Figure 2.36. AI profiles of clay soil (a) drying (b) water addition (Greve et al., 2010a).....	52
Figure 3.1. A schematic diagram of an automated multi-electrode resistivity system	59
Figure 3.2. The main components of the developed system	63
Figure 3.3. The shunt resistor used to log the current	65
Figure 3.4. The switching circuit for multiplexing electrodes	66
Figure 3.5. The main window of Resist	68
Figure 3.6. Defining a sequence of electrodes for automated data acquisition	69
Figure 3.7. Logging the resistivity data and other variables	69
Figure 3.8. Miller resistivity box	71
Figure 3.9. The circular resistivity cell.....	72
Figure 3.10. Circular resistivity cell (a) Wenner (B) Dipole Dipole (c) Square array	75
Figure 3.11. Calibration of the circular resistivity cell for three resistivity arrays.....	75
Figure 3.12. Miller resistivity box calibration	76
Figure 3.13. Square resistivity probe developed in this study	78
Figure 3.14. Square resistivity devices constructed in this study.....	78
Figure 3.15. Resistivity square array (a) α -resistivity (b) β -resistivity.....	79
Figure 3.16. A comparison between resistivity of KCl solutions measured using the system developed and HANNA conductivity meter	80
Figure 4.1. Accuracy and precision	84
Figure 4.2. Illustration of the difference between accuracy and precision.....	84
Figure 4.3. Measurement setup using a high precision reference resistor (ABEM, Terrameter SAS 300 C, instruction manual)	87
Figure 4.4. A comparison between the measured and actual readings using Resist.....	88
Figure 4.5. A comparison between the measured and actual readings using the Terrameter.....	88
Figure 4.6. The forward and backward readings and the percentage difference of 100 Ohm resistor test	90
Figure 4.7. The mean resistance and the measurement error of 100 Ohm resistor test	90
Figure 4.8. The automatic scanning of 100 Ohm resistor at different times during the test	91
Figure 4.9. A comparison between the actual and measured values of automated data acquisition.....	93
Figure 4.10. A correlation between the forward and backward readings of automated data acquisition.....	93

Figure 4.11. Normal resistance, reciprocal resistance and reciprocity error of 56 and 68 Ohm resistor test	95
Figure 4.12. Average resistance and measurement error of 56 and 68 Ohm resistor test	95
Figure 4.13. The measured normal and reciprocal readings	97
Figure 4.14. Reciprocity test results of clay specimen prepared at 25% water content.....	99
Figure 4.15. A correlation between normal and reciprocal readings of all soil specimens investigated	101
Figure 4.16. A correlation between resistivity of ten KCl solutions measured by Resist and HANNA conductivity meter for three arrays	103
Figure 4.17. The resistivity of BIONICS soil measured using the square array	103
Figure 4.18. The resistivity of BIONICS soil measured using Square, Wenner and Dipole- Dipole array	104
Figure 4.19. The resistivity-gravimetric water content relationship of BIONICS specimens obtained using the Terrameter.....	105
Figure 4.20. The resistivity-gravimetric water content relationship of BIONICS specimens obtained using Resist	105
Figure 4.21. A comparison between the average resistivity measured using Resist and the Terrameter for the BIONICS specimens	106
Figure 4.22. A correlation between normal and reciprocal data calculated using Resist and the Terrameter.....	106
Figure 4.23. Resistivity-gravimetric water content relationship of Kaolin specimen during drying	108
Figure 4.24. Resistivity-gravimetric water content of sand specimen during drying.....	108
Figure 4.25. Resistivity profile of the water-filled container (stage one).....	109
Figure 4.26. Resistivity profile of the water-filled container (stage two).....	110
Figure 4.27. Resistivity profile of the sand-filled container (stage one).....	111
Figure 4.28. Resistivity profile of the sand-filled container (stage two)	111
Figure 4.29. Resistivity sections of the water-filled container, Stage one, 2D sections; (a) Resist, (b) the Terrameter, resistivity profiles at different depths; (c) Resist, (d) the Terrameter	113
Figure 4.30. Resistivity sections of the water-filled container, Stage two, 2D sections; (a) Resist, (b) the Terrameter, resistivity profiles at different depths; (c) Resist, (d) the Terrameter	114
Figure 5.1. (a) Electrical resistivity-molding water content, (b) electrical resistivity-initial degree of saturation (Abu-Hassanein et al., 1996)	119
Figure 5.2. Resistivity-gravimetric water content relationship for different densities of clay soil (Seladji et al., 2010)	120
Figure 5.3. BS Light and BS Heavy compaction curves and the corresponding resistivity data	125
Figure 5.4. Resistivity-degree of saturation of specimens compacted using BS Light and BS Heavy compaction methods	126
Figure 5.5. Dry density-gravimetric water content of specimens compacted using different compaction efforts	127
Figure 5.6. Resistivity-gravimetric water content of specimens compacted using different compaction efforts.....	127

Figure 5.7. Electrical resistivity-gravimetric water content of the dynamically compacted specimens	129
Figure 5.8. Electrical resistivity-gravimetric water content of the statically compacted specimens	129
Figure 5.9. Electrical resistivity-dry density of the dynamically compacted specimens	131
Figure 5.10. Electrical resistivity-void ratio of the dynamically compacted specimens	131
Figure 5.11. Electrical resistivity-dry density of the statically compacted specimens	132
Figure 5.12. Electrical resistivity-void ratio of the statically compacted specimens	132
Figure 5.13. Resistivity, water content and dry density relationship (a) Dynamic compaction (b) Static compaction	134
Figure 5.14. Electrical resistivity-Gravimetric water content relationship at constant dry density (Dynamic compaction).....	135
Figure 5.15. Electrical resistivity-Gravimetric water content relationship at constant dry density (Static compaction).....	135
Figure 5.16. Resistivity-volumetric water content of the dynamically compacted specimens	136
Figure 5.17. Resistivity-volumetric water content of the statically compacted specimens	137
Figure 5.18. Resistivity-volumetric water content of BIONICS clay compared to different clays reported in the literature	137
Figure 5.19. Resistivity-degree of saturation relationship of the dynamically compacted specimens	139
Figure 5.20. Resistivity-degree of saturation relationship of the statically compacted specimens	139
Figure 5.21. Resistivity-volumetric water content relationship of all specimens	141
Figure 5.22. Resistivity-degree of saturation relationship of all specimens.....	141
Figure 6.1. Electrical resistivity-temperature relationships of different soils (Zhou et al., 2013).....	145
Figure 6.2. The resistivity-temperature relationship over a range of temperatures (Keller and Frischknecht, 1966)	148
Figure 6.3. Electrical resistivity-water content relationship for different pore water resistivity (Zha et al., 2010).....	149
Figure 6.4. Resistivity-salt content of clay soils at different sites (Long et al., 2012)	150
Figure 6.5. Air temperature variation in the lab for 48 hours at different dates.....	153
Figure 6.6. The measured resistivities at the lab temperature	153
Figure 6.7. Resistivity and temperature data of the cooling stage	154
Figure 6.8. The resistivity-temperature relationship of the cooling stage	154
Figure 6.9. Resistivity and temperature data of the heating stage	156
Figure 6.10. The resistivity-temperature relationship of the heating stage	156
Figure 6.11. Resistivity and temperature data of the freezing stage	157
Figure 6.12. The resistivity-temperature relationship of the freezing stage	157
Figure 6.13. The resistivity-temperature relationship of the BIONICS clay	158
Figure 6.14. A comparison between pore water resistivity measured by Resist and the conductivity meter	159
Figure 6.15. The pore water resistivity (measured by Resist)-salt concentration relationship of NaCl, KCl and MgCl ₂ solutions.....	160

Figure 6.16. The pore water resistivity (measured by HANNA)- salt concentration of NaCl, KCl and MgCl ₂ solutions.....	160
Figure 6.17. The influence of electrolyte type and concentration on resistivity of soil (w=25%)	162
Figure 6.18. The influence of pore water resistivity (measured by Resist) on resistivity of specimens prepared at 25% gravimetric water content with NaCl, KCl and MgCl ₂ electrolytes.....	162
Figure 6.19. The influence of pore water resistivity (measured by HANNA) on resistivity of specimens prepared at 25% gravimetric water content with NaCl, KCl and MgCl ₂ electrolytes	163
Figure 6.20. Resistivity-volumetric water content of specimens prepared using different KCl concentrations	164
Figure 6.21. The influence of KCl concentration on resistivity at constant volumetric water content	165
Figure 6.22. Resistivity-volumetric water content of specimens prepared using 0.1g/100ml KCl, 0.1g KCl and 0.1g NaCl/100ml and distilled water	167
Figure 6.23. Resistivity-volumetric water content of specimens prepared using 0.5g/100ml KCl, 0.5g KCl and 0.5g NaCl/100ml and distilled water	167
Figure 6.24. The influence of electrolyte composition on soil resistivity at constant volumetric water content (based on the regressions of the relationships in Figure 6.22)	168
Figure 6.25. The influence of electrolyte composition on soil resistivity at constant volumetric water content (based on the regressions of the relationships in Figure 6.23)	168
Figure 7.1. The experimental setup of the continuous procedures tests	175
Figure 7.2. Volume and mass measurements of drying test	175
Figure 7.3. The resistivity-gravimetric water content relationship of BIONICS clay	176
Figure 7.4. The resistivity-gravimetric water content relationship of Birtley clay	177
Figure 7.5. The resistivity-gravimetric water content relationship of the contaminated soil	177
Figure 7.6. The resistivity-gravimetric water content relationship of Kaolinite	180
Figure 7.7. The resistivity-gravimetric water content relationship of Bentonite	180
Figure 7.8. The resistivity-gravimetric water content of discrete drying (a) Compacted samples t1 and t2 (b) A comparison of t1 and t2 with the uncompact sample	182
Figure 7.9. Discrete drying and wetting test t3	184
Figure 7.10. Discrete drying and wetting test t4	184
Figure 7.11. A comparison between t3 and t4	185
Figure 7.12. The resistivity and gravimetric water content versus the elapsed time of test t5	186
Figure 7.13. The resistivity-gravimetric water content relationship of drying test t5	186
Figure 7.14. The resistivity-gravimetric water content of the continuous drying tests (t6 to t9) and t5	188
Figure 7.15. The resistivity-volumetric water content of the continuous drying tests (t6 to t9)	189

Figure 7.16. The resistivity-degree of saturation of the continuous drying tests (t6 to t9)	189
Figure 7.17. The resistivity-gravimetric water content of the continuous drying tests (t10 to t13)	190
Figure 7.18. The resistivity-volumetric water content of the continuous drying tests (t10 to t13)	191
Figure 7.19. The resistivity-degree of saturation of the continuous drying tests (t10 to t13)	191
Figure 7.20. The resistivity-degree of saturation of all continuous drying tests (t6 to t13)..	192
Figure 8.1. Flowchart shows resistivity modelling steps (Giao et al., 2011).....	197
Figure 8.2. XY slices of the 70mm depth crack model in dry soil	199
Figure 8.3. XZ slices of the 70mm depth crack model in dry soil	199
Figure 8.4. YZ slices of the 70mm depth crack model in dry soil	200
Figure 8.5. 3D visualization of the 70mm depth crack model in dry soil (a) the model (b) the model with XY cut	200
Figure 8.6. XY slices of the 70mm depth crack model in dry soil (5% added noise)	201
Figure 8.7. XZ slices of the 70mm depth crack model in dry soil (5% added noise)	202
Figure 8.8. YZ slices of the 70mm depth crack model in dry soil (5% added noise).....	202
Figure 8.9. 3D visualization of the 70mm depth crack model in dry soil (5% noise added) (a) the model (b) the model with XY cut.....	203
Figure 8.10. XY slices of the 70mm depth crack model in wet soil	204
Figure 8.11. XZ slices of the 70mm depth crack model in wet soil	204
Figure 8.12. YZ slices of the 70mm depth crack model in wet soil	205
Figure 8.13. 3D visualization of the 70mm depth crack model in wet soil (a) the model (b) the model with XY cut	205
Figure 8.14. XY slices of the 70mm depth crack model in wet soil (5% noise added)	206
Figure 8.15. XZ slices of the 70mm depth crack model in wet soil (5% noise added).....	206
Figure 8.16. YZ slices of the 70mm depth crack model in wet soil (5% noise added).....	207
Figure 8.17. 3D visualization of the 70mm depth crack model in wet soil (5% noise added) (a) the model (b) the model with XY cut.....	207
Figure 8.18. 3D visualization of 40mm depth crack model in dry soil (a) the model with XY cut out (b) the model with 5% resistivity noise	209
Figure 8.19. 3D visualization of the 40mm depth crack model in wet soil (a) the model with XY cut out (b) the model with 5% resistivity noise	209
Figure 8.20. 3D visualization of the 10mm depth crack model in dry soil (a) the model with XY cut out (b) the model with 5% resistivity noise	210
Figure 8.21. 3D visualization of the 10mm depth crack model in wet soil (a) the model with XY cut out (b) the model with 5% resistivity noise	210
Figure 8.22. Square resistivity devices used with the crack positions tested	212
Figure 8.23. Square resistivity measurements (a) electrode arrangement (b) the measurement procedure	213
Figure 8.24. Azimuthal resistivity stages of the manually created cracks test	214
Figure 8.25. Resistivity profile of parallel (PP) and perpendicular (PL) measurements across a manually introduced crack (70mm length, 50 mm depth and 1.5mm width).....	215
Figure 8.26. Influence of the depth of crack on soil resistivity (a=50mm)	217

Figure 8.27. Influence of the depth of crack on soil resistivity (a=100mm).....	217
Figure 8.28. Resistivity as a function of the depth of the crack	218
Figure 8.29. Influence of the length of the crack on soil resistivity (a=50mm).....	219
Figure 8.30. Influence of the length of the crack on soil resistivity (a=100mm).....	219
Figure 8.31. Influence of the width of the crack on soil resistivity (a=50mm).....	221
Figure 8.32. Influence of the width of the crack on soil resistivity (a=100mm).....	221
Figure 8.33. Influence of the orientation of the crack on soil resistivity (a=50mm).....	223
Figure 8.34. Influence of the orientation of the crack on soil resistivity (a=100mm).....	223
Figure 8.35. <i>AI</i> -depth profiles	225
Figure 8.36. <i>AI</i> changes at deferent depths for the created cracks	225
Figure 8.37. Polar diagram and <i>AI</i> - depth data for the initial non-cracked stage and for the subsequent stages with cracks of 10, 40 and 70mm depth (a) Polar diagram at 10mm depth (b) <i>AI</i> -depth profiles	226
Figure 8.38. Resistivity data of the initial non-cracked stage as a function of the azimuth.....	228
Figure 8.39. Resistivity of the original non-cracked soil on polar diagram (a) α , β and A_v resistivity (b) <i>AI</i> data	228
Figure 8.40. <i>AI</i> polar diagrams of the manually created cracks in stage 1, 2 and 3	229
Figure 8.41. Evolution of <i>AI</i> polar diagrams profiles (a) Stage 1 (b) Stage 2 and (c) Stage 3.....	230
Figure 8.42. <i>AI</i> polar diagrams of the first drying and wetting test	232
Figure 8.43. <i>AI</i> polar diagrams of the second drying and wetting test	234

LIST OF TABLES

	<u>Page</u>
Table 2.1. Atterberg Limits of the BIONICS fill material (Mendes, 2011).....	25
Table 2.2. Popular electrode arrangements (Samouëlian et al., 2005).....	31
Table 3.1. Resistivity of compacted specimens of different dimensions	81
Table 4.1. A comparison between Resist and the Terrameter for different reference resistors	87
Table 4.2. Summary of automatic data acquisition of the reference resistors tests	91
Table 4.3. Summary of normal and reciprocal readings of reference resistors	96
Table 4.4. Summary of reciprocity tests of clay and sand specimens.....	100
Table 5.1. List of tests performed on compacted specimens	123
Table 6.1. List of samples and electrolytes prepared	151
Table 7.1. Tests performed on compacted samples.....	181

Chapter 1

Introduction

1.1 Overview

An accurate knowledge of the water content of unsaturated soils is crucial to understand the geotechnical properties and behaviour of natural and engineered earth structures. Seasonal changes of soil water content can cause significant seasonal changes in pore pressures, which affects soil strength, making water content an important factor when considering stability and long-term serviceability of engineered earth structures such as embankments (e.g. Gunn et al., 2009; Toll et al., 2011). In clay soils, however, water content changes may cause cyclic processes of shrinkage and swelling, and that can adversely impact the engineering properties and behaviour of these soils, which is known to contribute to slope failures (e.g. Smethurst et al., 2006). Future climate forecasts indicate that the UK will be affected by higher temperatures and more extreme rainfall seasons (IPCC, 2007). These seasonal fluctuations in water content cause corresponding fluctuations in pore pressures. Therefore, in-situ monitoring of the water content in engineered earth structures is vitally needed.

Quantifying water content in unsaturated soils is difficult due to the complexity of unsaturated systems and the difficulties associated with gathering representative measurements. A large spectrum of techniques is available to measure soil water content ranging from small scale probes to regional, remote sensors. Various probes are used in practice to estimate water content by measuring soil properties that can be related to water content. These include; neutron scattering (e.g. Bell and McCulloch, 1966); dielectric methods such as Time Domain Reflectometry (TDR), Frequency Domain Reflectometry (FDR) and capacitance probes (e.g. Topp et al., 1980; Jones et al., 2002; Robinson et al., 2003; Huisman et al., 2006). Remote sensors such as passive (radiometer) and active (radar and scatterometer) sensors provide measurements at regional scale (Brocca et al., 2010).

Water content probes provide valuable information on a small volume (few cubic centimetres) of the soil. However, these techniques are destructive and offer measurements at point scale which make it sensitive to the disturbance of the soil itself during the installation with limited spatial resolution (Robinson et al., 2008). In addition, water content measurement in the vicinity of these probes might not be representative for heterogeneous soils, and moisture along fissures cannot accurately be measured which may lead to considerable errors (Sass, 2005). Furthermore, the measurements are related to the time and location of the probe and installation process which cannot be repeated at the same place prohibiting a reliable monitoring of moisture evolution. Moreover, the high cost of these instruments and soil specific calibrations are additional drawbacks (Muñoz-Carpena, 2002; Jones and Or, 2004). Although remote sensors can cover a much bigger area, key limitations of these techniques are the limited resolution, the small penetration depth and the measurements are largely affected by soil surface roughness (Vereecken et al., 2008).

The Electrical Resistivity Tomography (ERT) method has emerged recently as an alternative technique for quantifying soil water content at various scales. The technique offers non-invasive measurements that can be integrated on a large volume.

The method has routinely been used in geotechnical (Pellerin, 2002), environmental (Grellier et al., 2008), hydrogeological (Barker and Moore, 1998), agricultural (Petersen and Al Hagry, 2009), archaeological (Noel and Xu, 1991), and mineral (Mwenifumbo, 1997) investigations. It has been adopted to address a wide range of problems related to the hydraulic properties of the soil to investigate, for instance; soil water content (Cosentini et al., 2011), porosity (Dannovski and Yaramanci, 1999), saturation (Abu-Hassanein et al., 1996), structure (Tabbagh et al., 2000), compaction (Seladji et al., 2010), heterogeneities (Borsic et al., 2005), solute transport (Binley et al., 1996a), landslides (Chambers et al., 2011b), and pollution (Godio and Naldi, 2003).

In particular, soil resistivity is sensitive to water content changes. A proxy relationship between the resistivity and water content has been indicated by many researchers (e.g. McCarter, 1984; Russell and Barker, 2010). Changes in water content cause significant changes in the resistivity of the soil. Thus, mapping resistivity changes during wet and dry seasons provides a powerful tool to monitor the soil water content distribution at different scales ranging from laboratory (e.g. Brunet et al., 2010; Franz et al., 2011; Muñoz-Castelblanc et al., 2011) and field scales (e.g. Turesson, 2006; Cassiani et al., 2009; Nijland et al., 2010). Being rapid and cost-effective, this method is a very promising tool for providing in-situ 2D (e.g. Jackson et al., 2002), 3D (e.g. Zhou et al., 2001) and 4D (Chambers et al., 2014) tomographies of soil water content lacking from traditional techniques. In addition, the method has been indicated as an effective technique for the estimation of the spatiotemporal variability of water content (e.g. Calamita et al., 2012; Gunn et al., 2014), and to consider the effect of cracking in soil hydrodynamics (e.g. Amidu and Dunbar, 2007). Moreover, through time-lapse and real-time measurements, this method has been adopted as a new technology for long-term embankment warning systems (Gunn et al., 2010a; Chambers et al., 2011a; b; Gunn et al., 2014).

Significant advances in this method have taken place with the advent of automated resistivity systems that facilitate the acquisition of a large number of measurements in a limited time accompanied with robust data inversion software. Automated multi-electrode resistivity systems now allow rapid and efficient data acquisition of electrical resistivity measurements to address a wide range of problems. These advances have recently been reviewed by Samouëlian et al. (2005) and Loke et al. (2011; 2013).

Automatic multi-electrode systems have several desired advantages over traditional instruments (Tsourlos, 1995; Dahlin, 2001): (1) speedup the data acquisition process; (2) improve the resolution and confidence through collecting large data sets, (3) offer the flexibility to choose a suitable electrode array for a particular problem, which in turn reduces the time effort of laborious electrode switching using manual four electrode systems.

Recently, there have been rapid advances in resistivity instrumentation, resulting in more rapid and efficient data acquisition systems. The increased demand to develop flexible and non-destructive techniques that can address complex problems has led to the speed up in the research in this regard. The ongoing research is expected to continue (Dahlin, 2001). However, one of recent advances is the development of automated resistivity systems capable of acquiring real-time data to investigate transient phenomena (Loke et al., 2011). On a lab scale, interest has been focused on the development of systems and devices that can provide quick and efficient local tools to monitor water content (e.g. Damasceno et al., 2009; Stacey et al., 2009; Muñoz-Castelblanc et al., 2011; 2012), while on the field scale, automated resistivity systems have been developed to provide a continuous data acquisition (e.g. Ogilvy et al., 2009; Sherrod et al., 2012).

In geotechnical testing, there is an increasing need to develop efficient techniques to measure soil water content with volume integration, preferably in a non-invasive manner. Therefore, this thesis aims to develop an automated multi-electrode resistivity system and other devices for water content characterisation of unsaturated clay soil.

1.2 Thesis objectives

The main objectives of the work described in this thesis are:

1. To develop a flexible, automatic multi-electrode resistivity system and resistivity devices for laboratory water content measurements.
2. To investigate the water content characteristics of a mechanically compacted clay soil using the electrical resistivity method.

The main goal was to develop an automated resistivity system that can provide automated real-time measurements to monitor water content changes in unsaturated soils. Such a system would be useful for monitoring water content changes in the soil using small resistivity probes/devices in addition to collecting resistivity data for ERT studies. The second objective was to explore the potential of the resistivity technique for water content

characterisation of unsaturated clay soils, and to consider of the influence of drying, wetting and cracking on soil properties. Such data can be used to calibrate resistivity data from the field against water content.

1.3 Thesis structure

The thesis is organised in nine chapters. Following this introductory chapter, Chapter 2 presents the theoretical background and basis for the work contained in the subsequent chapters. The physical principles of the main water content measurement techniques are discussed. A review of the basic principles of the electrical resistivity technique, particularly its use for water content measurements is given.

Chapter 3 presents the design and construction of a new automated multi-electrode resistivity system developed in this study. The design, calibration and measurement procedures of a new resistivity probe for localised water content determination, and other resistivity devices are also presented

As for a new system, data quality and error of the developed system had to be examined. Therefore, Chapter 4 describes the laboratory calibration and validation procedures adopted to examine the developed system. A wide range of reference resistors and different types of soils were used to check the data quality of the system. The outputs were compared with those collected using commercial instruments.

Chapter 5 explores the water content characteristics of mechanically compacted clay soils determined using the resistivity method. Unsaturated clay specimens, compacted at various water content, were used to investigate the influence of the compaction key variables on soil resistivity. At each water content, the specimens were compacted using dynamic (standard Proctor and Modified) and static methods. Gravimetric water content, volumetric water content and degree of saturation were correlated with the measured resistivity for a range of dry densities.

In addition to the compaction conditions, the temperature and pore water conductivity have been indicated as important factors that affect the resistivity of the soil. Therefore, Chapter 6 investigates the role of temperature and pore water conductivity on resistivity measurements. The resistivity behaviour of the soil over a temperature range of -12 to 43°C is discussed. As the electrical conductivity of the pore water depends on the type and concentration of the dissolved salts, specimens of clay soils were mixed with different electrolyte types and concentrations, and the influence of the dissolved salt types and their concentration on soil resistivity is addressed.

Unsaturated soils are subjected to drying-wetting cycles. In addition to the negative pore pressures (or suctions), water content and volume changes are key controlling factors. Although a number of studies have been undertaken to investigate the effect of water content on soil resistivity, volume changes due to water content changes are rarely considered, as such measurements add complexity to these necessary laboratory tests. Therefore, Chapter 7 aims to investigate the use of the resistivity for characterising drying and wetting of clay soils. In addition to discrete drying/wetting, water content and volume change measurements were collected with the resistivity measurements in a real-time procedure.

Clay soil tends to shrink when it loses moisture, this shrinkage may cause cracking. Although soil cracks have complex patterns, their formation causes directional dependence of the electrical current flow, which makes resistivity promising for characterising soil cracks. Chapter 8 is dedicated to exploring the potential of the resistivity method to characterise the cracking of clay soils. Numerical and experimental techniques have been used to explore the influence of cracking parameters (i.e. depth, length, width, and orientation) on soil resistivity.

Finally, Chapter 9 summarises the results of the research study, provides conclusions and also gives recommendations for future work.

Chapter 2

Soil water content measurement: Background and literature review

Soil water content is a key variable for describing water and energy exchanges through soil-atmosphere interactions and for understanding a variety of hydrological and hydrogeological processes. Thus, the quantification of this variable is essential for different disciplines and Geo-engineering applications. In recent decades, a wide range of techniques has been introduced to measure soil water content. A substantial body of knowledge is available in the literature on the theory and application of these methods. Therefore, in this chapter, the main methods used to measure soil water content are reviewed. The physical principles behind these methods, their advantages and drawbacks, are discussed. In addition, the theoretical background of the resistivity method and its application for water content measurement of unsaturated soil is presented. This chapter is dedicated to providing a theoretical background and basis for the work contained in this thesis. Further details relevant to particular aspects of the current work will be provided in the subsequent chapters.

2.1 Soil water content

2.1.1 Background

Unsaturated soil, as a porous medium, consists of three phases: air, solid and water (Figure 2.1). The state of water in this soil can be defined in terms of the water content and water potential (i.e. suction). The former is an expression of the amount of water in the soil while the latter determines the energy status of the soil water (i.e. the energy associated with the forces that hold the water in the soil). The relationship between soil water content and suction can be defined through the soil water retention curve (also known as the soil

water characteristic curve), one of the most important relationships in the field of unsaturated soil (Fredlund and Rahardjo, 1993).

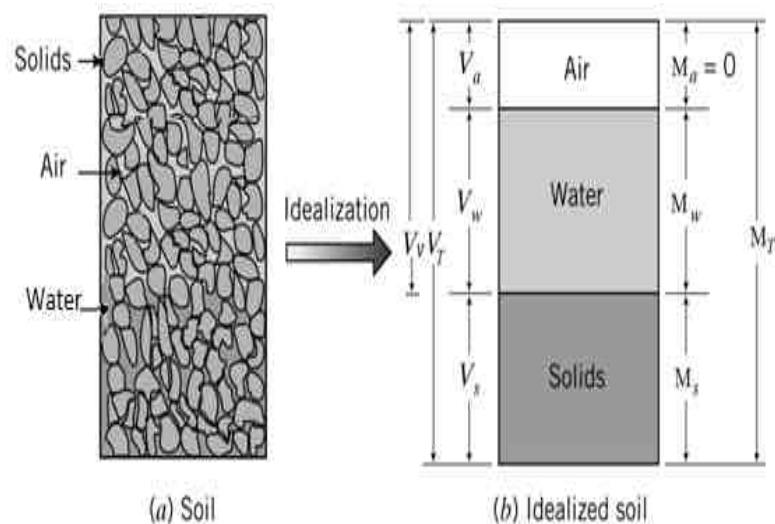


Figure 2.1. Schematic representation of soil phases (Budhu, 2011)

In particular, the amount of water in the soil can be determined on a mass basis as the gravimetric water content, w , expressed as the percentage ratio of the mass of water, M_w , to the mass of soil solids, M_s :

$$w = \frac{M_w}{M_s} \times 100\% \quad (2.1)$$

On a volume basis, volumetric water content, θ , defines the amount of water as the percentage ratio of the volume of water, V_w , to the total volume of the soil, V_T :

$$\theta = \frac{V_w}{V_T} \times 100\% \quad (2.2)$$

The relationship between gravimetric and volumetric water content can be given as:

$$\theta = w \left(\frac{\rho_d}{\rho_w} \right) \quad (2.3)$$

Where ρ_d is the dry density of the soil and ρ_w is the water density.

The water state can also be described in terms of the degree of saturation, S_r , defined as the fraction of porosity, \emptyset , that is occupied by water, expressed by the ratio of volume of water, V_w , to the volume of voids, V_v :

$$S_r = \frac{V_w}{V_v} = \frac{V_w}{V_T \cdot \emptyset} = \frac{\theta}{\emptyset} \quad (2.4)$$

S_r ranges from (0-1) or (0- 100%).

2.1.2 Clay soils: Mineralogy and microstructure

The chemical weathering of soils produces clay minerals of sheet structure chemically known as hydrous alumina-silicates. The bonding characteristics of the silica and alumina sheets play an important role in the mechanical properties of these minerals. Two basic flat, plate-like sheets structures can be identified: the tetrahedral sheet which consists of a silicon atom surrounded by four oxygen atoms; and the octahedral sheet which consists of an aluminium atom surrounded by six oxygen atoms (Figure 2.2). According to a combination of these fundamental structures, different clays (e.g. Kaolinite, Illite, and Montmorillonite) are available. Kaolinite consists of repeated layers of one silica sheet and one alumina sheet held together by hydrogen bonds; this structure is commonly known as 1:1 structure (Figure 2.3). The structure of Illite consists of repeated layers of one alumina sheet between two silicate sheets, and the layers are held together by potassium ions. This structure is known 2:1 structure. Montmorillonite is characterised by a structure similar to Illite, but the layers are held by weak van der Waals forces and exchangeable ions that allow water to easily infiltrate between layers and separate them causing swelling (Budhu, 2011).

Clay soils, commonly used as fills in earthworks, are susceptible to progressive failure due to the swell and shrink behaviour of clay minerals. This behaviour is mainly controlled by the microstructure of clay soils and water content changes related to climate effects.

CHAPTER 2: SOIL WATER CONTENT MEASUREMENT: BACKGROUND AND LITERATURE REVIEW

The soil absorbs the water during wet seasons and hence the volume increases, and dries out during the dry seasons and hence the volume decreases. As a consequence, shear strength of the soil reduces due to irreversible plastic strains accumulated within the soil (Lambe and Whitman, 1999). Shear zones, however, are characterised by water content changes, and the earlier identification of water content changes along these zones is crucial for monitoring the slopes.

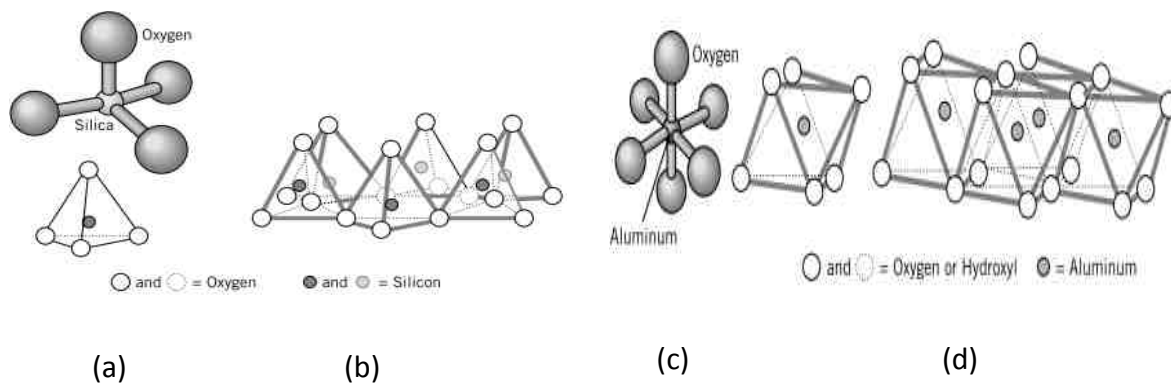


Figure 2.2. Clay minerals structure (a) Silica tetrahedron (b) Silica sheets (c) Aluminium octahedron and (d) Aluminium sheets (Budhu, 2011)

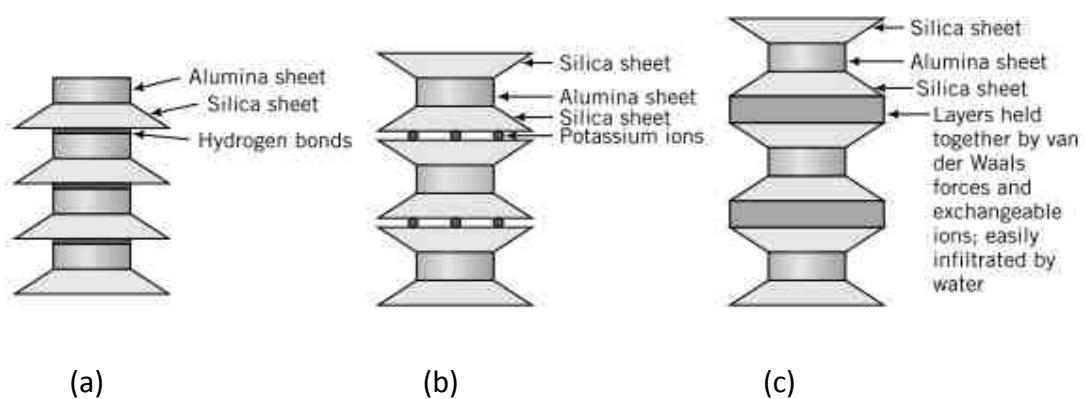


Figure 2.3. Clay minerals structure (a) Kaolinite (b) illite, and (c) montmorillonite (Budhu, 2011)

2.2 Soil water content measurement methods

2.2.1 Direct method: Gravimetric method

The amount of water in the soil can directly be obtained using the gravimetric method (BS 1377-2, 1990). The method is based on the measurement of the soil mass before and after oven drying at 105°C for 24 h. Soil water content can be derived as:

$$w = \frac{M_{wet} - M_{dry}}{M_{dry}} \times 100\% \quad (2.5)$$

Where M_{wet} and M_{dry} are the mass of the soil before and after drying, respectively. Although the actual value of water content can be determined using the gravimetric method, this method is time-consuming and impractical in the field since it requires a large number of specimens to overcome the spatial heterogeneity of the soil. Nonetheless, since all other methods are indirect, the gravimetric method represents the reference for calibrating all other methods.

2.2.2 Indirect methods

Indirect methods measure a soil physical property that can be related to the amount of the water through empirical relationships, commonly called calibration curves. A brief review of the main methods is given in the following sections. Their working principles, advantages and drawbacks are highlighted. For further details, recent reviews can be found in (Western et al., 2002; Robinson et al., 2003; Evett and Parkin, 2005; Muñoz-Carpena et al., 2006; Robinson et al., 2008; Vereecken et al., 2008; Seneviratne et al., 2010; Bittelli, 2011).

Neutron scattering probe

The neutron scattering probe (Figure 2.4), mounted on an access tube, employs fast neutrons emitted from a radioactive source that collide with soil atoms. The neutrons slow

down and lose their energy due to collision with hydrogen atoms in the water. A detector counts the number of slowed neutrons in a particular time interval, which can be related to the hydrogen content, or soil water content. This method offers robust and accurate measure of volumetric water content; however, the high cost of the instrument, soil specific calibration and safety hazards are the major drawbacks (Evet and Parkin, 2005; Muñoz-Carpena et al., 2006).



Figure 2.4. Neutron scattering probe (Muñoz-Carpena et al., 2006)

Dielectric methods

Dielectric methods estimate the volumetric water content of the soil by measuring the dielectric constant k (or the bulk permittivity) of the soil that determines the velocity of an electromagnetic wave through the soil (e.g. Topp, et al. 1980). Since the dielectric constant of water ($k=80$) is larger than of air ($k=1$) and soil constitutes ($k= 2-5$), the bulk permittivity is mainly governed by soil water content (Blonquist et al., 2005). To estimate volumetric water content from k , the empirical equation of Topp et al. (1980) is commonly used:

$$\theta = -5.3 \times 10^{-2} + 2.92 \times 10^{-2} k - 5.5 \times 10^{-4} k^2 + 4.3 \times 10^{-6} k^3 \quad (2.6)$$

The above relationship is independent of the soil type and valid for water volume below 50%. A specific calibration is needed for soils of high water or organic contents. Based on the sensor output signal (e.g. time, frequency and impedance), different dielectric sensors are available (Muñoz-Carpena et al., 2006).

Time domain reflectometry TDR

TDR is one of the most accurate and reliable methods for water measurements (e.g. Robinson et al., 2003; Huisman et al., 2006). The TDR probe (Topp et al., 1980; Jones et al., 2002) propagates high-frequency electromagnetic waves (usually 1MHz to 1GHz) along the cable attached to a probe inserted into the soil (Figure 2.5). The probe determines the dielectric constant k by measuring the propagation time t that it takes for an electromagnetic wave to propagate along the transmission line. Since the velocity v is a function of k of the soil, k is proportional to the square of the travel time t down and back along the transmission line:

$$k = (c/v)^2 = ((c \cdot t)/(2 \cdot L))^2 \quad (2.7)$$

$$\text{or, } t = \frac{2L\sqrt{k}}{c} \quad (2.8)$$

Where c is the velocity of the electromagnetic waves in free space (m/s) and L is the length of the probe embedded in the soil (m). Although TDR measurements are robust and accurate, they potentially suffer from limited applicability in highly saline soil, highly conductive clay contents and stony soils (Jones and Or, 2004)



Figure 2.5. TDR probes (Muñoz-Carpena et al., 2006)

Frequency domain FD: Capacitance, frequency domain reflectometry FDR

Frequency domain probes (plates, rods, or metal rings) shown in Figure 2.6 use a capacitor that is connected to an oscillator to measure the dielectric constant (as TDR) using electromagnetic waves at megahertz frequency. Water content changes in the soil can be estimated by detecting changes in the circuit operating frequency (Muñoz-Carpena, 2002; Gardner, 1986; Bittelli, 2011). In the capacitance type, k of the soil is calculated by measuring the charge time of a capacitor made with the soil while, in FDR, the oscillator frequency is controlled in a particular frequency range to determine the resonant frequency (i.e. the greatest amplitude) which reflects a measure of the water content.

The high resolution, accuracy and flexibility in the sensor design are main advantages of these sensors. However, as the operating frequency is usually below 100MHz, a soil specific- calibration is required as k is more affected by the density, salinity, temperature and clay content of the soil (Muñoz-Carpena et al., 2006).



Figure 2.6. FD probes (a) Capacitance (plates) (b) Capacitance (rods) and (c) FDR (rings)
(Muñoz-Carpena, 2002)

Amplitude domain reflectometry ADR: Impedance

ADR sensors use a fixed frequency signal generated by an oscillator through a coaxial transmission line and central metal rod surrounded by an array of rods (Figure 2.7). The impedance measurement is dependent on the dielectric constant of the soil between the metal rods. Compared to other dielectric probes, the ADR probe is less expensive and not sensitive to temperature. However, the probe is influenced by air gaps and stones in the soil, as are TDR probes (Muñoz-Carpena et al., 2006).

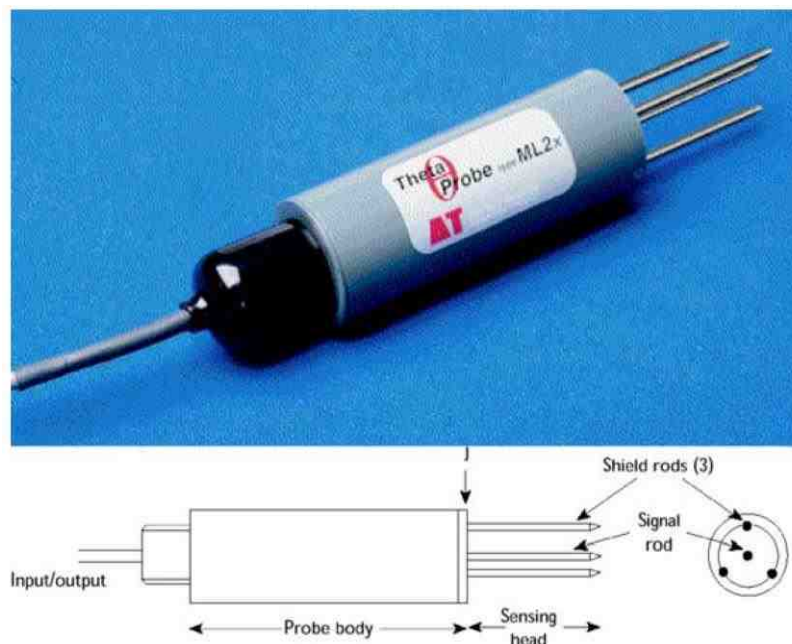


Figure 2.7. ADR probe (Muñoz-Carpena, 2002)

Ground penetrating radar: GPR

GPR uses the same principle as the TDR probe to measure water content at larger scales (Davis and Annan, 1989). The GPR system consists of transmitting and receiving antennas (Figure 2.8) to determine the travel time of high frequency (1MH-1GH) electromagnetic waves transmitted into the soil. The radar wave travel time is related to the dielectric constant through the Topp et al. (1980) equation (Huisman et al. 2003). Although robust and non-disturbing measurements can be collected across large areas, signal attenuation, especially in clay soils, severely limits the depth of penetration (Evelt and Parkin, 2005). However, new advancements in technology and interpretation techniques have led to significant improvements (Robinson et al., 2008).

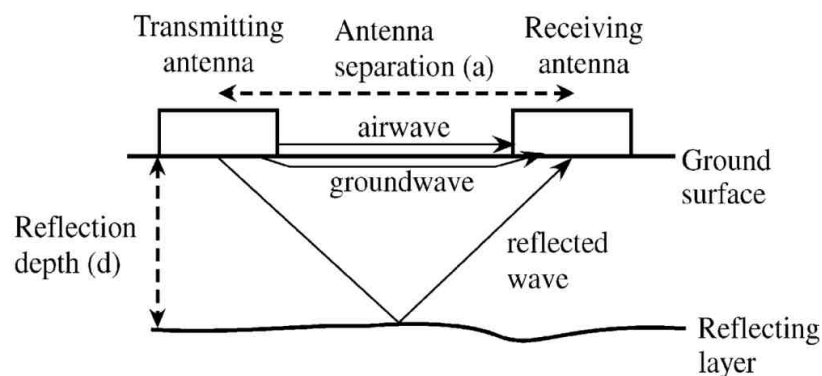


Figure 2.8. Schematic diagram showing the GPR working principle (Lunt et al., 2005)

Remote sensors

Measurement of soil water content changes at large scales is useful to improve the knowledge about the climate and hydrologic modelling (Western et al., 2002). Remote sensors can be operated from the ground; airborne or space-borne platforms. These sensors can be classified into passive (radiometer) and active (radar and scatterometer) sensors (Figure 2.9). In the first type, the instrument measures the self-emission of the soil surface. The fraction of the total radiation that is emitted is related to the dielectric properties of the soil. In the second type, the sensor measures radiation scattered back from the surface after the soil is illuminated using a source of radiation (Robinson et al., 2008; Brocca et al., 2010). Among others, low frequency (i.e. microwave) radar is the most effective type for measuring water content (Robinson et al., 2008) as it can penetrate through clouds and precipitation and has a relatively good penetrating depth. Although the remote sensors provide rapid and cost-effective information over large areas, they have limited depth of penetration (a few centimetres) and are sensitive to vegetation and soil surface roughness (Western et al., 2002; Vereecken et al., 2008).

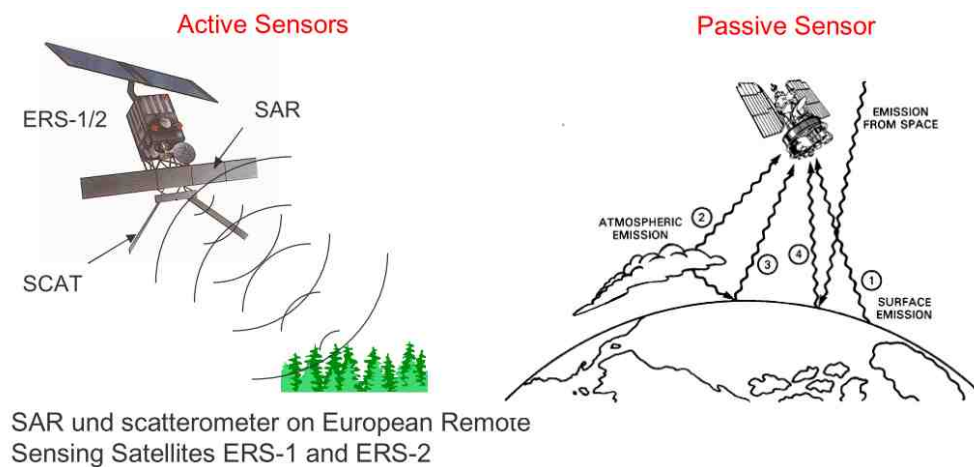


Figure 2.9. Passive (radiometer) and active (radar) sensors

2.3 Soil water content: Scaling issues

Soil water in unsaturated soil is highly variable, both in space and time, and many dependent processes are nonlinear and complex (Western et al., 2002). Because of the topography, land cover, evaporation, precipitation and soil heterogeneity, obtaining accurate and representative measurements of water content is difficult. As the heterogeneous distribution of soil water depends on several landscape factors, this leads to scaling effects and makes accurate predictions of the hydrologic system behaviour challenging (Brocca et al., 2010).

Water content probes provide measurements at point scale with limited spatial resolution (Robinson et al., 2008; Bittelli, 2011). Water content measurement in the vicinity of these probes however might not be representative for heterogeneous soils. Although remote sensors can cover a much larger area, key limitations of these methods are the limited resolution, the small penetration depth and the measurements being greatly affected by soil surface vegetation and roughness. In a review paper, Robinson et al. (2008) emphasised that measurements at small scale have advanced with a broad spectrum of in situ sensors while measurements at basin scale (2,500-25,000 km²) have advanced with

remote sensing. At present, there is an intermediate scale gap where we currently lack methods that describe field scale water content changes. Therefore, there is an increasing demand to explore new techniques that can map, at field scale, the spatiotemporal variability of soil water content (Sass, 2005, Robinson et al., 2009; Srayeddin and Doussan, 2009).

The ERT method has recently emerged as a non invasive technique that can offer measurements of water content at different scales with variable resolution. The method can produce 2D, 3D and 4D estimates of water content changes that are lacking using other techniques. It has the potential to be a rapid and cost-effective monitoring tool, and, if linked with other point based sensors, can effectively be used to map moisture build-up in engineered earthworks caused by seasonal water changes (e.g. Gunn et al., 2007; 2008; 2014).

2.4 Water content changes: Climate effects

Seasonal water content changes are strongly dependent on climate effects. Recent climate forecasts indicate that the UK will be subjected to higher temperatures and intense rainfall seasons (IPCC, 2007). These effects were already observed from the recent extensive floods which followed unusually large rainfalls, accompanied by slope failure observations along the transportation network. In the UK, thousands of kilometres of rail and road embankments have been built from materials that vary with the location, constructed using traditional and modern construction methods. The majority of these embankments were built in the 19th century using stiff clay with poor compaction techniques and experience problems associated with pore pressure changes related to water content changes. As water content increases, pore pressure increases (i.e. suction decreases) leading to loss of strength and slope failures (Toll et al., 2011). However, since the water content changes are seasonal, the climate effects are likely to affect the seasonal pore pressure cycle within the soil. Consequently, pore pressure will be higher during the wetter winter and lower in drier

summers that impact the stability of these structures. It is, therefore, important to predict the impact of climate change on the engineering performance and stability of earthworks such as embankments (Toll et al., 2008; Gunn et al., 2009; Mendes, 2011).

Although rainfall is the most frequent triggering factor that causes a slope to fail and is widely used as an early warning factor, the relationship between rainfall infiltration, water content change and suction is highly complex, nonlinear and hysteretic (Toll et al., 2011). The complex relationship between suction and water content, shown in Figure 2.10, reflects the complexity of the flow in unsaturated soils and emphasises the need for a better understanding of the influence of water content changes on these soils.

In clay soil, commonly used as a fill in earthworks, water content changes often cause cyclic processes of swelling and shrinkage. Clay minerals absorb water during wet periods, making them swell, and lose water during dry periods, making them shrink. The shrink- swell behaviour of clay and the corresponding volume changes are a well-known global problem. In the UK, the British Geological Survey considers the problem one of the most damaging hazards, particularly in the southeast (Figure 2.11a), costing the economy about £3 billion over the past decade (BGS, 2014a).

The degree of shrink-swell behaviour is controlled by the mineralogy and amount of clay in the soil and the seasonal water content changes. Based on the distribution of unstable slopes (Figure 2.11b), about 10% of Britain is classified as having moderate to significant landslide hazard potential and more than 7% of the transport network is located in areas of moderate and significant landslide potential, which brings significant challenges (Dijkstra and Dixon, 2010).

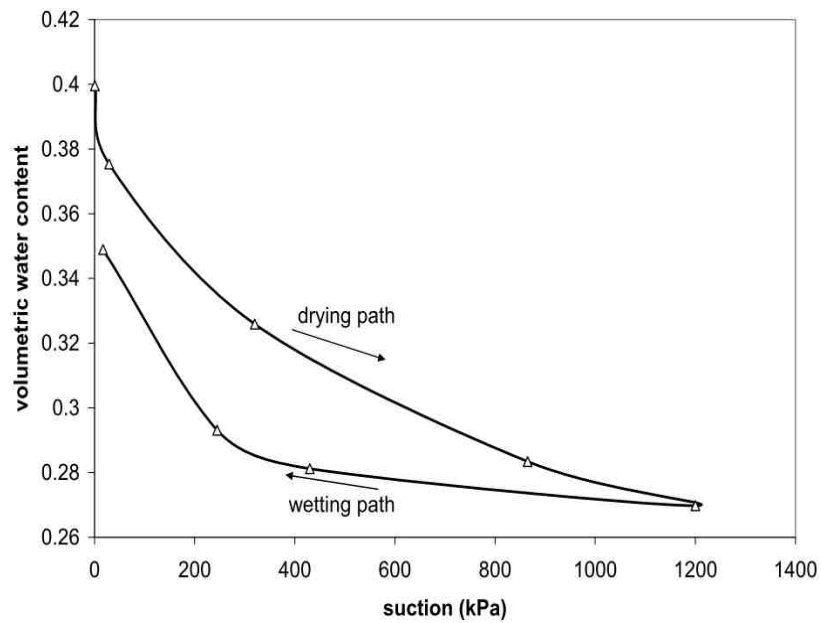


Figure 2.10. Soil water retention curve of BIONICS clay (Lourenço, 2008)

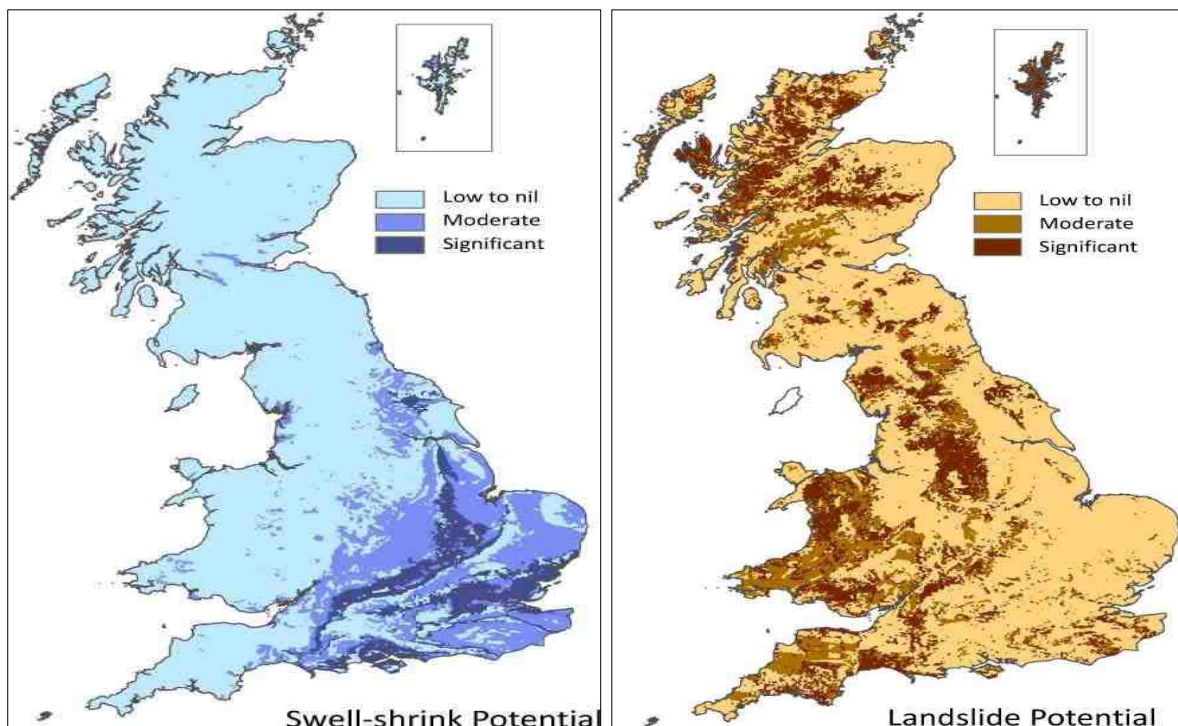


Figure 2.11. The UK map (a) Swell-shrink potential map (BGS, 2014a),
(b) Landslide potential map (BGS, 2014b)

Figure 2.12 shows the rainfall and landslide events monitored by the BGS in the UK for January 2012 to July 2014. Increasing rainfall events caused a marked increase in the number of the landslides. Increasing rainfall caused a variety of earthwork failures in the national rail network (Department of Transport, 2008), as shown in Figure 2.13.

Direct pore pressure measurements using high-capacity tensiometers (e.g. Lourenço, 2008) provide the most accurate and reliable information of the impact of climate change on the earthworks, such as embankments. Pore pressure changes are closely related to water content changes. Therefore, water content measurements can be used as a useful indicator to assess the state of these structures. Although in-situ measurements of soil water content using soil sampling and moisture sensors can provide an accurate assessment of water content at a local scale, these tools are intrusive and offer insufficiently representative information. Financial, operational and time limitations reduce the number of measurements at field scale.

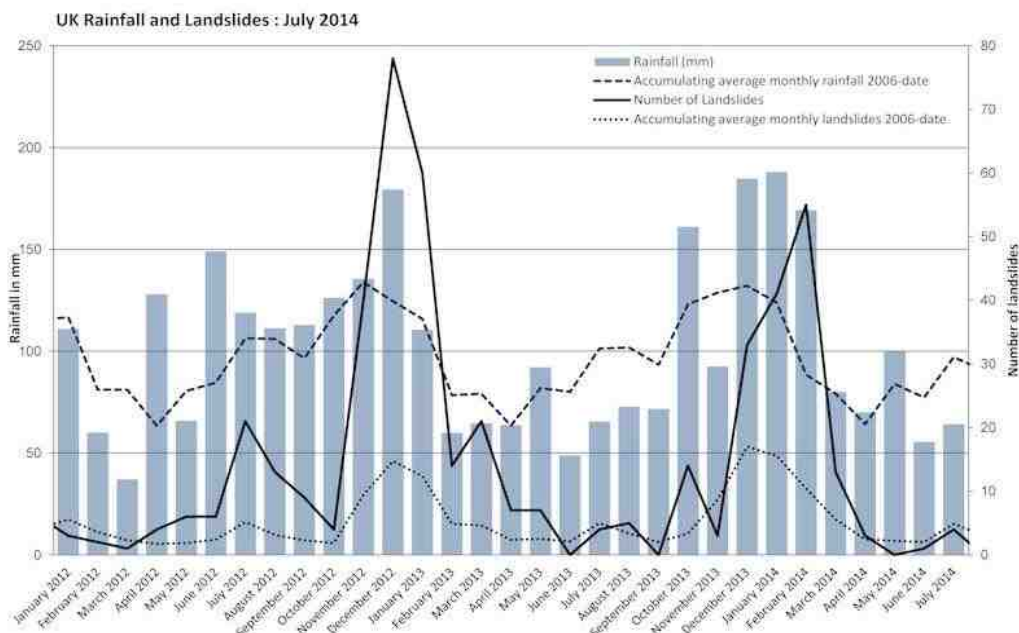


Figure 2.12. Rainfall and landslide events in the UK (January 2012 to July 2014) (BGS, 2014c)

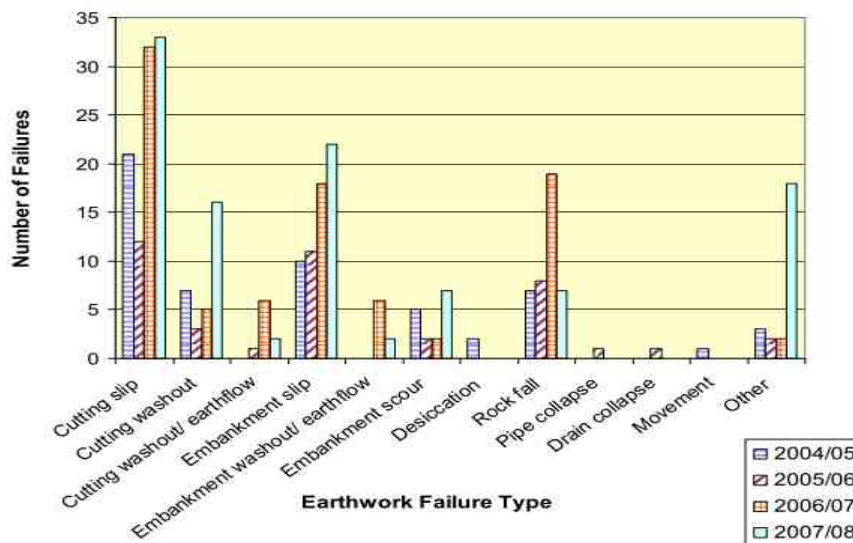


Figure 2.13. The earthwork failures in the UK rail network (2004-2008) (Department of Transport, 2008)

There is a need to research into new methods that can monitor water content changes related to the climate changes. As part of the BIONICS project, an experimental embankment was built to address the impact of climate changes on engineered earth structures.

2.5 BIONICS Project

The BIONICS project (BIOlogical and eNgeering Impacts of Climate change on Slopes), funded by the Engineering and Physical Research Council, is a large collaborative research project, involving academic partners and industrial stakeholders, aimed at investigating the impact of future climate changes on engineered earth structures. As part of the project, a full-scale experimental embankment was built near Newcastle, United Kingdom. The embankment was instrumented with monitoring network of piezometers, tensiometers, water content and temperature sensors, inclinometers and extensometers, as well as two resistivity arrays. Considerable efforts, modelling, laboratory and field testing, have been undertaken to investigate the effects of climate change on

infrastructure embankments in order to develop methodologies and generate data for models capable of addressing the impact of climate change on the serviceability and stability of these structures.

The soil used in the current study was sourced from the BIONICS embankment. Therefore, a brief description of the embankment and soil properties are provided. Full details about the design, construction, instrumentation and monitoring of the embankment can be found in Glendinning et al. (2006), Hughes et al. (2008; 2009) and Toll et al. (2008; 2011; 2012a; b).

2.5.1 The embankment

The BIONICS embankment (90m long, 29m width and 6m height) is a unique research facility constructed in 2005. The embankment (Figure 2.14) was divided into four main sections made using different types of construction methods. The two outer panels were poorly compacted to represent the old rail embankments built in Victorian times (over 100 years ago) while the inner panels were compacted according to modern compaction methods. The outermost panels were made for biological studies (Glendinning et al., 2006; Toll et al., 2012a).

A glacial till sourced from a stockpile in County Durham was used as fill material in the construction of the embankment. The general particle size distribution of the material is shown in Figure 2.15. The material consists of 12% gravel, 16% sand, 35% silt and 37% clay. It is, therefore, classified as well-graded sandy clay soil. According to the Atterberg limits obtained using (BS, 1990: Test 4.3 and 5.3) reported in Table 2.1, the material is classified as being of intermediate plasticity. Considering the PI and the percentage of clay, the fill material is considered as inactive (activity equals 0.53) (Mendes, 2011). Based on the BS Light compaction (Proctor) test (BS 1377, 1990: Tests 3.3), the maximum dry density of 1.71 Mg/m³ was achieved at optimum water content of 15.5% (Mendes, 2011). The soil exhibits a tendency for volume changes. A shrinkage limit of 14% was reported (Lourenço, 2008).

CHAPTER 2: SOIL WATER CONTENT MEASUREMENT: BACKGROUND AND LITERATURE REVIEW

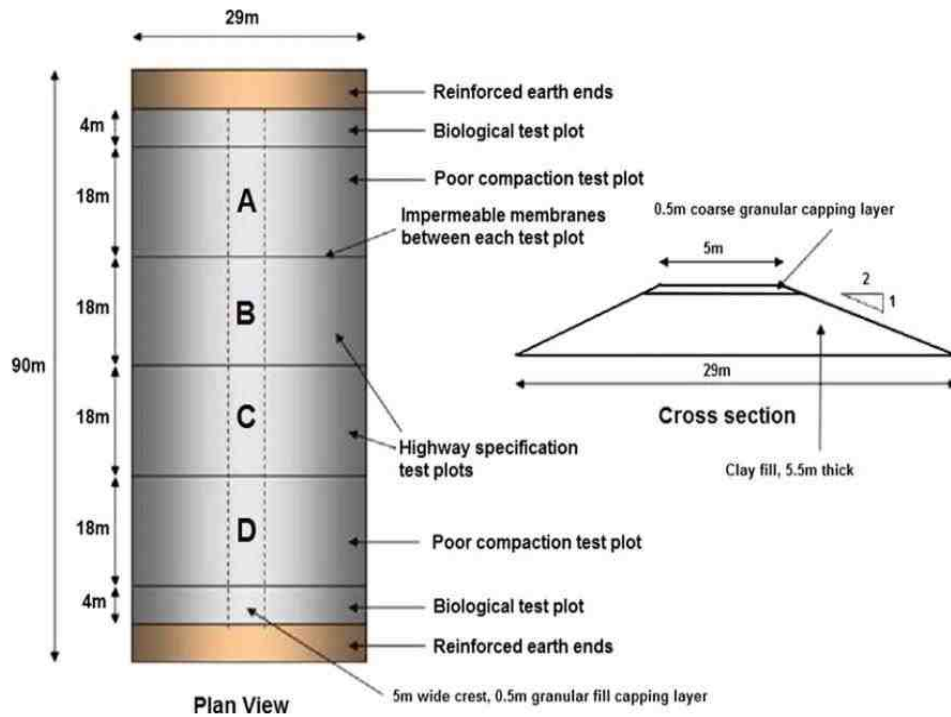


Figure 2.14. Plan view and cross-section of the BIONICS embankment (Toll et al., 2012a)

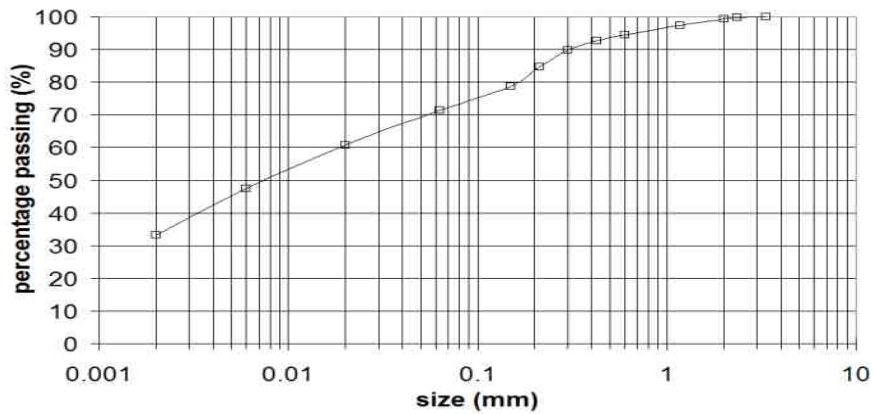


Figure 2.15. Particle size distribution of the material (Mendes, 2011)

Table 2.1 Atterberg Limits of the BIONICS fill material (Mendes, 2011)

Natural water content W _n (%)	Liquid limit LL (%)	Plastic Limit PL (%)	Plasticity Index PI	Liquidity Index LI
22.6	43.3	23.7	19.6	-0.05

CHAPTER 2: SOIL WATER CONTENT MEASUREMENT: BACKGROUND AND LITERATURE REVIEW

A study into the hydro-mechanical behaviour of the fill material used in the BIONICS embankment was carried out by Mendes (2011) which involved the determination of the soil water retention and the mechanical behaviour of the soil under unsaturated conditions. In addition, two resistivity arrays, oriented perpendicular to the embankment at the heavily and poorly compacted panels, were installed by BGS. Each array consisted of 32 electrodes with electrode spacing of 0.5m. Figure 2.16 shows a 2D ERT profile of the embankment that indicates the potential of the method for characterising the internal structure of the embankment. The section also provides valuable information about the resistivity variation within the embankment, which reflects the effect of water content changes and other variations, such as temperature and pore water chemistry variations, across the embankment (Sellers et al., 2010; 2012; Gunn et al., 2014). Detailed laboratory work is needed to further investigate these effects (Hen-Jones et al., 2014).

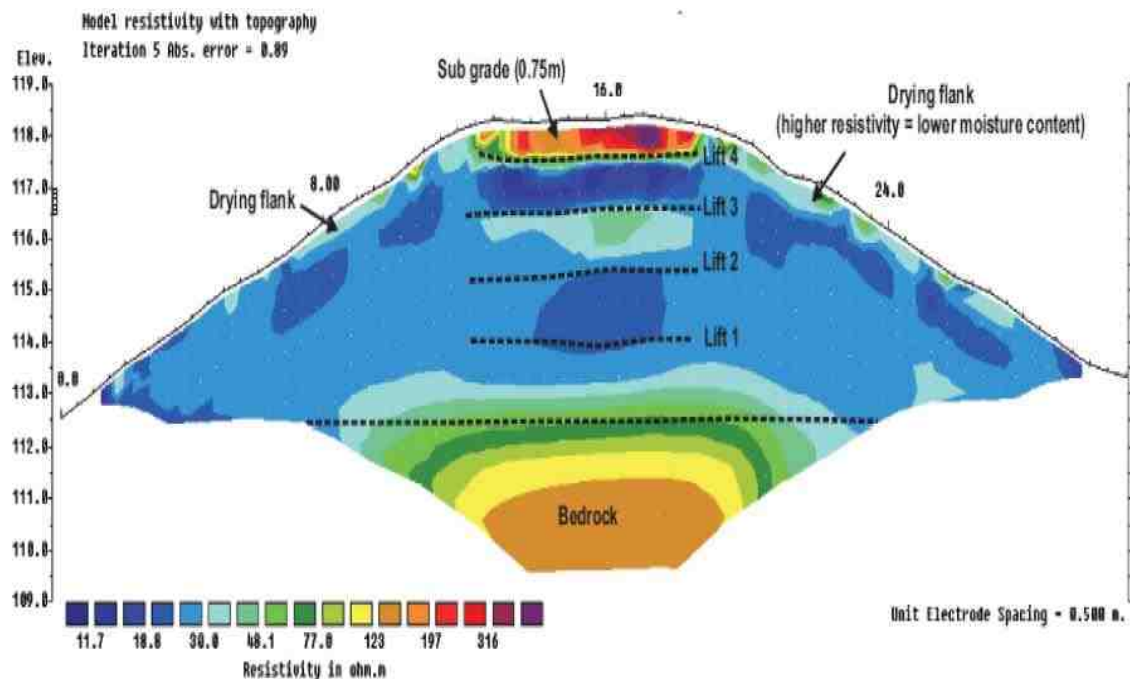


Figure 2.16. 2D ERT profile of the BIONICS embankment (Sellers et al., 2012)

2.6 Electrical resistivity method

Electrical resistivity is a physical property of a material that describes its ability to resist the flow of electrical current. The resistivity method is, therefore, based on the principle that the voltage drop associated with DC or low frequency current injected into the soil is strongly dependent on the resistivity of the soil. Electrical conduction takes place in soil and rocks in three ways: electrolytic, electronic and dielectric conduction. In soils and rocks, electrolytic conduction is the most common method where the current moves through the ions in the pore water. In electronic conduction, the current is carried by the free mobile electrons in the metals. The low resistivity (high conductivity) of metals is, therefore, explained by the large number of free electrons in their structure (Keller and Frischknecht, 1966). Dielectric conduction takes place in insulator materials when an external AC current is applied, which makes the electrons shift slightly. Using DC or low frequency AC current, dielectric conduction in soils can be neglected (Reynolds, 1997).

As electrical conduction takes place as a result of the movement of the ions, electrical properties of soils are mainly controlled by pore water content (Bryson, 2005; Friedman, 2005; Samouëlian et al., 2005). However, the solid phase characteristics affect the relative proportions of water and the air and the connectivity of pores (Friedman, 2005). Furthermore, the electrolytic current conduction is affected by the temperature (Campbell et al., 1948) and pore water salinity (Rinaldi and Cuestas, 2002).

The theoretical background of the ERT method, common electrode arrangements, measurement procedures and the recent advances are briefly reviewed. Further details can be found in several textbooks (e.g. Keller and Frischknecht, 1966; Telford et al., 1990; Reynolds, 1997; Sharma, 1997) and reviews (e.g. Samouëlian et al., 2005; Aizebeokhai et al., 2010; Loke et al., 2011; 2013).

2.6.1 Basic theory

Ohm's Law is a fundamental physical law that governs the flow of electrical current in the soil. The electrical resistance R (Ohm) of a conductor is defined as:

$$R = \frac{\Delta V}{I} \quad (2.9)$$

Where ΔV (volt) is the potential difference between two points in the conductor and I is the electrical current (Ampere). The resistance of the conductor (Figure 2.17) is found to be directly proportional to its length L (m) and inversely proportional to the cross-sectional area A (m²):

$$R = \frac{\rho L}{A} \quad (2.10)$$

Where ρ is the resistivity of the conductor (Ohm.m). Combining (Eq. 2.9) and (Eq. 2.10), the resistivity can be written as:

$$\rho = \frac{\Delta V}{I} \frac{A}{L} \quad (2.11)$$

In an infinite, homogeneous half-space medium with a single current source on its surface (Figure 2.18a), the current travels radially away from the point of the origin, and electrical potential lines are hemispherical. In this case, the resistance at any point from the source within the medium can be calculated by determining the radius, r , from the source and the surface area of the resulting equipotential surface, $2\pi r^2$. The resistance R (Eq. 2.10) can be rewritten as follows:

$$R = \rho \left(\frac{r}{2\pi r^2} \right) = \frac{\rho}{2\pi r} \quad (2.12)$$

The potential difference resulted from a single current source at a distance r can be expressed as:

$$\Delta V = IR = I \left(\frac{\rho}{2\pi r} \right) \quad (2.13)$$

In practice, four electrodes are commonly used. Two electrodes (C1 and C2) for injecting the current and two electrodes (P1 and P2) for measuring the potential difference between two points (Figure 2.18b). In this case, the potential difference between P1 and P2 for a general four electrode arrangement (Figure 2.19) is given as:

$$\Delta V = V_{P1} - V_{P2} = \left(\frac{I\rho}{2\pi r1} - \frac{I\rho}{2\pi r2} \right) - \left(\frac{I\rho}{2\pi r3} - \frac{I\rho}{2\pi r4} \right) \quad (2.14)$$

$$\Delta V = \frac{I\rho}{2\pi} \left(\frac{1}{r1} - \frac{1}{r2} - \frac{1}{r3} + \frac{1}{r4} \right) \quad (2.15)$$

Therefore, the resistivity of the medium can be determined as:

$$\rho = \frac{2\pi}{\left(\frac{1}{r1} - \frac{1}{r2} - \frac{1}{r3} + \frac{1}{r4} \right)} \frac{\Delta V}{I} = K \frac{\Delta V}{I} \quad (2.16)$$

Where K is the geometric factor which depends on the arrangement of the electrodes. In a homogeneous medium, the measured resistivity from Eq. 2.16 is constant and independent on the electrode configuration or location. In a heterogeneous medium, the measured resistivity is then termed the apparent resistivity (Keller and Frischknecht, 1966), which is the resistivity of an equivalent homogeneous medium that will give the same resistance value for the same electrodes arrangement (Loke et al., 2011). Therefore, the measured resistivity value is an average reading of the soil volume engaged during the measurements. Eq. 2.16 is the general equation for calculating the resistivity of any electrode arrangement.

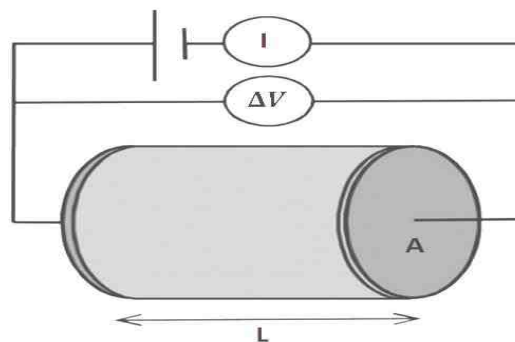


Figure 2.17. Ohm's law on simple conductor of length L and cross-sectional area A^2

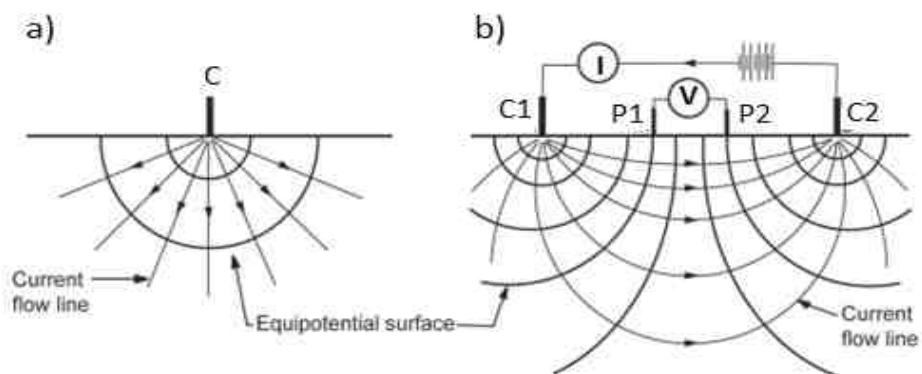


Figure 2.18. The current flow and potential distribution in a homogenous and half-space medium (a) a single current source (b) four-electrode method

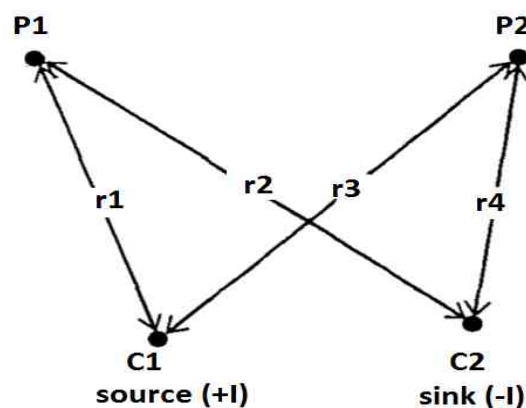


Figure 2.19. General four-electrode arrangement

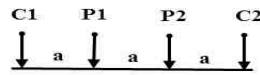
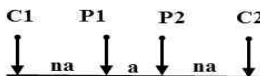

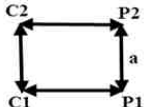
Theoretically, the four electrodes can be placed at any arbitrary locations on the soil surface. However, only a few electrodes arrays are popular and have been used for data acquisition (Szalai and Szarka, 2008). Each array has characteristic features that make it suitable for a particular application. Table 2.2 shows the popular electrode arrangements and the corresponding geometric factors: a is the electrode spacing and n is the spacing integer factor.

2.6.2 Data acquisition

Four-electrode resistivity systems: 1D resistivity method

Traditional four-electrode resistivity system consists of a resistivity meter, four metal stakes (electrodes) and cables to connect the electrodes to the resistivity meter. The system includes two essential components: the power unit and the voltage measuring unit connected to the current and voltage electrode through the cables (e.g. Samouëlian et al., 2005; Aizebeokhai, 2010). Figure 2.20 shows the basic parts of the traditional four-electrode resistivity system.

Table 2.2 Popular electrode arrangements (Samouëlian et al., 2005)

Array type	Electrode arrangement	Geometric factor (K)
Wenner		$2\pi a$
Wenner-Schlumberger		$\pi n(n + 1)a$
Dipole-Dipole		$\pi n(n + 1)(n + 2)a$
Square		$2\pi a/2\sqrt{2}$

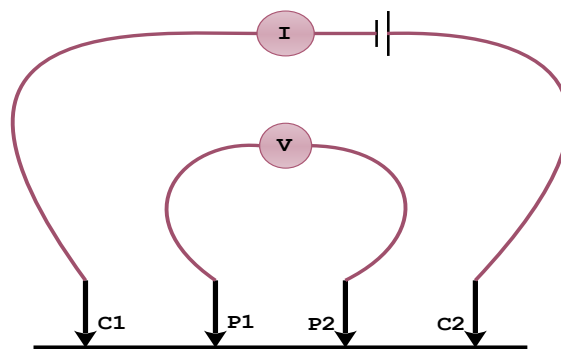


Figure 2.20. Traditional four-electrode resistivity system

In field studies, traditional 1D data acquisition is carried out using Vertical Electrical Sounding (VES), horizontal profiling or Constant Separation Traversing (CST) and horizontal mapping (Reynolds, 1997). VES can be performed by taking a number of measurements at a fixed array midpoint, where distances between the electrodes are progressively increased to obtain the resistivity variation with depth. Interpretation of VES curves assumes 1D horizontally layered resistivity models (Zohdy, 1989). This method has traditionally been used in hydrogeological and engineering applications for delineating the depth of bedrock, the water table and the thickness of horizontal layers. CST is achieved by moving an array with fixed electrode spacing along a profile to detect the lateral resistivity variations. The measurements obtained are interpreted qualitatively to map the location of vertical structures, such as faults, and to map the thickness of overburden layers. Horizontal mapping (i.e. combining several CST profiles) is useful to map lateral resistivity variations (Reynolds, 1997).

On a laboratory scale, the four-electrode method is described in BS 1377-3 (1990) and ASTM G57 (2006). Using a standard resistivity cell (e.g. Miller soil box), a quick measure of soil (or water) resistivity can be obtained. Figure 2.21 shows the measurement setup according to the four-electrode method. The outer two pins (or plates) are used to inject the current and voltage difference is measured between the inner voltage pins. The resistivity

can be calculated using Eq. 2.11, where A is the cross sectional area of the box (m^2) and L is the length between the voltage pins (m).

Using the two-electrode method (AASHTO T288-91, 2004; ASTM G187, 2005), the voltage pins are removed, and voltage wires are connected to the current ends. Therefore, L would be the distance between the outer electrodes. However, regardless of the method used (i.e. four-electrode or two-electrode), the measured resistivity of the soil should in theory be the same and independent of the method used.

In practice, the four-electrode (e.g. Abu-Hassanein et al., 1966; Taylor and Barker, 2002; Giao et al., 2003; Russell and Barker, 2010; De Vita et al., 2012), and two-electrode method (e.g. McCarter, 1984; Fukue et al., 1999) have been implemented using different cell shapes and dimensions. However, the former is superior in minimizing the polarization and contact resistance problems (e.g. Gupta and Hanks, 1972; Heaney, 2003; ASTM G57, 2006; Beck et al., 2011). Therefore, the four-electrode method was adopted for the laboratory work in this thesis.

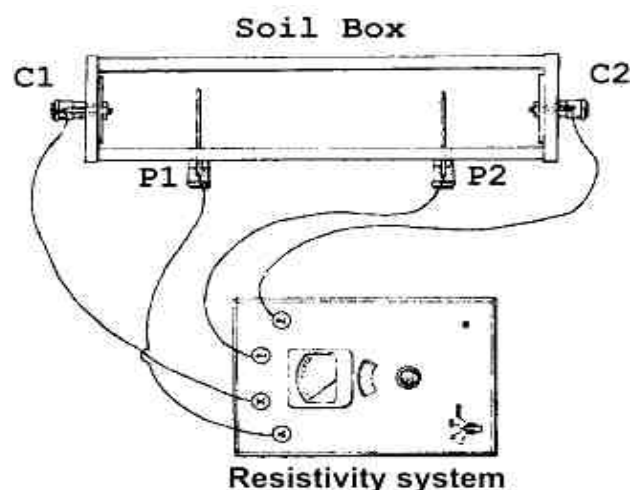


Figure 2.21. Standard four electrode resistivity method (ASTM G57, 2006)

In practice, various resistivity cells/devices have been implemented. Although the standard resistivity method using the Miller soil box is easy to use, the geometry and shape of the box do not offer the flexibility in procedures needed for development of resistivity-water content correlations (Kalinski and Kelly, 1993). Therefore, Kalinski and Kelly (1993, 1994) adopted a circular resistivity cell (Gupta and Hanks, 1972) to measure water content of high plasticity clay.

The cell (Figure 2.22) is typically an eight-equispaced electrode cell but is commonly called a four electrode circular cell; because only four electrodes are used each time to make individual resistance reading. The average independent eight resistances that can be collected are used to calculate the resistivity of the specimen. Several researchers (e.g. Borsic et al., 2005; Stacey et al., 2006; 2009; Beck et al., 2011) used similar cells, but with different shapes and electrode numbers. However, the cell requires specific calibration to consider the effect of its geometry on resistivity measurements (Kalinski and Kelly, 1993).

Recently, several researchers have developed small-scale resistivity probes/devices for local measurements where a quick and easy measure of soil resistivity can be obtained. For example, Sreedeeep et al. (2004) developed a resistivity probe based on Wenner arrangement. Using the same arrangement, Peixoto et al. (2010) presented a resistivity probe for geotechnical and geoenvironmental studies. A combined resistivity and temperature probe using a pole-pole arrangement was developed by Sherrod et al. (2011) for long-term field monitoring. Kim et al. (2011) presented an electrical resistivity cone probe (ERCP) to measure the resistivity of seashore soft soils and to estimate void ratio in the field. Commercially, similar probes have been developed, for example, by VERTEK, such as Soil Moisture, Resistivity and Temperature (SMRT) Module and Electric Conductivity (Resistivity) Module HT series.

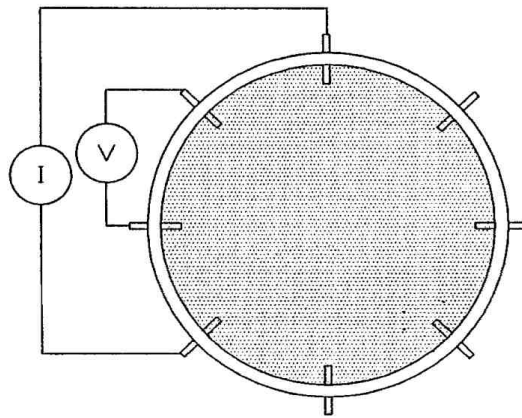


Figure 2.22. Typical circular four-electrode resistivity cell (Kalinski and Kelly, 1994)

However, these probes/devices are based on a similar principle of using a linear electrode arrangement (e.g. Wenner, pole-pole array), as the probes shown in Figure 2.23, for example. The resistivity measured by the linear arrays is affected by the azimuth of the line of the measurements (Habberjam and Watkins, 1967). In addition, these probes/devices contradict the non-invasive nature of the resistivity technique, which makes it attractive for a wide range of applications.

More recently, simultaneously with the current study, Muñoz-Castelblanco et al., (2011) developed a resistivity probe for local water content measurements of natural unsaturated soil subjected to drying and wetting cycles, and for local measurement of water content in a triaxial test (Muñoz-Castelblanco et al., 2012; 2014). The probe was constructed using four electrodes fixed in a silicon body (Figure 2.24). It was inspired from the surface probe presented by Maryniak et al. (2003). However, due to the poor contact with the soil, the probe required a slurry paste of clay to improve the contact; therefore, a specific calibration was needed to account for using the slurry in water content determination. Details about a new resistivity probe and other devices constructed in the current work, measurement and calibration procedures will be described in Chapter 3.

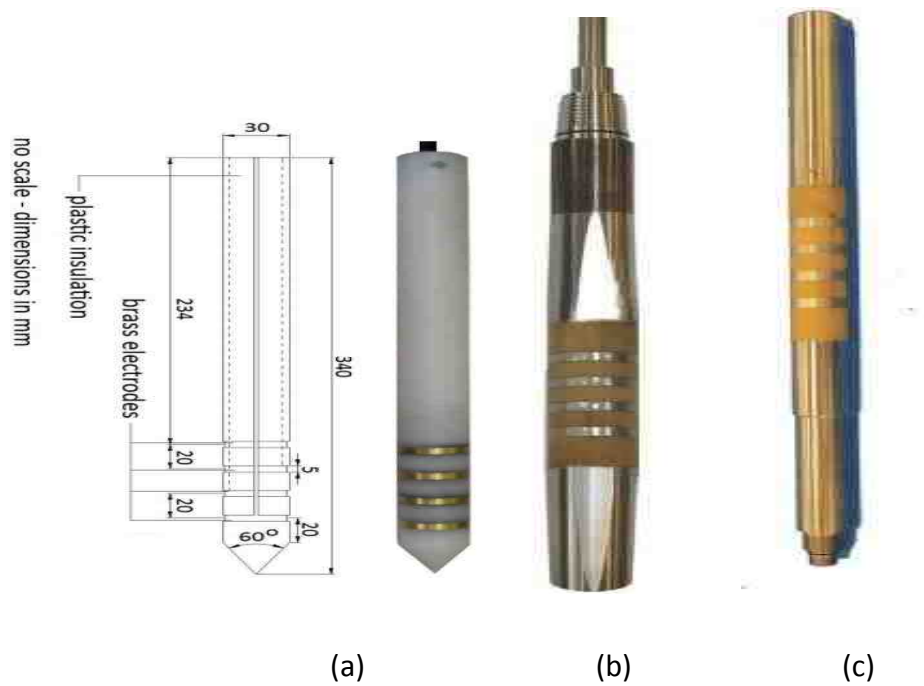


Figure 2.23. Resistivity probes (a) A probe for geotechnical and geoenvironmental studies (Peixoto et al., 2010) (b) Moisture, Resistivity and Temperature (SMRT) Module (VERTEK, 2013) (c), and Electric Conductivity (Resistivity) Module HT series (VERTEK, 2013)

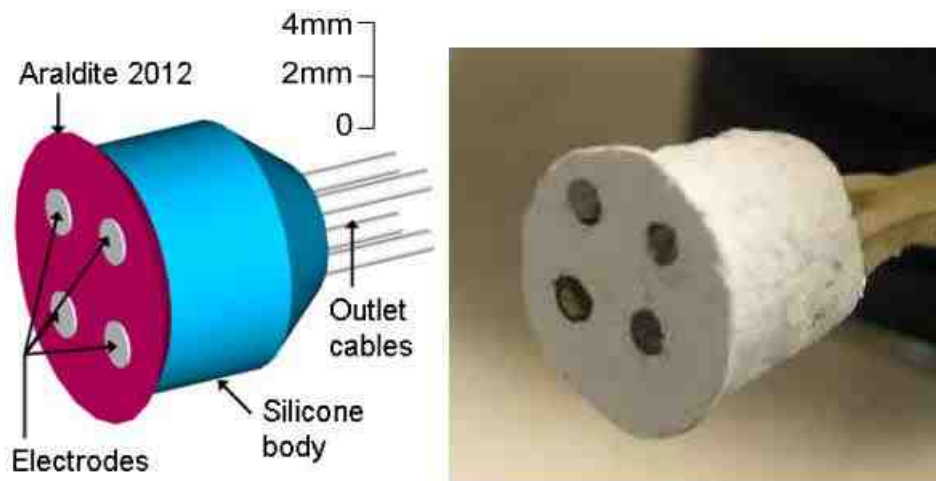


Figure 2.24. Resistivity probe for local water content monitoring (Muñoz-Castelblanco, 2011)

Multi-electrode resistivity systems: Electrical resistivity tomography

The advent of automated multi-electrode resistivity systems has led to rapid and efficient data acquisition of resistivity measurements. Using a number of electrodes attached to a resistivity system with a switching module makes it possible to carry out 2D, 3D and 4D imaging surveys with tremendously increased efficiency and productivity.

Multi-electrode resistivity systems, however, are based on using the principle of a four-electrode method and the adoption of multiplexing of a number of electrodes. A computer controlled switching module chooses four predefined electrodes for each single measurement, sends the current, and measures the potential drop from which the resistance can be calculated (Loke et al., 2011). Using a number of various combinations of transmitting and receiving pairs of electrodes, 2D/3D resistivity images can be constructed using appropriate inversion software. Moreover, using time-lapse 3D resistivity technique, 4D resistivity data can be obtained (Chambers et al., 2013). These improvements provide much more detailed information than the traditional 1D resistivity sounding, profiling and mapping.

Multi-electrode resistivity systems provide an imaging technique to infer the electrical resistivity distribution within a medium by taking measurements on its boundary (Binley et al., 1996a; b; Barker, 1997). On a laboratory scale, the electrodes are attached to the medium, which can be a closed geometry, such as a small circular resistivity cell (Damasceno et al., 2009) or a large lysimeter (Garré et al., 2011), and half-space experiments (e.g. a small tank) (Sentenac and Zielinski, 2009). In the field, the electrodes can be distributed along the surface in profiles/grids (Zhou et al., 2001) or placed down boreholes (Binley et al., 2002). Based on a set of sufficient combinations of four-electrode readings, a resistivity model of the medium can be inferred using an appropriate image reconstruction technique. Resistivity data, however, can be obtained using different array arrangements. An example of 2D data collection using 20 electrodes with a Wenner array (Loke et al., 2013), is shown in Figure 2.25.

CHAPTER 2: SOIL WATER CONTENT MEASUREMENT: BACKGROUND AND LITERATURE REVIEW

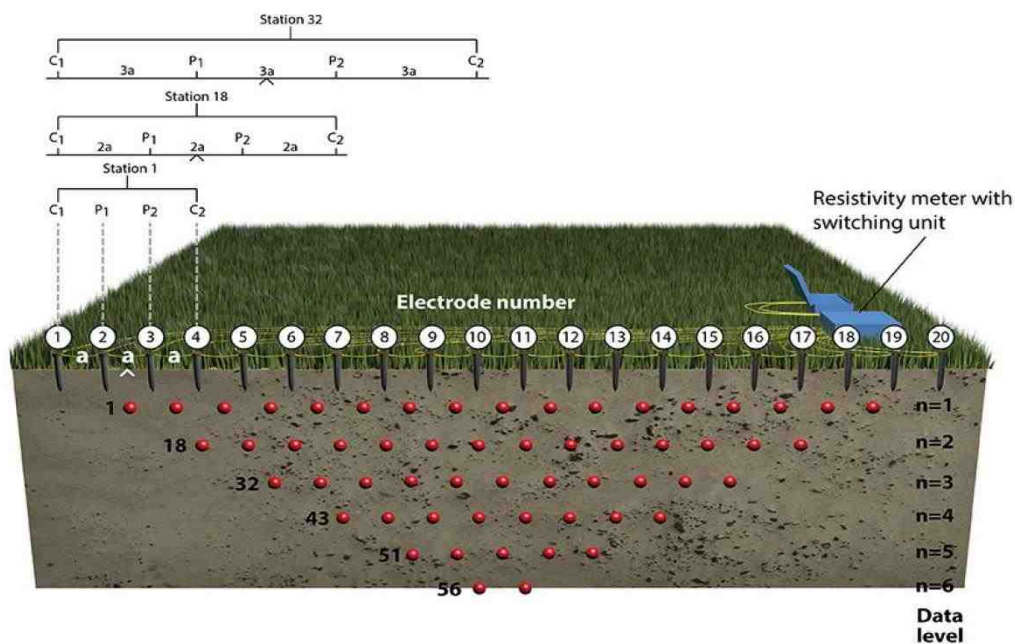


Figure 2.25. 2D data collection using multi-electrode resistivity system (Loke et al., 2013)

This setup is applicable for both lab and field applications. In 2D mode, a number of electrodes are installed along a line connected to the resistivity meter through multi-core cables. The measurements are progressively recorded for particular electrode spacing a and a number of acquisition levels (Griffiths and Barker, 1993). However, as the spatial distribution of electrical properties is inherently 3D in nature, the 3D model can provide more accurate results, especially in environmental and engineering applications where the subsurface is highly complex (Aizebeokhai et al., 2010). In this mode, a number of electrodes are laid out in a square or rectangular grid with constant electrode spacing. For complete 3D data, a large number of measurements are required (Tsourlos, 2004). Therefore, Loke and Barker (1996b) suggested a cross-diagonal method in which measurements are only acquired at electrodes along the X and Y directions. In practice, two approaches are commonly implemented. The first, a quasi 3D data set, is obtained by reconstruction of a number of parallel 2D lines (Tsourlos, 2004). The second is the use of the square array for a rectangular grid of electrodes (Samouëlian et al., 2004).

CHAPTER 2: SOIL WATER CONTENT MEASUREMENT: BACKGROUND AND LITERATURE REVIEW

Recently, the development of multichannel systems has significantly reduced the measurement acquisition time. In these systems, two electrodes are used to inject the current while the potential difference is measured across a different pair of voltage electrodes. Moreover, a pulled-array recording system for continuous dynamic measurements using steel-cylinder electrodes (Sørensen, 1996) or spiked wheels (Panissod et al., 1998) offer rapid data collection over large areas. More recently, automated monitoring systems have been introduced for monitoring transient phenomena that require automated data acquisition. Such sophisticated systems have emerged recently as a new technology for embankment warning systems (Gunn et al., 2010a; b). A fully automated resistivity system, ALERT-ME (Automated time-Lapse Electrical Resistivity Tomography) developed by BGS is now being deployed remotely. The system (Figure 2.26) is powered by renewable energy and controlled through wireless telemetry (GPRS) to communicate with an office-based PC, providing a 24h monitoring system. Recent advancements in resistivity instrumentation and the design and construction of new multi-electrode resistivity system will be discussed further in Chapter 3.

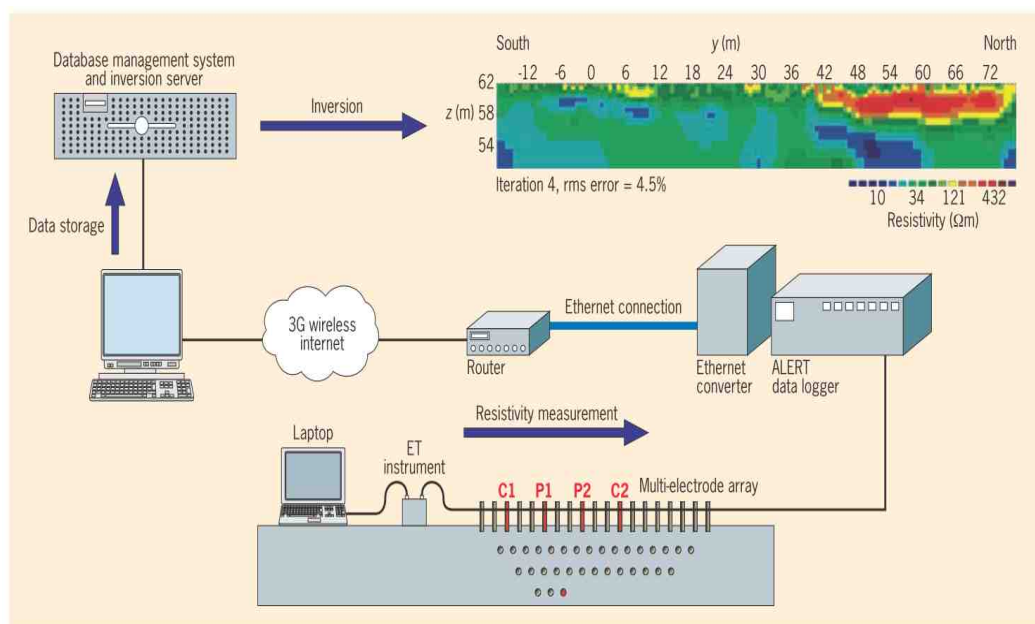


Figure 2.26. The ALERT-ME system developed by BGS (Gunn et al., 2010b)

CHAPTER 2: SOIL WATER CONTENT MEASUREMENT: BACKGROUND AND LITERATURE REVIEW

Modern multi-electrode systems have effectively been used to map water content changes in earthworks such as embankments. For instance, Jackson et al. (2002) mapped a rapid build-up of moisture on embankment shoulder a few days before a shallow failure (Figure 2.27). As the seasonal changes in water content control the seasonal resistivity changes, water content anomalies can be extracted from time-lapse measurements (Figure 2.28) that can be used as an early warning of moisture build-up in engineered earthworks (Chambers et al., 2007; 2008; 2009). Gunn et al. (2014) adopted ERT for mapping the spatial and temporal water content changes in clay embankments. Mapping water content using ERT requires a calibration of the resistivity against water content, usually performed in the laboratory.

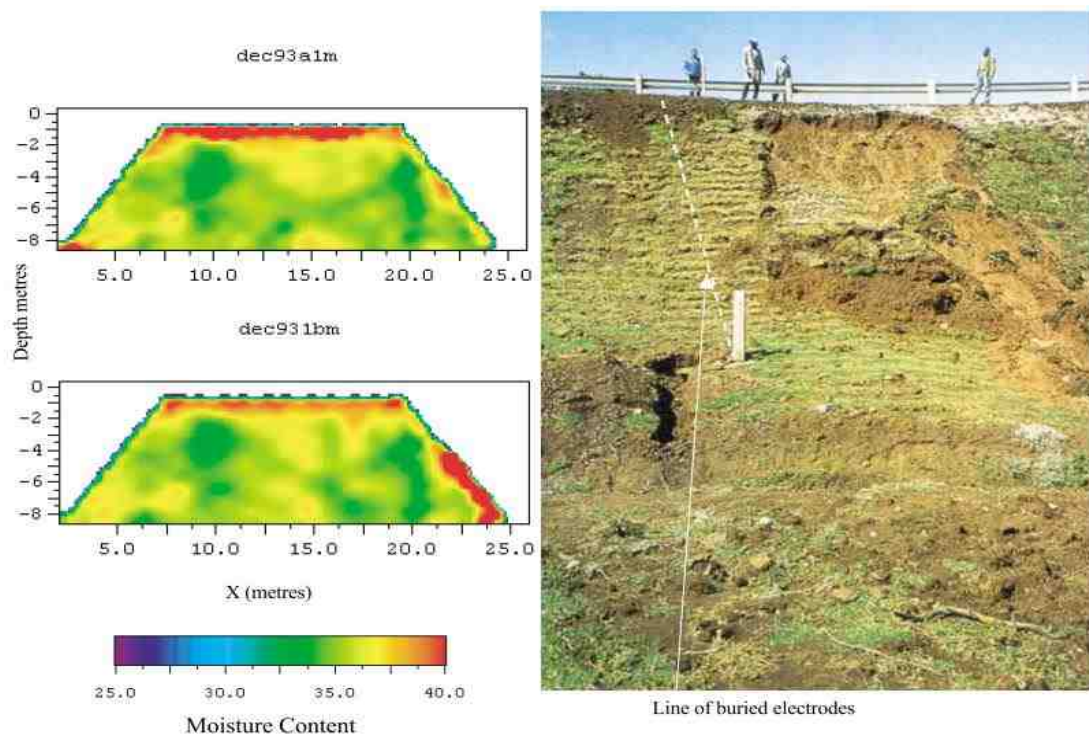


Figure 2.27. Build-up of moisture prior to slope failure, inferred using 2D ERT (Jackson et al., 2002)

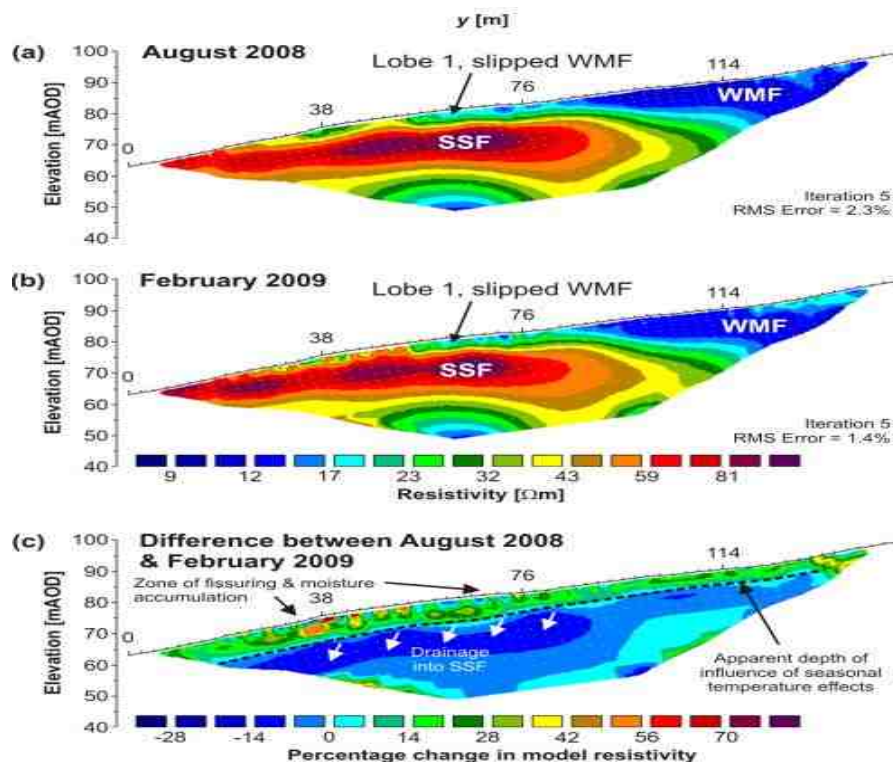


Figure 2.28 Time-lapse 2D resistivity sections (Chambers et al., 2009)

2.7 Resistivity method for water content characterisation

2.7.1 Soil resistivity-water content relationship

In order to use the resistivity method to map soil water changes, it is necessary to establish the soil resistivity-water content relationship that applies to the particular soil of interest. Like other indirect methods, ERT provides a measure of physical property (i.e. resistivity) that can be related to the soil water content. Therefore, quantifying soil water content is a two-step procedure (e.g. Goyal et al., 1996, Amidu and Dunbar, 2007; Zhou et al., 2007; Di Maio and Piegari, 2011; Gunn et al., 2014). Firstly, the soil resistivity distribution is derived and, secondly, the water content is estimated from these sections using a calibration curve. Figure 2.29 illustrates the approach of using ERT to map soil water content

mapping using ERT. Figure 2.30 shows examples of the laboratory calibration for different types of clays (McCarter, 1984; Fukue et al., 1999; Michot et al., 2003).

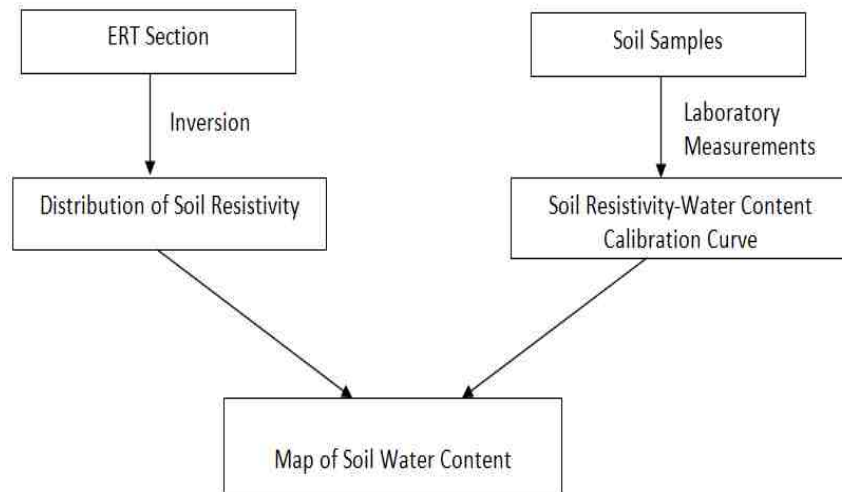


Figure 2.29. A schematic diagram illustrating the approach of water content mapping using ERT (Di Maio and Piegari, 2011)

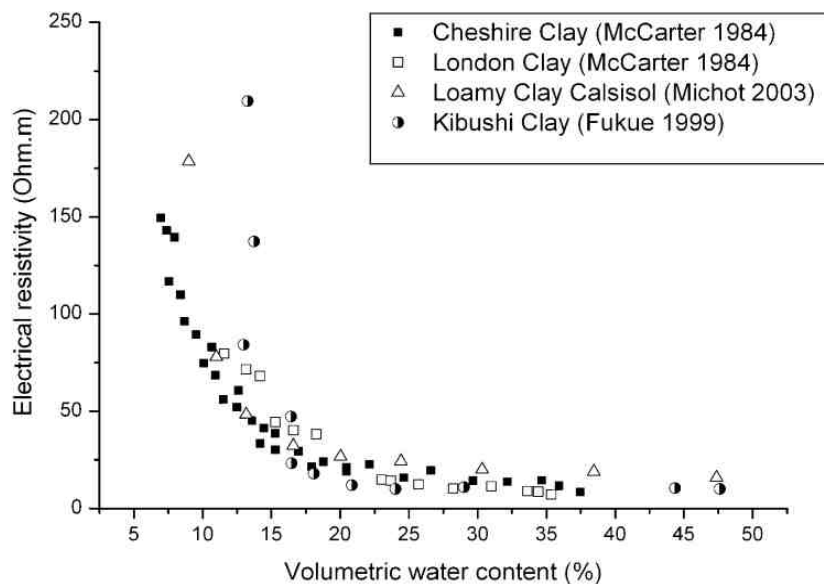


Figure 2.30. Electrical resistivity-volumetric water content relationship of different types of clay (Samouëlian et al., 2005)

A large number of authors have reported similar, explicit relationships between resistivity and water content. These can be grouped into theoretical (Mualem and Friedman, 1991), laboratory (e.g. Archie, 1942; Kalinski and Kelly, 1993; Zhou et al., 2001; Russell and Barker, 2010; Yan et al., 2012) and field-based (e.g. Michot et al., 2003; Amidu and Dunbar, 2007; Schwartz et al., 2008; Celano et al., 2011; Calamita et al. 2012) studies. Considerable efforts have been made to understand this relationship and a number of models have been introduced.

Archie (1942) pioneered resistivity-water content studies in the oil industry. In saturated soil, he related soil resistivity ρ_o , pore water resistivity ρ_w and porosity n in a common relationship called Archie's law:

$$\rho_o = \rho_w n^{-m} \quad (2.17)$$

Where m is a fitting constant related to the soil characteristics (Friedman, 2005).

In unsaturated soil, a decrease in the saturation is accompanied by an increase in resistivity due to the partial replacement of pore water with air. Archie's Law for unsaturated soil is expressed as:

$$\rho = \rho_w n^{-m} S_r^{-b} \quad (2.18)$$

$$\rho = \rho_o S_r^{-b} \quad (2.19)$$

Where ρ is resistivity of unsaturated soil, S_r is the degree of saturation and b is a saturation exponent (Keller and Frischknecht, 1966).

Archie's relationships, or modified forms, have successfully been implemented by a number of authors to estimate water content (e.g. Turesson, 2006; Werban et al., 2008). Rhoades et al. (1976) presented a second order polynomial formula. Kalinski and Kelly (1993) implemented this relation to estimate water content of clay soil with 0.009 standard

error. Other authors (e.g. Pozdnyakova, 1999; Ozcep et al., 2009; Bery and Saad, 2012; Yan et al., 2012) adopted an exponential relationship to relate resistivity with water content.

For a limited range of water content, a first order linear relationship has been reported (Goyal et al., 1996; Zhu et al., 2007). In the literature, nonlinear resistivity-water content models (polynomial, power and exponential) expressions have been adopted. However, the differences between them are statistically insignificant, particularly in a limited range of water content (Pozdnyakov et al., 2006; Calamita et al., 2012).

Recently, the resistivity-water content relationships reported in the literature have been reviewed by Shah and Singh (2005) and Calamita et al. (2012). Based on extensive experimental study, Shah and Singh (2005) proposed 'a generalized Archie's Law' for fine-grained soils expressed as:

$$\rho = \rho_w \theta^{-m} \quad (2.20)$$

Where ρ is the soil resistivity, θ the volumetric water content, ρ_w is a fitting parameter related to pore water resistivity and m is a constant. Similar power law relationships have been adopted by a large number of authors (e.g. McCarter, 1984; Fukue et al., 1999; Hymer et al., 2000; Walker and Houser, 2002; Michot et al., 2003; Amidu and Dunbar, 2007; Liu and Yeh, 2004; Brunet et al., 2010; Celano et al., 2011; Yan et al., 2012). Calamita et al. (2012) correlated the resistivity and volumetric water content relationships reported in the literature (Figure 2.31). The figure highlights the power law relation. These studies show that the resistivity of different soils decreases with increasing water content and, at low water content, resistivity decreases more rapidly.

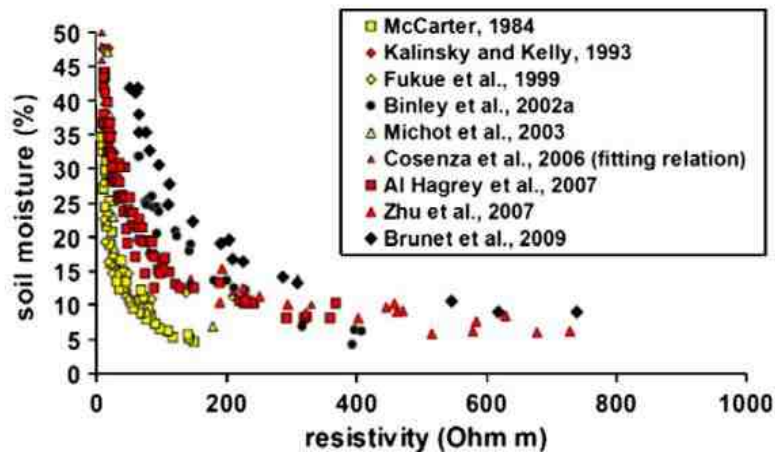


Figure 2.31. Resistivity-volumetric relationships reported in the literature for different soils (yellow: clay, Red: loam, Black: sand) (Calamita et al., 2012)

2.8 Resistivity method for characterising drying and wetting of clay soils

Although numerous studies have considered the influence of water content on soil resistivity, the impact of drying and wetting and the associated volume changes has rarely been addressed. Amidu and Dunbar (2007) used the resistivity method to characterise the seasonal drying and wetting of Vertisol (clay content >30%) of high shrink–swell potential. Laboratory measurements were used to generate soil moisture–resistivity relationships to calibrate the field data. However, the calibration was based on measuring the resistivity of the soil as the soil sample dried in the laboratory, and the volume of the sample was measured manually. Russell and Barker (2010) provided one of the first studies of the electrical characteristics of clays during drying. They reported the resistivity behaviour of seven geographically distributed British clays and pure clays during moisture loss. However, only the gravimetric water was considered (Figure 2.32). Muñoz-Castelblanco et al. (2011) reported the influence of water content changes of Loess soil (16–25% clay fraction) during drying and wetting cycles. It was concluded that the resistivity was mainly related to the water content of the soil. However, the volume changes were not appreciated.

In the above-mentioned studies, the soil resistivity was measured in a discrete style (i.e. stage drying/wetting). According to the author's knowledge, no tests have been conducted where resistivity and volume changes are monitored continuously and simultaneously on soil specimens subjected to drying/wetting cycles.

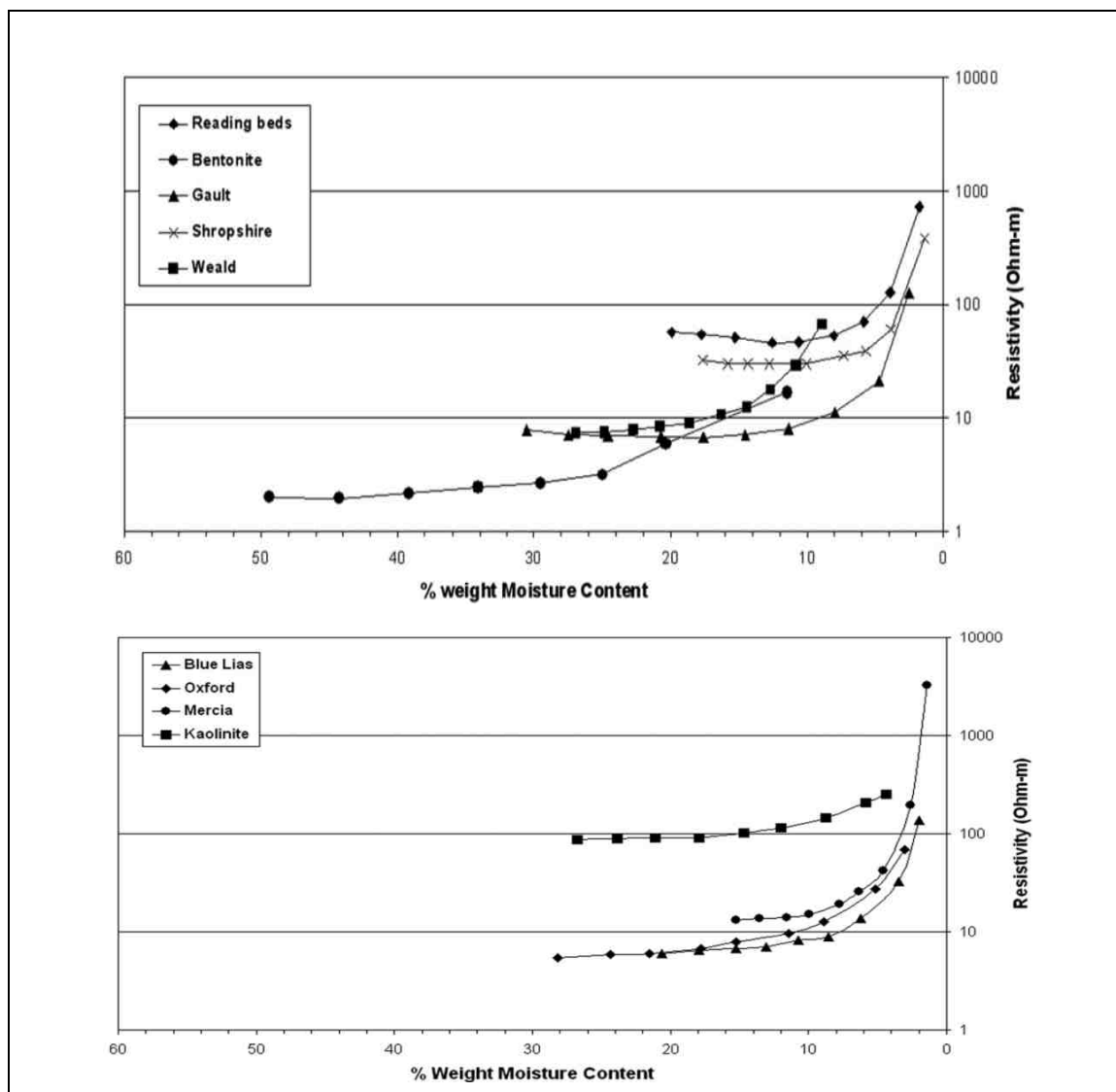


Figure 2.32. Resistivity-water content relationships of different local and pure clay soils (Russell and Barker, 2010)

2.9 Resistivity method for characterising cracking of clay soils

2.9.1 Cracking mechanism

Clay soil tends to shrink when it loses moisture, such shrinkage of clay commonly often causes cracking. In addition to the water content, the cracking process is governed by a large number of factors, (e.g. soil heterogeneity, mineral composition, temperature, evaporation, layer thickness, land cover, etc.). Therefore, the precise mechanism of cracking dynamics is not perfectly understood (Tang et al., 2011). Nevertheless, the development of tensile stresses due to shrinkage of the soil has widely been accepted as the common cause of the cracks. As the water evaporates from the surface of the soil, the matric suction develops and progressively increases. Consequently, the soil consolidates and shrinks. Increasing matric suction induces tensile stress at the soil surface and, once the tensile stress exceeds the tensile strength, the soil cracks. The stresses concentrate at the tip of the crack, causing the crack tip to propagate until the stresses are reduced below the local tensile strength of the cracking soil (Inci, 2008; Tang et al., 2011). However, continuous drying and shrinkage of clays might lead to the development of interconnected cracks to form polygonal blocks. This might, in turn, lead to the development of shear zones beneath the soil and, hence, slope failure (Konrad and Ayad, 1997; Kodikara et al., 2000).

2.9.2 Application of the resistivity method for characterising cracking of soils

In theory, the resistivity method is based on the assumption that the subsurface is continuous, and measuring the voltage drop associated with the current injected into the soil provides information about the subsurface resistivity distribution. In a medium with conductive anomalies, the current flow lines tend to concentrate while, in a medium with resistive anomalies, the current lines tend to deviate around them (Figure 2.33).

As cracks are normally filled with air that is infinitely electrically resistive, cracks form barriers that disturb the flow of current, resulting in greater voltage drop relative to that measured for the surrounding intact soil. Therefore, cracks are expected to alter soil resistivity distribution significantly (Samouëlian et al., 2003a; Amidu and Dunbar, 2007; Jones et al., 2012; 2014).

Electrically, clays are classified into a single group with a typical resistivity of 1-100 Ohm.m (e.g. Reynolds, 1979; Telford et al., 1990). However, resistivity values of more than 100 Ohm.m have been reported with low water content (e.g. McCarter, 1984; Fukue, 1999; Michot et al., 2003). Although the actual resistivity of a dry crack can be assumed infinite (Greve, 2009), the measured resistivity of the clay soil containing cracks is far lower, as the resistivity measurement includes the intact soil as well (Jones et al., 2012; 2014). However, in resistivity sections, the resistivity contrast between the cracks and the surrounding soil is high enough to be detected, and, therefore, cracks can be identified as isolated spots with high resistivity values compared to intact soil (Figure 2.34) (Sentenac and Zielinski, 2009; Jones et al., 2012; 2014).

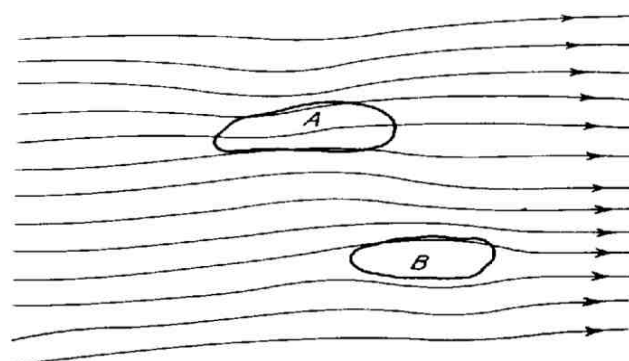


Figure 2.33. Distortion of current flow lines in (A) high and (B) low conductive anomaly

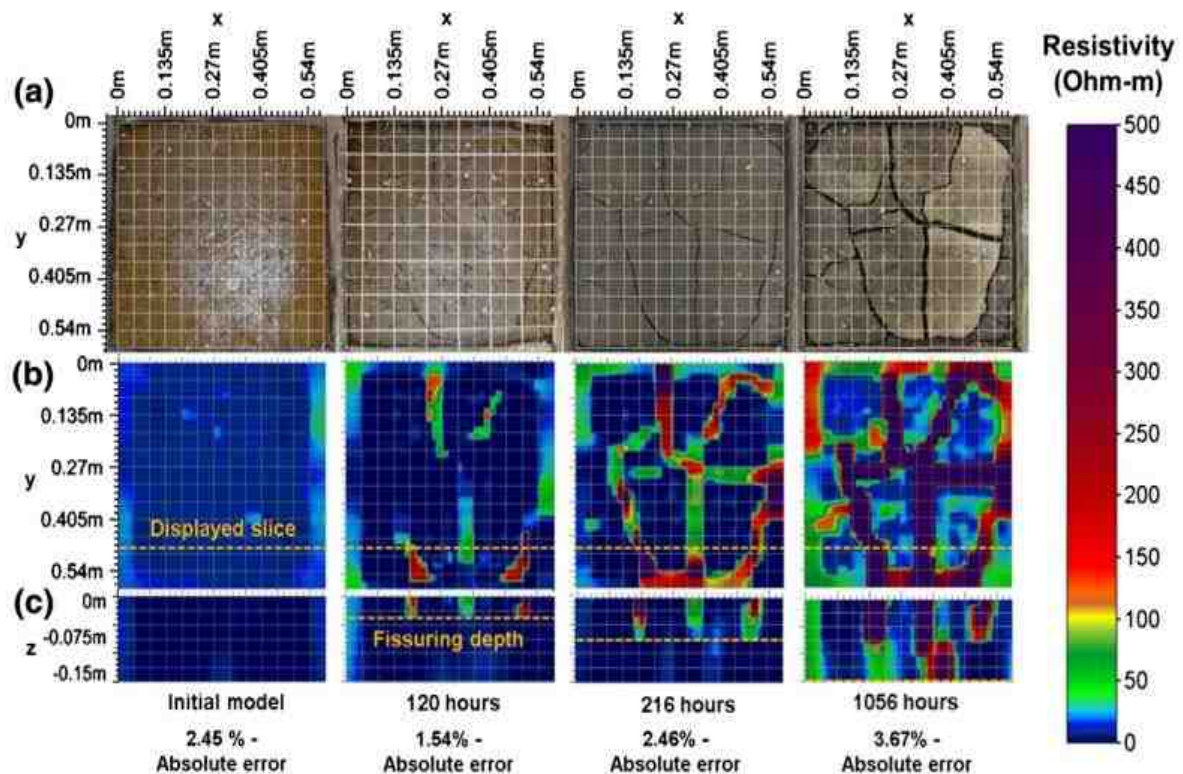


Figure 2.34. Development of cracking in clay soil sampled from flood embankment located near Thorngumbald in England: (a) photographs showing surface cracks development; (b) resistivity section, model layer ($z=0.01$ m) (c), vertical slice at $x\approx 38$ cm (Jones et al., 2014)

In Material Science, the resistivity method has proven successful in detecting cracks in metals (e.g. Farrell et al., 2008). In concrete studies, the method has been used to assess water content (e.g. Su et al., 2002) and the formation of cracks (e.g. Wiwattanachang and Giao, 2011). In soil sciences, early studies have focused on detecting joints and fractures in rocks to: determine strike of jointed bedrock (Taylor and Fleming 1988); map fractures pattern (Raju and Reddy, 1998; Seaton and Burby, 2002); locate flow pathways in conductive fracture zones (Slater et al., 1997; Cassiani et al., 2009); and monitor migration of a saline tracer (Rugh and Burbey, 2008).

Anisotropy, is a material's directional dependence of a physical property, has been found promising for characterising fractured soils. In ERT, the electrical anisotropy is defined as the variation of resistivity with the azimuth (Al Hagrey, 1994). This property has traditionally been used for identification of fractures (e.g. Lane et al., 1995; Busby, 2000; Busby and Jackson, 2006). In these studies, the shape of the resistivity ellipsoid of azimuthal measurements (Taylor and Fleming, 1988) is interpreted as being indicative of the fracture anisotropy. Using nonlinear arrays, such as the square array, minimum resistivity was measured when the current was injected parallel to the fracture, while a maximum value was measured when the current was injected perpendicular to the fracture (Figure 2.35). Therefore, the minor axis of the ellipse is used to identify the direction of the structural feature (Busby and Jackson, 2006; Massoud et al., 2009). LaBrecque et al. (2004) showed that 2D ERT can be used to detect fractures in wet and dry limestone blocks. However, conductive fractures showed a much smaller response than the resistive case.

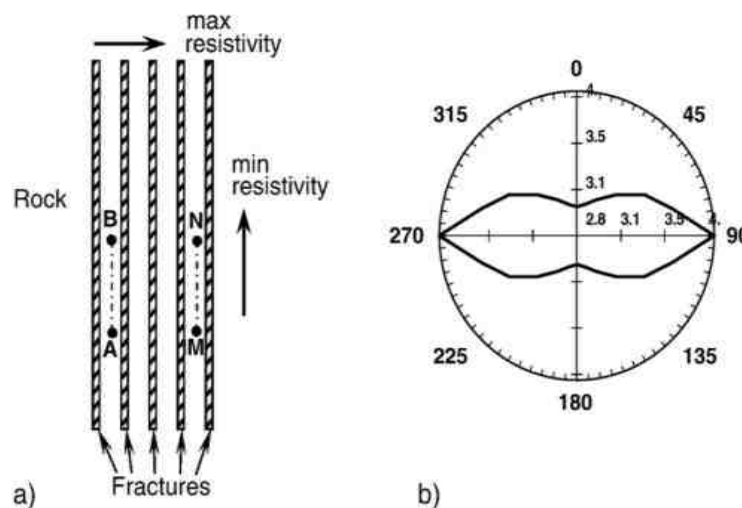


Figure 2.35. Azimuthal resistivity measurements (a) Parallel fractures (b) Polar diagram using square array (Busby and Jackson, 2006)

A number of studies have focused on using ERT to map cracks forming in clay soils. In the first reported 2D experiment, Samouëlian et al. (2003a) demonstrated the efficiency of the method to detect an artificial crack of 2mm wide on a compacted clay soil. However, only the depth of cracks was considered. To detect surface cracks, Samouëlian et al. (2004) used anisotropy index AI of a square array, defined as the ratio between resistivity in two perpendicular directions, conventionally named α and β resistivity:

$$AI = \frac{\rho_{\alpha}}{\rho_{\beta}} \quad (2.21)$$

As the presence of a crack results in an anisotropic alteration of the electrical field (Samouëlian et al., 2004), it is the most likely cause for AI to deviate from unity. As a consequence, they used AI data to provide information on the presence, position, and extension of the cracks. Chen et al. (2007) found that soil resistivity increases rapidly with increasing depth of vertical artificial fissures, as air becomes the predominate factor that controls the resistivity.

As studies involving electrical anisotropy seem to be promising, Greve (2009) showed that deviation of AI due to a simple crack introduced in the soil is a function of its depth, length and orientation. However, increasing crack width caused only slight increases in AI deviations. No AI response was noticed for cracking oriented at 45° , as reported by Samouëlian et al. (2004). On a lysimeter scale, Greve et al. (2010a) measured temporal changes in the AI profiles (Figure 2.36) of a series of coplanar electrode squares installed at regular depth intervals. They related the development of soil cracks to the gradual increase in AI , which allowed the detection of cracking dynamics in the hidden area under the surface. During drying, AI increased progressively, with the largest increase at the top of the soil. This was found to be consistent with a downward extension of the cracking network during drying (Johnston and Hill, 1944). During water addition, the AI profile returned to its initial state before drying, with a 2% difference.

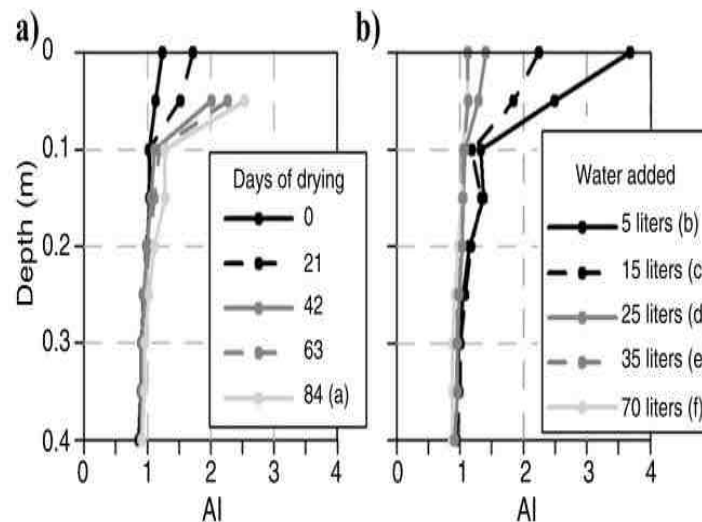


Figure 2.36. AI profiles of clay soil (a) drying (b) water addition (Greve et al., 2010a)

Later, Greve et al. (2011; 2012) used AI profiles to monitor water-preferred flow pathways in cracking clays. Using an analogue experiment, Szalai et al. (2010) showed that any fissure system makes isotropic medium anisotropic and, as cracking in soil is multi-directional, this also results in multi-directional anisotropy.

Kong et al. (2012) demonstrated that changing cracking parameters, such as depth, length, width, number and angle of manually created cracks, produces strong changes in the electrical properties of Laterite. However, resistivity measurements were only performed when the current was injected perpendicular to the cracks. Recently, ERT has been used to map cracking networks forming in clay soil under laboratory conditions. Sentenac and Zielinski (2009) adopted a miniaturised 2D ERT experiment to monitor clay fine fissuring induced by the natural desiccation process. The position and development of the vertical fissures were clearly identified as they formed. Jones et al. (2012) used 3D ERT to map fissure networks forming in compacted clays using linear Schlumberger, Dipole–Dipole and combined arrays. The fissure networks were successfully defined and compared very well with networks observed in the soil. Using miniature and large-scale 2D and 3D field surveys,

Jones et al. (2014) mapped desiccation cracks formed in a flood embankment. The extent of fissure zones was detected using a large-scale array where individual cracks could not be identified. However, the resolution of cracks was improved with a miniature array, where subsurface fissures were successfully imaged. The results were validated by numerical modelling.

2.10 Chapter Summary

This chapter has reviewed the theoretical background of the main water content measurement methods. The basic theory of the resistivity method and its application for water content characterisation of clay soil are discussed.

In addition to the direct gravimetric method, a large spectrum of indirect methods is available, ranging from small probes to regional, remote sensors. These methods are based on measuring a soil physical property that can be calibrated against water content. However, more research is needed to explore new techniques that can measure soil water content at different scales and to consider of the influence of drying and wetting on soil properties. The resistivity method reviewed in this chapter has the potential to provide relatively quick, non- invasive measurements of soil water content.

The application of the resistivity method for water content characterisation was reviewed to identify the knowledge gaps. Recent advances in resistivity instrumentation have focused on the development of automated multi-electrode systems and to develop resistivity devices that offer quick estimates of water content. The use of the resistivity method for water content characterisation of unsaturated clay soils subjected to drying and wetting cycles requires an automated system that offers automated real-time data collection. In the literature, many small-scale resistivity probes/devices have been developed. However, there is an increasing demand to develop efficient non-invasive techniques to measure water content with volume integration. The design and construction of a new automated multi-electrode resistivity system and resistivity probe developed in the

current thesis will be described in Chapter 3. Calibration and validation of the system will be presented in Chapter 4.

Although a large number of authors have reported explicit relationships between resistivity and water content, resistivity of clay soils is affected, in addition to water content, by various interlinked parameters that need to be considered. The water content characteristics of compacted BIONICS clay soil will be discussed in Chapter 5.

Recent work on BIONICS clay has reported resistivity variations across the embankment, that can be attributed mainly, in addition to water content, to variations in temperature and water salinity. Therefore, it is essential to address these effects. The influence of temperature and pore water chemistry on the soil resistivity will be discussed in Chapter 6.

In addition, although numerous papers have been published describing the resistivity-water content relationship, little interest has been paid to investigating the influence of drying and wetting and the accompanied volume changes on resistivity of clay soils. The application of the resistivity method for characterising drying and wetting of clay soil and the associated volume changes will be addressed in Chapter 7.

The application of the resistivity method for characterising cracking of clay soils will be discussed in Chapter 8. Numerical and experimental techniques are used to investigate the directional dependence of resistivity measurements in cracking clays and the effects of cracking depth, length, width and orientation on soil resistivity.

Chapter 3

Design and construction of an automated multi-electrode resistivity system

The electrical resistivity technique has been in use for more than one hundred years. Significant advances in instrumentation, survey designs, data acquisition techniques and interpretation software have taken place over the past few decades. Multi-electrode and multi-channel systems nowadays allow efficient and rapid data acquisition to investigate a large number of applications. Recently, there have been major advances in resistivity instrumentation to develop automated monitoring systems for detecting transient phenomena that require continuous data acquisition (e.g. Loke et al., 2013). Therefore, this chapter presents the design and construction of a new automated multi-electrode resistivity system for laboratory testing. A flexible data acquisition and control software package has been developed to obtain real-time resistivity data using different electrode arrangements. The user can set the current and voltage, switching 64 electrodes interchangeably as either current or voltage electrodes in a fully automated procedure. The design and measurement procedures of a new resistivity probe and other devices are also presented.

3.1 Introduction

The advent of multi-electrode resistivity systems over the past few decades has triggered a revolution in the use of the electrical resistivity method to address a wide range of applications.

A marked increase in the application of the four electrode DC resistivity method has taken place with the development of multi-electrode resistivity systems and robust data inversion software (e.g. Griffiths and Barker, 1993; Loke and Barker, 1996a, b). Using these systems, the ERT method has become widely applicable to map areas of complex geology

for different engineering and environmental applications. The effectiveness of this method in engineering and environmental applications is well discussed by Dahlin (1996), Barker (1997), Reynolds (1997), Pellerin, (2002) and Loke et al. (2011; 2013).

A number of authors (e.g. Niininen and Kehl, 1979; Beck, 1997; Avants et al., 1999; Herman, 2001; Olowofela et al., 2005; Awotoye and Selemo, 2006; Sheffer et al., 2007; Igboama and Ugwu, 2011; Lachhab and Booterbaugh, 2011) have fabricated low cost four electrode resistivity systems. Such systems have traditionally been used to collect 1D resistivity data for laboratory and field studies. However, for 2D and 3D ERT investigations, which incorporate collecting a large number of measurements, traditional four electrode systems are time consuming and impractical. Therefore, the advent of multi-electrode systems (e.g. Dahlin, 1996), a pulled-array recording systems (e.g. Christensen and Sørensen, 2001), and distributed data acquisition systems (e.g. Stummer et al., 2002) has substantially increased the efficiency and flexibility to acquire a large number of measurements in a reasonable time.

In particular, multi-electrode resistivity systems speed up data acquisition times; provide large data sets to construct 2D and 3D resistivity tomography images and offer the flexibility to choose a suitable electrode arrangement for a particular problem, this in turn reduces the effort and the laborious electrode switching using manual four electrode systems (Tsourlos,1995; Dahlin, 2001).

Multi-electrode resistivity systems have been developed by many commercial companies, as well as academic and research institutions using different measurement strategies. For example, multi-electrode systems that support automatic electrode multiplexing have been developed by commercial companies such as Campus Ltd., UK; Iris Instruments, France; ABEM Instruments, Sweden; GeoSys, Germany; Scintrex Ltd., Canada; and Oyo Geoelectric, Japan. In addition, several systems have been developed by academic institutions such as the University of Birmingham, UK (Griffiths et al., 1990); the University of Waterloo, Canada (Schneider et al., 1993); the University of Leicester, UK (Meju and

Montague, 1995); Lund University, Sweden (Dahlin, 1996); Stanford University, USA (Stacey et al., 2006) and University of Wisconsin–Madison, USA (Damasceno, 2009).

Other researchers have contributed to the ongoing research in different ways. For instance, Dickin and Wang (1995) described the design and operation of a flexible ERT system for laboratory and plant-scale process instruments. Werkema et al. (1998; 2000) developed windows based multi-electrode acquisition system that can collect resistivity data using a commercial resistivity meter. Stummer et al. (2002) developed a distributed data acquisition system, which introduced the concept of real-time experimental design.

In theory, the greater the number of electrodes used, the more independent the measurements that can be obtained, which results in higher resolution and confidence in the inferred resistivity distribution (Xu and Noel, 1993). However, the practical constraints of wiring and computational time limit the number of electrodes that can be used. To solve this problem, Van Weereld et al. (2001) used an array of 192 electrodes carried on a flexible printed circuit and wrapped around a core sample. A fast DC current pulse was used to measure resistance. Due to practical constraints, Polydorides (2002) suggested that a 16 electrode system is optimum for laboratory scale measurements, compromising between computational time and the noise introduced by using a large number of electrodes. Stacey et al. (2006) adopted this suggestion to develop a system consisting of three rings, each of 16 electrodes. A DC current with a switch matrix and data acquisition were controlled by an automated program developed in LABview. The system was used to estimate soil saturation (Stacey et al., 2009).

To speed up the data collection, continuous dynamic resistivity systems for land and water have been introduced. An array pulled by a vehicle was used for continuous land profiling (e.g. Sørensen, 1996) and a floating electrode array connected to a cable pulled by a boat was used for water surveys (e.g. Mansour and Slater, 2007).

Automated multi-electrode resistivity systems are increasingly becoming popular. For laboratory testing, Damasceno et al. (2009) presented a design for a low cost ERT acquisition system. The system consisted of 16 electrodes used to monitor chemical diffusion in a saturated sand specimen. Similarly, Bera and Nagaraju, (2011) developed an automatic electrode switching module with four 16:1 analog multiplexers connected to 16 surface electrodes. Devadasi et al., (2014) presented automatic switching system for resistivity profiling. Analog multiplexers were used for switching the electrodes.

Recently, automated monitoring systems have been introduced for continuous monitoring of complex transient phenomena such as water seepage (Sjödahl et al., 2008), active landslides (Chambers et al., 2011) and hydraulic processes in porous media (Kuras et al., 2009). For long-term monitoring, Dahlin and Jonsson (2011) presented a data acquisition system for automatic monitoring of embankment dams. Similarly, Jinguuji (2011) developed high speed and multi-transmission system suitable for high speed geological monitoring. For down hole studies, Sherrod et al. (2011) presented a low-cost resistivity and temperature system; a comparison was made using a Syscal R2 resistivity meter and all measurements within 10% difference were deemed acceptable. Korteland, (2013) developed a flexible and high speed ERT system for quantitative characterisation of solute transport processes in porous media. A pulsed DC current source and eight channels were used to control 128 electrodes. Using permanently installed in situ and remotely controlled electrodes via wireless telemetry (GSM, GPRS, WiFi or satellite telecommunications) and an IT infrastructure, an automated time lapse electrical resistivity tomography (ALERT) system has been recently developed by the British Geological Survey to collect 4D resistivity data (Chambers et al., 2013) rarely offered by other technologies.

An increased demand to develop efficient, non destructive, relatively easy and inexpensive techniques that can provide high resolution data to address complex problems has led to the speeding up of research in this direction. Therefore, the ongoing development of multi-electrode resistivity systems is expected to continue (Dahlin, 2001).

The current work aims to develop an automated multi-electrode resistivity system for laboratory measurements using the DC resistivity method. The system consisted of flexible data acquisition and control system that automatically switches 64 electrodes to acquire resistivity data using different electrode arrangements in a real-time procedure.

3.2 Multi-electrode resistivity system: Main components

Automated multi electrode resistivity systems are based on the principle of the traditional four electrode method and involve multiplexing a number of electrodes. A typical computer controlled system (Dahlin, 2000; Stacey et al., 2006; Damasceno et al., 2009; Sherrod et al., 2012) consists of three main parts (Figure 3.1): (1) data acquisition and control system; (2) electrode configuration and connection; and (3) a third party reconstruction software. The system, however, must offer flexible control of the current and voltage readings, high speed data acquisition and appropriate computer interfacing (Polydorides, 2002; Stummer et al., 2002; Damasceno et al., 2009).

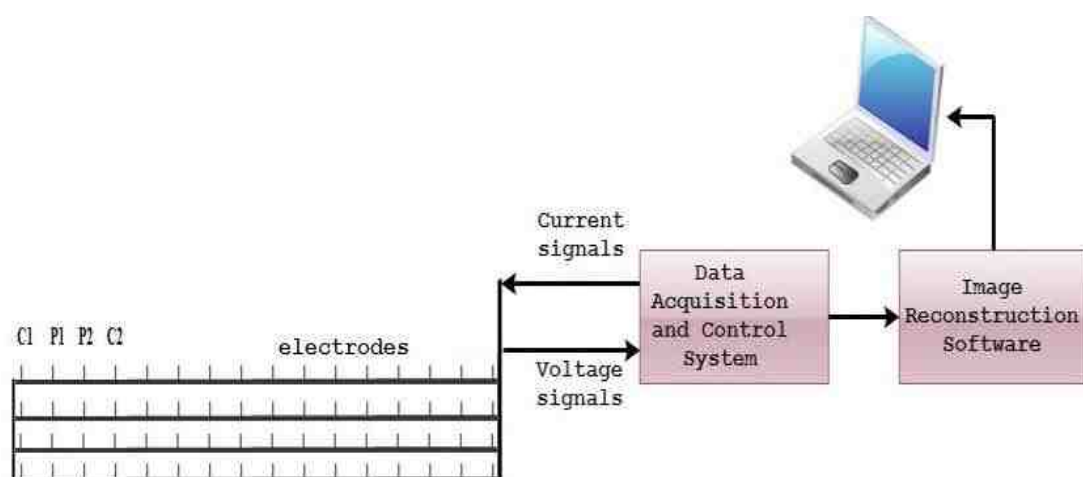


Figure 3.1. A schematic diagram of an automated multi-electrode resistivity system

The main requirements to construct the data acquisition and control system are: (1) a constant current source; (2) multiplexing or switching system and (3) data acquisition and controlling software running in a high-speed computer (Tourlos, 1995; Dahlin, 2001; Stacey, 2006).

The current source can be either direct DC, commutated direct (the source is attached to a commutator to change the polarity of the current), or low frequency alternating AC current, typically below 100 Hz (ASTM G57, 2006). However, the analysis and interpretation of the data are made based on DC measurements (Loke et al., 2011). Using an unaltered DC source, the polarization effect, which is related to the contact between the electrode (electronic conduction) and the soil (ionic conduction) has to be considered (Tsourlos, 1995; Dahlin, 2000; LaBrecque and Daily, 2008). This effect causes an accumulation of charges on the electrodes that gradually increases with time and, therefore, the measured resistances will gradually increase too. Using signals of unchanged direct current can effectively polarize the electrodes when the current is injected in one direction for a long time. Specific considerations have to be followed regarding the switching mechanism between the electrodes (Dahlin, 2000), when the electrode is used for current and then for voltage while still polarized. The problem of polarization can be tackled by periodically reversing the current electrode polarity (Tsourlos, 1995; ASTM G57, 2006) or by using special non-polarized electrodes (Samouëlian et al., 2005); however, they are difficult to implement and expensive (Wilkinson et al., 2012). Stainless steel electrodes have been found to be less affected by polarization (LaBrecque and Daily, 2008). Practically, adopting special measurement sequences and considering an adequate time delay between using an electrode to inject current and to measure voltage can significantly reduce the polarization effect (Dahlin, 2000; Wilkinson et al., 2012). An AC source at low frequency can be used to prevent an accumulation of ions so that electric polarization is minimized. However, electromagnetic effects have to be considered (Tsourlos, 1995).

In the literature, a DC current source (e.g. van Weereld et al., 2001; Kalinski and Vemuri, 2005; Stacey, 2006; 2009; Korteland, 2013) was used as it can greatly simplify the instrumentation and reduce the cost, compared to the AC current source, where phase angle has to be considered (Szczepanik and Rucki, 2000; Korteland, 2013). A DC power source can be used if the current and voltage polarity is regularly reversed, and readings are averaged for each polarity (ASTM G57, 2006).

The current and voltage electrodes in multi-electrode resistivity systems are switched by means of multiplexers. The switching mechanism should be reliable for any electrode arrangement (Loke et al., 2011). In the literature, different strategies have been adopted to achieve the electrode switching. Cost and practical limitations have been considered. In the first type, a central switching unit is used in which the main switching module is incorporated within the main resistivity unit, and the electrodes are connected via multi-core cables (Overmeeren and Ritsema, 1988). In these systems, the number of electrodes is limited to the number of electrode take-outs. Depending on the application, the electrode take-out spacing varies from less than 1 to 25 m or more (Dahlin, 2001). In the second type, the switching unit is connected to the resistivity meter through a system bus. This type can significantly increase the number of electrodes used, but is not practical in forested areas. In the third type, a switching circuitry is placed at each electrode instead of a central unit (Stummer et al., 2002). Although the latter provides high flexibility, the cost of switches can be higher than that of the central one and it requires greater programming effort. Recently, to reduce the acquisition time, multichannel systems have been introduced where only a pair of electrodes is used to inject the current, and the voltage difference is measured with different pairs of electrodes simultaneously (Loke et al., 2013).

The data acquisition and controlling software integrate the hardware and control the acquisition processes. The software should be efficient to choose the electrodes for each single measurement, sends the current, and measures the voltage drop from which the resistance and resistivity can be calculated and stored for interpretation.

Commercially, four electrode resistivity systems, such as the Allied Ohmega system of Allied Associates Ltd, U.K., costs about £4,600, while the Allied Tigre system of 64 electrodes costs about £17,800 (personal communication). In the subsequent sections, the design and construction of the system developed will be described.

3.3 Design and construction of the multi-electrode resistivity system

The system developed in the current study (Figure 3.2) consists of: a DC current power source, a Datascan data logger, a switching system and data acquisition and control software.

A programmable DC power supply was used to inject the current. A Datascan logger, connected to a PC via RS232 interface, was used to measure the voltage and log the current. Windows based data acquisition and controlling software named Resist (Toll and Hassan, 2014) has been developed to integrate the hardware and to control the data acquisition process.

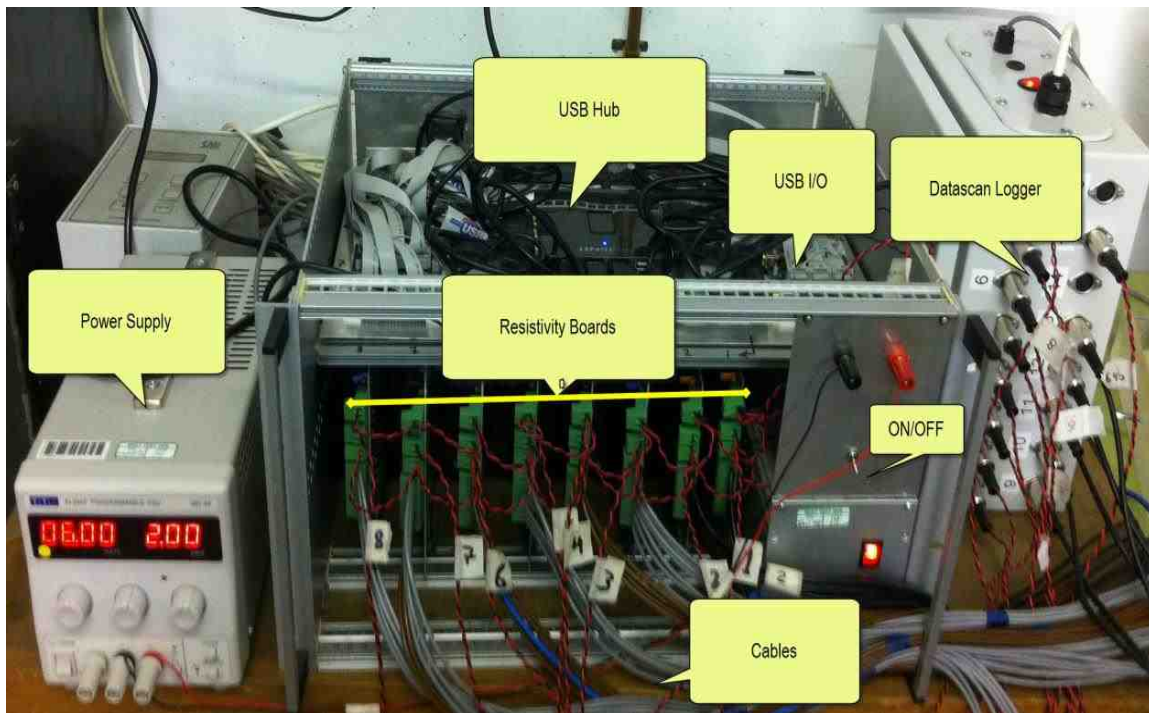


Figure 3.2. The main components of the developed system

3.3.1 Power source

In the current system, a 30V/2A power supply type EL302P, with an isolated RS-232 interface of 9-pin D connector, was used. The EL302P is a digitally programmable power source that offers remote control functions: set the voltage, set the current, read the voltage, and read the current. A typical current used in resistivity instruments ranges from 2 to 500 mA. Therefore, the power source used offers the range of current needed to cover of a wide range of resistivity values. In addition, although the desired voltage and current can be chosen manually (i.e. local operation mode), using a command list, the current and voltage can be controlled remotely (i.e. remote operation mode), which makes the power supply suitable for automated current injection needed for automated resistivity systems.

3.3.2 Datascan logger

To calculate the resistivity, a measure of the injected current and the resultant voltage drop is needed. MSL (Measurement Systems Ltd.) Datascan 7220 series connected with a PC via RS-232 cable was used for continuous data collection and communication. It has 16 integral analog channels individually configurable for DC voltage, current and thermocouple measurements. The module has an input impedance of 30M Ohms which makes the MSL7220 suitable for logging voltages and sensing the current via a shunt resistor. Therefore, the MSL7220 was adopted for data logging and communication to read the voltage drop and to sense the transmitted current by measuring the voltage drop across a one-Ohm high precision shunt resistor (Gupta and Hanks, 1972; Abu-Hassanein et al., 1996) shown in Figure 3.3. A similar approach has been adopted in the commercial instruments (e.g. MPT/ERT 2004 system) of Multi-Phase Technologies, LLC (MPT) (LaBrecque and Daily, 2008).

A shunt resistor can be used to measure the current in a circuit by measuring the voltage drop that the current creates across the resistor. According to Ohm's Law ($I=V/R$), the transmitted current can be determined straightforward by measuring the voltage drop across a resistor of known resistance. Different shunt resistors were examined during the construction of the system. After a series of tests, a high precision 1 Ohm resistor was used. In this case, the transmitted current equals to the voltage drop measured across the shunt resistor.

As the data logger supports 16 channels, the extra channels can be used to collect additional data, such as monitoring soil volume changes and suction of the soil. Unlike other resistivity systems, this makes the developed system multifunctional that can provide full laboratory monitoring in addition to measuring soil resistivity.

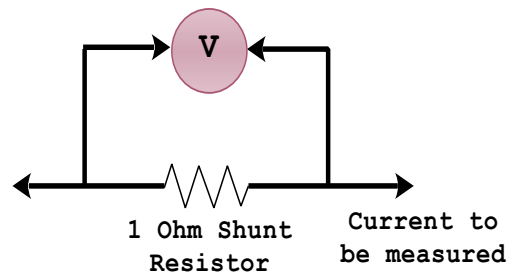


Figure 3.3. The shunt resistor used to log the current

3.3.3 Switching system

The switching system has been designed and fabricated at Durham University (Figure 3.4). Each switching board can control 8 electrodes and each electrode can be individually switched between five states: C+ (connected to the +ve side of the current source provided by the Power supply); C- (connected to the -ve side of the current source); P+ (connected to the +ve side of the data logger channel for measurement of voltage); P- (connected to the -ve side of the data logger channel) or Disabled (disconnected).

The switching is done through a USB I/O 24 module (Elexol Pty Ltd) that can provide digital output signals. Each I/O module has 24 individually programmable input/output pins grouped into 3 ports, and features a serial number which means the PC can identify each module uniquely, allowing multiple modules, connected via a USB hub, to be used for a single application. Three data bits are required to switch each electrode; 1 pin is used to enable/disable the electrode, the 2 other pins are used to switch between C+, C-, P+, P- using the configuration in Figure 3.4 (i.e. setting both pins to logic level zero (00) selects a C+ state; setting both pins to a logic level 1 (11) selects P-; C- is selected using (01) and P+ using (10)). Therefore, the USB 24 pin I/O can control 8 electrodes (8×3 pins).

CHAPTER 3: DESIGN AND CONSTRUCTION OF AN AUTOMATED MULTI-ELECTRODE RESISTIVITY SYSTEM

In the current system, eight switching boards (each with a USB I/O module) have been used. The resistivity boards are used to control 64 electrodes. However, the number of electrodes is only limited by the number of modules that can be used.

For laboratory studies, where only short cables are needed, the current and voltage electrodes are wired and connected to the system individually, instead of using multi-core cable (Barker, 1981). This approach offers versatility and flexibility in the measurement to choose any electrode arrangement (Werkema et al., 2000)

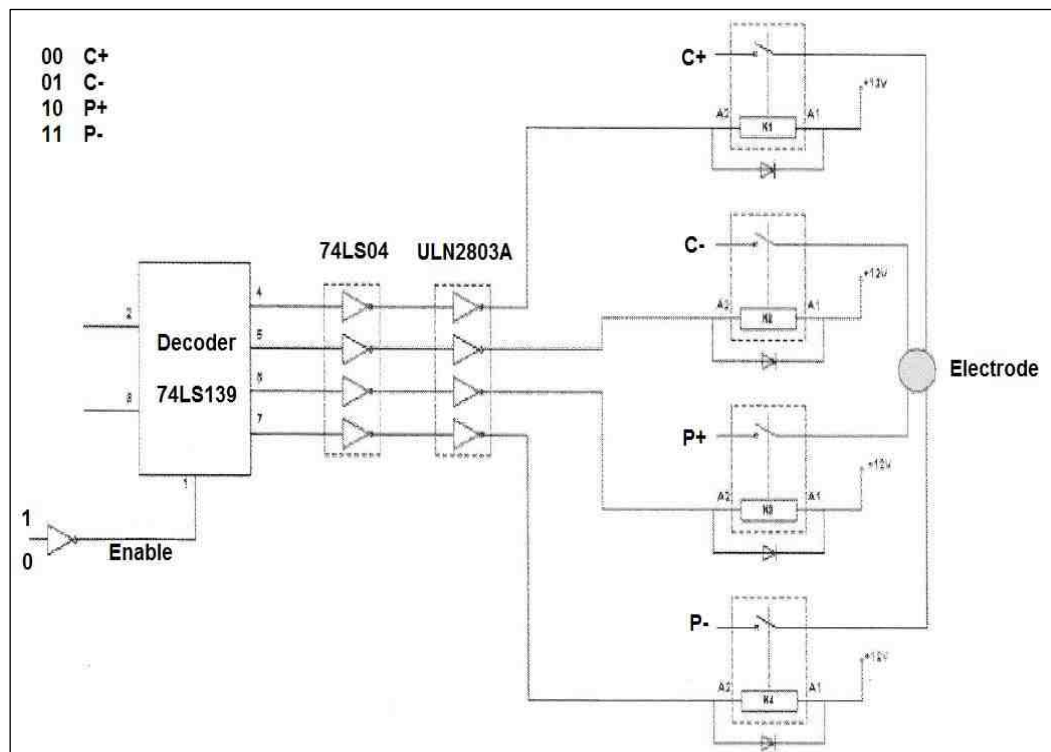


Figure 3.4. The switching circuit for multiplexing electrodes

3.3.4 Data acquisition and control software

A user friendly controlling and acquisition software named RESIST has been developed to integrate the hardware and control the overall processes. It is based on the TRIAX program used for other geotechnical laboratory control and data acquisition function (Toll, 1999). RESIST allows remote functions for controlling the power supply: set voltage, set current, set output On/Off and for acquiring data through the data logger to read current and voltage, thereby offering a fully automated control procedure. In modern resistivity systems, short current pulses are used (Dahlin, 2001). Similarly, RESIST sends short current pulses to the selected current electrodes; reads voltage difference via potential electrodes; and measures the current via the shunt resistor. To prevent polarization (ASTM G57, 2006), the polarity of the electrodes is reversed periodically and an average of current I (Amps) and voltage V (Volts) is collected to calculate the resistance R (Ohms). Moreover, using a predefined sequence of electrodes and appropriate geometric factors, resistivity ρ (Ohm. m) of any array can be collected and tabulated in a real-time procedure.

On the main window (Figure 3.5), the user can set the current and voltage, specify the current pulse time, the delay time between the readings and the number of inversions needed (i.e. the number of times needed to reverse the polarity of the electrodes). The user can also specify the active electrodes C1, P1, P2 and C2 for each reading. On the same window, the user can define the sequence of the measurements using the sub-window shown in Figure 3.6. Using a predefined sequence of electrodes and a particular delay time, the user can collect resistivity measurements using up to 64 electrodes. Since the electrodes are wired individually, resistivity of any electrode arrangement can be gathered straightforward by applying appropriate geometric factors. The outputs of the system can be logged using 'scan' window (Figure 3.7), where the user can choose the variables to be logged (e.g. date, time, current, potential, resistance, resistivity...etc.). The user can also define the scanning time interval needed for the automated acquisition.

CHAPTER 3: DESIGN AND CONSTRUCTION OF AN AUTOMATED MULTI-ELECTRODE RESISTIVITY SYSTEM

The system described above offers fully automated data acquisition, which makes it suitable for monitoring transient phenomena such as monitoring water content changes and drying and wetting of soils that require continuous real time data collection, one of the main interests in the current thesis.

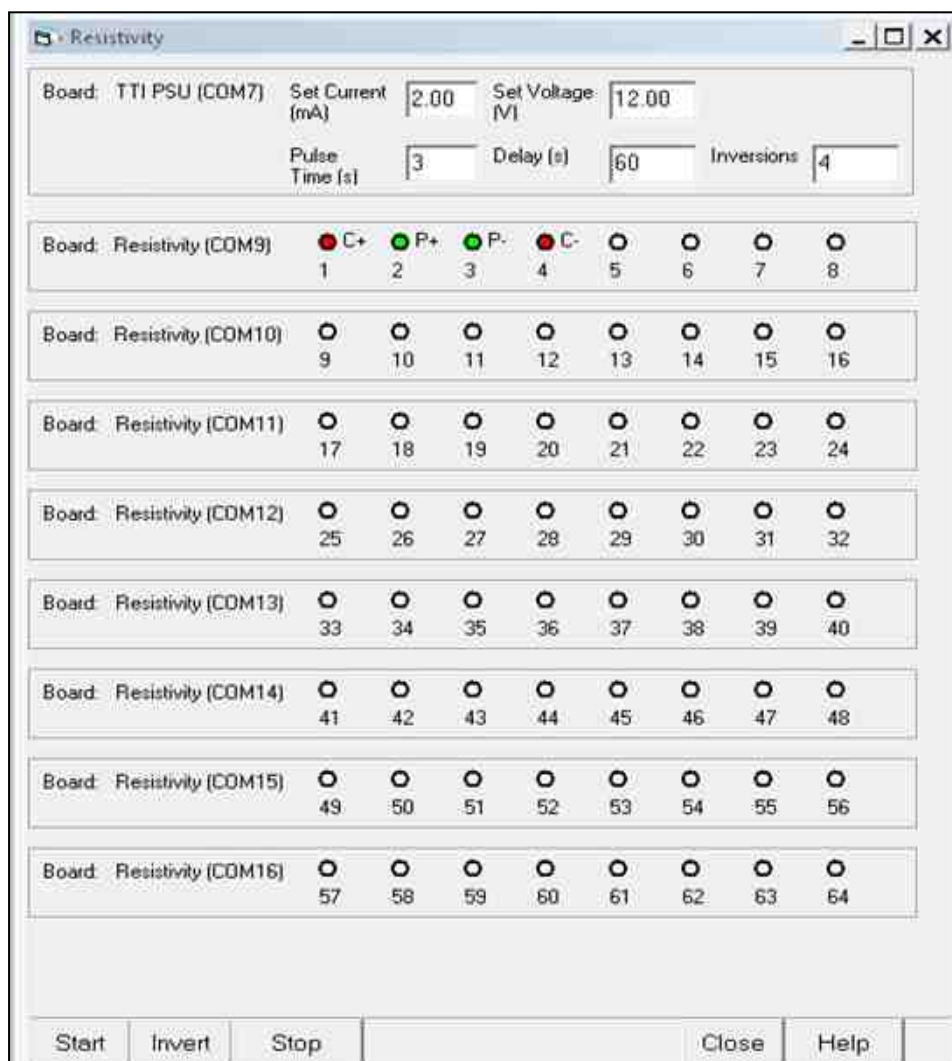


Figure 3.5. The main window of Resist

CHAPTER 3: DESIGN AND CONSTRUCTION OF AN AUTOMATED MULTI-ELECTRODE RESISTIVITY SYTEM

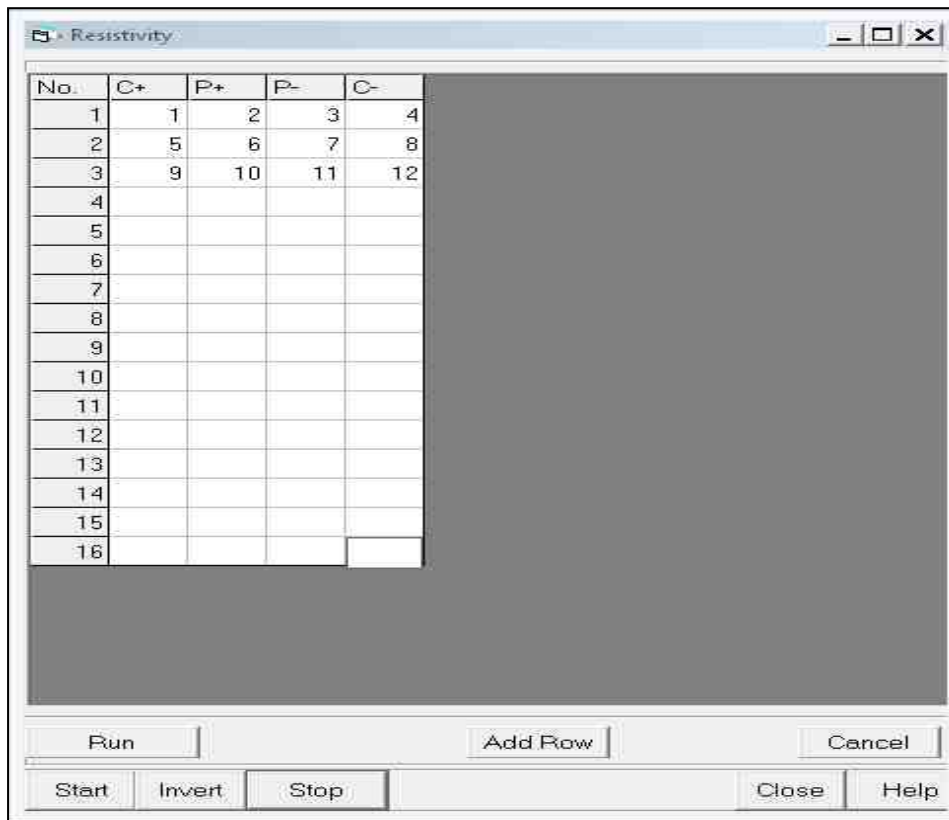


Figure 3.6. Defining a sequence of electrodes for automated data acquisition

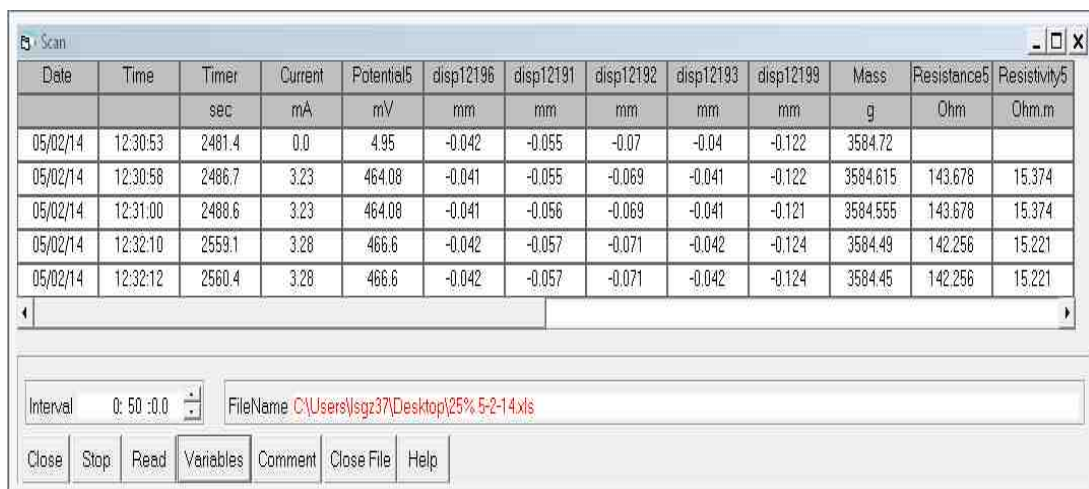


Figure 3.7. Logging the resistivity data and other variables

3.4 Laboratory resistivity devices constructed and measurement procedures

The following sections describe the laboratory resistivity devices constructed in the current work and measurement procedures. Specific experimental designs will be provided in the subsequent chapters.

3.4.1 Miller resistivity box

Miller resistivity box was constructed using non-conductive Plexiglas material (Figure 3.8). Stainless steel current and potential electrodes were used to minimize the effect of electrode polarization and to maintain good contact with soil (Dahlin, 2001; LaBrecque and Daily, 2008). The dimensions of the box were designed according to M.C. Miller Company (<http://www.mcmiller.com>) specifications, Soil Box Cat. # 37006 (\$137). The cross sectional area $A=7.2\text{cm}^2$ (i.e. $3\text{cm}\times 2.4\text{cm}$) and the interior pin separation $L=7.2\text{cm}$. The box was constructed to satisfy the standard four electrode method and two electrode method. For the four electrode method, the geometric factor A/L (Eq. 2.11, Chapter 2) equals 1cm and the measured resistance, $R(\text{Ohm})$ equals the sample resistivity, ρ ($\text{Ohm}\cdot\text{cm}$) directly. For the two electrode method, the interior voltage pins were not used, and current ends serve as both current and voltage electrodes. Therefore, the electrode separation (L) equals to the distance between current electrodes. The soil box described above was used as a standard device to test the system developed.

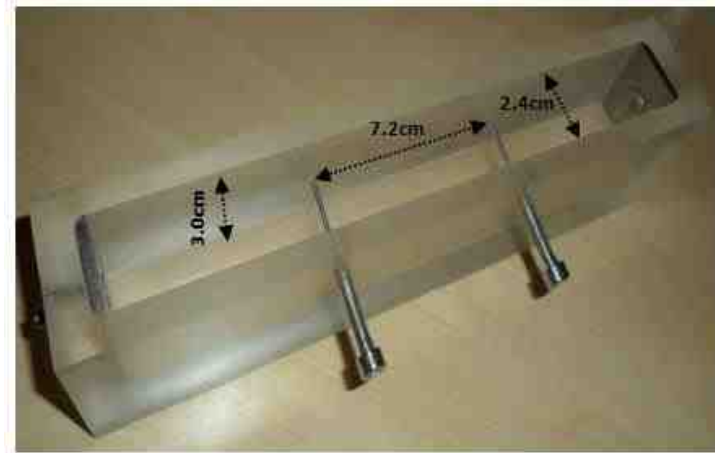


Figure 3.8. Miller resistivity box

3.4.2 Circular resistivity cell

A circular resistivity cell (120mm diameter and 60mm depth) shown in Figure 3.9 was constructed using a Plexiglas container equipped with eight stainless steel electrodes. Using the four electrode method, an average of eight independent resistances was used to calculate the resistivity using three electrode arrangements; Wenner, dipole-dipole, and square arrangements. The cell was used to test and validate the system using solutions of known conductivities (Chapter 4), and to investigate the potential of the resistivity technique for characterising cracking of clay soil (Chapter 8). Although the circular cell can provide more accurate representative resistivity value of the soil, and more relevant for compacted specimens using standard compaction methods, the cell requires calibration to consider the influence of 3D geometry of the cell on the measurements (Kalinski and Kelly, 1993).

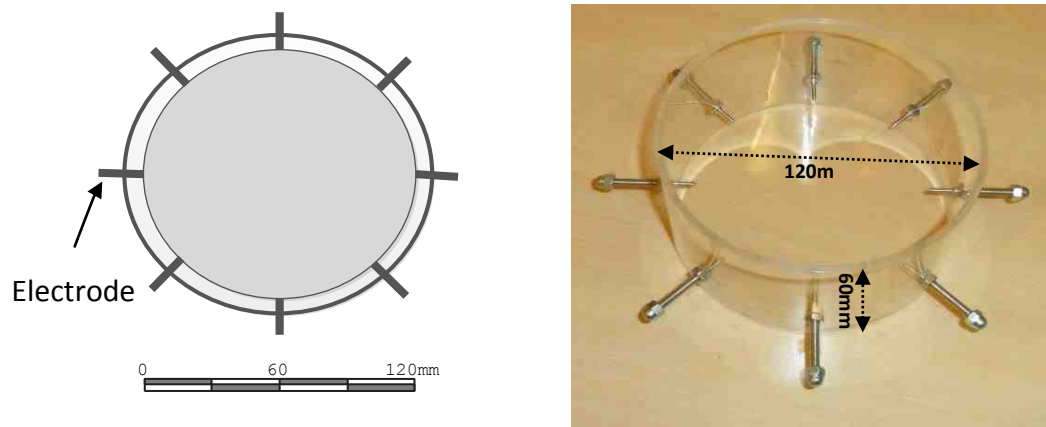


Figure 3.9. The circular resistivity cell

Circular resistivity cell calibration

The analytical geometric factor, K (e.g. $2\pi a$ for Wenner array) applies to simple and most frequent situation (i.e. a half-space infinite medium) for which an analytical expression can be defined for different arrays (see Table 2.2, Chapter 2). For a medium of "finite" volume (e.g. circular resistivity cell at a laboratory scale), border effects arising from the 3D geometry of the cell have to be considered. Two options are feasible (Beck et al., 2011; Du Plooy et al., 2013):

1. The experimental calibration: In this method, the geometric factor can be obtained by measuring the resistance of chemical solutions (e.g. KCl or NaCl) of known resistivity (Kalinski and Kelly, 1993; ASTM G57, 2006; Sreedeeep et al., 2004; 2005). First, resistance, $R = (V/I)$ is measured when the cell is filled with a solution for which the resistivity, ρ (or conductivity σ) can independently be assessed by means of a commercial conductivity meter, itself calibrated using a standard solution. Comparing the measured resistance to the independently measured resistivity leads to an empirical geometric factor ($\rho = K.R$). In this procedure, although one solution can be used (e.g. Kibria and Hossain, 2012), one has to cover a range of conductivities, in order to generate a calibration curve. A number of

authors (e.g. Kalinski and Kelly, 1993; Sreedeeep et al., 2004, 2005; Sheffer et al., 2007; Kibria and Hossain, 2012) adopted the experimental procedure. According to ASTM G57 (2006), laboratory calibration is recommended to be performed at 20°C. However, when the resistivity measurements are performed at the same temperature of the calibration, any temperature correction factor equals 1.0 (Kalinski and Kelly, 1993). This procedure has to be implemented for each electrode configuration, and the drawbacks are linked to defining an accurate and repeatable experimental protocol (Beck et al., 2011).

2. Numerical calibration: in this method, one can simulate the above experiment (a cell of a same geometry, and the desired electrode configuration) in a homogeneous medium of resistivity equal to one. The numerically modelled resistances then lead to the geometric factor of the corresponding configuration (Marescot et al. 2006). In this method, the geometrical factor K can be expressed as:

$$K = \frac{\rho_o}{R_o} \quad (3.1)$$

Where ρ_o is the resistivity of a homogenous medium of R_o resistance for the same cell geometry. The above procedure leads to geometric factor that can be used to calculate soil resistivity. Beck et al. (2011) and Du Plooy et al. (2013) adopted the numerical procedure. However, this procedure needs to be validated experimentally (Beck et al., 2011).

Alternatively, one can always compare resistance measurements carried out on various soils, as long as the cell geometry and electrode configuration remain the same since all these measurements share the same geometric factor.

As the resistivity is the reciprocal of the conductivity (i.e. $\rho = 1/\sigma$), a correlation between the resistivity/conductivity measured by conductivity meter and resistivity/conductivity measured by the resistivity system should be a 1:1 relationship. This relationship provides a method to validate the resistivity system, where the resistivity is

assessed independently by means of commercial electrical conductivity meter. This method has been adopted by several authors to validate the outputs of new resistivity systems (e.g. Sheffer et al., 2007; Damasceno et al., 2009).

In the literature, the Wenner electrode arrangement is commonly used to calibrate the resistivity cell (e.g. Gupta and Hanks 1972; Kalinski and Kelly, 1993; Borsic et al. 2005). In this study, three arrangements were used. Measurement procedures and calibration results will be discussed in the following section.

Measurement procedure using the circular resistivity cell

Three electrode arrangements namely Wenner, dipole-dipole and square arrangements were implemented, see Figure 3.10. For each arrangement, eight independent resistance readings were collected by switching from one to the next neighbouring four electrodes. The average of these readings was calculated.

Ten KCl solutions with different electrical conductivities were prepared using distilled water (ASTM G57, 2006). A portable conductivity meter type HI 9835 of HANNA instruments, itself calibrated using a standard solution HI 70031, was used to measure the electrical conductivity of these solutions. The geometric factors for three arrays were calculated using the regression of the relationship between the measured resistances using the system and the independently assessed resistivities using the conductivity meter. The results are shown in Figure 3.11. In this process, all the materials and the instruments were accommodated in a temperature-controlled lab. The temperature was $\sim 20^{\circ}\text{C}$.

CHAPTER 3: DESIGN AND CONSTRUCTION OF AN AUTOMATED MULTI-ELECTRODE RESISTIVITY SYSTEM

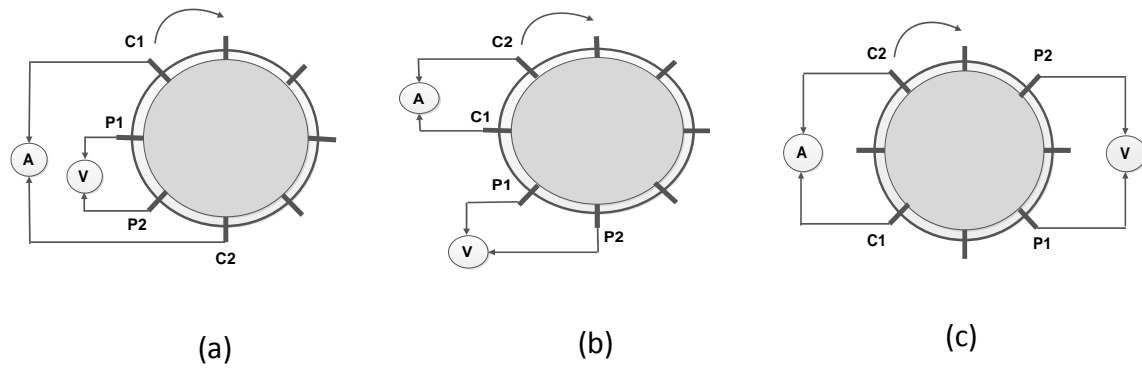


Figure 3.10. Circular resistivity cell (a) Wenner (B) Dipole Dipole (c) Square array

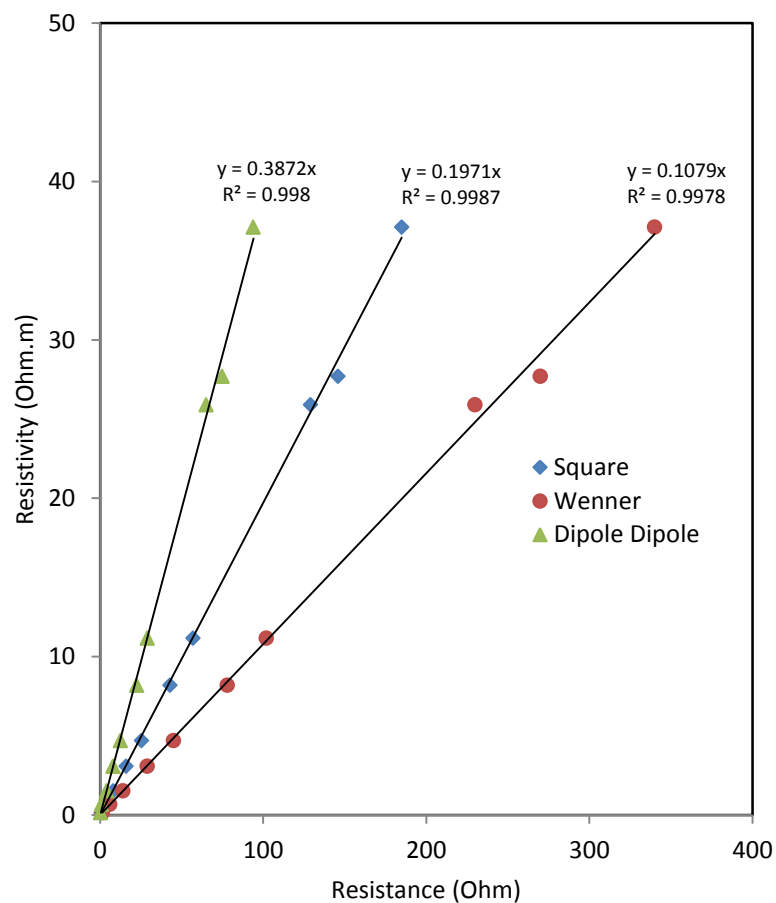


Figure 3.11. Calibration of the circular resistivity cell for three resistivity arrays

CHAPTER 3: DESIGN AND CONSTRUCTION OF AN AUTOMATED MULTI-ELECTRODE RESISTIVITY SYTEM

Using the above calibration, the resistivity of KCl solution was compared with independently assessed measurements using a HANNA conductivity meter as a method of validation. The comparison will be presented in Chapter 4. Furthermore, as mentioned earlier, the Miller soil box was constructed so that the geometric factor, $K=1\text{cm}$ or 0.01m . Following the procedure described above, the geometric factor was obtained for KCl solutions as shown in Figure 3.12. The obtained geometric factor (0.0105m) confirms the validity of the procedure adopted.

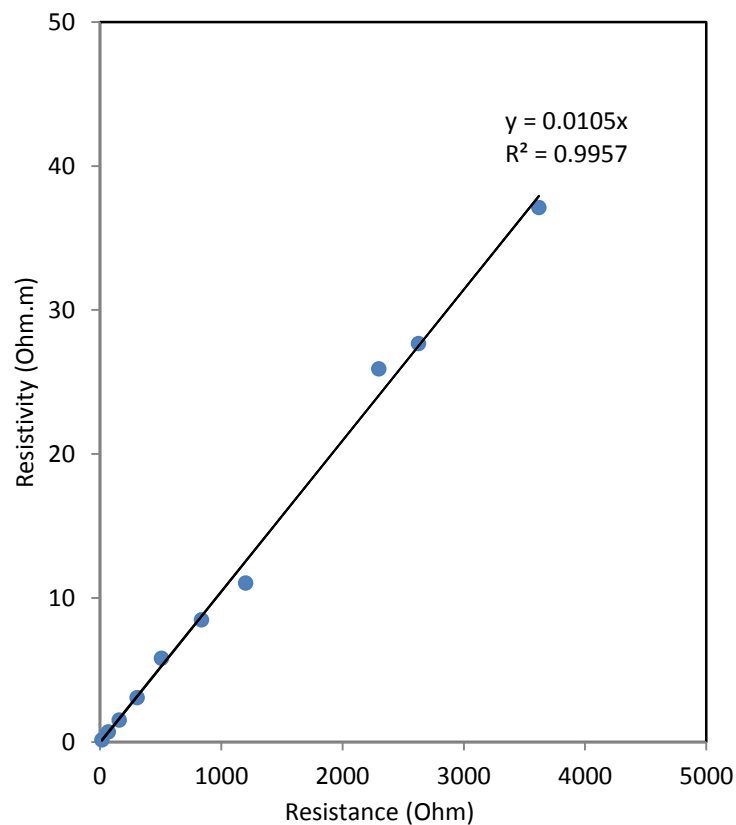


Figure 3.12. Miller resistivity box calibration

3.4.3 Resistivity devices for local measurements

As mentioned in chapter 2, many authors have developed small-scale resistivity probes/devices for quick local resistivity measurements implemented for different geotechnical and geoenvironmental applications, particularly for water content monitoring.

In the current study, resistivity devices based on the square arrangement were constructed, and used for local resistivity measurements. A new resistivity probe (Toll et al., 2013) was developed for localised water content determination, and used to investigate the soil water content characteristics of compacted clay soil described in Chapter 5, the role of pore water conductivity on soil resistivity described in Chapter 6 and drying and wetting of compacted clay samples described in Chapter 7. The probe (Figure 3.13) consisted of four stainless steel electrodes with an inter-electrode spacing of 10mm. The electrodes were fixed at the base of a PVC frame (16mm diameter and 12.5mm depth). To avoid the interference between the electrodes, the frame was filled with silicone.

Using the same arrangement, four stainless steel electrodes with 15mm inter-electrode spacing were fixed on a perspex plate (Figure 3.14a), and used to monitor water content changes during drying and wetting of uncompacted clay soils described in chapter 7. In addition, two devices with 50mm and 100mm inter-electrode spacings (Figure 3.14b) was used to investigate the influence of cracking parameters (i.e. depth, width, length, number and direction) on soil resistivity described in chapter 8.

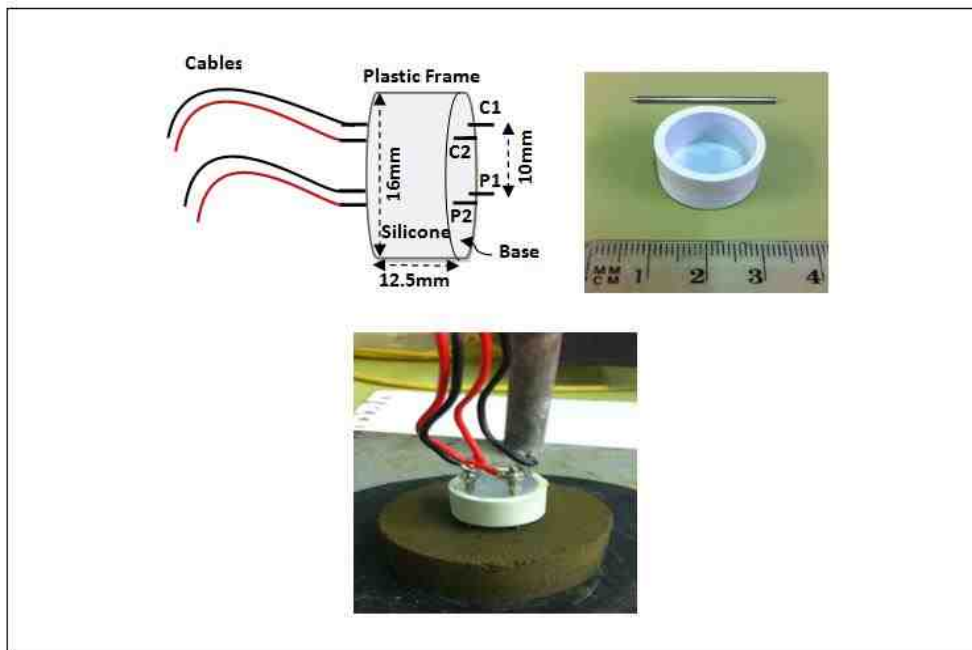


Figure 3.13. Square resistivity probe developed in this study

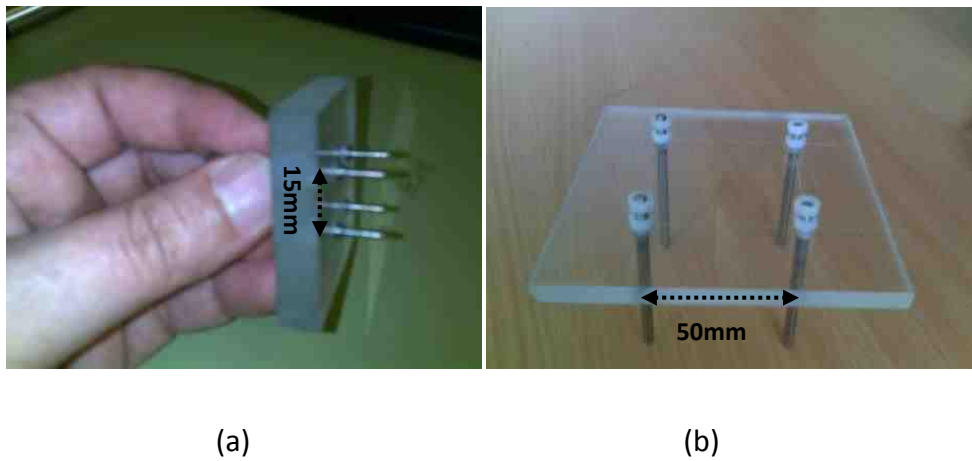


Figure 3.14. Square resistivity devices constructed in this study

In the current thesis, the square arrangement (Habberjam and Watkins, 1967) was adopted largely for the resistivity measurements. This arrangement provides a compact current flow pattern that is less dependent on the line of electrodes compared to linear arrays, thus eliminating effects of the soil container (Russell and Barker, 2010), and unlike other arrays, this arrangement offers two perpendicular readings (Figure 3.15), conventionally named α -resistivity and β -resistivity (ρ_α and ρ_β , respectively) (Samouëlian et al., 2004). An average resistivity of these two reading uniquely averages out soil heterogeneity (Russell and Barker, 2010; Greve et al., 2011), offering a more representative resistivity value of the soil specimen, and the ratio of ρ_α and ρ_β has been used to characterise cracking soils (e.g. Samouëlian et al., 2004; Greve et al., 2009; 2010a; b). Moreover, the small resistivity probe provides an easy and quick measure of soil resistivity that does not require calibration for the geometric factor K (Russell and Barker, 2010), which can be calculated using the following formula:

$$K = \frac{2\pi a}{2 - \sqrt{2}} \quad (3.2)$$

Where, a is the inter-electrode spacing.

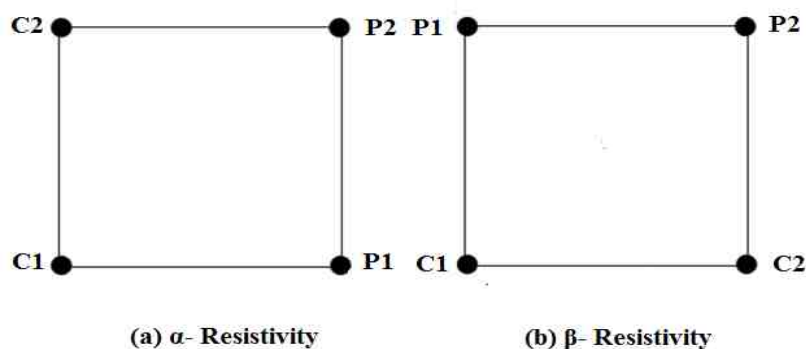


Figure 3.15. Resistivity square array (a) α -resistivity (b) β -resistivity

To confirm the validity of the geometric factor used, Figure 3.16 shows a comparison between resistivity of KCl solutions measured by the system (K is calculated according to Eq. 3.2), and the conductivity measured by HANNA conductivity meter. The solutions were placed in a plastic container (55mm diameter, 80.5mm height). The near unity 1:1 relationship confirms the validity of using the geometric factor calculated according to Eq. 3.2.

Furthermore, to explore the influence of the specimen size on the measured resistivity, a BIONICS clay specimen compacted at 20% gravimetric water content using BS light compaction (BS1377, 1990: Tests 3.3) was trimmed to specimens of different sizes. The measured resistivities using the probe (K was calculated according to Eq.3.2) are reported in Table 3.1. The table shows that trimming the specimen does not change the resistivity of the soil.

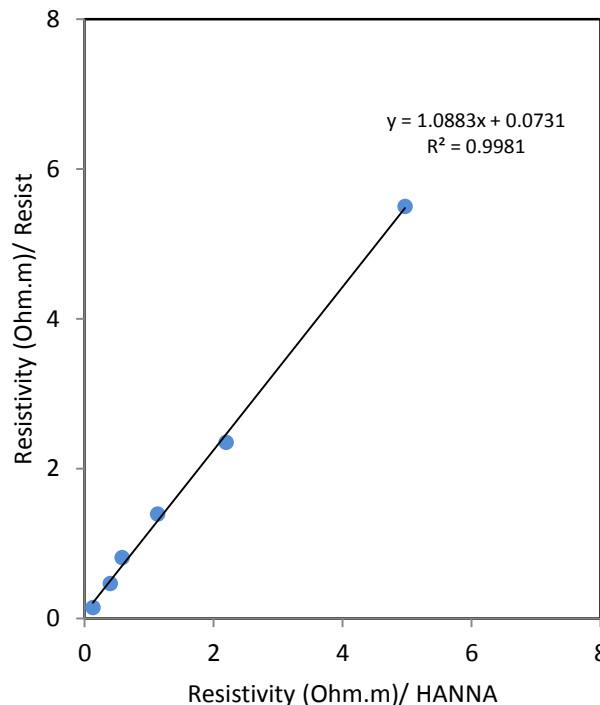


Figure 3.16. A comparison between resistivity of KCl solutions measured using the system developed and HANNA conductivity meter

Table 3.1 Resistivity of compacted specimens of different dimensions

Specimen dimension (diameter, height) mm	α -resistivity Ohm.m	β -resistivity Ohm.m	Average Resistivity Ohm.m
105, 115	14.37	14.63	14.50
105, 50	14.52	14.62	14.57
75, 20	14.42	14.52	14.47
50, 20	14.37	14.41	14.39

3.5 Chapter summary

This chapter described the design and construction of a new automated multi-electrode resistivity system for laboratory testing, and a new resistivity probe and devices for local resistivity measurements.

An automated data acquisition and control system has been developed to acquire resistivity data using different arrays. The system controls 64 electrodes interchangeably as current and voltage electrodes, reads the output current and voltage, and stores the calculated resistivity data for interpretation in fully automated procedure.

The system offers a continuous real-time data collection, which is one of the recent advances in the resistivity instrumentation. This advantage makes it relevant to carry out experimental studies to monitor water content changes in unsaturated soil submitted to drying and wetting cycles.

To monitor water content, a new resistivity probe was developed for localised water content determination. The probe offers a quick and easy tool to monitor water content changes in unsaturated soil subjected to drying and wetting procedures.

CHAPTER 3: DESIGN AND CONSTRUCTION OF AN AUTOMATED MULTI-ELECTRODE RESISTIVITY SYTEM

The resistivity devices constructed, and used in the subsequent chapters were described. Due its unique characteristics, the square arrangement was chosen. The measurement procedures used were discussed.

After a series of tests conducted (described in Chapter 4), the system was adopted to carry out the laboratory work presented in this thesis.

Chapter 4

Calibration and validation of the multi-electrode resistivity system

This chapter describes the calibration and validation of the multi-electrode resistivity system developed in the current thesis. The main goal was to check the data quality of the system in order to produce reliable data with minimum error. The system was tested using a wide range of high precision reference resistors and different soils. The outputs were correlated with those acquired with commercial instruments. Accuracy, precision and resolution of the measurements are assessed.

4.1 Introduction

As for any new instrument, calibration; a process of evaluating and adjusting its accuracy (i.e. the agreement or closeness of a measured value to its well known true value) and precision (i.e. the degree to which repeated measurements, under the same conditions, give the same results) is necessary to ensure the reliability of the outputs of the instrument (BS ISO 5725-1, 1994; JCGM 200, 2008). Figures 4.1 and 4.2 illustrate the difference between accuracy and precision. In addition, resolution (i.e. the ability to distinguish between slightly different measurements) is also important to determine the fineness to which an instrument can measure. Measurements with high accuracy, precision and resolution are required to produce reliable data. Instrument validation, on the other hand, is a process that confirms that the instrument is working correctly to fulfil its intended use. This process proves the performance validity of the instrument.

To ensure accurate outputs, calibration of the instrument needs to be carried out regularly. The process involves (1) selection, over the range of the measurement interest, a number of standards with well-known values; (2) measuring the standards using the custom

instrument to be calibrated; (3) a functional correlation between the actual and measured values (i.e. Calibration curve); and (4) using the calibration curve to correct all the measurements accordingly. Using the above procedure, a measurement error of an instrument can be defined as the percentage difference between the measured and actual value of the quantity being measured, where:

$$Error(\%) = \frac{(Measured\ value - Actual\ value)}{Actual\ value} \times 100 \quad (4.1)$$

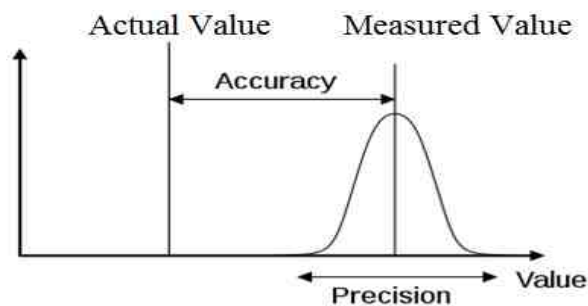


Figure 4.1. Accuracy and precision

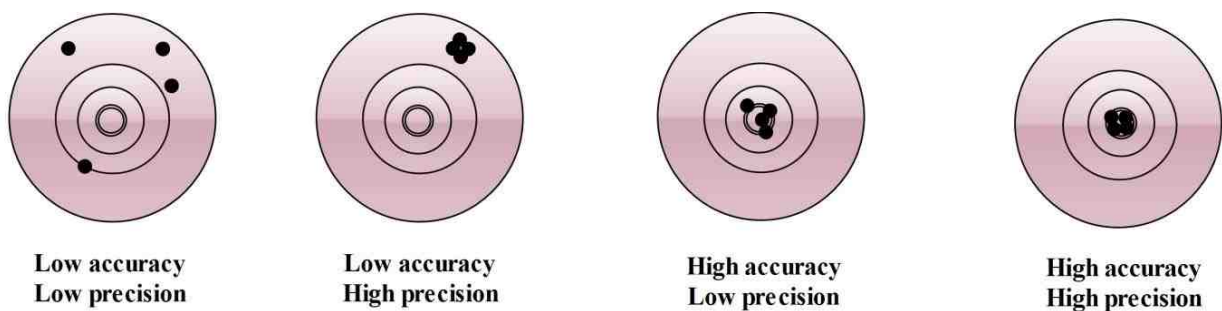


Figure 4.2. Illustration of the difference between accuracy and precision

4.1.1 Calibration and validation of resistivity instrument

Since a resistivity instrument measures the resistance of the materials, reference resistors of known values are commonly used to calibrate the system and to determine the measurement error of the instrument (ASTM G57, 2006; Korteland, 2013). According to ASTM G57, a 5% error is accepted and a calibration curve should be used if the error exceeds this limit. To validate the instrument, the outputs can be compared with those acquired using a standard resistivity system (e.g. Awotoye and Selemo, 2006; Igboama and Ugwu, 2011; Lachhab and Booterbaugh, 2011), or a standard conductivity meter (Sheffer et al., 2007; Damasceno et al., 2009).

Firstly, a wide range of reference resistors was used. Accuracy, precision, and resolution of the measurements were assessed. Secondly, the outputs of the system were compared with those collected using a Terrameter SAS 300 C resistivity system (ABEM), and a conductivity meter type HI 9835 (HANNA instruments).

4.1.2 Data quality and error

The resistivity measurement is subject to a variety of error sources, such as poor electrode contact, electrode polarization and random errors introduced by the measurement instrument (e.g. Heaney, 2003; Chambers et al., 2004; LaBrecque and Daily, 2008). However, the user can reduce the errors by adopting appropriate measurement design and electrode arrangements. Therefore, it is recommended to check the data quality and the expected error of resistivity measurements. Repeatability (stacking), reverse electrode polarity and reciprocity have been found suitable to achieve this goal (e.g. Binley et al., 1995; Slater et al., 2000; Nimmer et al., 2007; Korteland, 2013). With repeatability, the measurements are repeated making sure that temporal affects are not induced by the instrument itself. In the second method, the polarity of current (C+ and C-) and voltage (P+ and P-) is reversed, which should result in identical readings (Binley et al., 1995). Differences between normal and reverse polarity readings indicate inconsistency in the data acquisition.

However, it has been reported that reciprocity (i.e. exchanging current and potential electrodes) is optimum to check data quality of resistivity instrument (Chambers et al., 2004; Nimmer et al., 2007; LaBrecque and Daily, 2008; Robert et al., 2011). Ideally, normal and reciprocal readings should be identical. The difference between them might indicate errors and can reveal inconsistency of the measurements (Parasnis, 1988). Therefore, reciprocity error R_E is commonly used to assess data errors in resistivity measurements, defined as:

$$R_E = |R - R_{\text{recip}}| / R_{\text{mean}} \% \quad (4.2)$$

Where R , R_{recip} and R_{mean} are the normal resistance, the reciprocal resistance and the mean resistance, respectively. If the measurement system is noise free, resistance (Voltage/Current) readings of reference resistors should be exactly reciprocal, although small errors are expected due to random noise of the measurement system (LaBrecque and Daily, 2008). For soils, a 5% target reciprocity error has been accepted (Chambers et al., 2004; Nimmer et al., 2007).

4.2 Calibration: Reference resistors

4.2.1 A four electrode method

Reference resistors of a wide range were used to check the data quality of the system using the measurement setup shown in Figure 4.3.

A comparison between resistance readings of the system developed (hereafter called Resist) with those obtained using a Terrameter SAS 300 C system (hereafter called Terrameter) is reported in Table 4.1, with the individual error of each resistor. The table indicates high accuracy measurements with a maximum error of 0.8% compared to a 2.0% maximum error of the Terrameter, and high resolution (e.g. the ability to distinguish between 2 and 4 Ohm, or 10 and 11 Ohm resistor). This high resolution is attributed to the

high resolution ($0.625 \mu V$) of the Datalogger used to log the current and the voltage, which can be considered as the actual resolution.

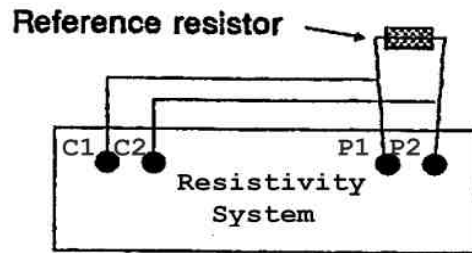


Figure 4.3. Measurement setup using a high precision reference resistor (ABEM, Terrameter SAS 300 C, instruction manual)

Table 4.1. A comparison between Resist and the Terrameter for different reference resistors

Reference Resistor (Ohm)	Terrameter		Resist	
	Average Reading (Ohm)	Percentage Error (%)	Average Reading (Ohm)	Percentage Error (%)
2	1.99	0.50	1.99	0.50
4	3.98	0.50	3.97	0.75
10	9.9	1.00	10.00	0.00
11	11.1	0.90	11.01	0.09
56	56.1	0.18	56.3	0.54
100	98.0	2.00	99.2	0.80
120	119.3	0.58	120.2	0.17
150	149.0	0.67	150.1	0.07
220	217.0	1.36	218.9	0.50
270	268.0	0.74	270.5	0.19
370	368.0	0.54	368.9	0.30
490	486.0	0.82	489.0	0.20
590	585.0	0.85	589.1	0.15
1000	996.0	0.40	998.4	0.16
1120	1118.0	0.18	1118.4	0.14
1220	1217.0	0.24	1215.9	0.33
3300	3328.6	0.86	3311.9	0.36
		Maximum error 2.00%	Maximum error 0.80%	

To determine the measurement error of the system, the measured and actual readings are plotted in Figure 4.4 and 4.5 for Resist and the Terrameter, respectively. The measurement error is 0.19% and 0.50% for Resist and the Terrameter, respectively.

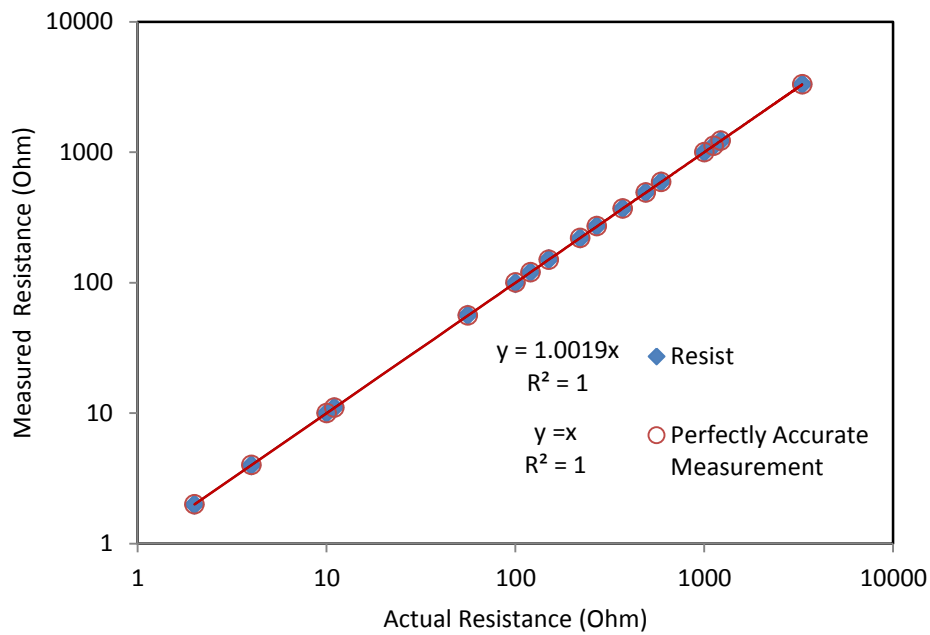


Figure 4.4. A comparison between the measured and actual readings using Resist

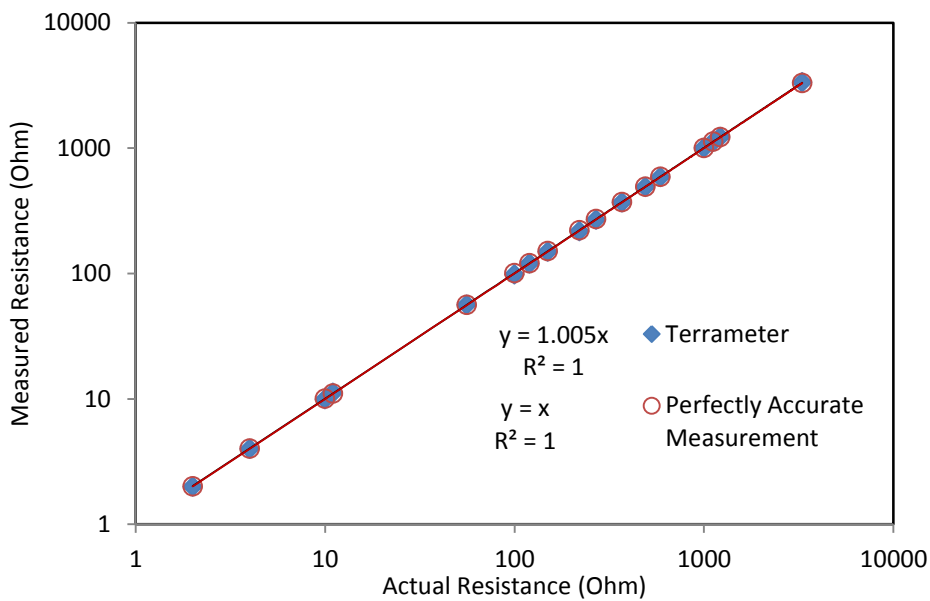


Figure 4.5. A comparison between the measured and actual readings using the Terrameter

4.2.2 Automated data acquisition

As mentioned in Chapter 3, one of the most recent advances in resistivity instrumentation is the development of automated systems. Therefore, reference resistors of different values were used in fully automated data acquisition tests. Reverse electrode polarity (i.e. forward and backward) and reciprocity (i.e. swapping current and voltage electrodes) tests were carried out. Automated readings at different scanning time intervals and acquisition periods were collected. The accuracy of the measurements was assessed. To examine the dispersion of the readings under the same condition (i.e. constant resistance), standard deviation was calculated. This can reveal the consistency or the reproducibility of the measurements (i.e. the precision).

Forward and Backward readings

In this test, automated forward and backward readings were collected. The percentage difference between the forward and backward readings, mean resistance (i.e. the average of forward and backward readings), the standard deviation and the measurement error, were calculated. One example is presented in this section. The rest of tests are shown in Figures A.1 to A.16 in Appendix A. Table 4.2 summarises the results.

Figure 4.6 shows the forward and backward readings of a 100 Ohm resistor test acquired at a 5 minute scanning interval for 89 hours of automated data acquisition, and the percentage difference. Figure 4.7 shows the mean resistance and the measurement error. Figure 4.8 shows screen shots of the data scanning at different times during the test.

The average forward and backward reading was 99.527 Ohm and 99.525 Ohm, respectively. The forward and backward readings are nearly identical with an average difference of 0.014% (Minimum 0%, maximum 0.083%). The average resistance was 99.526 Ohm (standard deviation 0.017), with an average measurement error of 0.474%. The high accuracy and precision of the readings are clearly indicated.

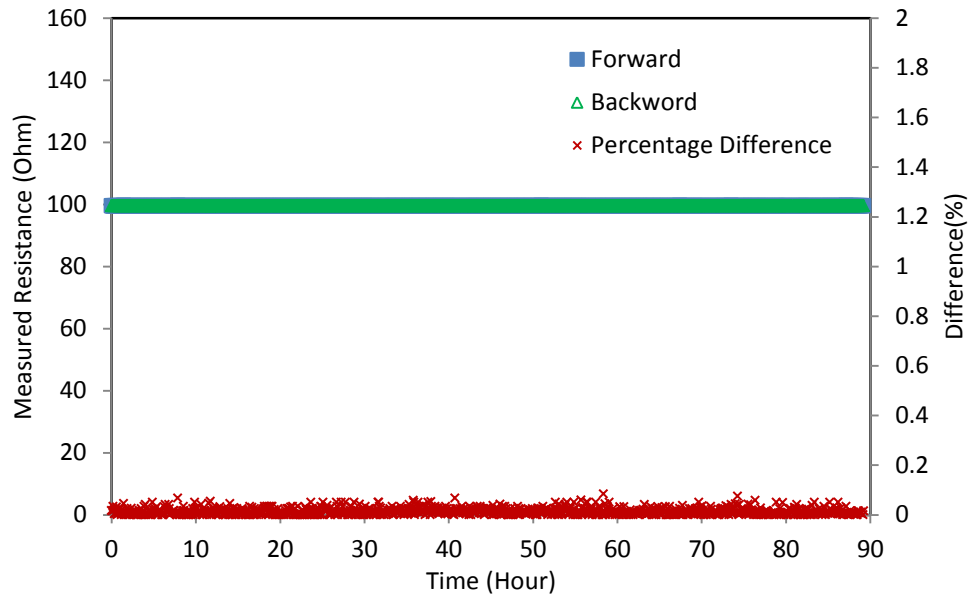


Figure 4.6. The forward and backward readings and the percentage difference of 100 Ohm resistor test

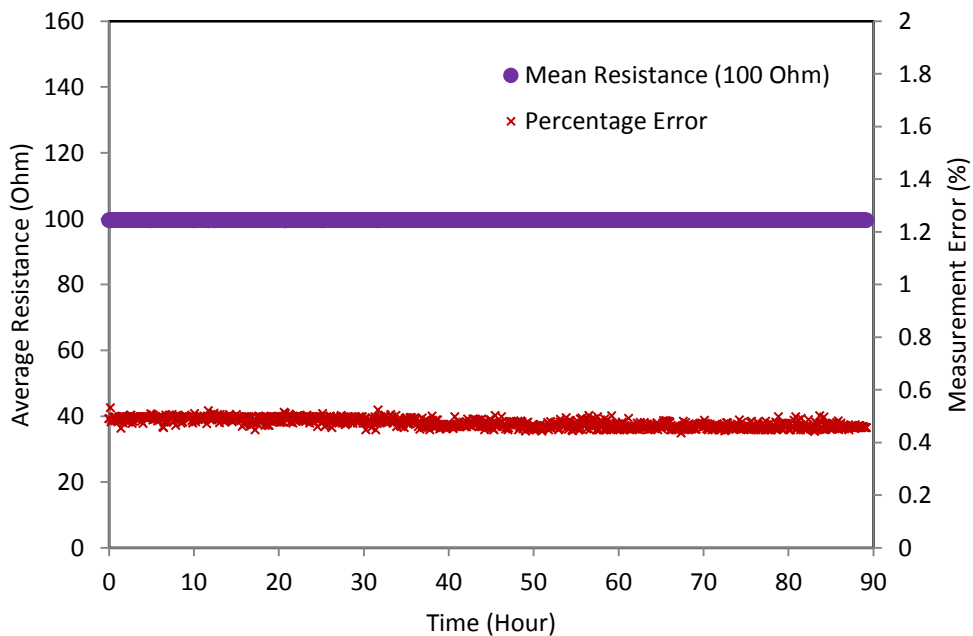


Figure 4.7. The mean resistance and the measurement error of 100 Ohm resistor test

Date	Time	Timer	Current	Potential2	Resistance2	Comments
		sec	mA	mV	Ohm	
10/10/13	15:54:27	174542.4	19.69	1960.14	99.55	Forward:
10/10/13	15:54:27	174542.9	19.69	1959.82	99.534	Forward:
10/10/13	15:55:01	174576.7	19.69	1960.14	99.55	Backward:
10/10/13	15:55:01	174577.3	19.69	1960.14	99.55	Backward:

Date	Time	Timer	Current	Potential2	Resistance2	Comments
		sec	mA	mV	Ohm	
10/10/13	16:38:13	177169.	19.69	1960.14	99.55	Forward:
10/10/13	16:38:14	177169.5	19.69	1959.82	99.534	Forward:
10/10/13	16:38:48	177203.5	19.69	1960.14	99.55	Backward:
10/10/13	16:38:48	177204.	19.69	1960.14	99.55	Backward:

Date	Time	Timer	Current	Potential2	Resistance2	Comments
		sec	mA	mV	Ohm	
11/10/13	12:23:29	70183.2	19.68	1958.19	99.502	Forward:
11/10/13	12:23:30	70184.2	19.68	1958.19	99.502	Forward:
11/10/13	12:24:04	70217.8	19.68	1958.19	99.502	Backward:
11/10/13	12:24:04	70218.3	19.68	1958.19	99.502	Backward:

Date	Time	Timer	Current	Potential2	Resistance2	Comments
		sec	mA	mV	Ohm	
11/10/13	15:03:47	79801.4	19.68	1958.19	99.502	Forward:
11/10/13	15:03:48	79802.2	19.67	1958.19	99.552	Forward:
11/10/13	15:04:22	79835.9	19.68	1958.19	99.502	Backward:
11/10/13	15:04:22	79836.4	19.68	1958.19	99.502	Backward:

Figure 4.8. The automatic scanning of 100 Ohm resistor at different times during the test

Table 4.2. Summary of automatic data acquisition of the reference resistors tests

Reference resistor used (Ohm)	The electrodes used	Scanning time interval (Min)	Average forward resistance (Ohm)	Average backward resistance (Ohm)	Average difference (%)	Average resistance (Ohm)	Standard deviation	Average measurement error (%)
18	1,2,3 and 4	40	17.9172	17.9171	0.021	17.917	0.003	0.460
33	5,6,7 and 8	20	32.848	32.847	0.090	32.847	0.040	0.467
56	25,26,27 and 28	30	55.890	55.887	0.034	55.889	0.014	0.199
100	14,10 ,22 and 18	05	99.527	99.526	0.014	99.526	0.017	0.474
328	47,55,58 and 48	15	327.218	327.229	0.086	327.223	0.365	0.237
470	17,18,19 and 20	30	468.242	468.248	0.023	468.245	0.115	0.373
560	37,38,39 and 40	55	557.184	557.196	0.019	557.190	0.121	0.502
1000	49, 50, 51 and 52	45	1002.229	1002.228	0.018	1002.228	0.232	0.223
3300	61,62,63 and 64	60	3308.228	3308.201	0.006	3308.214	0.294	0.249

Figures 4.6 to 4.8, Figures A.1 to A.16 in Appendix A and Table 4.2 demonstrate that reversing electrode polarity gave almost identical forward and backward readings with a very low percentage difference ranging from 0.006 to 0.09%, which indicates good data quality. In addition, the calculated individual measurement error was very small ranging from 0.199 to 0.502%, which indicates highly accurate measurements. The standard deviation ranges from 0.003 to 0.365 which demonstrates that the readings tend to vary very close to the average, which indicates the high precision of the measurements.

To determine the measurement error of the resistance ranges investigated, Figure 4.9 shows a comparison between the actual and measured values for the data included in the Table 4.2. The low measurement error of 0.21% of the automatic data acquisition mode indicates high accuracy measurements. This error is very close to 0.19% obtained in the four electrode mode which reflects the consistency of the automated acquisition for long periods. Figure 4.10 shows a correlation between the forward and backward readings. The forward and backward readings are almost identical which reflects the high quality of the data collected.

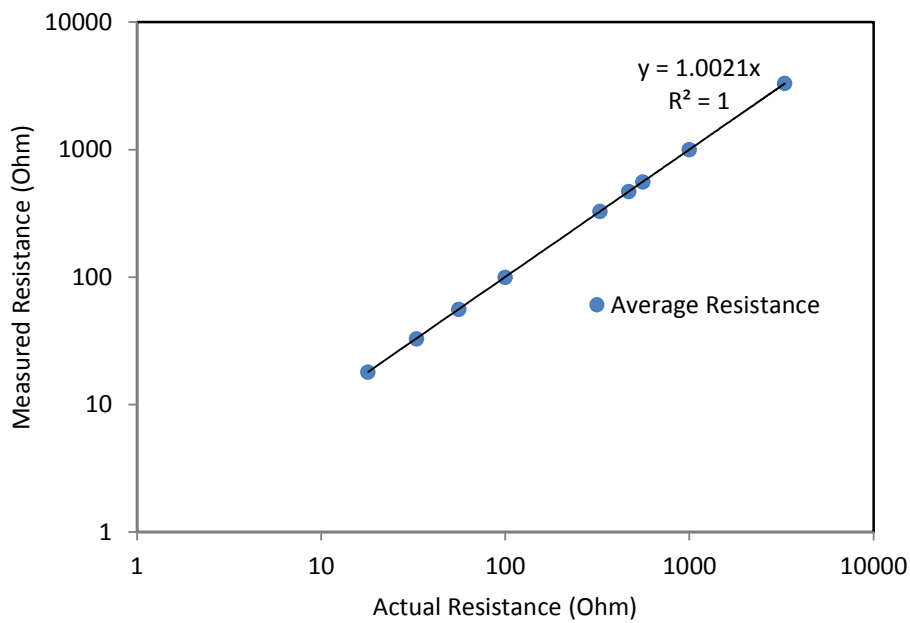


Figure 4.9. A comparison between the actual and measured values of automated data acquisition

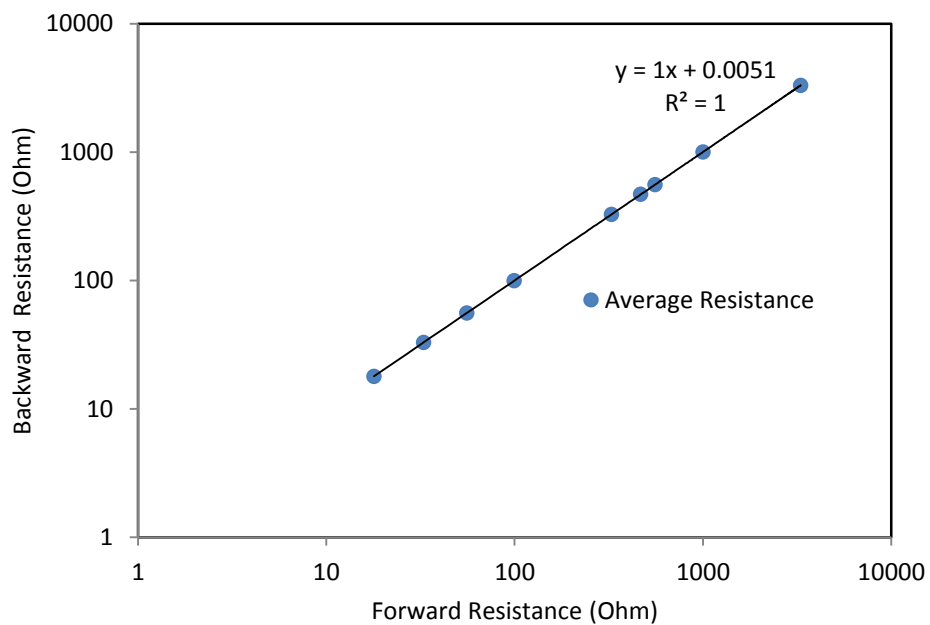


Figure 4.10. A correlation between the forward and backward readings of automated data acquisition

Reciprocity test: Reference resistors

As mentioned earlier, the reciprocity test (swapping current and voltage electrodes) has been considered to be ideal to reveal the consistency of the data acquisition. To examine the switching capability of the system, two and three resistors were attached at the same time to one or more resistivity board. Forward and backward of normal and reciprocal measurements were collected automatically. The reciprocity error, the mean resistance (i.e. the average of normal and reciprocal resistance) and the measurement error were calculated.

One example is presented in this section. The rest of the tests are shown in Figures A.17 to A.22 in Appendix A. Table 4.3 summarises the results.

Figure 4.11 shows normal resistance, reciprocal resistance and reciprocity error of 56 and 68 Ohm resistors tested for 66 hours of automated data acquisition. Figure 4.12 shows the average resistance and the measurement error. The average of normal and reciprocal readings was, respectively, 55.991 and 55.939 of 56 Ohm resistor. For the 68 Ohm resistor, the average of normal and reciprocal readings was, respectively, 67.634 and 67.712 Ohm. The reciprocity error was 0.099 and 0.125% for the 56 and 68 Ohm resistors, with average measurement error of 0.063% and 0.481%, respectively. The low reciprocity error indicates the high quality of the measurements. In addition, the low measurement error demonstrates the high accuracy of the data collected. The low standard deviation of 0.019 and 0.026 for the 65 and 68 Ohm resistors, respectively, confirms the high precision of the measurements.

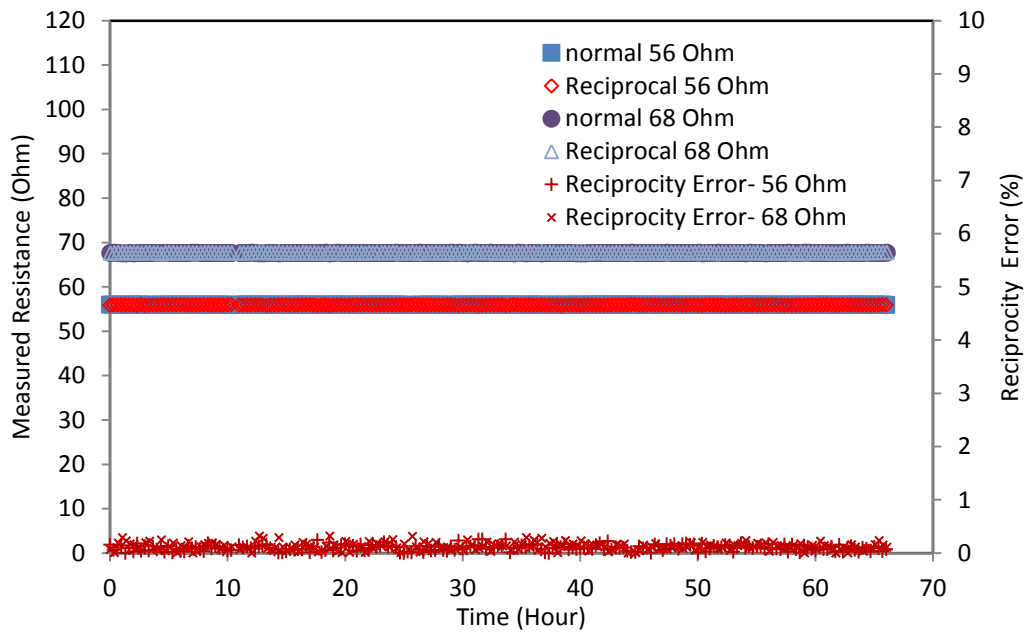


Figure 4.11. Normal resistance, reciprocal resistance and reciprocity error of 56 and 68 Ohm resistor test

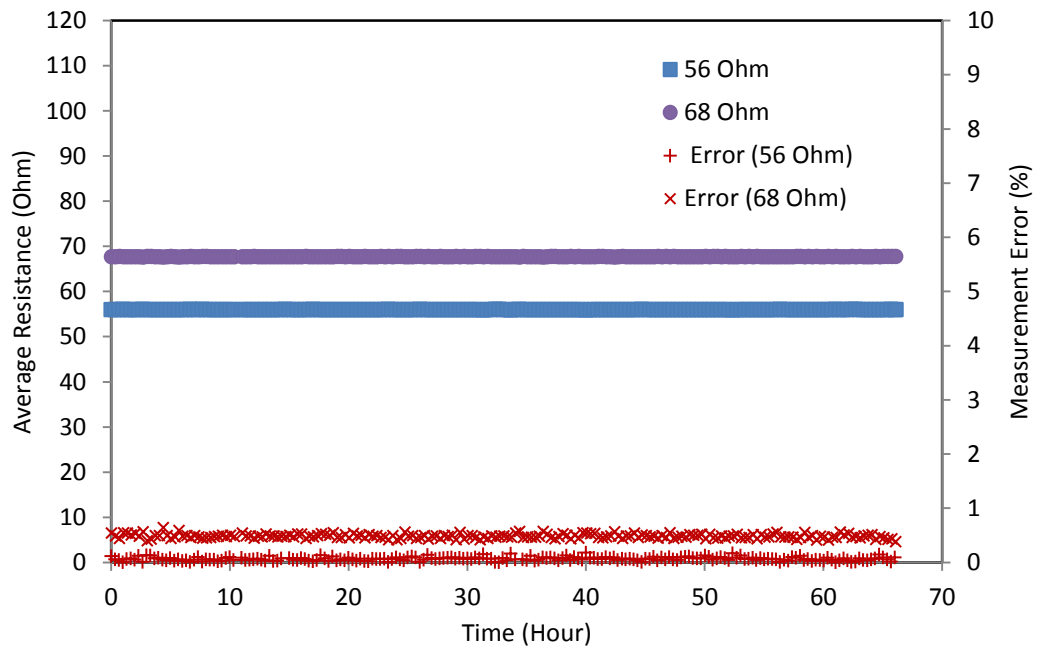


Figure 4.12. Average resistance and measurement error of 56 and 68 Ohm resistor test

Table 4.3. Summary of normal and reciprocal readings of reference resistors

Reference resistor used (Ohm)	Average normal resistance (Ohm)	Average reciprocal resistance (Ohm)	Reciprocity error (%)	Average resistance (Ohm)	Standard deviation	Average measurement Error (%)
13	13.073	13.064	0.077	13.069	0.022	0.731
43	42.700	42.732	0.077	42.715	0.035	0.461
56	55.991	55.939	0.099	55.965	0.019	0.063
68	67.634	67.712	0.125	67.673	0.026	0.481
100	99.211	99.202	0.012	99.206	0.006	0.793
390	389.091	389.042	0.013	389.067	0.018	0.239
470	466.727	466.748	0.019	466.737	0.089	0.694
560	557.204	557.360	0.034	557.282	0.108	0.485
1000	1002.026	1002.069	0.015	1002.047	0.129	0.205

Figures 4.11 and 4.12, Figures A.17 to A.22 in Appendix A and Table 4.3 demonstrate that swapping current and voltage electrodes polarity gave nearly identical readings with a low reciprocity error ranging from 0.012 to 0.125%, and low measurement error ranging from 0.063 to 0.793%, indicating highly accurate measurements. The low standard deviation ranges from 0.006 to 0.129 means that the readings tend to vary very close to the accurate average.

Figure 4.13 shows a correlation between normal and reciprocal readings for the data included in Table 4.3. Normal and reciprocal measurements are very well correlated which reflects the consistency of the measurements.

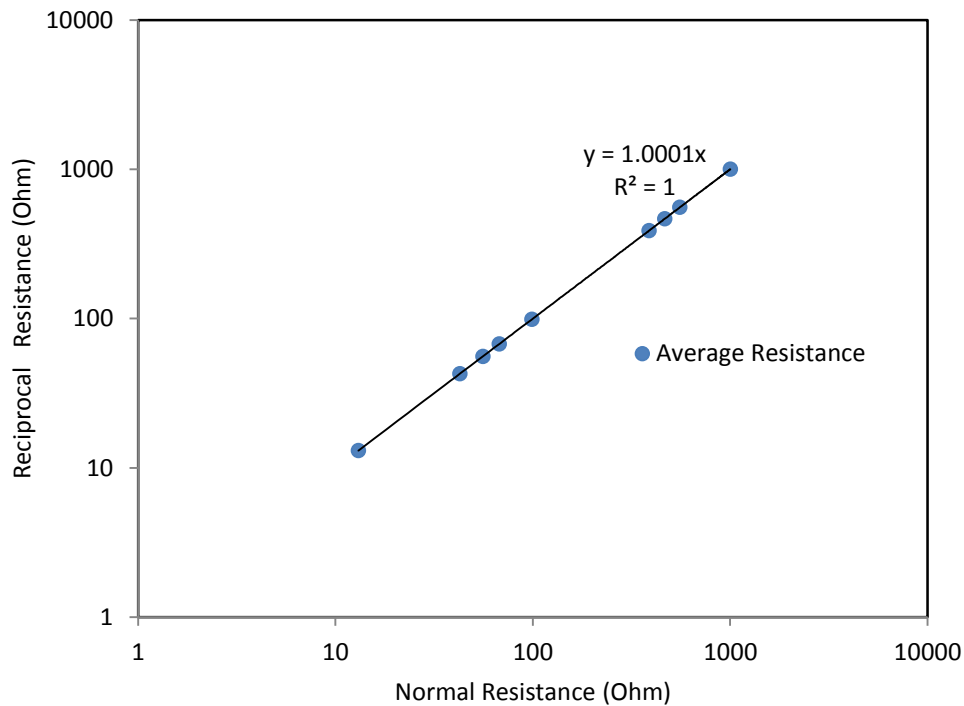


Figure 4.13. The measured normal and reciprocal readings

To summarise, the automated data acquisition of a wide range of reference resistors demonstrates that reversing electrode polarity and swapping current and voltage electrodes give, as should be, almost identical readings with a low measurement error that does not require calibration (ASTM G57, 2006). The low measurement error indicates the high accuracy of the measurements, and the measurement system (electronic circuits) has a low noise (LaBrecque and Daily, 2008), which is one of the requirements for any efficient resistivity system (Damasceno et al., 2009). The low standard deviation demonstrates that the measurements tend to vary close to the "accurate" average which means that the readings are consistent with high precision. However, the system needs to be tested using soils with a wide range of resistivity. Therefore, a series of tests were carried out using different soils, and the outputs were compared with those collected using standard resistivity instrument, as will be described in the subsequent sections.

Reciprocity test: Soils

A series of the reciprocity error tests was carried out using clay and sand specimens to cover a wide range of resistivity. To better examine the precision of the data collection, normal and reciprocal resistivity readings were first collected at constant water content for sealed specimens prepared at different gravimetric water contents. This can show the degree to which repeated measurements under the same conditions (i.e. constant water content) gives the same results. Normal resistivity, reciprocal resistivity, average resistivity and reciprocity error were calculated. Since normal and reciprocal measurements use different signal paths (LaBrecque and Daily, 2008), small differences between normal and reciprocal readings are expected due to soil heterogeneity. However, high reciprocity error might indicate inconsistency in the data acquisition due to, for example, bad electrode contact and random noise induced by the equipment itself. Therefore, this test can reveal the inconsistency of the data collected.

Reciprocity tests were conducted on BIONICS clay specimens prepared at 25%, 20%, 15%, 12% and 10% gravimetric water content. To better check the reproducibility of the data, two tests were conducted on two specimens prepared at 15% water content. To examine the system using soil with a higher resistivity, reciprocity tests were also conducted using sand specimens prepared at 30% and 15% gravimetric water content. The automated measurements were collected continuously for 48 hours. One example is presented in this section. The rest of the tests are presented in Figures A.23 to A.29 in Appendix A. Table 4.4 summarises the results of all specimens tested.

Figure 4.14 shows the reciprocity test results of clay specimen prepared at 25% water content. The average of normal resistivity, reciprocal resistivity, average resistivity and reciprocity error was 10.64 Ohm.m, 10.86 Ohm, 10.75 Ohm.m and 2.05%, respectively. The standard deviation was 0.126.

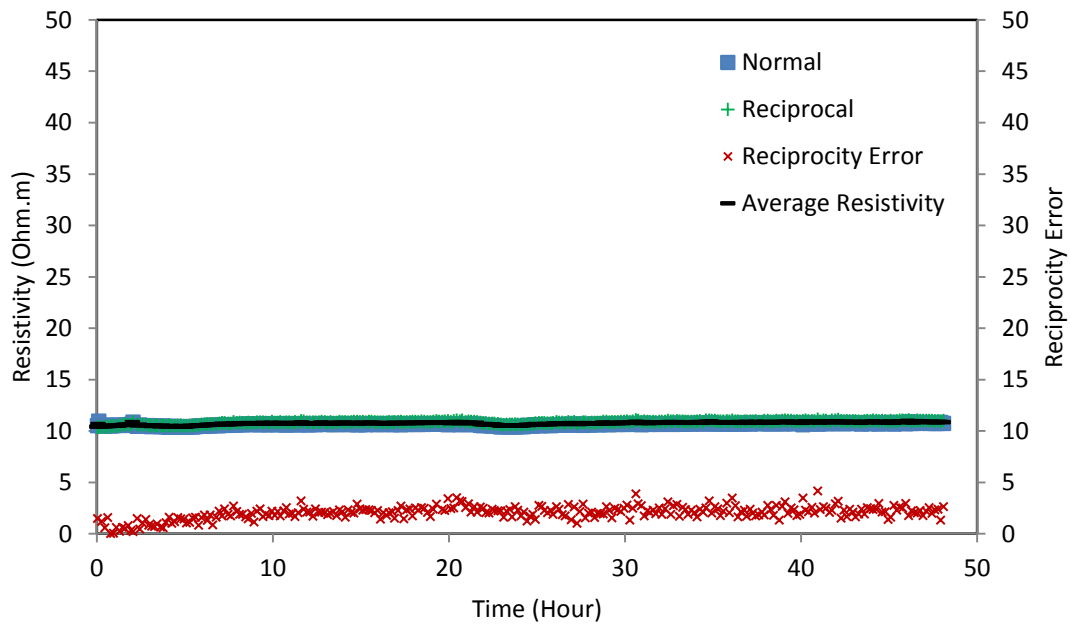


Figure 4.14. Reciprocity test results of clay specimen prepared at 25% water content

Table 4.4. Summary of reciprocity tests of clay and sand specimens

Soil	Gravimetric water content (%)	Average normal resistivity (Ohm.m)	Average reciprocal resistivity (Ohm.m)	Average resistivity (Ohm.m)	Standard deviation	Average reciprocity error (%)
Clay	25	10.64	10.86	10.75	0.126	2.05
Clay	20	12.57	12.77	12.67	0.044	1.51
Clay	15 (1)	14.15	14.26	14.20	0.091	0.81
Clay	15 (2)	14.17	14.54	14.35	0.044	2.57
Clay	12	20.68	21.35	21.02	0.120	3.20
Clay	10	36.72	38.32	37.52	0.808	4.24
Sand	30	140.32	142.92	141.62	0.576	1.84
Sand	15	305.25	310.09	307.67	1.659	1.59

Figure 4.14, Figures A.23 to A.29 in Appendix A and Table 4.4 show that the reciprocity error for the specimens tested ranged from 0.81 to 4.24 %. This indicates the consistency of the data collected. However, at low water content (e.g. 12 and 10%) of BIONICS clay, the error was relatively high. At low water content, where pores are partially filled with air, differences in saturation are expected. Therefore, electrical paths become discontinuous (Fukue et al. 1999), and the current might follow different pathways causing a relatively high reciprocity error "difference" between the normal and reciprocal readings (LaBrecque and Daily, 2008). Nevertheless, the overall reciprocity error is acceptable (<5%). In addition, the two tests conducted on BIONICS clay prepared at 15% water content indicate the high repeatability of the measurements, as the average resistivity was 14.20 and 14.35 Ohm.m, with a standard deviation of 0.091 and 0.044, for specimens (1) and (2), respectively. Moreover, at a relatively unchanged condition (i.e. constant water content), the measurements show high precision with low standard deviation ranges from 0.044 to 1.659. The redistribution of water in the soil during the test could cause differences in the reciprocity error measured over the time.

It can be seen from Table 4.4 that resistivity decreases with increasing gravimetric water content of clay and sand specimens. Increasing the water content makes more water available for electrical conduction, and, therefore decreases the resistivity. To determine the overall reciprocity error for the resistivity range investigated, average normal and reciprocal resistivity readings of all specimens included in Table 4.4 are plotted in Figure 4.15. Normal and reciprocal readings are highly correlated with low reciprocal error of 1.67%.

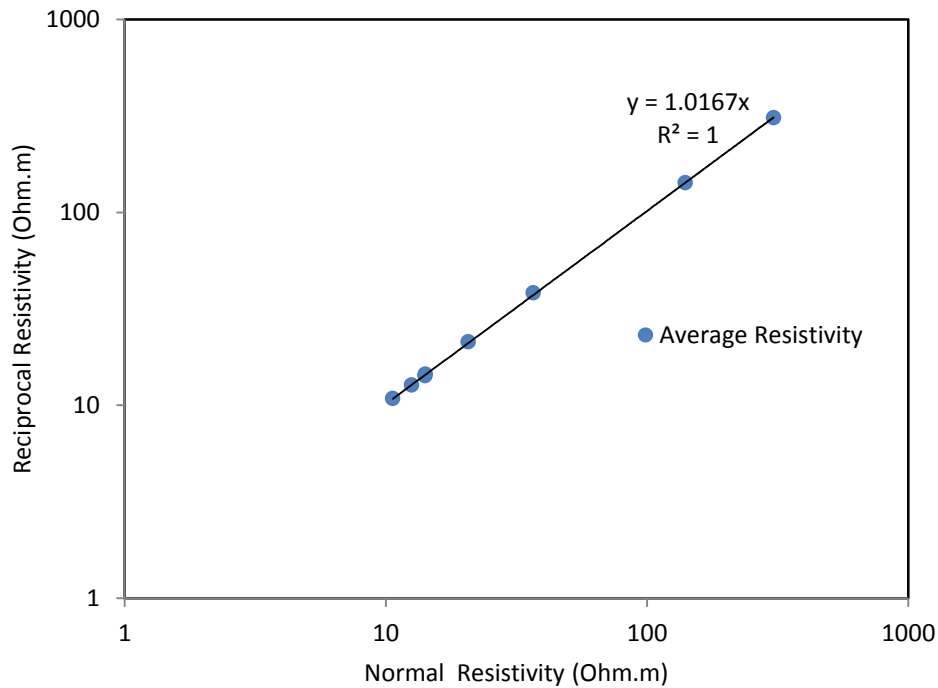


Figure 4.15 A correlation between normal and reciprocal readings of all soil specimens investigated

4.3 Validation

Resistivity of soil may vary within a range. Therefore, to validate the outputs, a comparison with a standard resistivity system is useful. This comparison proves the performance validity of the instrument and confirms that the measurement method adopted is valid for future tests. Therefore, a series of tests were conducted to compare the outputs of Resist with standard commercial instruments, as described below.

4.3.1 Resistivity and conductivity

Resistivity is the inverse of the conductivity. Therefore, a comparison between the resistivity measured using Resist, and conductivity measured using a conductivity meter of chemical solutions was used to validate the outputs of the system.

Using the measurement and calibration procedures described in Chapter 3, the electrical conductivity of ten KCl solutions placed in the circular cell was measured using a HANNA HI 9835 conductivity meter, calibrated using a standard solution type HI 70031. The corresponding average resistivity of eight readings obtained by Resist (using the experimental geometric factors obtained from Figure 3.11 in Chapter 3), for three arrays Square (0.1971), Wenner (0.1079) and Dipole-Dipole (0.3872) were used to produce the correlation shown in Figure 4.16. The near-unity linear correlation confirms the validity of the measurements (Sheffer et al., 2007; Damasceno et al., 2009). A similar correlation using KCl solution from Sreedeeep et al., (2005) is shown for comparison.

Using the experimental geometric factors, the average of normal and reciprocal resistivity of square, Wenner and Dipole- dipole arrays of BIONICS sample (w=40%) placed in the circular cell were calculated. Figure 4.17 shows α -resistivity, β -resistivity, $A\nu$ - resistivity and AI of square array. The measured resistivities of eight readings, and AI (close to 1) indicate the homogenous background of the soil. Similarly, Figure 4.18 shows the average of normal and reciprocal resistivity of Square, Wenner and Dipole-Dipole arrays. The measured resistivities using different arrays are consistent. This indicates the validation of the experimental geometric factors obtained.

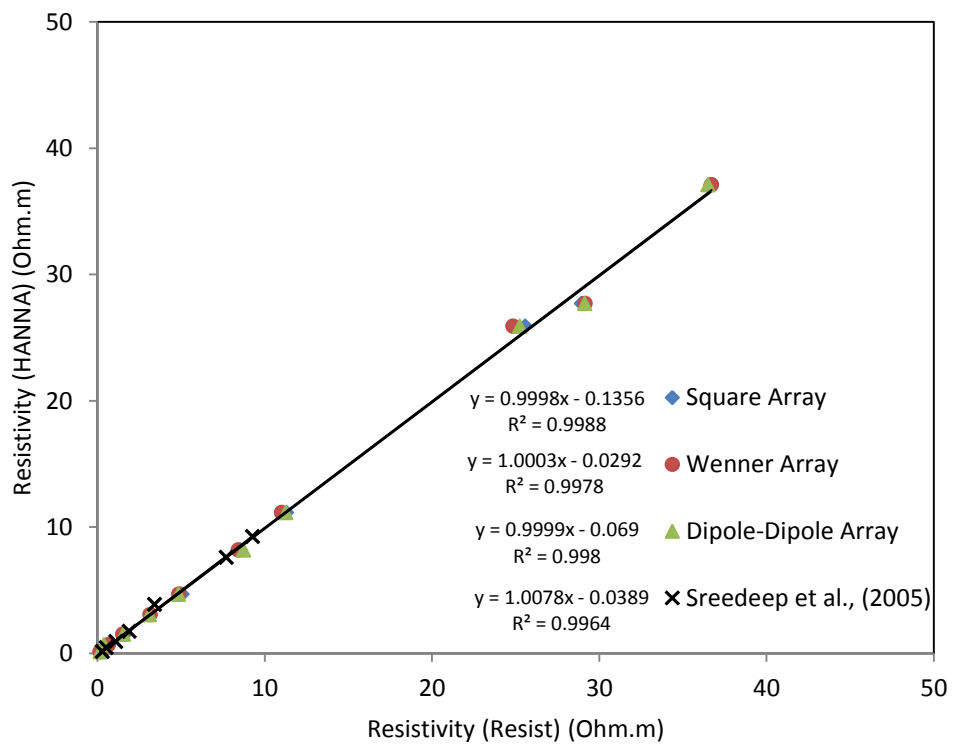


Figure 4.16. A correlation between resistivity of ten KCl solutions measured by Resist and HANNA conductivity meter for three arrays

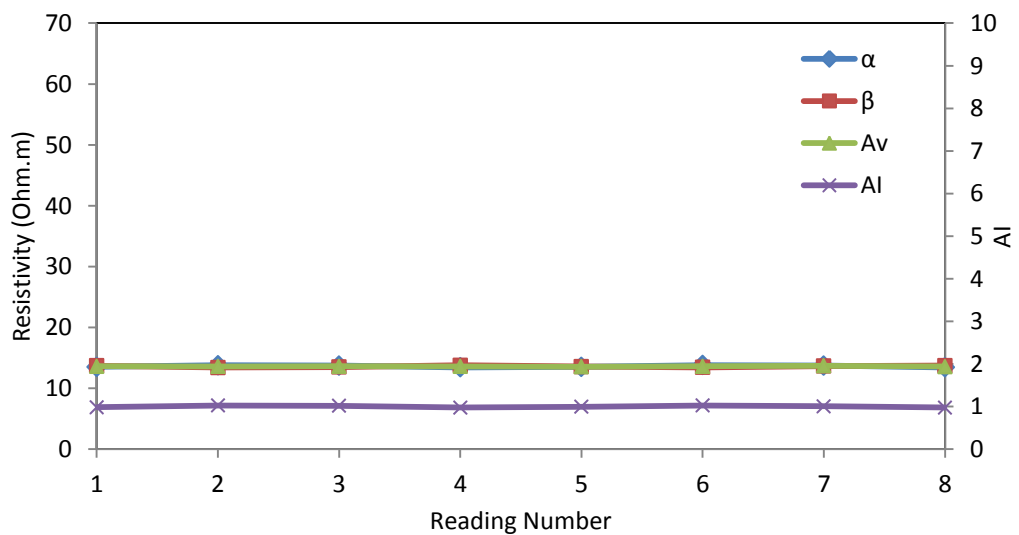


Figure 4.17. The resistivity of BIONICS soil measured using the square array

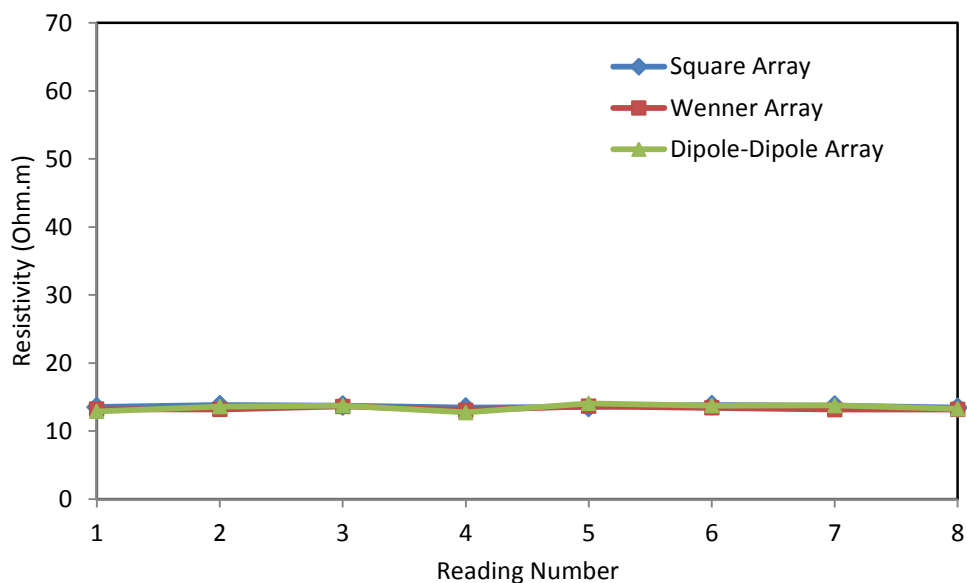


Figure 4.18. The resistivity of BIONICS soil measured using Square, Wenner and Dipole-Dipole array

4.3.2 Resist and Terrameter SAS 300 C

A four electrode method

Figure 4.19 and 4.20 show the resistivity-gravimetric water content relationship of BIONICS clay specimens using a Miller resistivity box, obtained using the Terrameter and Resist, respectively. Normal resistivity, reciprocal resistivity and reciprocity error were calculated. The average reciprocity error of the Terrameter and Resist readings was 1.22% and 2.07%, respectively. Again, at low water content, the reciprocity error was relatively high. The maximum error was 4.46% and 5.91% for the Terrameter and Resist, respectively.

Figure 4.21 shows a comparison of the average resistivity measured using the Terrameter and Resist with the reciprocity error. Figure 4.22 shows a correlation between the normal and reciprocal data calculated. A good comparison between the Terrameter and Resist readings can be noticed with an average difference of 1.12%. The normal and reciprocal readings are highly correlated.

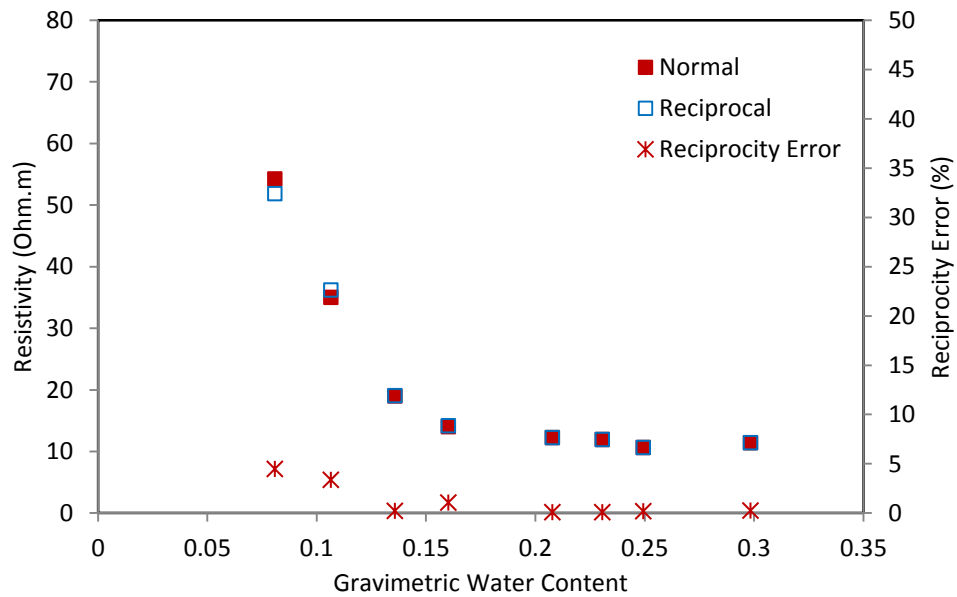


Figure 4.19. The resistivity-gravimetric water content relationship of BIONICS specimens obtained using the Terrameter

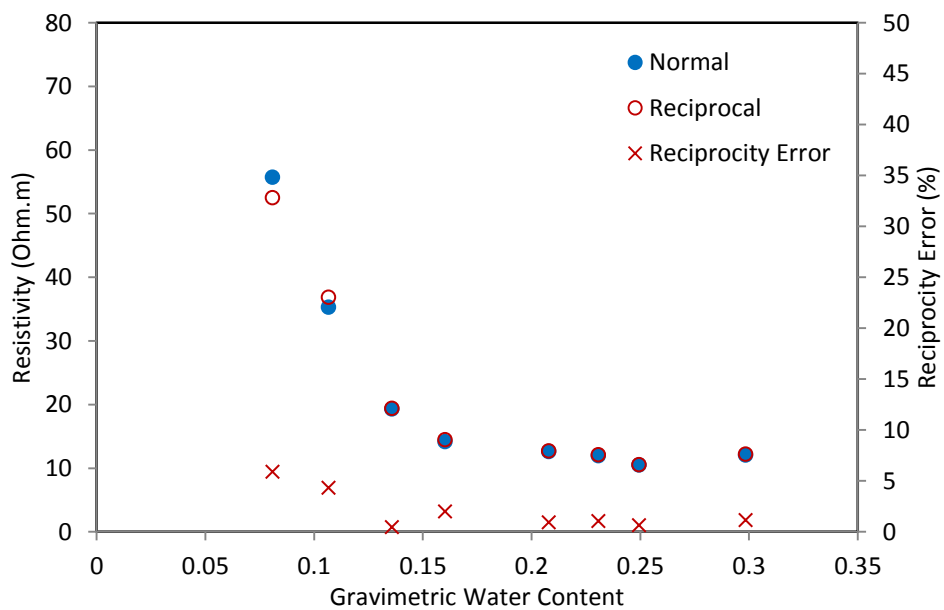


Figure 4.20. The resistivity-gravimetric water content relationship of BIONICS specimens obtained using Resist

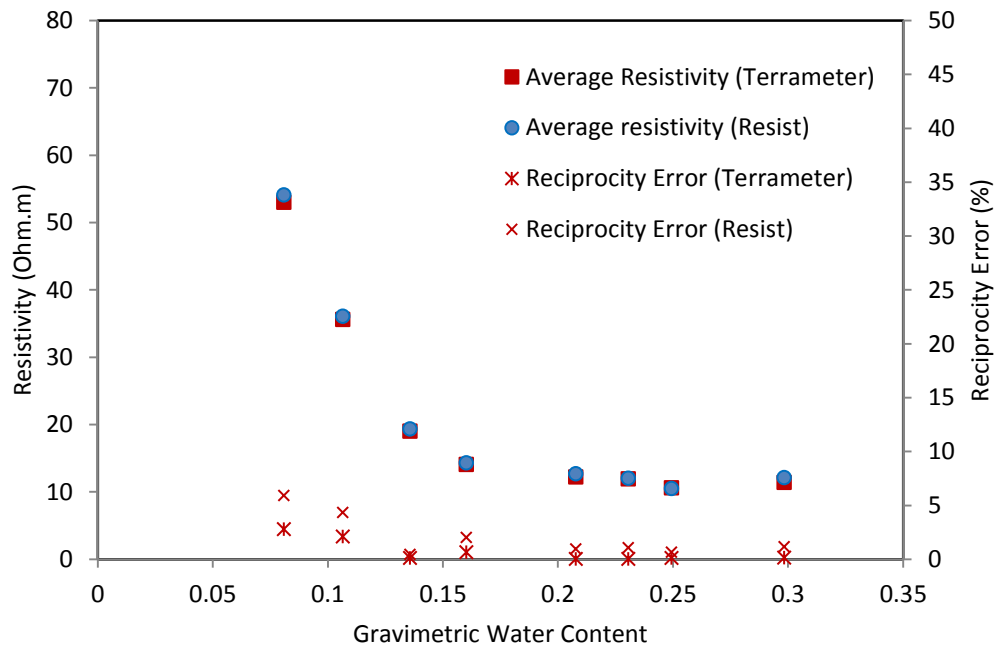


Figure 4.21. A comparison between the average resistivity measured using Resist and the Terrameter for the BIONICS specimens

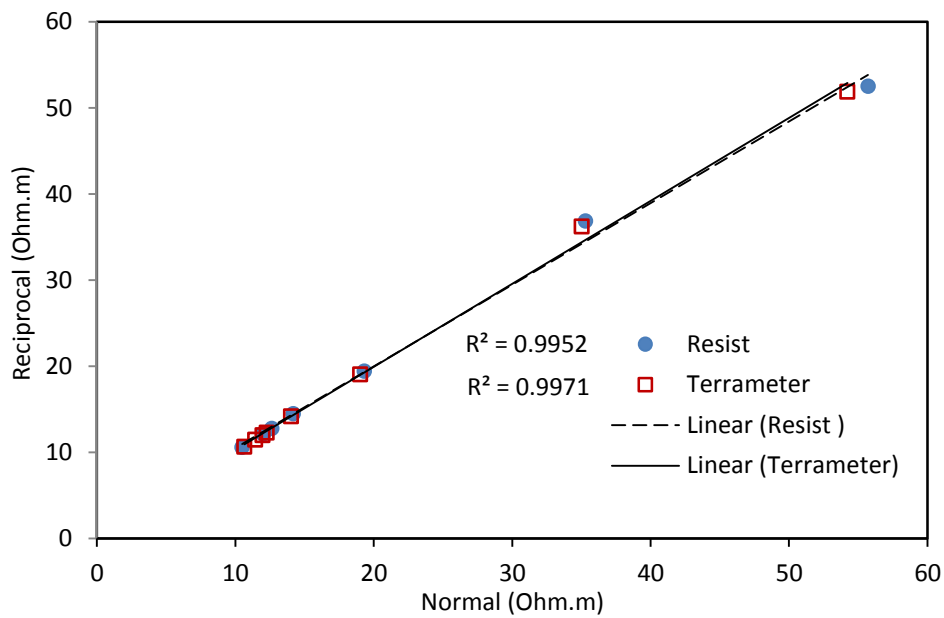


Figure 4.22. A correlation between normal and reciprocal data calculated using Resist and the Terrameter

In general, the range of the measured resistivity is within the typical resistivity range of clay soils, and the resistivity-water content relationship follows the power law relationship reported in the literature (e.g. Calamita et al., 2012). Resistivity decreases with increasing water content, and at low water content, resistivity decreases more rapidly. Since electrical conduction takes place via ions in the pore water, at high water content, more ions are accessible for the current and therefore low resistivity. At low water content, pore water is partially replaced by air and therefore high resistivity, and the resistivity changes more rapidly. These general findings are consistent with numerous papers (e.g. Russell and Barker, 2010; Yan et al., 2012). The soil water content features of BIONICS clay will be further analysed in Chapter 5.

Monitoring water content changes of the clay soil during drying and wetting is one of the objectives of the current thesis. Therefore, a drying test was conducted on Kaolin and sand specimens, and a correlation was made between the resistivity data collected using Resist and the Terrameter. Figures 4.23 and 4.24 show the resistivity-gravimetric water content relationship of a Kaolin and fine-grained sand specimens, respectively. As expected, resistivity increases as water content decreases because of drying.

A good comparison between Resist and the Terrameter can be seen with a maximum difference of 1.6%, 3.8% for Kaolin and sand, respectively. A relatively high difference was noticed at low water content in Figure 4.24 probably due to the electrode contact resistance at this level of water content (Gupta and Hanks, 1972). Further drying and wetting tests on BIONICS, local and pure clays will be presented in chapter 7.

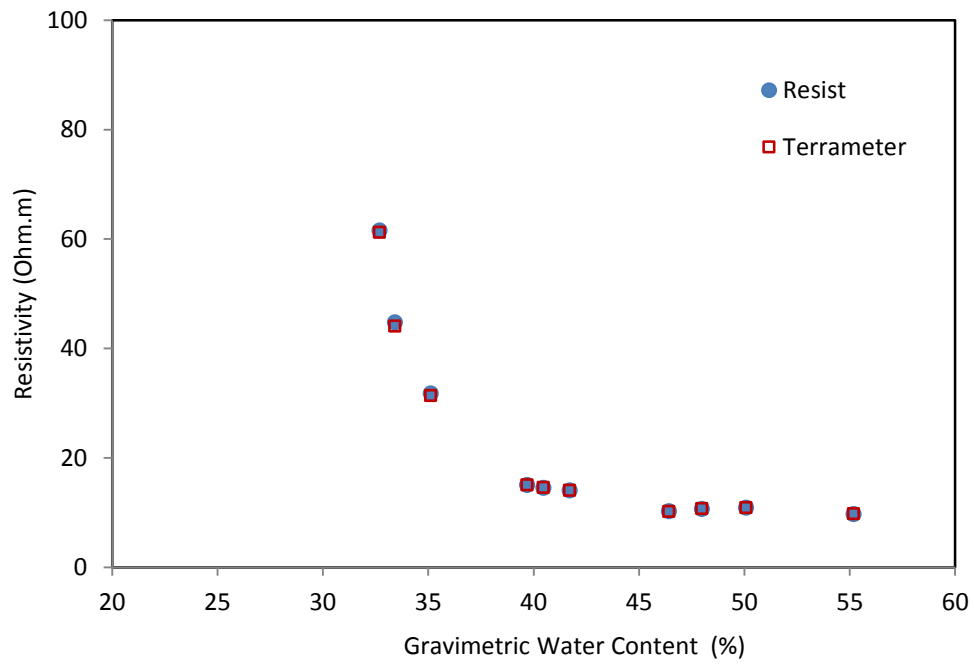


Figure 4.23. Resistivity-gravimetric water content relationship of Kaolin specimen during drying

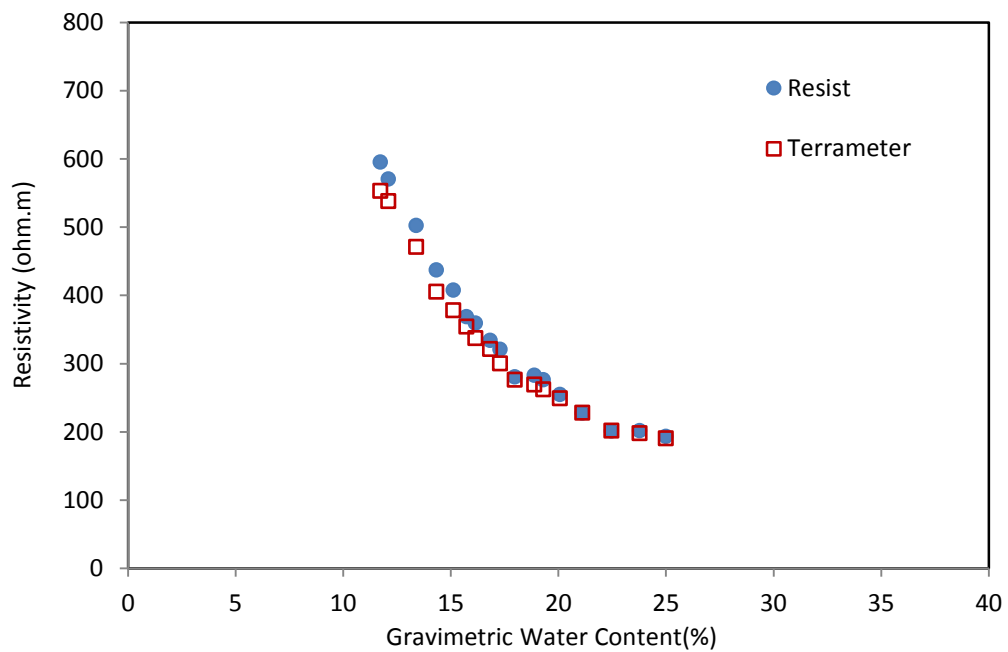


Figure 4.24. Resistivity-gravimetric water content of sand specimen during drying

Horizontal profiling

Horizontal profiling or Constant Separation Traversing CST can be performed by moving an array with fixed electrode spacing along a profile to detect the lateral resistivity variations. As a common practice, water is used to test the proposed setup in laboratory studies, as water represents a homogenous medium for resistivity measurements (e.g. Chambers et al., 2004; LaBrecque and Daily, 2008). Adopting the Werkema et al. (2000) procedure, a plastic container (60x40x25cm) filled with tap water, and equipped with 16 electrodes fixed in a wood strip, was used in a CST test.

In the first stage, the measurements were collected using Wenner array with constant electrode spacing of 3 cm by Resist and the Terrameter as shown in Figure 4.25. In the second stage, the procedure was repeated with a plastic sheet (3cm depth, 0.5cm width and 14cm length) inserted between the electrode 8 and 9 (i.e. at 0.225cm X distance), as shown in Figure 4.26. Plastic/glass sheets have commonly been used to assess the capabilities of resistivity equipment and the experimental setup (e.g. Werkema et al., 2000; Leontarakis and Apostolopoulos, 2012).

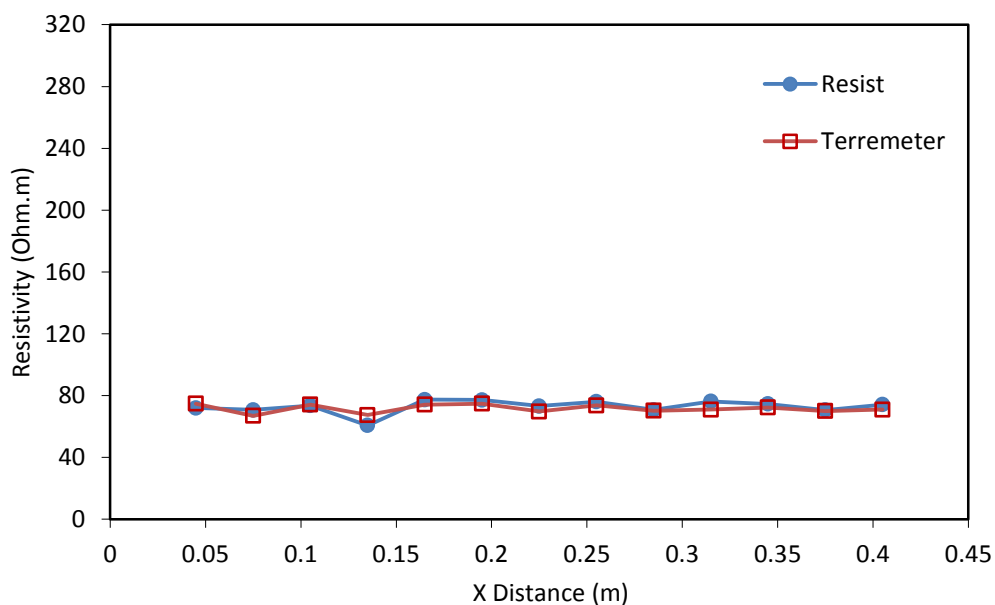


Figure 4.25. Resistivity profile of the water-filled container (stage one)

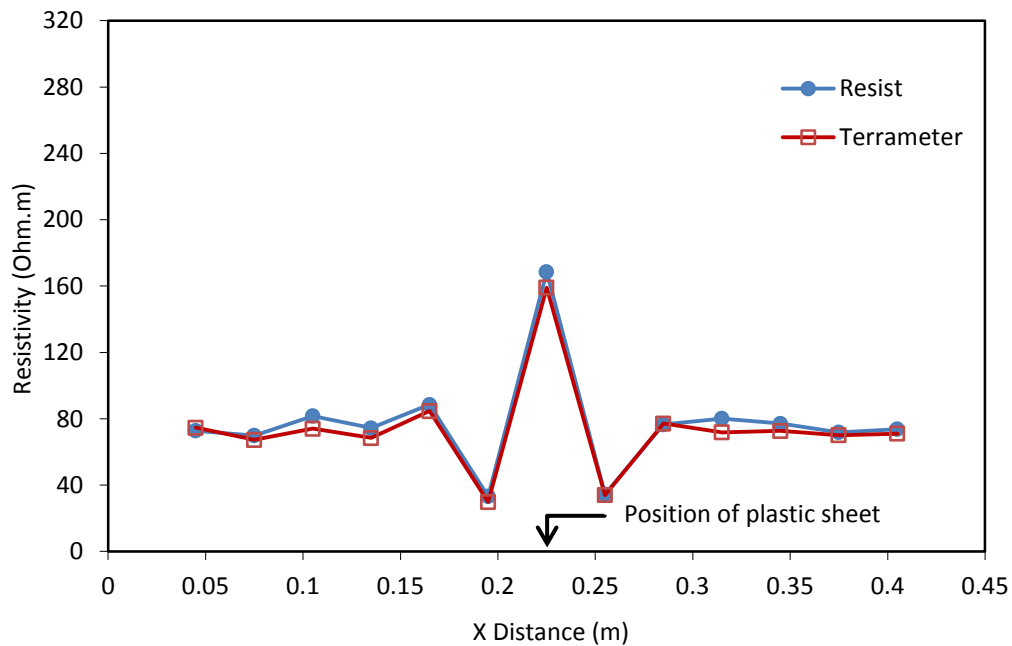


Figure 4.26. Resistivity profile of the water-filled container (stage two)

The CST profile in Figure 4.25 shows that the resistivity does not change horizontally which reflects the homogenous resistivity of the medium. As the resistivity of plastic is high, inserting the plastic sheet causes an increase in resistivity at 0.225 cm X distance, as shown in Figure 4.26. A good comparison between Resist and the Terrameter can be seen with a maximum difference of 5.3% and 5.5% in stage one and stage two, respectively.

The experiment was repeated using a manually compacted sand ($w=20\%$). Again, a good comparison between Resist and the Terrameter can be seen with a maximum difference of 2.3% and 6.1% in stage one Figure 4.27 and stage two Figure 4.28, respectively. Small resistivity differences were noticed during the experiment due to a rise of water because of the capillary action.

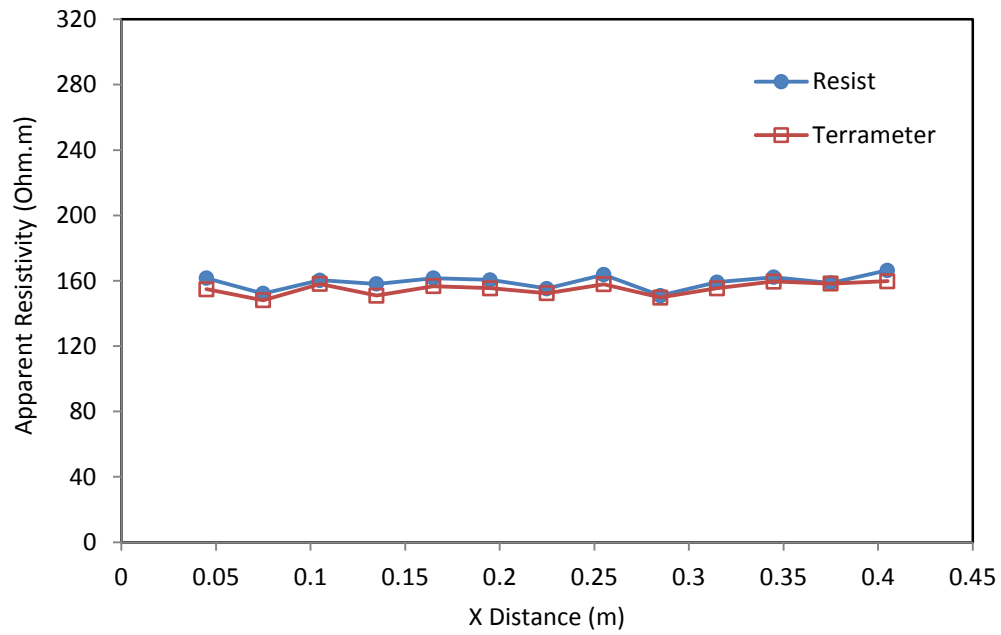


Figure 4.27. Resistivity profile of the sand-filled container (stage one)

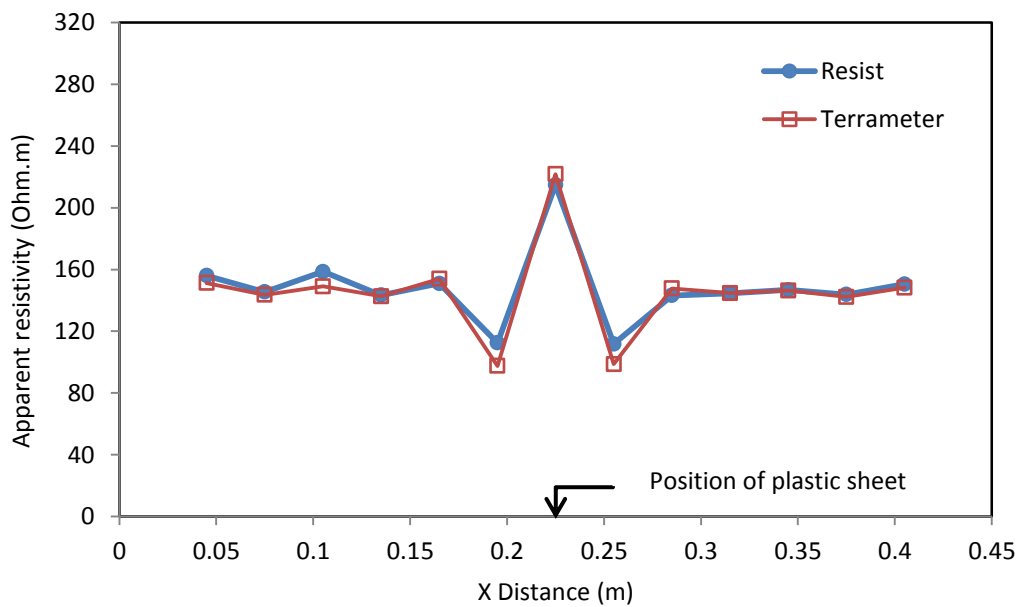


Figure 4.28. Resistivity profile of the sand-filled container (stage two)

A 2D ERT test

A 2D ERT test was conducted using the same setup described in CST test. Wenner array was used for four acquisition levels with a minimum electrode spacing of 3 cm. The plastic container was filled with water in the first stage then a plastic sheet (3 cm depth, 0.5 cm width, and 7 cm length) was inserted at 0.225 cm X distance in the second stage to examine the imaging ability of the system. The measurements were collected using Resist and the Terrameter.

2D ERT profiles were constructed using smoothness constrained method of ZONDRES2D software (<http://zond-geo.ru/english/zond-software/ert-and-ves/zondres2d>). Figure 4.29 shows the resistivity sections of stage one. A homogenous resistivity background can be seen in Figure (4.29a&b) which were obtained using Resist and the Terrameter, respectively. Resistivity profiles at different depths plotted in Figure (4.29c&d) which were obtained using Resist and the Terrameter, respectively, indicate that resistivity does not change with depth.

Figure 4.30 shows the resistivity sections of stage two. The high resistivity of the plastic sheet is clearly visible in the resistivity sections, as shown in Figure 4.30a&b, which were obtained using Resist and the Terrameter, respectively. Resistivity profiles at different depths Figure 4.30c&d obtained, respectively, using Resist and the Terrameter, show that resistivity changes considerably with depth at 0.22 X distance.

Figures 4.29 and 4.30 indicate a good correlation between 2D ERT sections collected using Resist and the Terrameter. Some differences in resistivity were expected due to local changes in water resistivity. However, this test demonstrates the ability of the system to resolve resistivity changes introduced by structures of small dimensions such as soil cracks. In all models tested, a good convergence between the observed and the calculated model was achieved, as indicated by the small RMS errors (Loke, 2014).

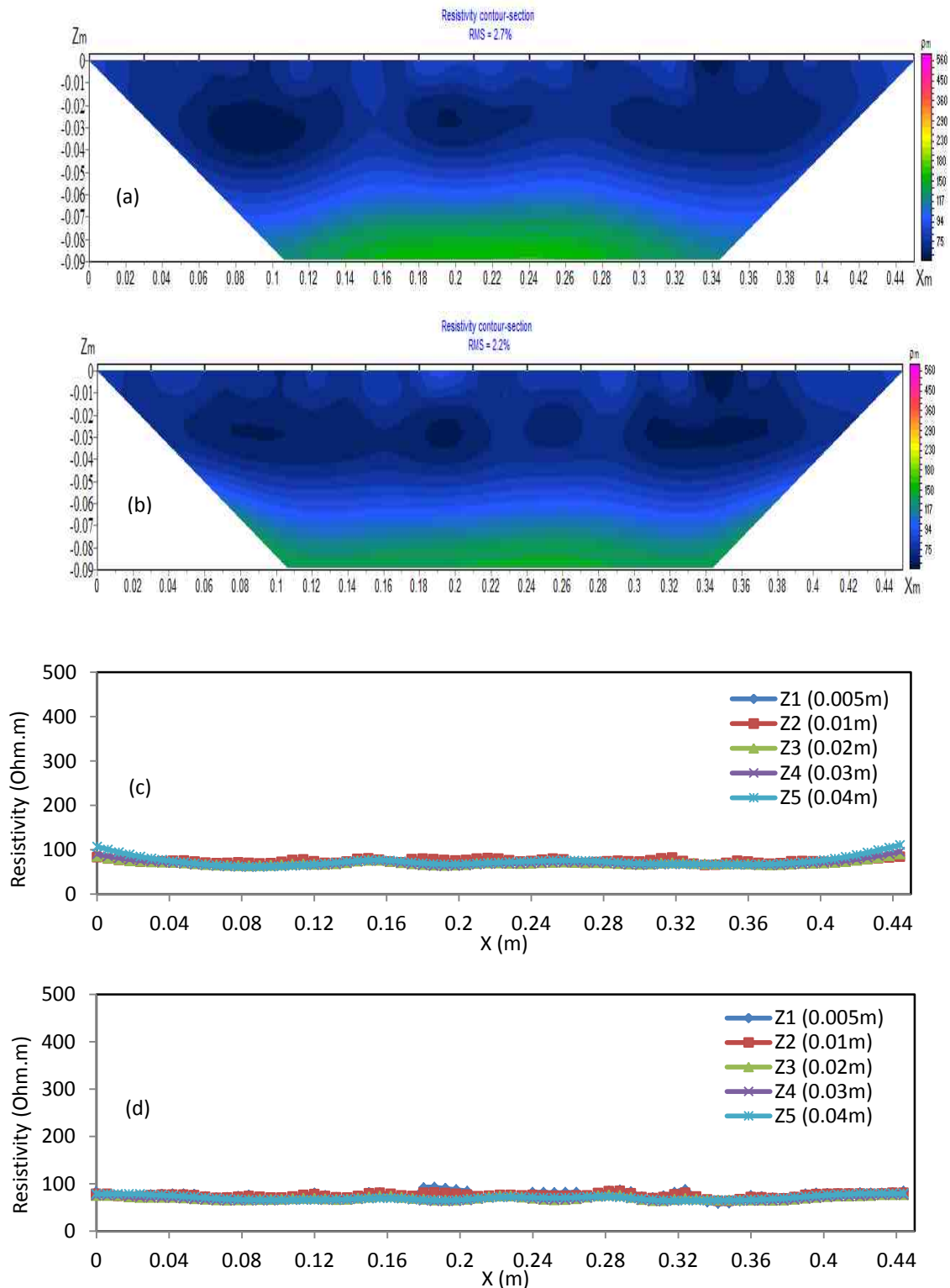


Figure 4.29. Resistivity sections of the water-filled container, Stage one, 2D sections; (a) Resist, (b) the Terrameter, resistivity profiles at different depths; (c) Resist, (d) the Terrameter

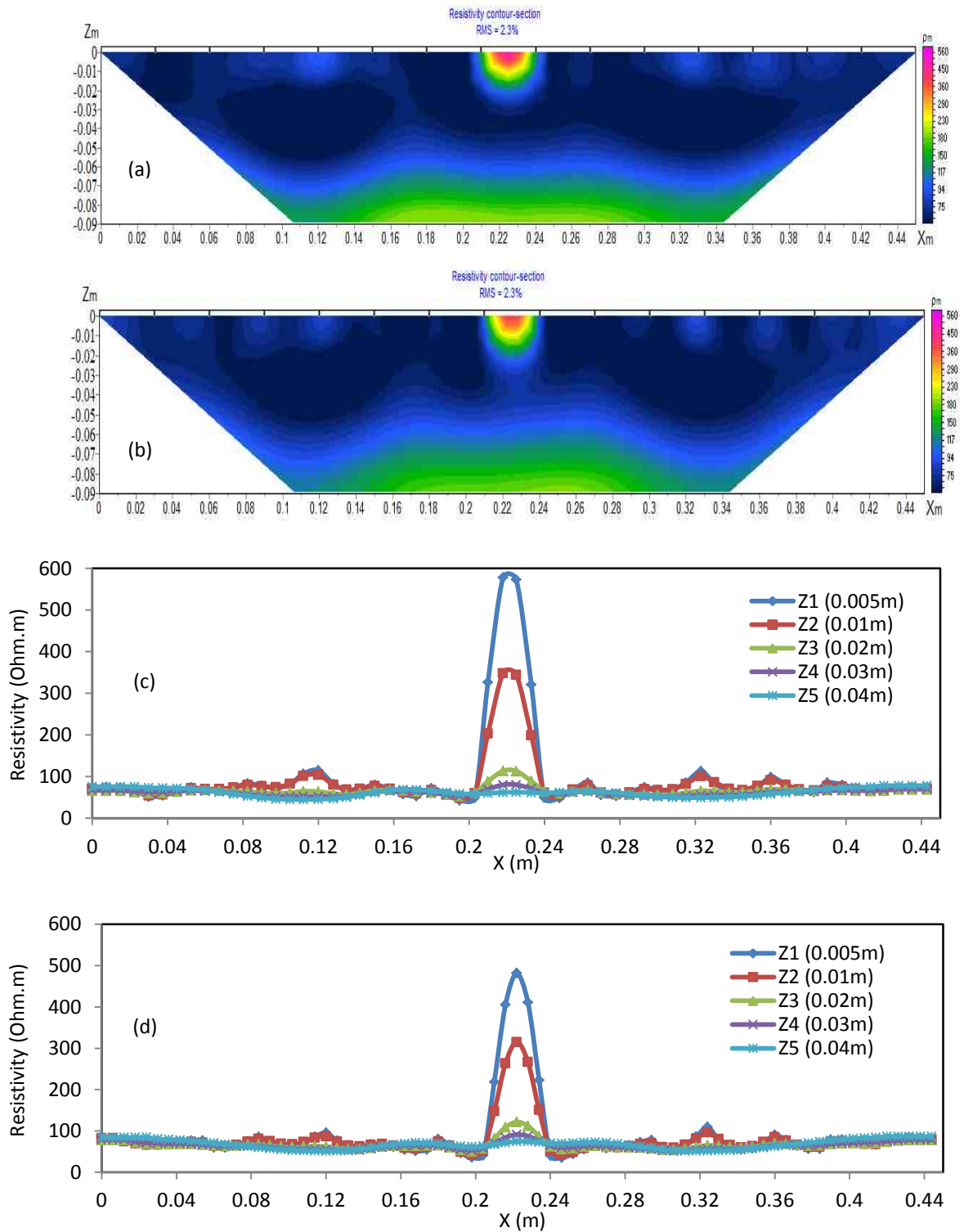


Figure 4.30. Resistivity sections of the water-filled container, Stage two, 2D sections; (a) Resist, (b) the Terrameter, resistivity profiles at different depths; (c) Resist, (d) the Terrameter

4.4 Chapter summary

This chapter described the calibration and validation of the resistivity system developed in the current thesis. A wide range of reference resistors and different soils was used to check the data quality of the system. Accuracy, precision and resolution of the measurements were assessed. The outputs were correlated with those collected with standard commercial instruments at different situations.

Using a wide range of reference resistors, high accuracy and precision measurements were indicated. The results showed that reversing electrode polarity and swapping current and voltage electrodes give almost identical readings with a low measurement error. The measurement error was 0.19% in four electrode method and 0.21% in the automated and continuous data acquisition. This reflects the high accuracy of the system developed and the consistency of the automated data acquisition for long periods. The low standard deviation of the readings demonstrates that the measurements tend to vary close to the "accurate" average which means that the readings are consistent with high precision.

To validate the system, the outputs were compared with those collected using standard conductivity and resistivity meters. For a range of solutions with different concentrations, the readings correlated very well with conductivities measured using a conductivity meter. The outputs of the system were also compared with Terrameter SAS 300 C resistivity system in a four-electrode method, horizontal profiling and 2D ERT tests. The results showed a good comparison with low percentage difference for different soils.

The laboratory results confirmed the validity of the system for automated data collection which is one of the recent advances in the resistivity instrumentation. Therefore, the system was adopted to carry out the laboratory work described in this thesis, particularly to investigate the water content characteristics of unsaturated clay soil and to consider the influence of wetting, drying and cracking of the soil.

Chapter 5

Water content characteristics of mechanically compacted clay soil

For geotechnical testing, a number of lab and field based techniques have been developed to investigate soil water content characteristics. Among others, the electrical resistivity method provides a non-invasive, quick and low cost estimate of water content. However, electrical resistivity values of compacted clay soils is influenced, in addition to water content, by various interlinked parameters that all need to be addressed to obtain reliable water content measurements. This chapter is dedicated to investigating the water content characteristics of mechanically compacted clay soil using the resistivity method. Clay specimens from the source used in the construction of the BIONICS embankment, and compacted at various water contents, were used to investigate the influence of compaction key variables (e.g. water content, density, compaction method and compaction effort) on soil resistivity. At each gravimetric water content, the specimens were compacted using dynamic (standard Proctor and Modified) and static methods for a range of dry densities. To measure soil resistivity, a small resistivity probe, described in Chapter 3, was used. Gravimetric water content, volumetric water content and degree of saturation were correlated with the measured resistivity. The results are discussed according to the microstructure characteristics of compacted clay soils.

5.1 Introduction

A wide range of techniques has been developed to measure in situ soil water content. Numerous reviews (e.g. Western et al., 2002; Robinson et al., 2003; Evett and Parkin, 2005; Muñoz-Carpena et al., 2006; Robinson et al., 2008; Vereecken et al., 2008; Seneviratne et al., 2010; Bittelli, 2011) have been published. The advantages and drawbacks

of these techniques were discussed in Chapter 2. However, there is an increasing interest in exploring efficient techniques to measure soil water content at laboratory and field scales.

Compared to in situ water content sensors, the resistivity method is non invasive and the measurements can be integrated into a larger 3D volume by increasing the electrode spacing. Moreover, the method has been indicated as an effective technique for the estimation of the spatiotemporal variability of water content at various scales (e.g. Walker and Houser, 2002; Calamita et al. 2012).

The resistivity method has been in used in geotechnical testing for evaluating soil compaction (e.g. McCarter, 1984; Sawazaki et al., 2009; Seladji et al., 2010; Zha et al., 2010), monitoring water content changes (e.g. Jackson et al., 2002; Amidu and Dunbar, 2007; Muñoz-Castelblanc et al., 2011) and investigating correlations with other parameters such as soil void ratio (Kim et al., 2011), dry density (Beck et al., 2011), pore water conductivity (Rinaldi and Cuestas 2002) and hydraulic conductivity (Abu-Hassanein et al., 1996). In a review paper, Bryson (2005) evaluated the geotechnical parameters using the resistivity method. He concluded that the parameters that affect the hydraulic flow also affect the electrical conduction in soils; therefore, there is the likelihood that the resistivity method can be used to address some geotechnical properties of soils.

In particular, a proxy relationship between soil resistivity and water content has been indicated in numerous studies. As reviewed in Chapter 2, a number of authors have reported the usefulness of using the resistivity method to estimate water content at various scales. However, in addition to water content, the hydraulic properties of compacted clay soils are affected by other compaction key variables such as density, compaction method and compaction effort (Mitchell et al., 1965). These variables affect the shape, size and connectivity of pores (Benson and Daniel, 1990; Daniel and Benson, 1990). Like water, electrical conduction paths are affected by pore properties; therefore, soil resistivity is expected to be influenced by the above mentioned compaction variables (Abu-Hassanein et

al., 1996; Bryson, 2005). It is, therefore, important to address these variables in compacted clay soils commonly used in engineered structures such as road embankments.

5.2 Compaction key variables

Compaction, the densification of the soil by expulsion of the air, improves the mechanical properties of the soil. It increases the shear strength, lowers the compressibility, reduces the void ratio and, hence, the water flow through the soil.

Mechanical (dynamic or static) energy is applied to rearrange the grains into a dense state. In the laboratory, dynamic (standard and modified) compaction tests (BS1377, 1990: Tests 3.3 and 3.5) have been developed. For a given compaction effort, a compaction curve that relates dry density and gravimetric water content can be developed, from which a maximum dry density at the optimum water content OMC is determined, which serves as a criterion to control compaction process specifications in the field (Powrie, 2009). Increasing the compaction effort increases the maximum dry density and reduces the optimum water content of the soil. According to the specification required, maximum strength can be achieved dry of the optimum and minimum hydraulic conductivity can be achieved wet of the optimum. In static compaction, the soil is usually compacted in a confined mould using a piston that provides a gradual static load.

Soil water content and density are key factors to assess the stability and serviceability of engineered structures such as road embankments. The resistivity method has proven sensitivity to water content and the dry density of soils. As the electrical conduction in soils is controlled by pore water, resistivity is found to be sensitive to water content (e.g. Kalinski and Kelly, 1993; Abu-Hassanein et al. 1996), and, as the resistivity of air is infinite, the method has proven sensitivity to the density of the soil (Beck et al., 2011; Bai et al., 2013)

In the literature, a number of authors have discussed the influence of water content and other compaction key variables on soil resistivity. For instance, some authors (e.g.

McCarter, 1984; Yan et al., 2012) reported that the resistivity of compacted clay soil is a function of volumetric water content and degree of saturation. Abu-Hassanein et al. (1996) found that the resistivity is sensitive to the compaction conditions (Figure 5.1a), the higher the compaction effort, the lower the soil resistivity. However, at high water content, resistivity is less affected by compaction. A unique relationship between resistivity and the degree of saturation independent of the compaction effort was noticed (Figure 5.1b). At constant density, Seladji et al. (2010) reported that the resistivity of clay soil decreases with increasing water content, as shown in Figure 5.2.

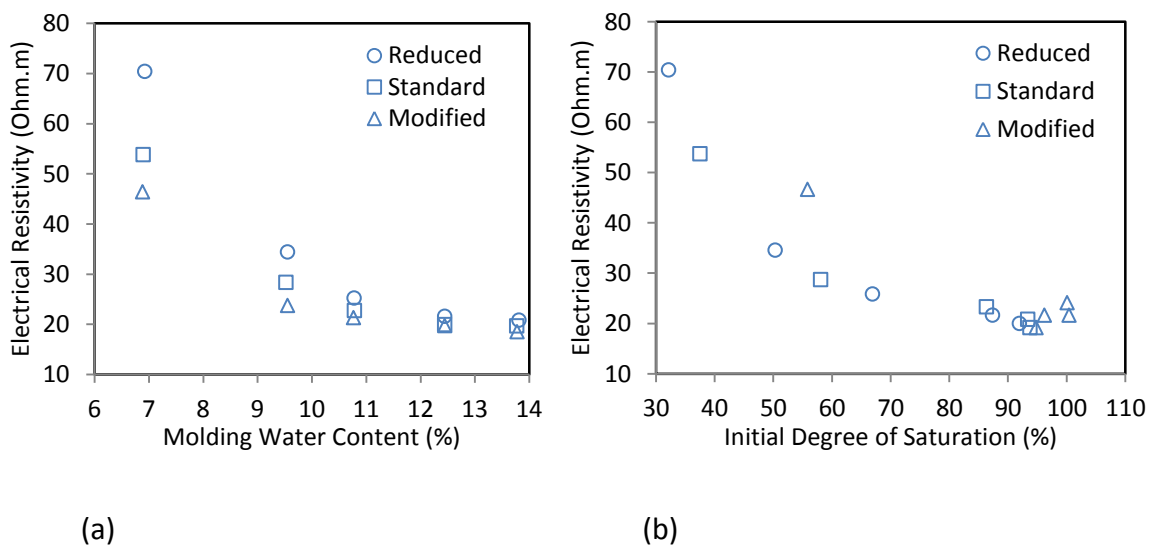


Figure 5.1. (a) Electrical resistivity-moulding water content, (b) electrical resistivity-initial degree of saturation (Abu-Hassanein et al., 1996)

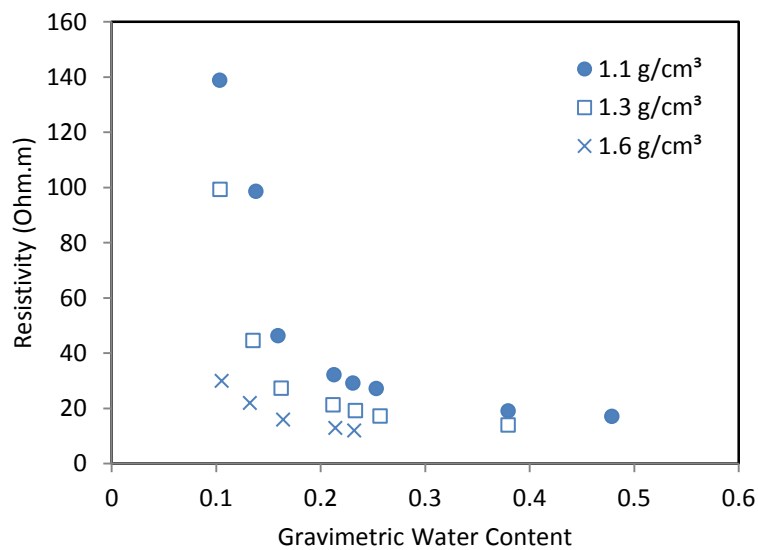


Figure 5.2. Resistivity-gravimetric water content relationship for different densities of clay soil (Seladji et al., 2010)

According to Alonso et al. (1999), intra-aggregate voids (or micro porosity) and inter-aggregate voids (or macro porosity) can be distinguished in clay aggregates. Compaction reduces the inter-aggregate voids and improves the particle to particle contact, leading to an increase in soil density. Electrically, several authors highlighted the influence of the clay microstructure in resistivity of compacted clay soils. Fukue et al. (1999) reported that the resistivity is influenced by structural characteristics of clay soil. At high water content, the continuity of pore water provides pathways for current and, therefore, results in low resistivity. At low water content, the discontinuity of pore water causes abrupt resistivity changes. They introduced the concept of "critical water content", where the electrical conduction behaviour can be divided into two segments of low and high resistivity separated by a critical water content value. The resistivity changes abruptly at a point where water becomes discontinuous. Robain et al. (2001) related the low and high resistivity values, respectively to the macro and micro porosity. Zha et al. (2010), Beck et al. (2011) and Kibria and Hossain, 2012 noticed that the critical water content falls close to the optimum water content. It is worth mentioning that, based on soil water retention studies (e.g.

Romero and Vaunat, 2000); two distinct segments of high and low suctions have been correlated with intra-aggregate and inter-aggregate water, respectively. Therefore, some recent studies have shown similarities between the soil resistivity-water content trend and water retention curve (e.g. Muñoz-Castelblanco, 2011; De Vita et al., 2012; Yan et al., 2012). Pozdnyakov et al. (2006) related resistivity behaviour of clay to the state of pore water molecules. The resistivity decreases rapidly with increasing water content in the first range (adsorbed, film and film-capillary water) then decreases less rapidly in the second range (capillary and gravitational water). At high water content close to saturation, the resistivity is independent of water content, as paths for electrical currents are achieved and the electrical charges are not affected by the mobility of water molecules.

To explore the water content characteristics of BIONICS clay, the specimens were compacted using dynamic (standard Proctor and Modified) and static methods. The specimens were prepared at various gravimetric water contents and dry densities.

5.3 Experimental setup

5.3.1 Specimen preparation

A reliable sample preparation procedure is an important step to replicate the results of any laboratory tests. Preliminary compaction tests of the fill material of the BIONICS embankment (Mendes, 2011) showed that the presence of large particles causes significant differences in the achieved densities. Therefore, the soil was sieved through a 2.8 mm sieve to reduce these differences. Compaction tests of the sieved soil showed a good repeatability. In the current work, the following soil preparation procedure was adopted:

1. The soil was dried to the atmosphere.
2. The soil was crushed and sieved through a 2.8 mm sieve to remove the large particles from the soil.
3. The soil was oven dried for 24 hours.

4. Distilled water (ASTM G57, 2006) was mixed with the soil to the desired gravimetric water content and left in a sealed plastic bag for 24 hours for water content homogenisation.

5. At each gravimetric water content, the specimens were compacted to a range of dry densities. For dynamic compaction, the soil was compacted according to BS light (Proctor) and BS heavy (Modified Proctor) compaction standard (BS1377, 1990: Tests 3.3 and 3.5), using a drop-hammer compaction machine.

In addition, to investigate the effect of dry density/void ratio, degree of saturation and the compaction effort, at each gravimetric water content, five specimens were compacted using different compaction efforts, by increasing the number of blows from 15 to 55 to cover the wide range of dry density that can be found in practice. For static compaction, soil specimens were compacted in three layers in a brass mould using a piston that provided a gradual static load. At each gravimetric water content, five specimens were prepared. Extra tests (5 specimens) were prepared at low, intermediate and high gravimetric water content, 0.075, 0.15, and 0.25, respectively. Table 5.1 lists the tests conducted. A total of 132 specimens were prepared.

5.3.2 Resistivity measurements

The resistivity measurements were performed using the resistivity probe described in Chapter 3. Two perpendicular resistivity readings named ρ_α and ρ_β , were collected. The average resistivity of ρ_α and ρ_β was used as the resistivity of the specimen (Russell and Barker, 2010). All measurements were performed in a temperature controlled laboratory.

Table 5.1 List of tests performed on compacted specimens

Gravimetric water content	Compaction method	Dry density range Mg/m ³	Number of the specimens
0.07-0.244	Light Proctor	1.58-1.73	9
0.048-0.246	Heavy proctor	1.58-1.89	8
0.065	Light (Modified)	1.56-1.73	5
0.075	Light (Modified)	1.56-1.76	5
0.0105	Light (Modified)	1.61-1.78	5
0.120	Light (Modified)	1.63-1.84	5
0.135	Light (Modified)	1.65-1.87	5
0.15	Light (Modified)	1.69-1.85	5
0.17	Light (Modified)	1.70-1.78	5
0.20	Light (Modified)	1.66-1.70	5
0.22	Light (Modified)	1.58-1.63	5
0.25	Light (Modified)	1.52-1.54	5
0.075	Static Compaction	1.55-1.71	10
0.095	Static Compaction	1.52-1.78	5
0.105	Static Compaction	1.52-1.80	5
0.12	Static Compaction	1.61-1.83	5
0.135	Static Compaction	1.57-1.84	5
0.15	Static Compaction	1.65-1.83	10
0.17	Static Compaction	1.72-1.77	5
0.20	Static Compaction	1.66-1.69	5
0.23	Static Compaction	1.57-1.61	5
0.25	Static Compaction	1.52-1.58	10
			Total=132

5.4 Results and discussion

5.4.1 Compaction and compaction effort

Figure 5.3 presents the dry density-gravimetric water content of specimens compacted using BS Light and BS heavy compaction methods, and the corresponding resistivity data. The same data is plotted in terms of the degree of saturation in Figure 5.4.

Figure 5.3 shows that the resistivity decreases with increasing water content. For BS Heavy compaction, there is a 3.44% resistivity increase for water content decrease from 0.246 to 0.048. For BS Light compaction, there is a 4.09% resistivity increase for water content decrease from 0.244 to 0.069. The resistivity is relatively low when the soil is compacted wet of the optimum (OMC=0.156 for BS Light, OMC= 0.127 for BS Heavy), while resistivity is high when the soil is compacted dry of the optimum. The resistivity increases abruptly dry of the optimum, while it seems to be independent of water content wet of the optimum. Moreover, increasing the compaction effort decreases soil resistivity. However, resistivity is not sensitive to the compaction, or the compaction effort, used when the soil is compacted wet of the optimum, whereas this effect is more significant when the soil is compacted dry of the optimum. This behaviour can be explained in terms of fabric changes during compaction. When the soil is compacted dry of the optimum, or with low compaction effort, the clods of clay are difficult to remould, with large air-filled pores (Benson and Daniel, 1990) and, therefore, high resistivity. In contrast, when the soil is compacted wet of the optimum, or at higher compaction effort, the clods of clay are easy to remould with small pores that are filled with water and, therefore, low resistivity. These observations are consistent with observations by Abu-Hassenein et al. (1996), Sawazaki et al. (2009) and Seladji et al. (2010), for different types of clay.

Moreover, at a distinct point of water content close to the optimum, soil resistivity starts to change rapidly. Similarly, a "critical water content" close to the optimum has been reported in the literature (e.g. Zha et al., 2010; Beck et al., 2011; Kibria and Hossain, 2012). Electrically, the discontinuity of pore water at low water content causes a relatively high resistivity, while at high water content the continuity of pore water is enhanced, causing a rapid decrease in the resistivity. At saturation levels close to 100% saturation, the influence of water on resistivity is insignificant, as the pores are almost filled with water and the electrical paths are accessible (Fukue et al., 1999). This behaviour suggests that the microstructure of compacted clay soils plays an important role in soil resistivity. Two distinct trends can be distinguished in Figure 5.3, separated by a critical water content reported in

the literature that falls close to optimum water content. This distinction can be related to the intra-aggregate and inter-aggregate fabrics that characterise the microstructure of clay soils.

The resistivity-degree of saturation relationships, displayed in Figure 5.4, show independency of the compaction effort. A similar unique relationship that is independent of compaction is reported by Abu-Hassanein et al. (1996) for ten clay soils (See Figure 5.1b). Eq. 2.19 in Chapter 2 was fitted to the experimental data, giving $b=1.23$ and 1.16 for Light and Heavy compaction, respectively. Abu-Hassanein et al. (1996) reported a range of 0.6-2.29 for different clays.

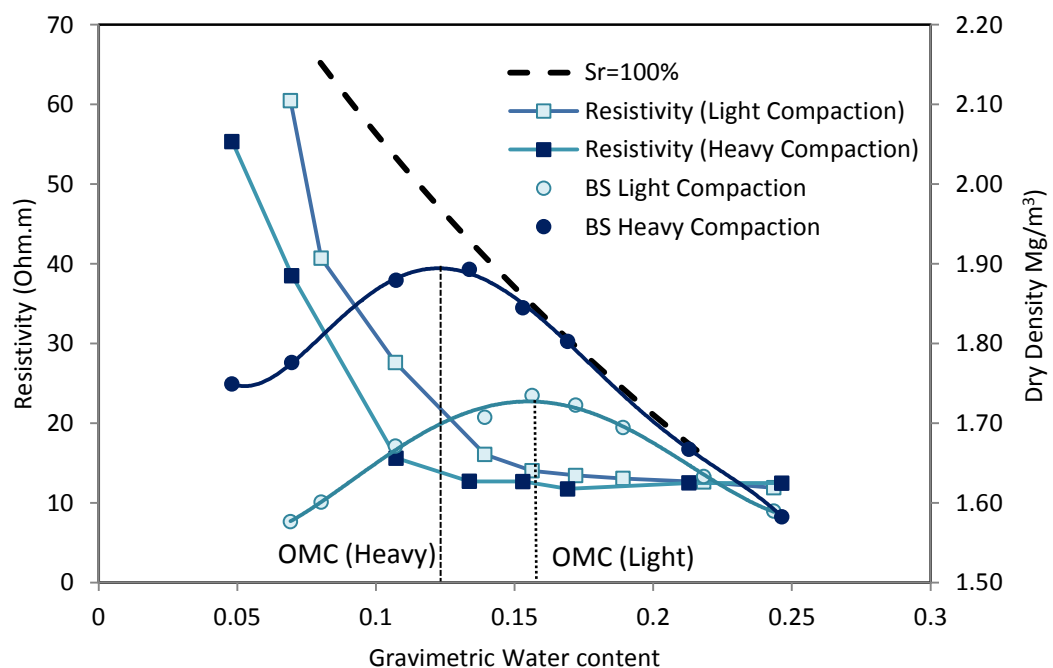


Figure 5.3. BS Light and BS Heavy compaction curves and the corresponding resistivity data

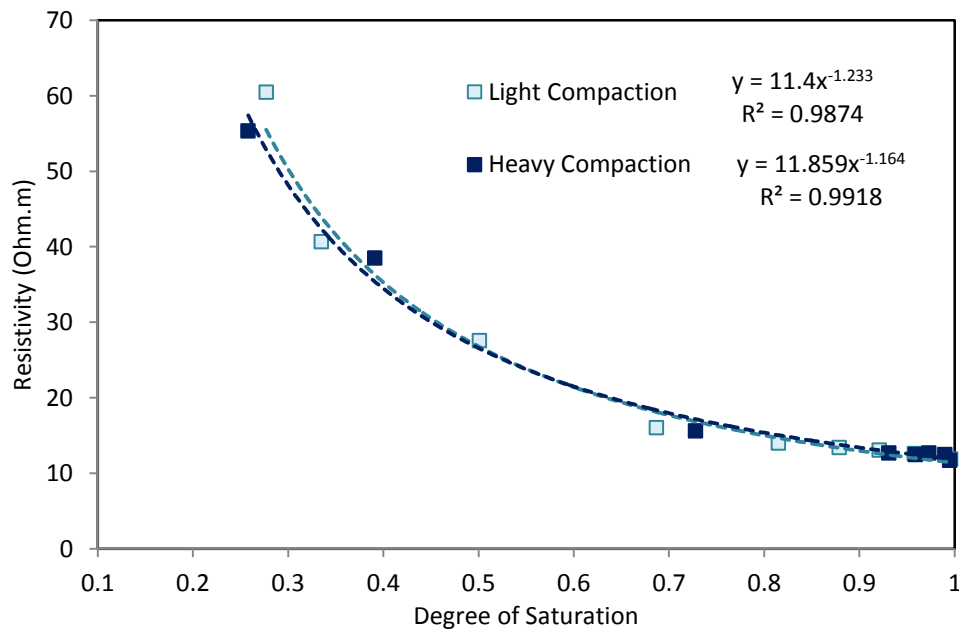


Figure 5.4. Resistivity-degree of saturation of specimens compacted using BS Light and BS Heavy compaction methods

To better emphasize the influence of the compaction effort, Figure 5.5 and Figure 5.6 present, respectively, the dry density-gravimetric water content relationship and the corresponding resistivity data of specimens compacted using different compaction efforts by changing the number of the blows of the compaction machine from 15 to 55. Increasing the compaction effort increases the maximum dry density and decreases the optimum water content. Again, increasing the compaction effort (the number of blows) helps in reducing the voids that are filled with air and, therefore, lowers soil resistivity. At low water content (0.065), the resistivity decreases from 70.33 to 40.93 Ohm.m as the number of the blows increases from 15 to 55 blows. However, for specimens compacted at high water content (0.25), where the pores are almost filled with water with a high degree of saturation, resistivity is low (~12 Ohm.m) and not affected by increasing the compaction effort or water content (Abu-Hassanein et al., 1996; Sawazaki et al., 2009).

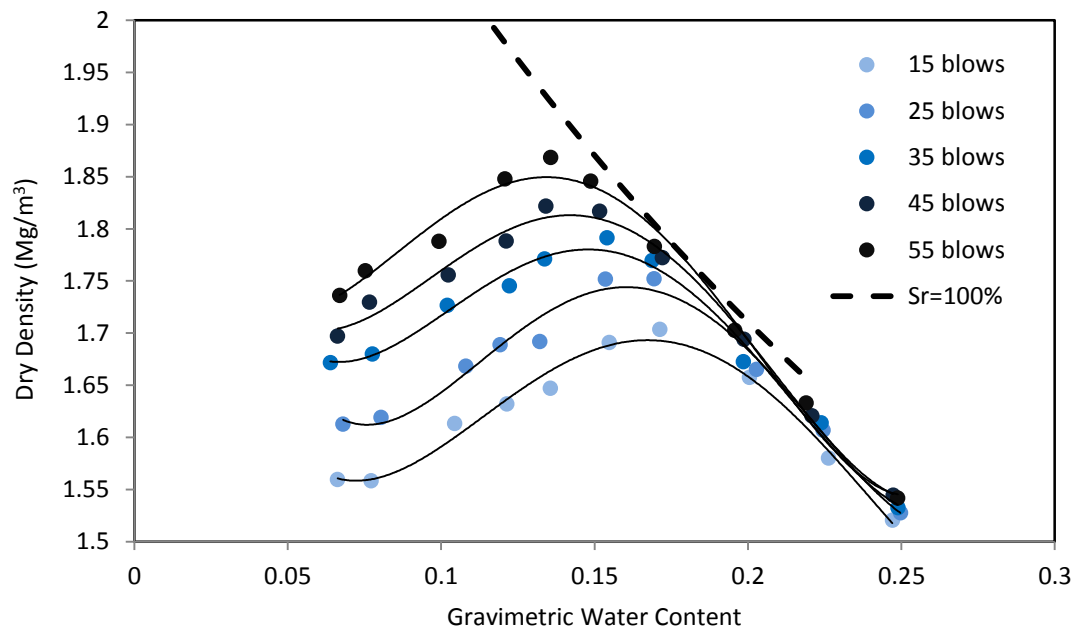


Figure 5.5. Dry density-gravimetric water content of specimens compacted using different compaction efforts

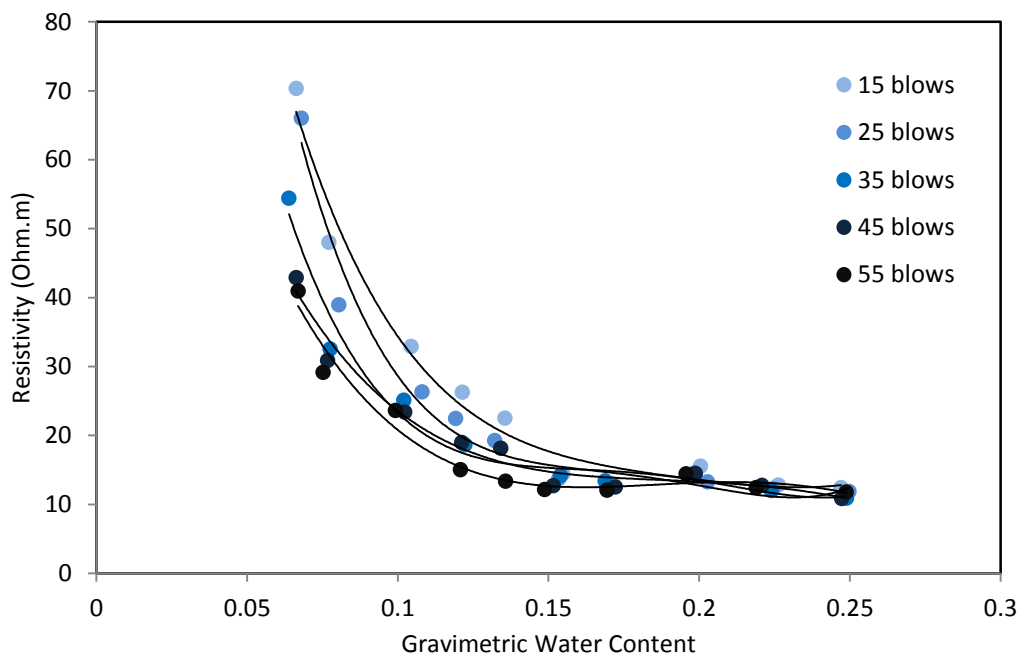


Figure 5.6. Resistivity-gravimetric water content of specimens compacted using different compaction efforts

5.4.2 Gravimetric water content

Development of laboratory correlations between soil resistivity and water content is practically useful, enabling field resistivity data to be used to estimate in situ water content (e.g. Kalinski and Kelly, 1993).

Figure 5.7 shows the resistivity-gravimetric water content relationship of dynamically compacted specimens. At low water content (e.g. 0.065), the resistivity changes largely from 40.93 to 70.33 Ohm.m for samples compacted at the same gravimetric water content, but different dry densities (as will be discussed in the next section). At high water content (e.g. 0.25), the dry density varies in a limited range; therefore, resistivity varies in a limited range, too. Similarly, Figure 5.8 shows the resistivity-gravimetric water content relationship of statically compacted specimens. At low water content (e.g. 0.075), the resistivity changes largely from 49.64 to 63.98 Ohm.m for samples compacted at the same gravimetric water content, but different dry densities. At high water content (e.g. 0.25), the dry density varies in a limited range; therefore, resistivity varies in a limited range, too. This suggests that the dry density/void ratio has an important role in soil resistivity, due to changes in the degree of saturation, particularly at low water content. Figure 5.7 and Figure 5.8 demonstrate that using gravimetric water content as a criterion to calibrate resistivity against water content in remoulded soils can be erroneous, as soils may be found at identical gravimetric water content, but at different degrees of saturation (McCarter, 1984).

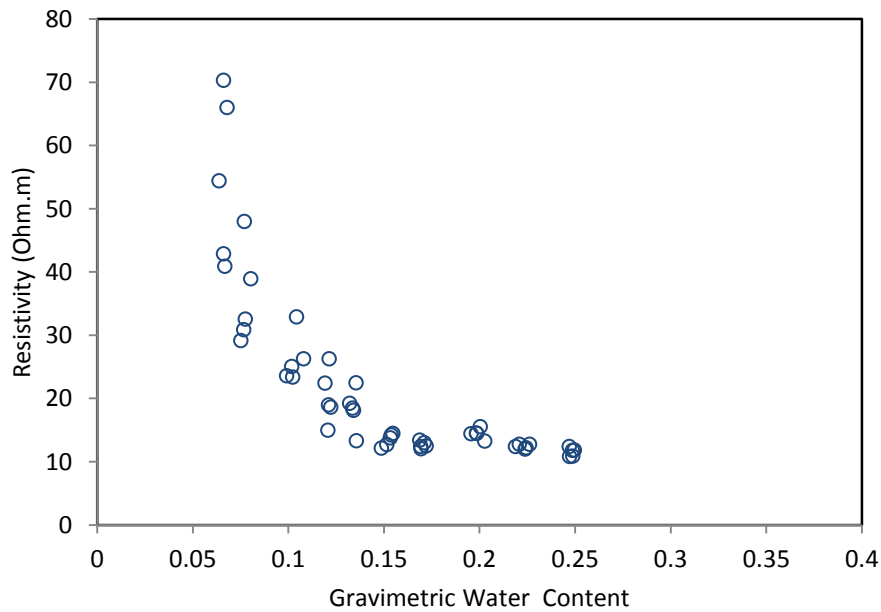


Figure 5.7. Electrical resistivity-gravimetric water content of the dynamically compacted specimens

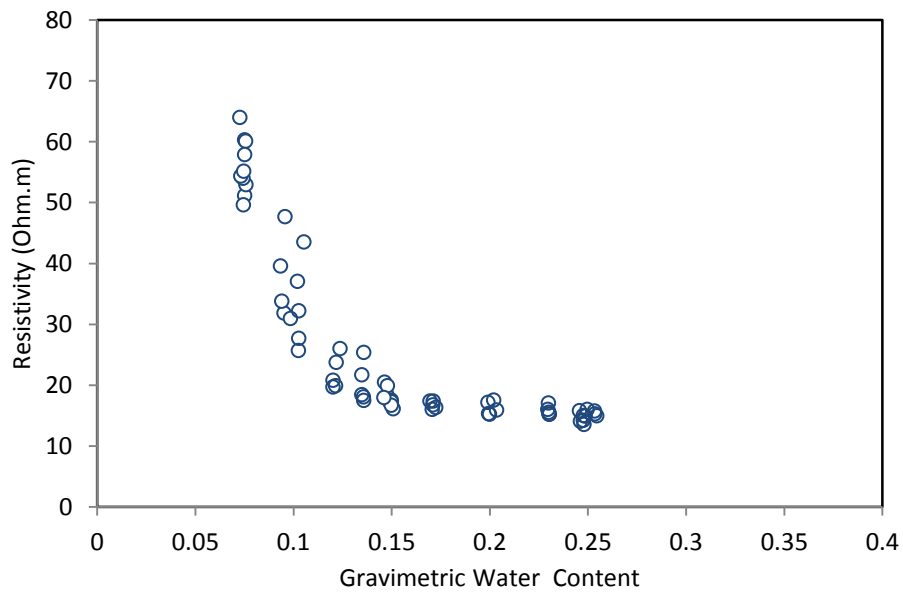


Figure 5.8. Electrical resistivity-gravimetric water content of the statically compacted specimens

5.4.3 Dry density and void ratio

To support the above discussion, soil resistivity is plotted against dry density and void ratio in Figure 5.9 and Figure 5.10, respectively, for the dynamically compacted specimens. Similarly, the resistivity is plotted against dry density and void ratio in Figure 5.11 and Figure 5.12, respectively, for the statically compacted specimens.

For a particular gravimetric water content, resistivity decreases linearly with increasing dry density/decreasing void ratio (Beck et al., 2011). However, the slope of the relationship is flattened with increasing water content. The extra tests (five specimens) that were prepared at low, intermediate and high gravimetric water content, 0.075, 0.15, 0.25, respectively, in Figure 5.11 and Figure 5.12 confirmed the stability of the trend.

This behaviour can be explained by changing of the soil properties during compaction. For soil compacted at low water content, the pores are partially filled with air. At water content dry of optimum, air is expelled from the soil, making the particles more close to each other in a denser state (dry density increases), while, at high water content (wet of optimum), the compaction effort cannot expel more air and the water added prevents densification (Budhu, 2011). Electrically, this behaviour can be explained by the continuity/ discontinuity of water phase in the soil (Fukue et al., 1999), as discussed earlier.

More importantly, the linear regressions shown in Figure 5.9 and Figure 5.10 can be distinguished into two groups with different slopes. The slope of the regression line decreases with increasing water content, and at particular water content (~ 0.15) close to the OMC (0.156), the slope flattens and remains constant, which can be attributed to the microstructure changes of the compacted soil.

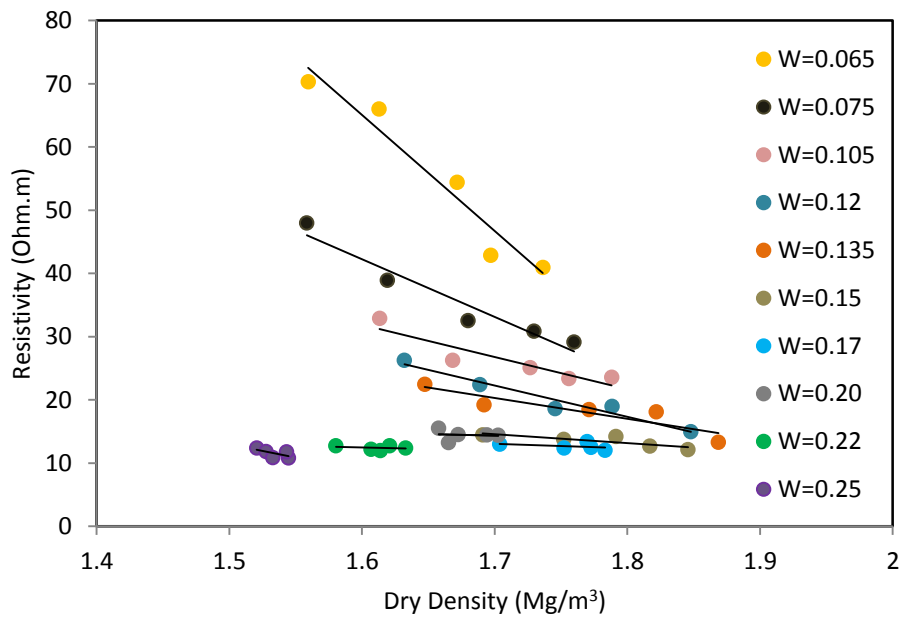


Figure 5.9. Electrical resistivity-dry density of the dynamically compacted specimens

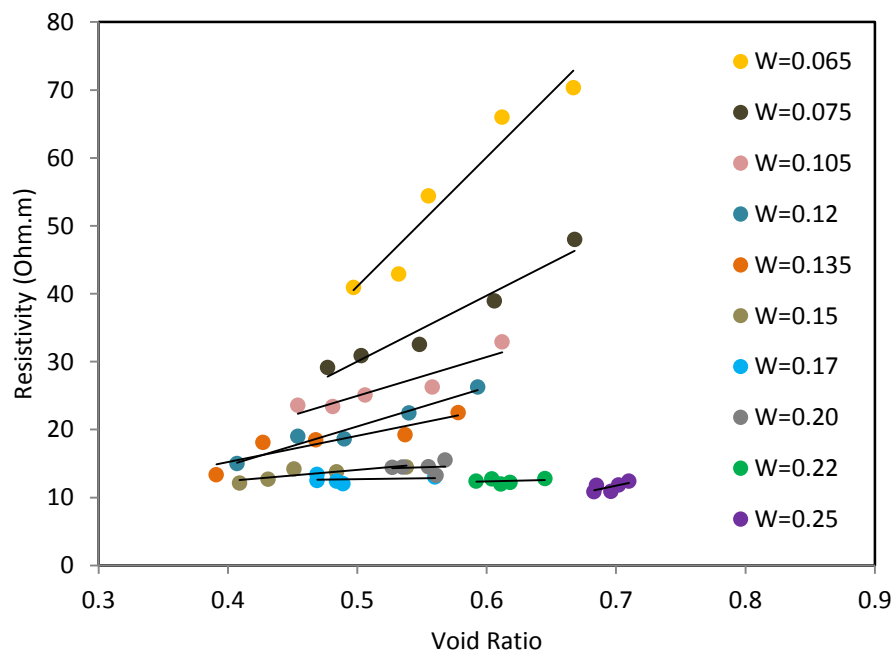


Figure 5.10. Electrical resistivity-void ratio of the dynamically compacted specimens

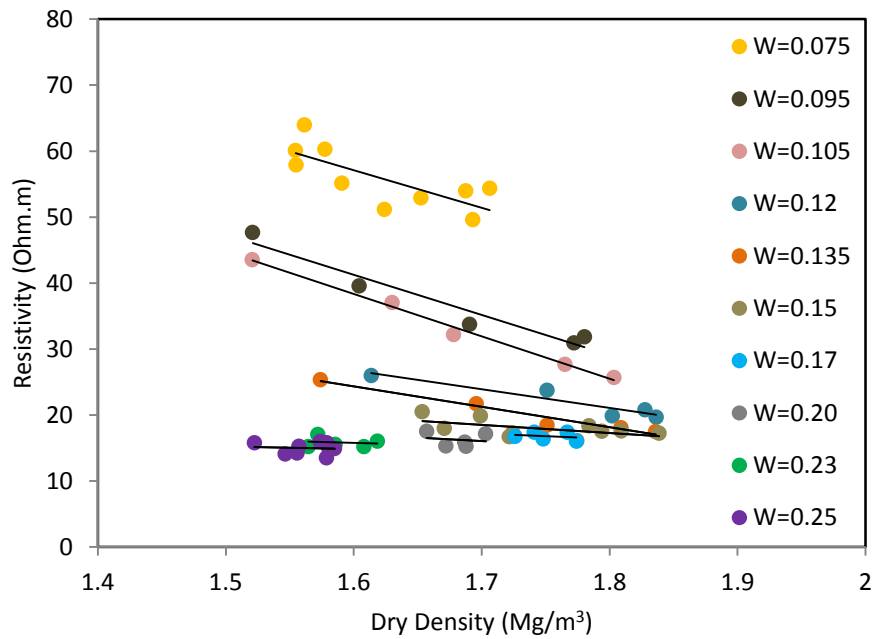


Figure 5.11. Electrical resistivity-dry density of the statically compacted specimens

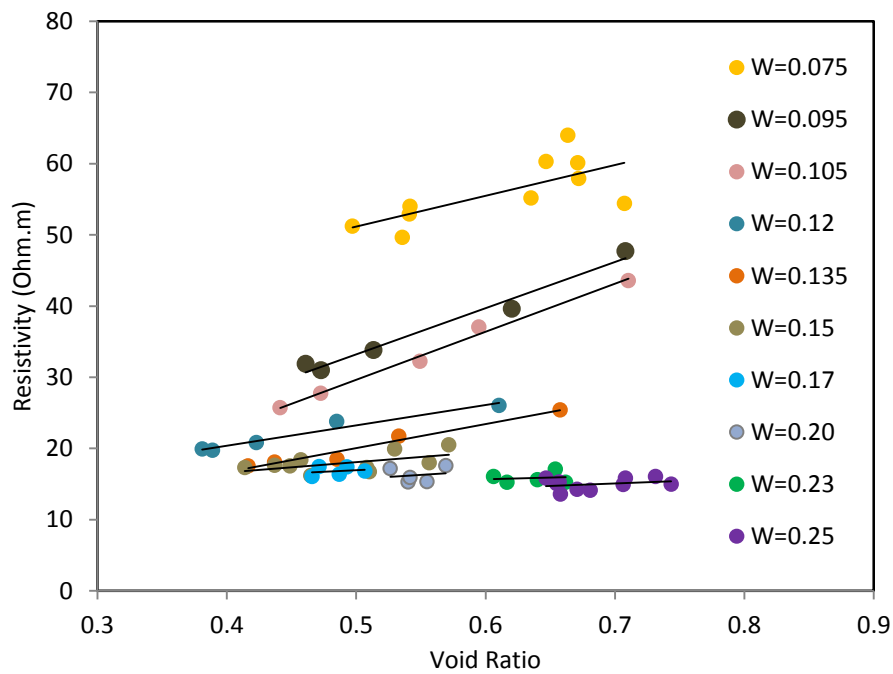
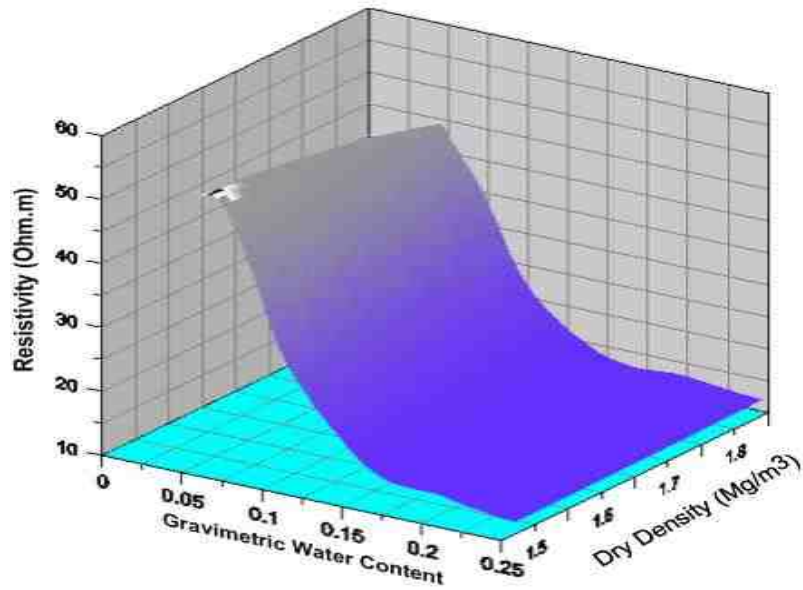


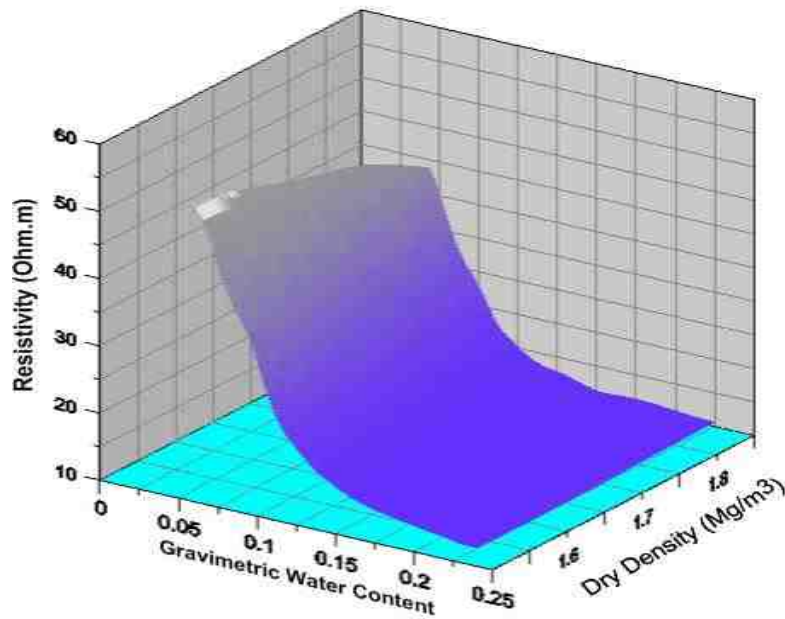
Figure 5.12. Electrical resistivity-void ratio of the statically compacted specimens

As both gravimetric water content and dry density affects soil resistivity, a 3D surface that relates resistivity, gravimetric water content and dry density, as suggested by Kibria and Hossain, (2012), is shown in Figure 5.13. The figure shows that resistivity decreases with increasing water content and dry density. At high water content and dry density, the surface flattens and becomes horizontal.

By making use of the linear regressions of Figure 5.9 and Figure 5.11, the influence of gravimetric water content on soil resistivity at a constant dry density can be calculated, as shown in Figure 5.14 and Figure 5.15, for dynamic and static compaction, respectively. At a constant dry density, resistivity increases with decreasing the gravimetric water content and this influence is more significant at low water content (Seladji et al., 2010; Beck et al., 2011). Figure 5.14 shows that at a constant dry density (e.g. 1.65 Mg/cm^3), the resistivity increases from 55.92 to 14.34 Ohm.m as water content decreases from 0.20 to 0.065. As the dry density increases (the void ratio decreases), more voids are filled with water (more water accessible for electrical conduction), and, therefore, soil resistivity decreases.



(a) Dynamic compaction



(b) Static compaction

Figure 5.13. Resistivity, water content and dry density relationship (a) Dynamic compaction

(b) Static compaction

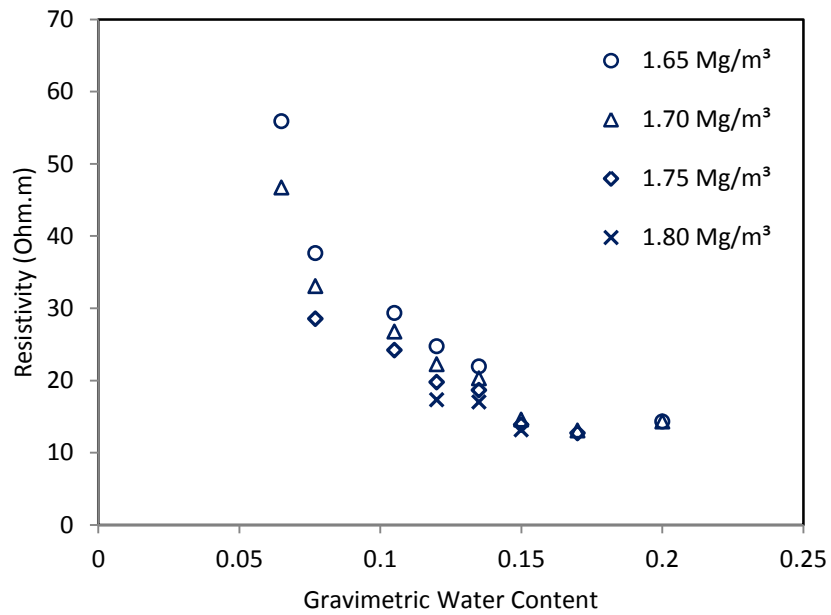


Figure 5.14. Electrical resistivity-Gravimetric water content relationship at constant dry density (Dynamic compaction)

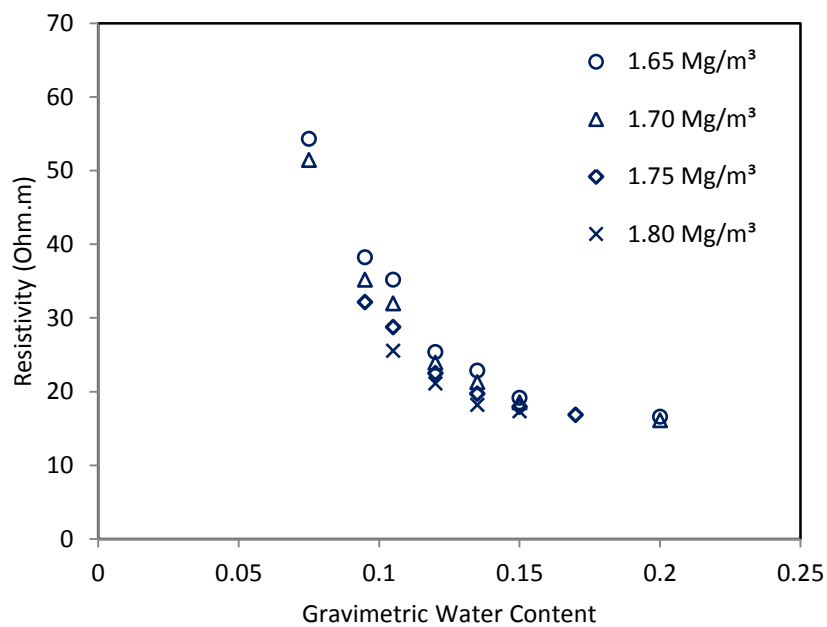


Figure 5.15. Electrical resistivity-Gravimetric water content relationship at constant dry density (Static compaction)

5.4.4 Volumetric water content

Volumetric water content integrates both gravimetric water content and dry density into one geotechnical parameter (Eq. 2.3, Chapter 2), offering a volume-integrated assessment of water content. Figure 5.16 and Figure 5.17 show the resistivity-volumetric water content relationships of the dynamically and statically compacted specimens, respectively. It can be seen that the resistivity decreases with increasing volumetric water content (e.g. Michot et al., 2003; Kalinski and Vermuri, 2005; Yan et al., 2012). Figure 5.18 shows the resistivity-volumetric water content of the dynamically compacted specimens compared to different clays reported in the literature. The high correlation coefficient for the wide range of water content covered suggests that this relationship can reasonably be used to calibrate resistivity against volumetric water content (e.g. Celano et al., 2011; Calamita et al., 2012).

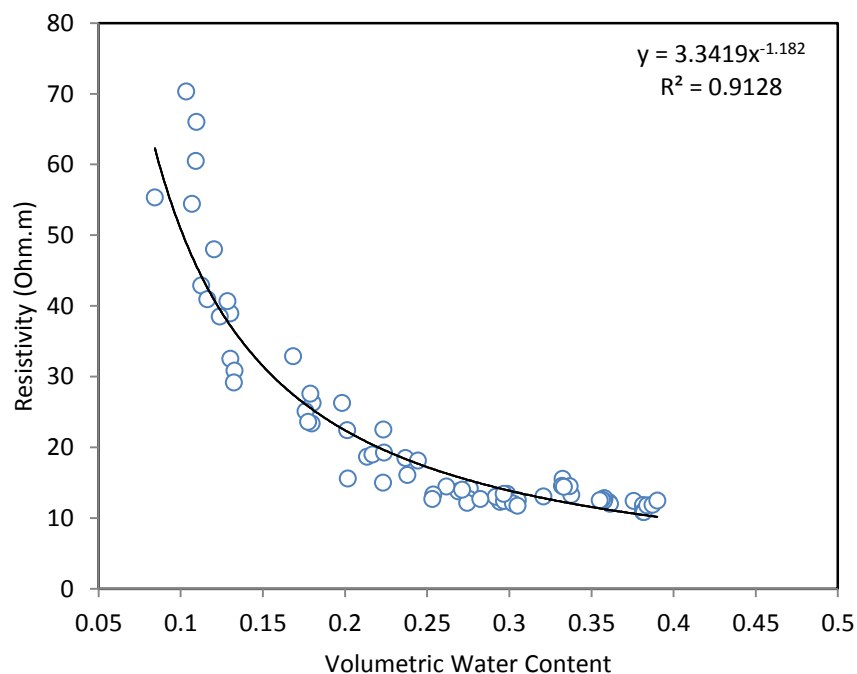


Figure 5.16. Resistivity-volumetric water content of the dynamically compacted specimens

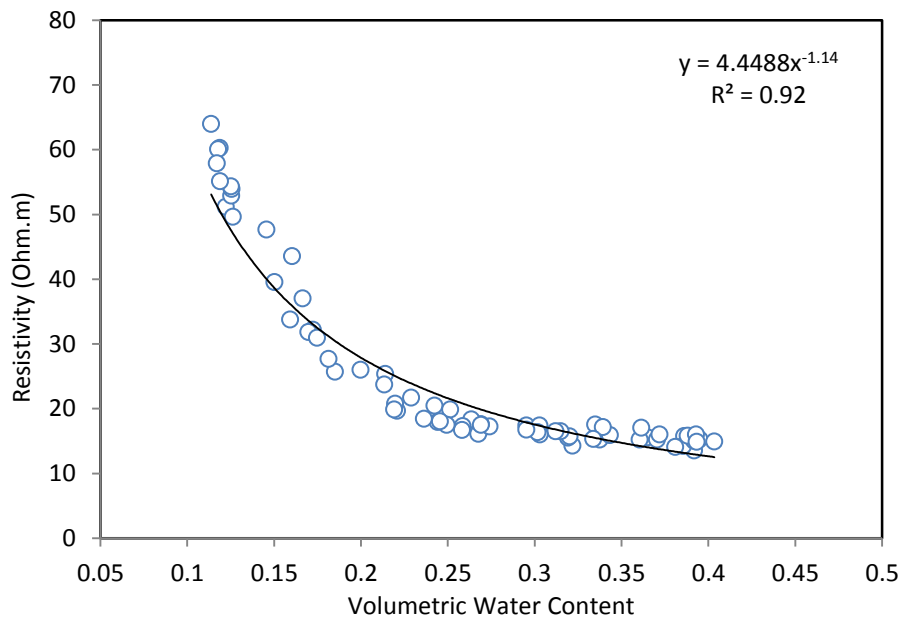


Figure 5.17. Resistivity-volumetric water content of the statically compacted specimens

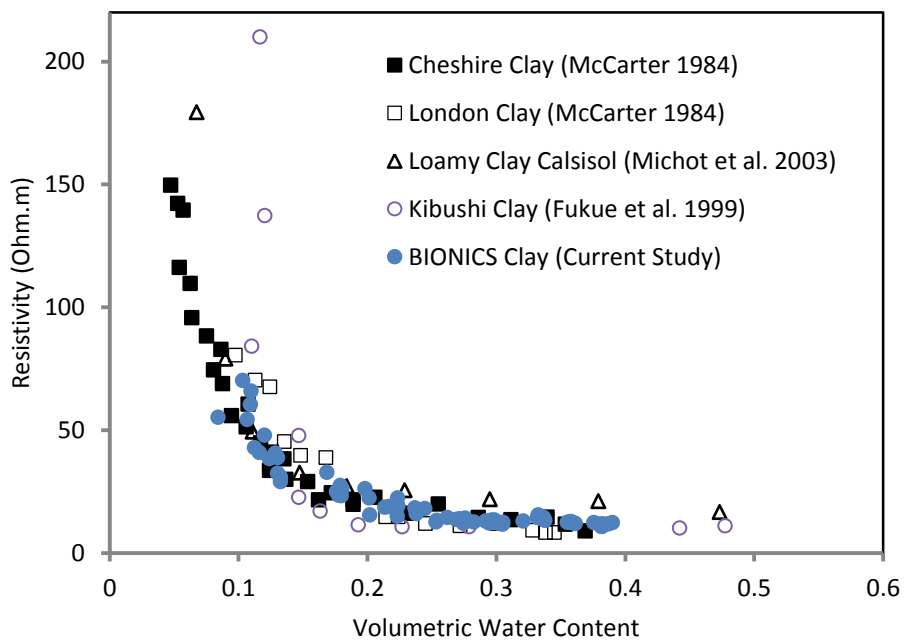


Figure 5.18 Resistivity-volumetric water content of BIONICS clay compared to different clays reported in the literature

5.4.5 Degree of saturation

According to Archie's Law, a decrease in the degree of saturation of the soil is accompanied by an increase in the resistivity, due to the partial replacement of pore water with air. Therefore, the variation of soil resistivity can be interpreted by means of the degree of saturation. Figure 5.19 and Figure 5.20 show the resistivity-degree of saturation relationship of the dynamically and statically compacted specimens, respectively. It can be noticed that increasing the degree of saturation decreases soil resistivity and that, at low degree of saturation, the resistivity changes more rapidly (Abu-Hassanein, 1996; McCarter 1984; Zha et al., 2010; Yan et al., 2012; Zhang et al., 2012).

Again, at low degrees of saturation, the continuity of pore water needed for current conduction does not reach a satisfactory level. Therefore, the resistivity is relatively high and changes rapidly. Increasing the degree of saturation improves the continuity of pore water and electrical conduction, causing a decrease in the resistivity. At a degree of saturation close to 100%, the electrical paths are well achieved for the electrical current. Therefore, the influence of water content on the resistivity becomes insignificant.

The high correlation coefficients of the resistivity-degree of saturation relationships suggest that the resistivity is strongly correlated with the degree of saturation of the soil.

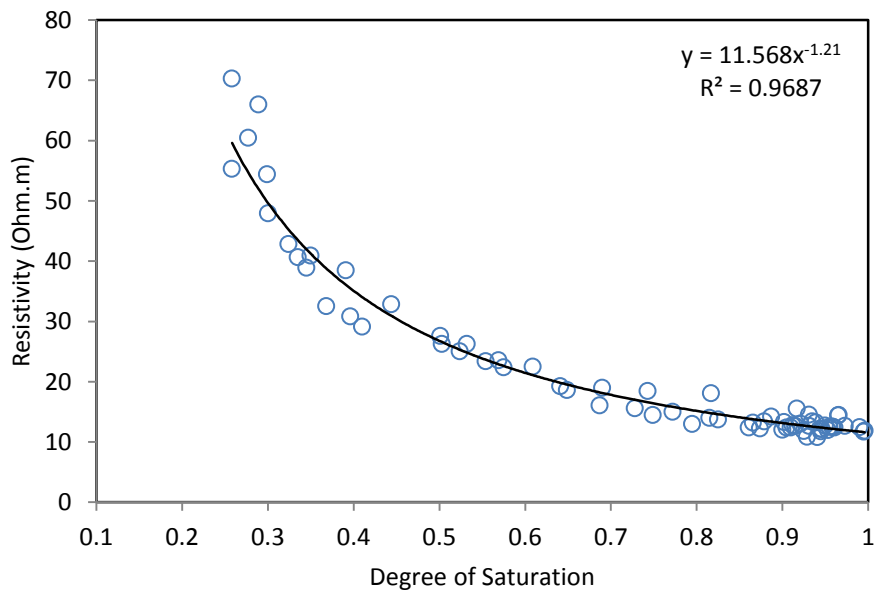


Figure 5.19. Resistivity-degree of saturation relationship of the dynamically compacted specimens

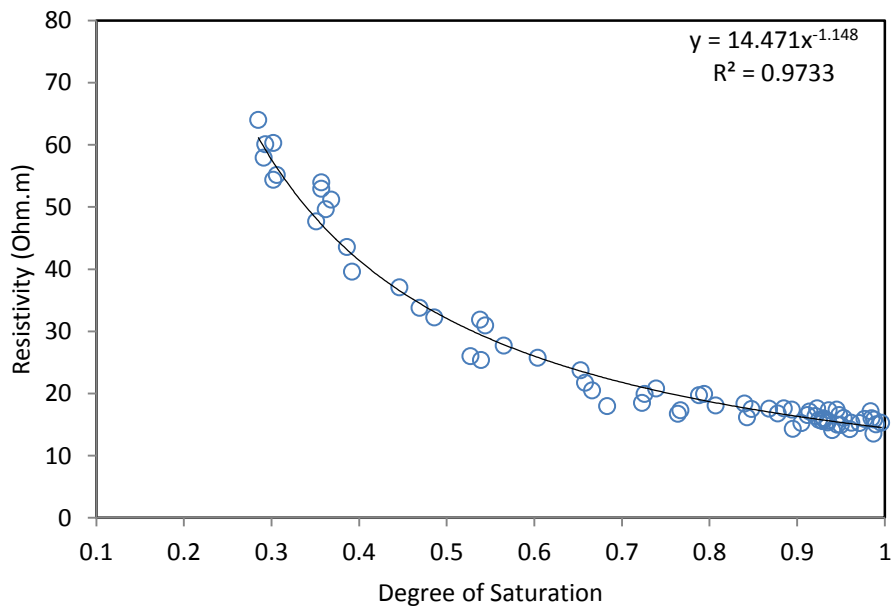


Figure 5.20. Resistivity-degree of saturation relationship of the statically compacted specimens

5.4.6 Compaction mechanism

Resistivity data of all specimens examined in this work, whether compacted using static or dynamic compaction, and the corresponding volumetric water content and the degree of saturation data are shown in Figure 5.21 and Figure 5.22, respectively.

For both compaction mechanisms, resistivity varies inversely with the volumetric water content and degree of saturation, as reported in the literature. However, the resistivity of the dynamically compacted specimens is slightly lower than the resistivity of the statically compacted specimens. Although the difference is not huge, this difference can be attributed to the microstructure differences in the compaction mechanism. The falling hammer of the compaction machine breaks the aggregates of the particles and bridges the voids, and, therefore, the resistivity is relatively low, while, in the static compaction, the load increases gradually, keeping more connectivity of macro voids, and, therefore, the resistivity is relatively high.

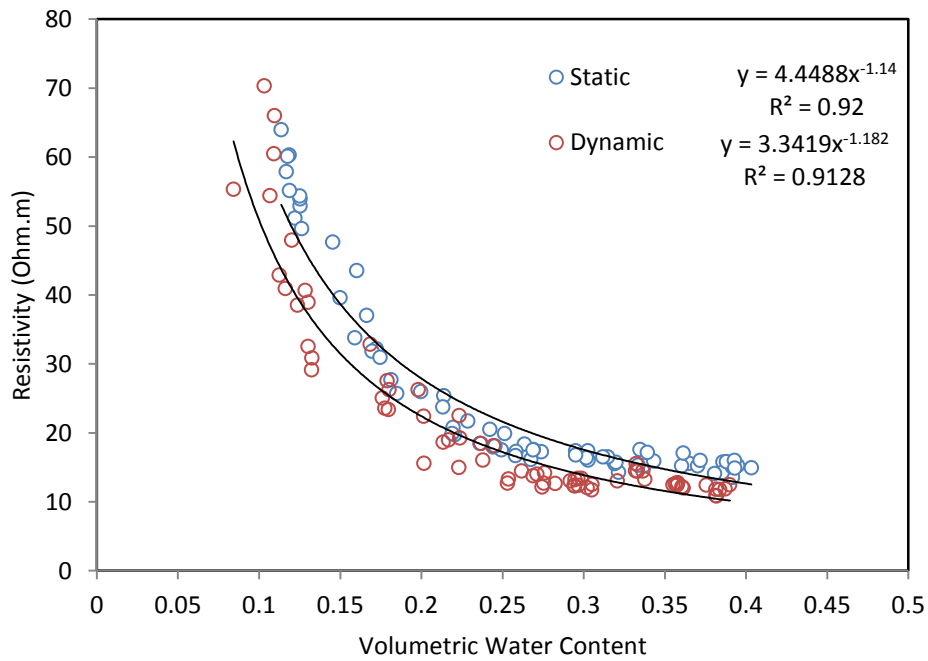


Figure 5.21. Resistivity-volumetric water content relationship of all specimens

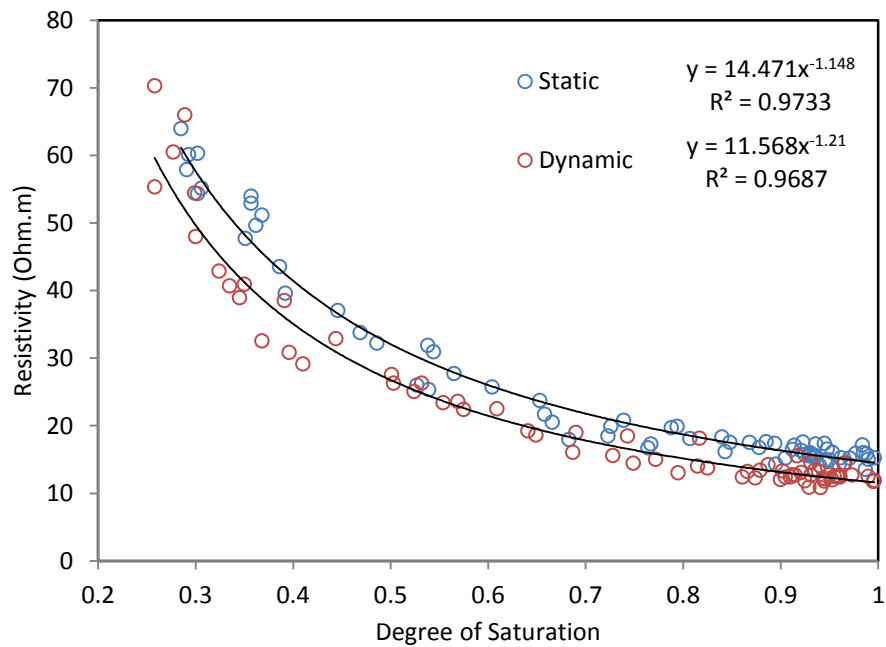


Figure 5.22. Resistivity-degree of saturation relationship of all specimens

5.5 Chapter summary

The water content characteristics of a mechanically compacted clay soil have been investigated using the resistivity method. BIONICS clay specimens compacted using dynamic (standard Proctor and Modified), and static methods were used. Soil resistivity was measured using the resistivity probe developed in the current thesis. Gravimetric water content, volumetric water content and degree of saturation were correlated with the measured resistivity for a range of dry densities. The results showed that the resistivity of compacted clay soils is sensitive to the compaction key variables and conditions. The key findings can be summarized as follow:

1. The soil resistivity of the mechanically compacted clay soil is strongly affected by compaction. The resistivity is relatively low for specimens compacted wet of the optimum, while resistivity is relatively high for specimens compacted dry of the optimum. This behaviour is explained by changing the soil properties during compaction.
2. The effect of the compaction effort on soil resistivity is significant when the soil is compacted at low water content or dry of the optimum; the more the compaction effort, the lower the resistivity. However, this effect is less significant when soil is compacted at high water content or wet of the optimum, where the pores are almost filled by water with a high degree of saturation.
3. For each gravimetric water content, resistivity changes with changing dry density/void ratio, particularly at low water content. Therefore, using gravimetric water content as a criterion to calibrate resistivity against water content can be erroneous, as soils may be found at identical gravimetric water content, but at different degrees of saturation.
4. Soil resistivity is inversely related to the volumetric water content and the degree of saturation. A unique relationship between resistivity and the degree of saturation that is independent of the compaction effort was achieved.

5. The resistivity is controlled by the degree of saturation. An increase in soil water content, dry density or the compaction effort causes an increase in the degree of saturation. At low degrees of saturation, the discontinuity of pore water causes a relatively high resistivity, while, at high degrees of saturation, the continuity of pore water is improved, causing a decrease in the resistivity. At water content levels close to saturation, the influence of water on resistivity is insignificant, as the electrical paths are achieved for electrical conduction.

6. An increase in the degree of saturation is also accompanied by changes in clay microstructure. According to the microstructure of clay, two distinct trends in the resistivity can be distinguished, separated by a critical water content as reported in the literature. This distinction is related to intra-aggregate and inter-aggregate fabrics of clay soil.

7. It is suggested that the degree of saturation or volumetric water content is more reliable than the gravimetric water content to calibrate the resistivity against water content, and resistivity investigation on remoulded soils must consider a range of specimens with various degrees of saturation for better water content estimates.

8. The resistivity of mechanically compacted clay soil is influenced by several interlinked parameters that need to be considered to obtain reliable water content estimates.

Chapter 6

The role of temperature and pore water conductivity on resistivity of clay soil

As the electrical conduction in soils takes place via the displacement of the ions in pore water, the resistivity of the soils is affected by temperature and pore water conductivity. However, in most studies, the assumption is made that the influence of soil temperature is relatively less significant than the water content variation to capture the variability of soil resistivity (e.g. Chrétien et al., 2014), or the resistivity has been corrected to a reference temperature based on correction models developed in the literature using soil solution extracts or natural waters, but then widely used for soils (e.g. Zhou et al., 2013). Similarly, variation of pore water conductivity is assumed relatively constant and hence its effect can be neglected comparing to water content variations (Samouëlian et al., 2005). Consequently, very little interest has been given to investigating the influence of pore water conductivity on soil resistivity (Rinaldi and Cuestas, 2002).

Recent work conducted by the British Geological Survey on the BIONICS embankment has shown resistivity variations across the embankment, mainly attributed to water content variation, however, variations could also be due to variations in temperature and/or pore water conductivity. It is, therefore, essential to investigate these effects on the measured resistivities. This chapter is dedicated to exploring the role of temperature and pore water conductivity on the resistivity of BIONICS clay. The resistivity behaviour of the soil for a range of temperature (-12 to 43°C) is discussed, and the effect of the salt type and concentration on resistivity is addressed.

6.1 Introduction

The electrical conduction in soils is influenced, among other factors, by the mobility of ions in the pore water. Mobility of the ions, however, is controlled by temperature, salt type and concentration (Campbell et al., 1948; Rhoades et al., 1976). The mobility of the ions increases with increasing temperature as the viscosity of the water is decreased. Therefore, the resistivity of soils decreases with increased temperature (Figure 6.1). In addition, increasing the concentration of salts in the pore water provides more ions for electrical conduction. As salts have to be in an ionized form to be able to conduct the current, the amount of water controls the available paths for electrical conduction in soils. When an electric field is applied, cations are accelerated toward the negative pole and anions to the positive pole. Therefore, the pore water conductivity is expected to have an important role on soil resistivity.

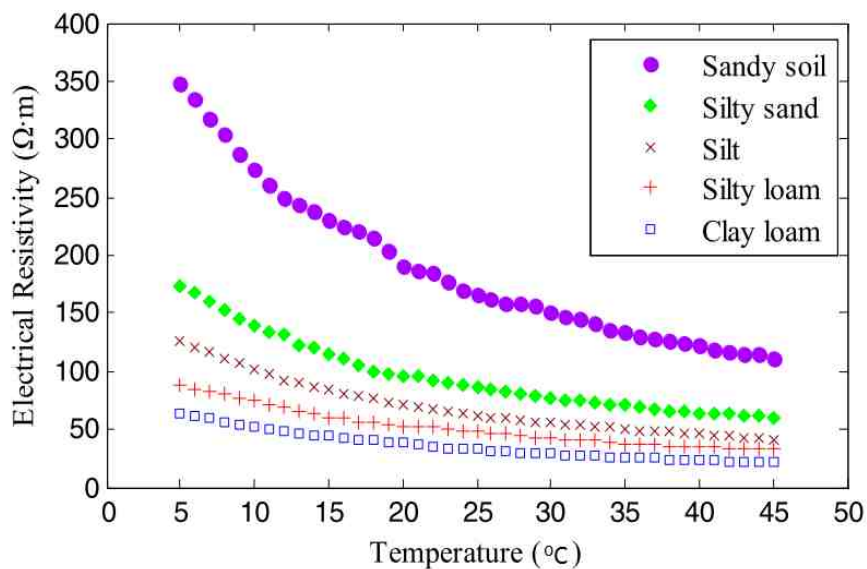


Figure 6.1. Electrical resistivity-temperature relationships of different soils (Zhou et al., 2013)

6.1.1 The temperature correction

Comparisons of resistivity data conducted at various temperatures need to be corrected to a standard reference temperature. In studies where the temperature effect is not considered, an assumption is made that temperature is constant when the measurements are performed over a short period. However, for measurements collected over a long period, temperature correction due to seasonal temperature variations is essential to compare resistivity data collected at the same location but on different dates (Samouëlian et al., 2005).

Several temperature correction models such as linear (e.g. Campbell et al., 1948), exponential (e.g. Corwin and Lesch, 2005) and power (e.g. Besson et al., 2008) have been reported. Most of these models have been developed and parameterized based on measurements of the electrical conductivity of soil solution extracts (Campbell et al., 1948), electrolyte solutions (Keller and Frischknecht, 1966) or natural waters (groundwater and seawater) with different salinities and chemical compositions (Hayashi, 2004). However, they have been used widely to correct resistivity data of different soils. Recent papers showed that the available models have limits of validity based on experimental data conducted on different soils (Zhou et al., 2013), and they are inconsistent with each other (Ma et al., 2011).

Significant difference between the resistivity of BIONICS clay samples measured in the laboratory and the in situ values has been reported, which are mainly attributed to the temperature variations that need to be addressed (Hen- Jones et al., 2014). Therefore, it is essential to quantify the influence of temperature on the resistivity of the soil. This would be useful to aid the interpretation of the field data.

The electrical conductivity-temperature relationship of natural waters is nonlinear (Millero, 2001). The degree of nonlinearity, however, is relatively small particularly at a

temperature range of (0-33°C), and the relationship can reasonably be approximated by a linear equation (Hayashi, 2004). Therefore, a linear model (Campbell et al., 1948; Keller and Frischknecht, 1966) has been widely adopted, expressed as:

$$\rho_T = \frac{\rho_o}{1 + \alpha (T - T_o)} \quad (6.1)$$

Where ρ_T is the resistivity at the ambient temperature T , ρ_o is the resistivity measured at a reference temperature T_o (e.g. 18°C or any other reference temperature (Keller and Frischknecht, 1966)) and α is the temperature coefficient of resistivity (~0.025 for most electrolytes).

Figure 6.2 shows the resistivity behaviour for fine-grained material over a range of temperatures. At temperatures below freezing, the effect of temperature on resistivity is significantly high comparing to its effect at a moderate temperature range as the resistivity of ice is very high compared to the water. Studies have shown that resistivity measured at -12°C is about 10 to 100 times larger than the resistivity measured at 18°C (Keller and Frischknecht, 1966). A moderate effect of temperature on resistivity is noticed at the freezing point due to the presence of salts in the pore water which makes freezing take place over an extended temperature range. In frozen ground, Hauk (2002) showed that, at temperatures above the freezing point, resistivity changes linearly with temperature due to changes in pore water resistivity following the Campbell model, while at temperatures below the freezing point, resistivity increases exponentially with temperature.

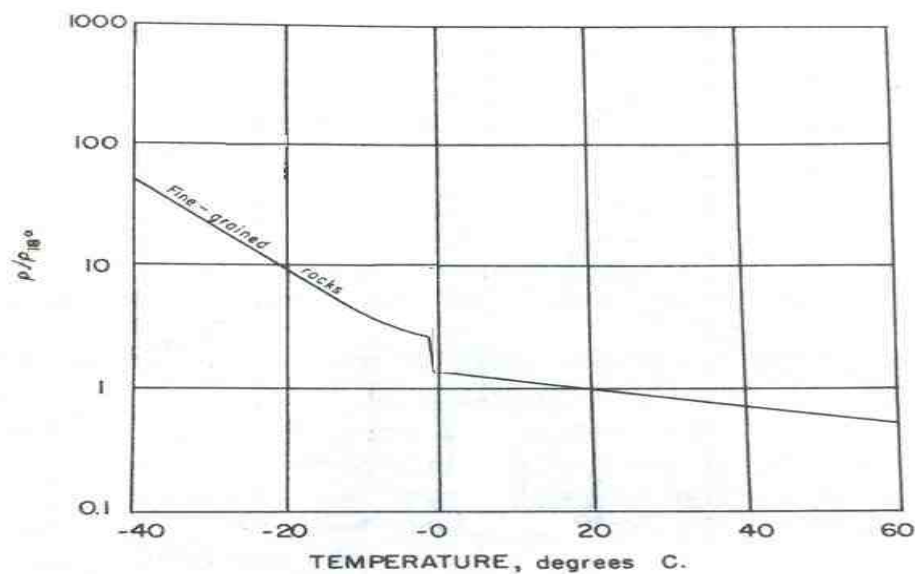


Figure 6.2. The resistivity-temperature relationship over a range of temperatures (Keller and Frischknecht, 1966)

6.1.2 The influence of pore water conductivity

According to Archie's law (Archie, 1942), the electrical resistivity of the soil is proportional to the pore water resistivity. Pore water resistivity is controlled by salt type and concentration in the water. Using a four electrode resistivity probe, Shea and Luthin (1961) reported a strong relationship between salinity and resistivity. This relationship was used for measuring soil salinity in situ.

Sen et al. (1988) found that the resistivity is non-linearly related to the pore water conductivity of clayey sandstone. Kalinski and Kelly (1993) demonstrated that pore water solutions of the same concentrations, but different compositions, were characterised by different conductivity, as different ions have different mobility. Consequently, the ions (e.g. Na^+ , K^+ , Cl^- , etc.) affect the pore water conductivity in different manners. Similarly, Rinaldi and Cuestas, (2002) showed that the electrical resistivity of compacted silty clay is mainly influenced by salt concentration and volumetric water content. However, soil with different

CHAPTER 6: THE ROLE OF TEMPERATURE AND PORE WATER CONDUCTIVITY ON RESISTIVITY OF CLAY SOIL

pore water composition showed different electrical resistivity, and specimens mixed with NaCl solutions showed the lowest resistivity.

Using solutions of different NaCl concentrations, Zha et al. (2006; 2010) found that soil resistivity decreases with increasing the salinity of water, and the influence of salinity is less significant for soils prepared at high water content or high concentrations (Figure 6.3). For fifteen marine clay sites, Long et al. (2012) reported that the resistivity of clay soil decreases rapidly with increasing salt content, and the resistivity becomes relatively constant at high salt content (Figure 6.4).

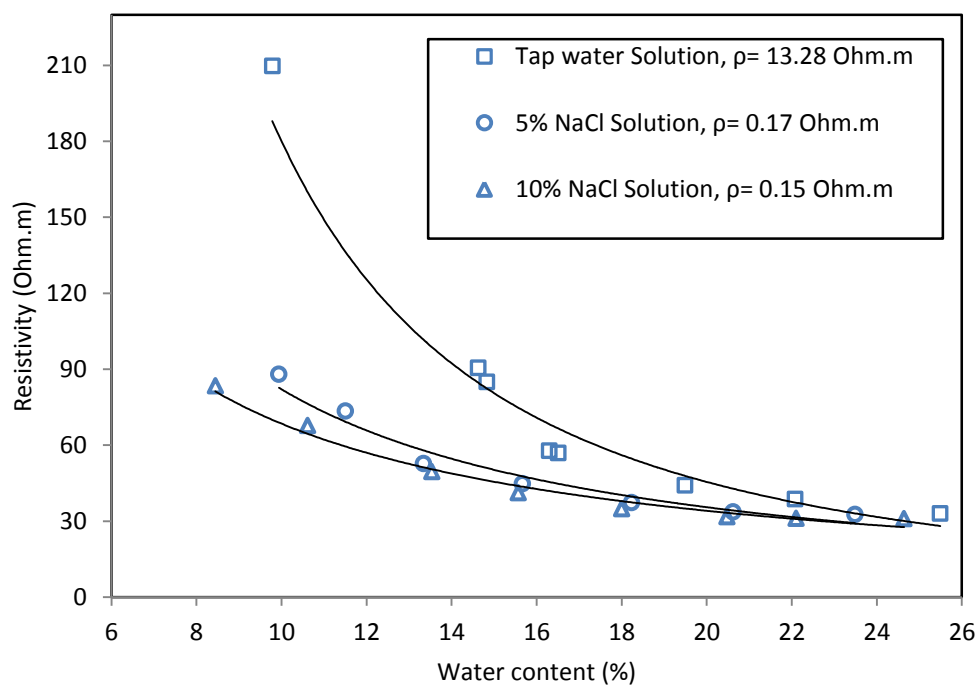


Figure 6.3. Electrical resistivity-water content relationship for different pore water resistivity (Zha et al. 2010)

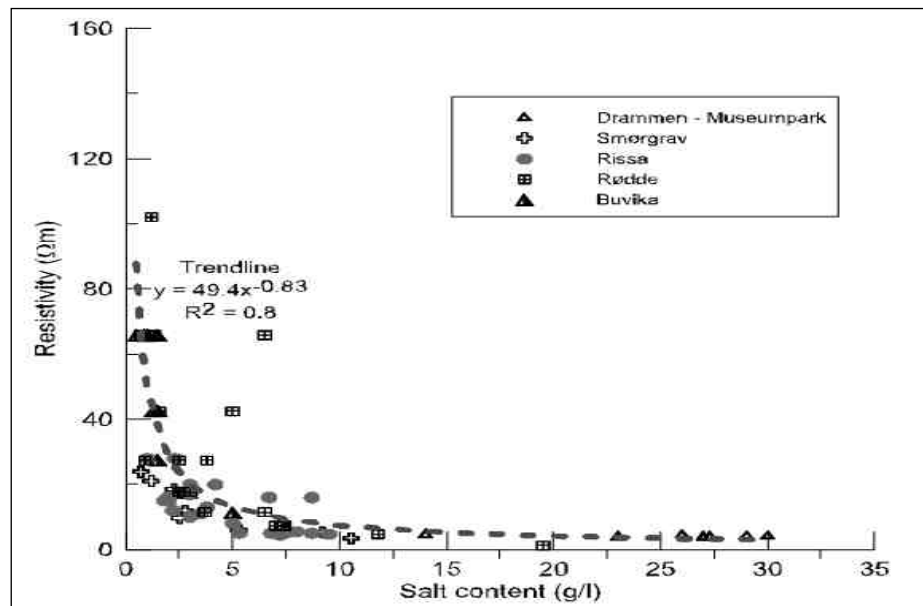


Figure 6.4. Resistivity-salt content of clay soils at different sites (Long et al., 2012)

6.2 Experimental setup

6.2.1 Sample Preparation

A specimen of BIONICS clay, compacted at 20% water content in the resistivity box, was used to investigate the influence of temperature on soil resistivity over a temperature range of (-12 to 43°C). To prevent water content changes, the specimen was sealed during the test, and conditioned in a temperature controlled lab where the mass and the temperature were monitored for 48 hours. Cooling was achieved using a freezer to -12°C while heating was achieved by means of an oven up to 43°C.

To address the influence of pore water conductivity on soil resistivity, the soil was mixed with different electrolytes of different concentrations. The electrolytes were prepared in a 100 ml flask using distilled water. Three common electrolytes; Potassium chloride (KCl), Sodium chloride (NaCl), and Magnesium chloride (MgCl₂) were used (as Rinaldi and Cuestas, 2002). The electrolytes were mixed with soil at different water

contents, and sealed in plastic bags for 24 hours period of equalisation. The specimens were compacted in a brass mould, and left for 24 hours for equalisation. Firstly, the specimens were compacted at 25% gravimetric water content with different salts at different concentrations. Secondly, the specimens were compacted at different water content and electrolyte concentration. Table 6.1 lists the samples prepared.

6.2.2 Resistivity measurements

The resistivity of the compacted specimens was measured using the four electrode method. The resistivity box and probe, described in Chapter 3, were used respectively to address the influence of temperature and the pore water conductivity on resistivity of the soil. As electrical resistivity and conductivity are inversely proportional to each other, the electrical resistivities of the solutions were measured using the same method as for measuring soil resistivity (Rinaldi and Custe, 2002). Therefore, the solutions were placed in a plastic container (55mm diameter, 80.5mm height), where the electrical resistivity was measured using the resistivity probe. To evaluate this procedure, comparisons between pore water resistivities measured using Resist and a HANNA conductivity meter were used.

Table 6.1 List of samples and electrolytes prepared

No	Salt type	Salt concentration (g/100ml)	Type	No of samples
1	NaCl, KCl, MgCl ₂	0.1-3.0	soil	15
2	KCl	0.1-1.5	soil	21
3	NaCl, KCl	0.2	soil	7
4	NaCl, KCl	1.0	soil	7
5	Distilled water	0	soil	7
6	NaCl	0.1-3.0	electrolyte	6
7	KCl	0.1-3.0	electrolyte	6
8	MgCl ₂	0.1-3.0	electrolyte	6

6.3 The experimental results and discussion

6.3.1 The influence of the temperature

The measurements conducted in this work were performed in a temperature controlled laboratory. The temperature was logged for 48 hours at different dates as shown in Figure 6.5. The temperature was kept at $\sim 20 \pm 0.5^\circ\text{C}$. The resistivity of the prepared specimen was first monitored at the lab temperature for 48 hours as shown in Figure 6.6. The measured resistivity ranged from (13.35-13.69) Ohm.m.

In the second stage, the specimen was cooled down to $\sim 7^\circ\text{C}$. The specimen was then allowed to equilibrate in the lab, where the temperature and resistivity were measured every five minutes until the specimen reached the lab temperature ($\sim 20^\circ\text{C}$). Figure 6.7 shows the measured resistivity and temperature for this stage. As expected, resistivity of the soil decreases with increasing the temperature. The resistivity decreases by 48.56% for temperature increasing from 6.7 to 20.3°C . Figure 6.8 shows the resistivity-temperature relationship. The Campbell model (Eq. 6.1) was fitted to the experimental data using $\alpha=0.025$.

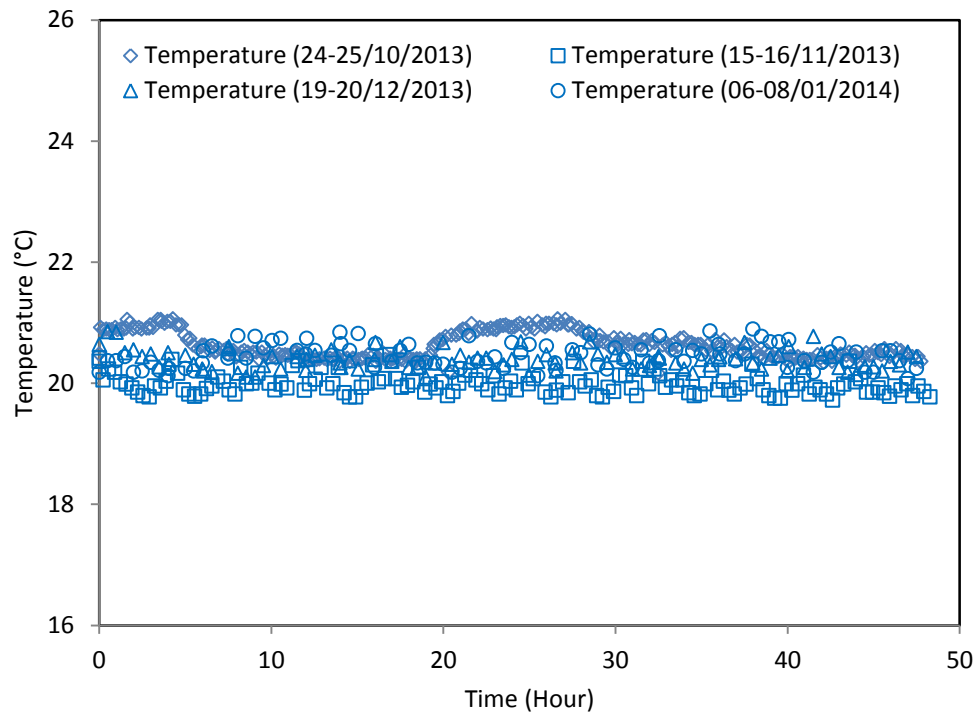


Figure 6.5. Air temperature variation in the lab for 48 hours at different dates

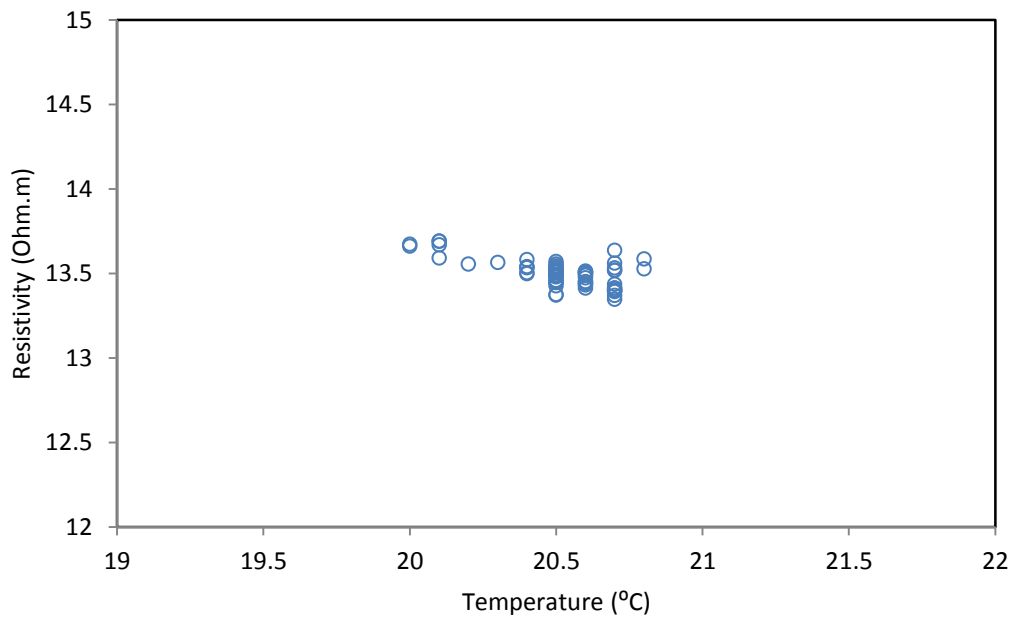


Figure 6.6. The measured resistivities at the lab temperature

CHAPTER 6: THE ROLE OF TEMPERATURE AND PORE WATER CONDUCTIVITY ON RESISTIVITY OF CLAY SOIL

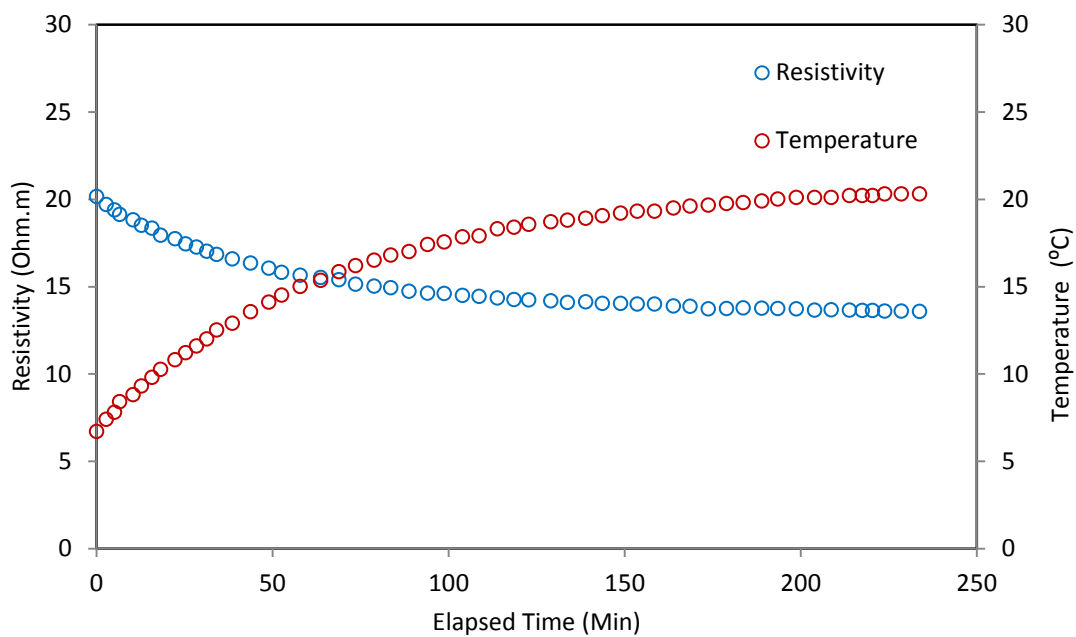


Figure 6.7. Resistivity and temperature data of the cooling stage

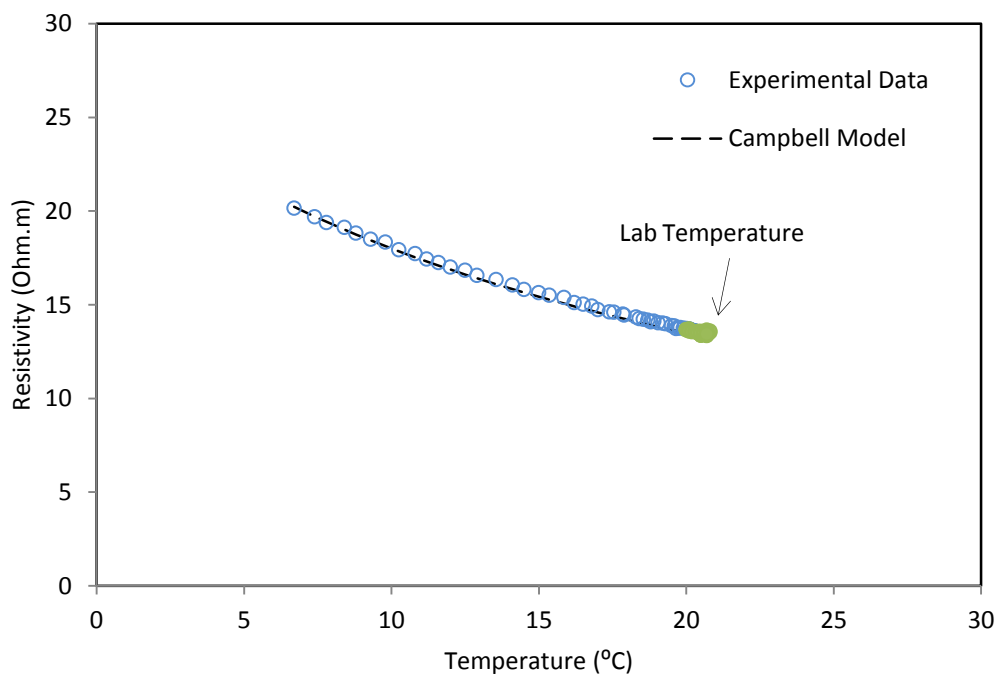


Figure 6.8. The resistivity- temperature relationship of the cooling stage

In the third stage, the temperature of the specimen was increased up to 43 °C using an oven. The specimen was then allowed to equilibrate in the lab, where the temperature and resistivity were measured every five minutes until the specimen reached the lab temperature. Figure 6.9 shows the measured resistivity and temperature for this stage. Soil resistivity increases with decreasing the temperature. The resistivity increases by 56.17% for temperature decreasing from 43.0 to 20.2°C. Figure 6.10 shows the resistivity-temperature relationship. The Campbell model was fitted to the experimental data using $\alpha=0.025$.

In the fourth stage, the temperature was decreased to -12°C using a freezer. The specimen was then allowed to equilibrate in the lab, where the temperature and resistivity were measured until the specimen reached the lab temperature. Figure 6.11 shows the measured resistivity and temperature for this stage. Figure 6.12 shows the resistivity-temperature relationship. At sub frozen temperatures, the resistivity is considerably higher due to the high resistivity of ice, and the resistivity decreases abruptly with the temperature decreasing. At temperatures above freezing, the resistivity is low due to the low resistivity of the water, and the resistivity decreases gradually with temperature (Keller and Frischknecht, 1966; Hauk, 2002). Figure 6.11 shows that the freezing took place over an extended temperature range where the resistivity decreases abruptly. The Campbell model fits well for the resistivity data above the freezing point. However, at temperatures close to freezing the model does not fit very well.

Figure 6.13 shows the resistivity-temperature relationship over the range of temperatures tested. The influence of temperature on resistivity at temperatures below freezing is significantly higher than its influence at temperatures above the freezing. The measured resistivity at the end of each stage (~13.50 Ohm.m) was as the same as the value measured at the lab temperature.

CHAPTER 6: THE ROLE OF TEMPERATURE AND PORE WATER CONDUCTIVITY ON RESISTIVITY OF CLAY SOIL

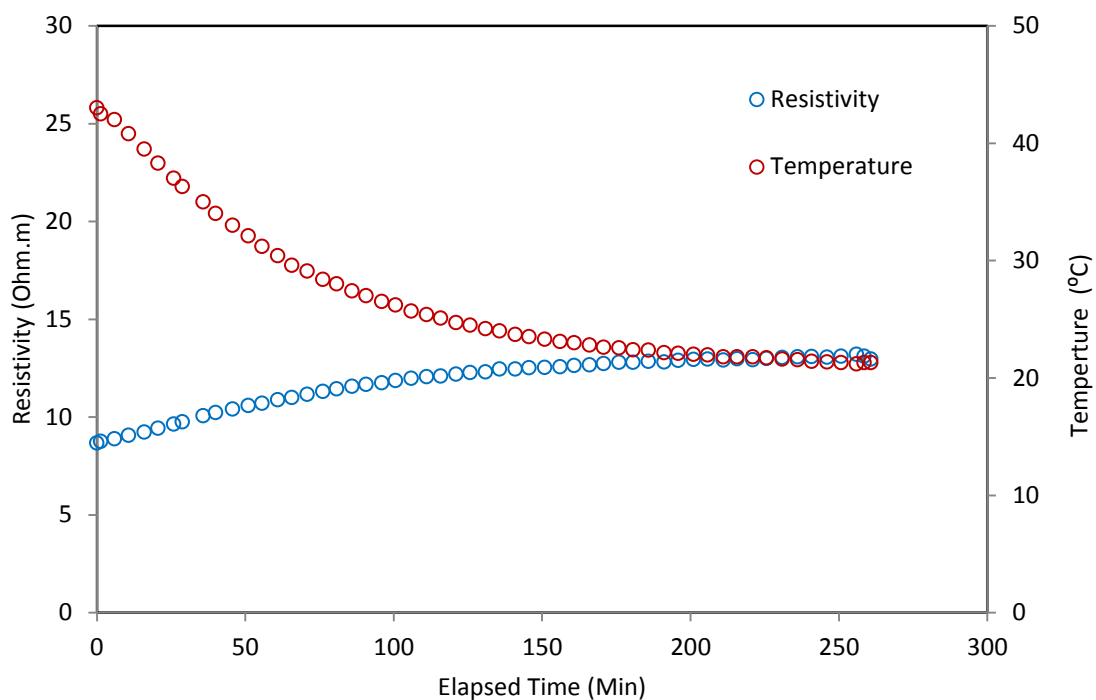


Figure 6.9. Resistivity and temperature data of the heating stage

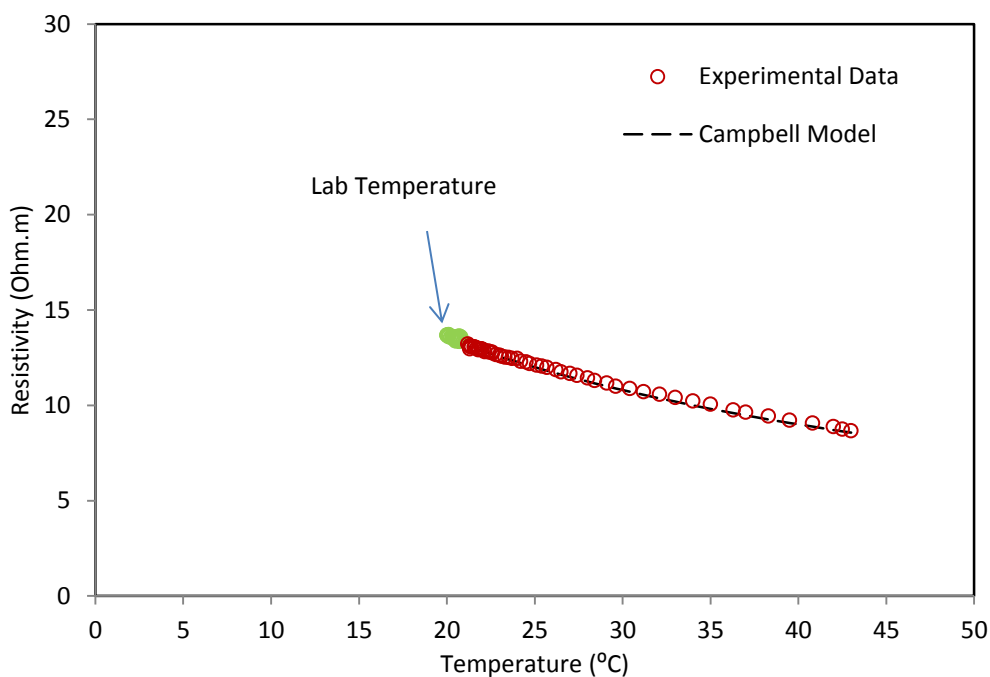


Figure 6.10. The resistivity- temperature relationship of the heating stage

CHAPTER 6: THE ROLE OF TEMPERATURE AND PORE WATER CONDUCTIVITY ON RESISTIVITY OF CLAY SOIL

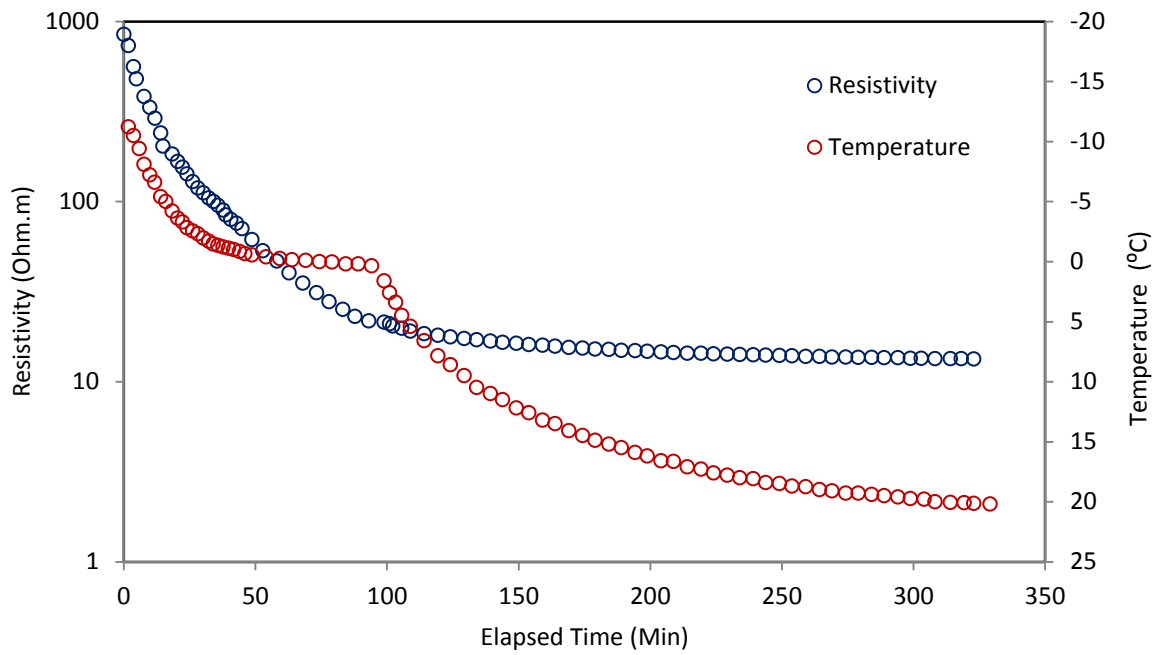


Figure 6.11. Resistivity and temperature data of the freezing stage

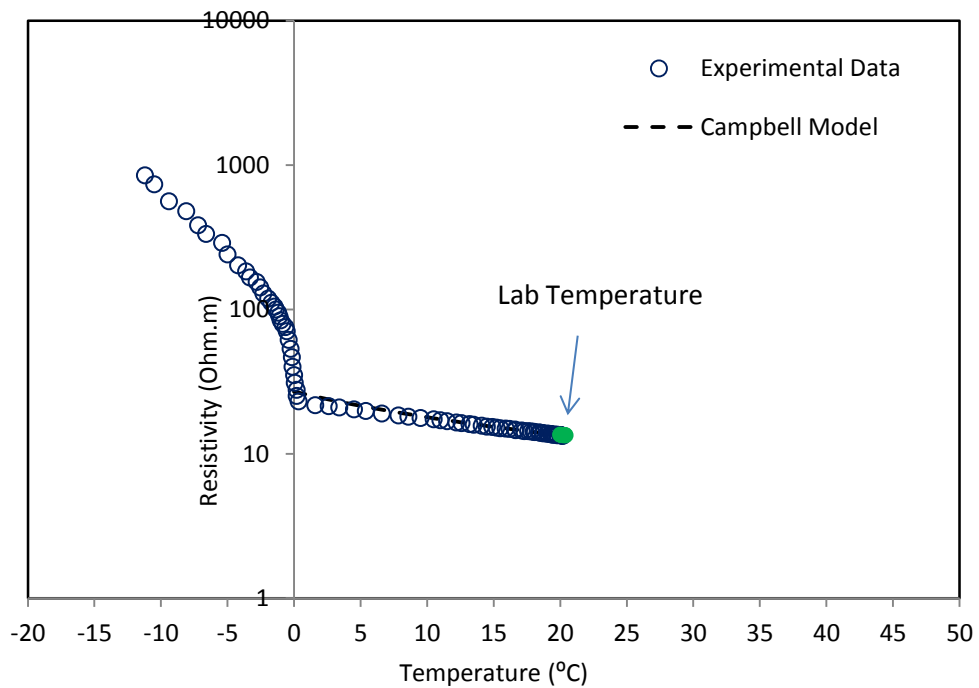


Figure 6.12. The resistivity- temperature relationship of the freezing stage

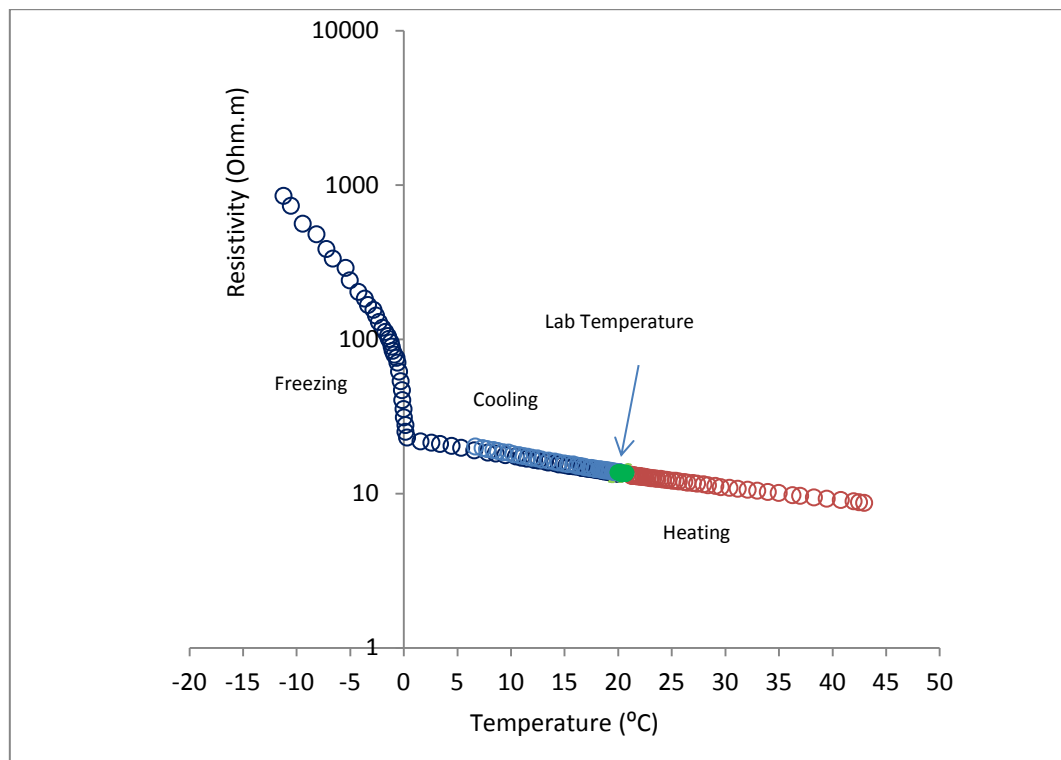


Figure 6.13. The resistivity- temperature relationship of the BIONICS clay

6.3.2 The influence of salt type and concentration on pore water resistivity

Electrical resistivity of the electrolytes

Before testing the effect of salt type and concentration on the soil, the electrical resistivity of the electrolyte solutions prepared was measured using the resistivity probe and Resist. To evaluate the procedure adopted, the electrical conductivity of the electrolytes used was first measured using a HANNA conductivity meter, calibrated using a standard solution. The obtained electrical conductivities were converted into electrical resistivities and compared with those calculated using Resist as shown in Figure 6.14. A good agreement can be seen which confirms that the procedure adopted was performed satisfactory.

Figures 6.15 and Figure 6.16 show the pore water resistivity-salt concentration (expressed by weight) obtained using Resist and the HANNA conductivity meter, respectively. It can be seen that the pore water resistivity decreases with increasing salt concentration. However, at a relatively low salt concentration, the pore water resistivity changes more rapidly, where only a little quantity of salt is added. At high concentration, the influence of salt concentration is less significant, as the ionic density is high and, therefore, the pore resistivity is low and not affected by salt concentration. The salts used showed similar response, but different resistivities as they have different ionic mobility or conductivity (Kalinski and Kelly, 1993). Figure 6.15 and 6.16 indicate a good comparison between the results obtained using Resist and the HANNA conductivity meter.

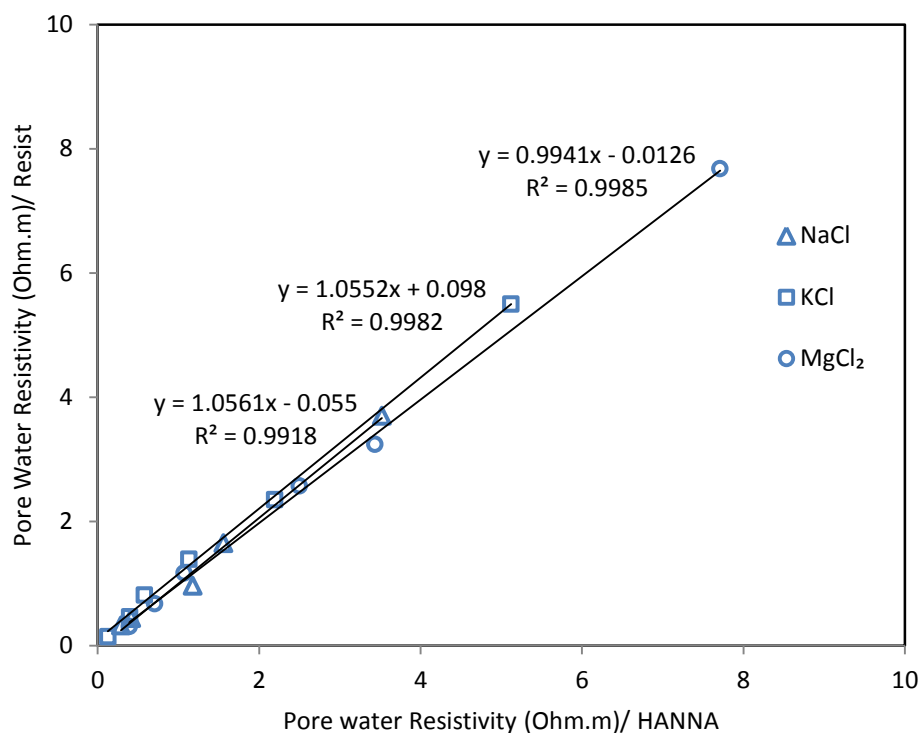


Figure 6.14. A comparison between pore water resistivity measured by Resist and the conductivity meter

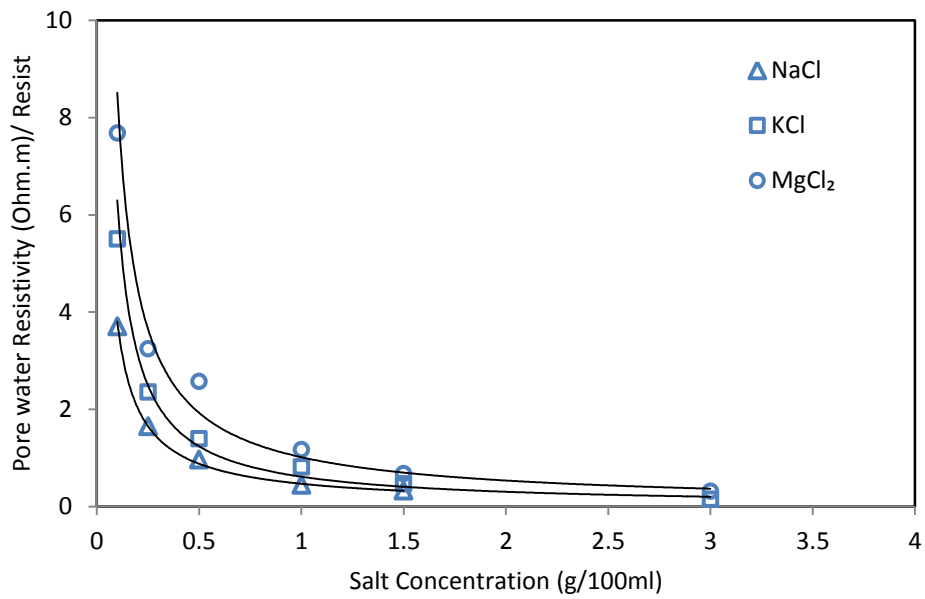


Figure 6.15. The pore water resistivity (measured by Resist) - salt concentration relationship of NaCl, KCl and MgCl₂ solutions

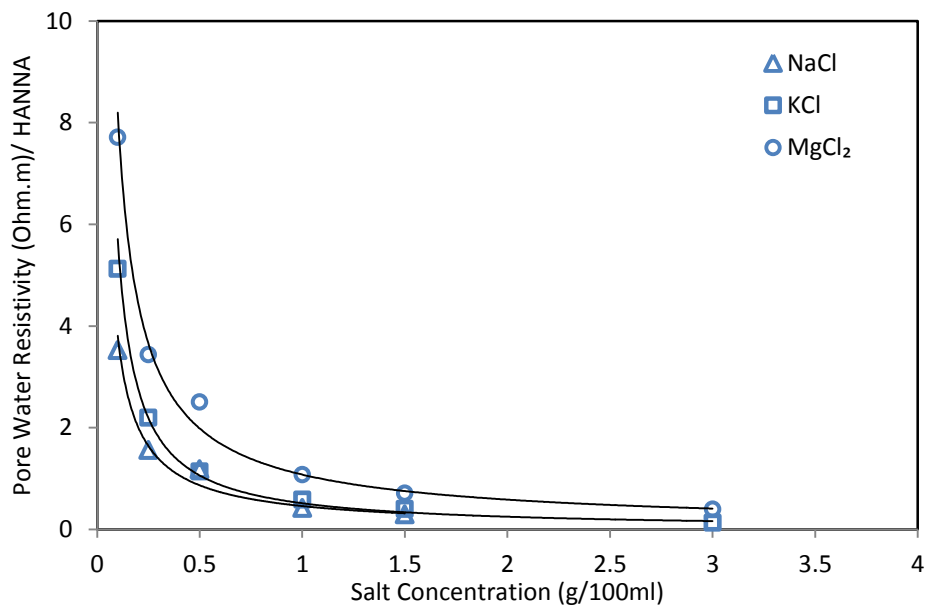


Figure 6.16. The pore water resistivity (measured by HANNA)-salt concentration of NaCl, KCl and MgCl₂ solutions

The influence of salt type and concentration of pore fluid on soil resistivity

The influence of salt type and concentration on soil resistivity was first investigated on specimens prepared at the same gravimetric water content (25%) with NaCl, KCl and MgCl₂ electrolytes of different concentrations. Figure 6.17 shows the influence of electrolyte type and concentration on soil resistivity. It can be seen that resistivity of the soil decreases with an increase of the electrolyte concentration as reported previously by Rinaldi and Custe (2002). The resistivity of soil mixed with NaCl electrolyte decreases from 9.33 to 1.98 Ohm.m. Similarly, the resistivity of soil mixed with KCl electrolyte decreases from 6.59 to 2.83 Ohm.m. The resistivity of soil mixed with MgCl₂ electrolyte decreases from 8.42 to 2.05 Ohm.m. Increasing the salt concentration means more ions are available for current conduction and hence low resistivity. However, the solutions used show different influences on resistivity of the soils, particularly at low concentration. As mentioned by Kalinski and Kelly (1993) and Rinaldi and Custe (2002), electrolytes of the same concentration, but different composition are characterised by different mobility. Therefore, these solutions have different influence on soil resistivity. At high concentrations, the electrical paths are very well achieved, and the influence of electrolyte type and concentration is less significant comparing to low concentration electrolytes. Increasing the salt concentration decreases the pore water resistivity, and hence the soil resistivity.

Increasing the electrolyte concentration decreases the pore water resistivity hence lowers soil resistivity. Figure 6.18 and Figure 6.19 show, respectively, the influence of pore water resistivity measured using Resist and HANNA conductivity meter on soil resistivity. The resistivity increases with increasing pore water resistivity (Zha et al., 2006). Again, different salts have different influence on soil resistivity.

CHAPTER 6: THE ROLE OF TEMPERATURE AND PORE WATER CONDUCTIVITY ON RESISTIVITY OF CLAY SOIL

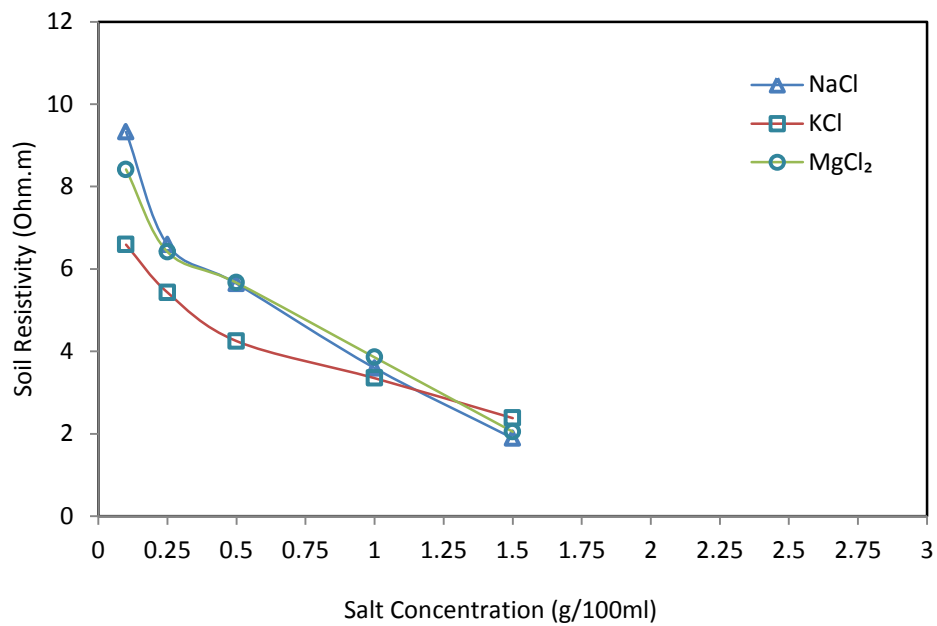


Figure 6.17. The influence of electrolyte type and concentration on resistivity of soil (w=25%)

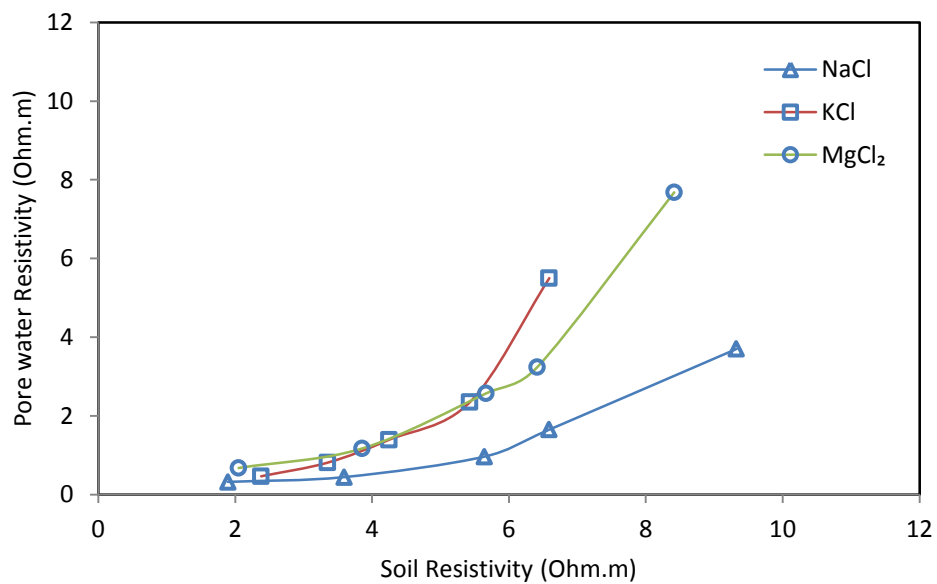


Figure 6.18. The influence of pore water resistivity (measured by Resist) on resistivity of specimens prepared at 25% gravimetric water content with NaCl, KCl and MgCl₂ electrolytes

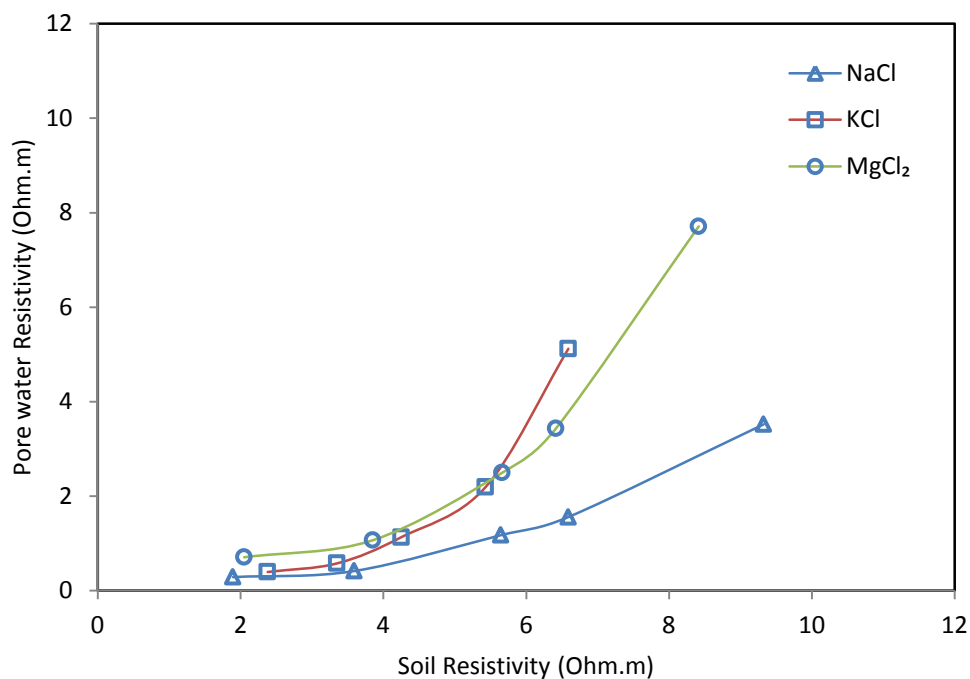


Figure 6.19. The influence of pore water resistivity (measured by HANNA) on resistivity of specimens prepared at 25% gravimetric water content with NaCl, KCl and MgCl₂ electrolytes

The influence of salt concentration on resistivity of soils of different water content

To address the influence of salt concentration on resistivity of specimens prepared at different water content, specimens were prepared using KCl solutions of 0.1, 0.5 and 1.5 g/100ml concentration of distilled water. The resistivity-volumetric water content relationship of these specimens is shown in Figure 6.20. Soil resistivity increases with decreasing the volumetric water content. The resistivity increases from 13.34 to 48.06 Ohm.m for specimens prepared using distilled water while the resistivity increases from 2.87 to 15.26 Ohm.m for specimens prepared using 1.5g/100ml KCl solution. Increasing the salt concentration decreases soil resistivity. However, this influence is less significant at high water content (Zha et al., 2006; 2010), and high salt content (Long et al., 2012).

In addition, using the regressions of the relationships presented in Figure 6.20, the influence of salt concentration on soil resistivity at constant volumetric water content was calculated as shown in Figure 6.21. For a given volumetric water content, resistivity decreases when the salt concentration increases (Kalinski and Kelly, 1993). This explains the differences in soil resistivity resulted from the variations of ionic concentration and composition in soils with the same water content. At 15% volumetric water content, the resistivity decreases from 31.58 to 11.97 Ohm.m for KCl concentration range of 0-1.5 g/100ml. At 35% volumetric water content, the resistivity decreases from 12.69 to 3.30 Ohm.m for the same range of KCl concentration.

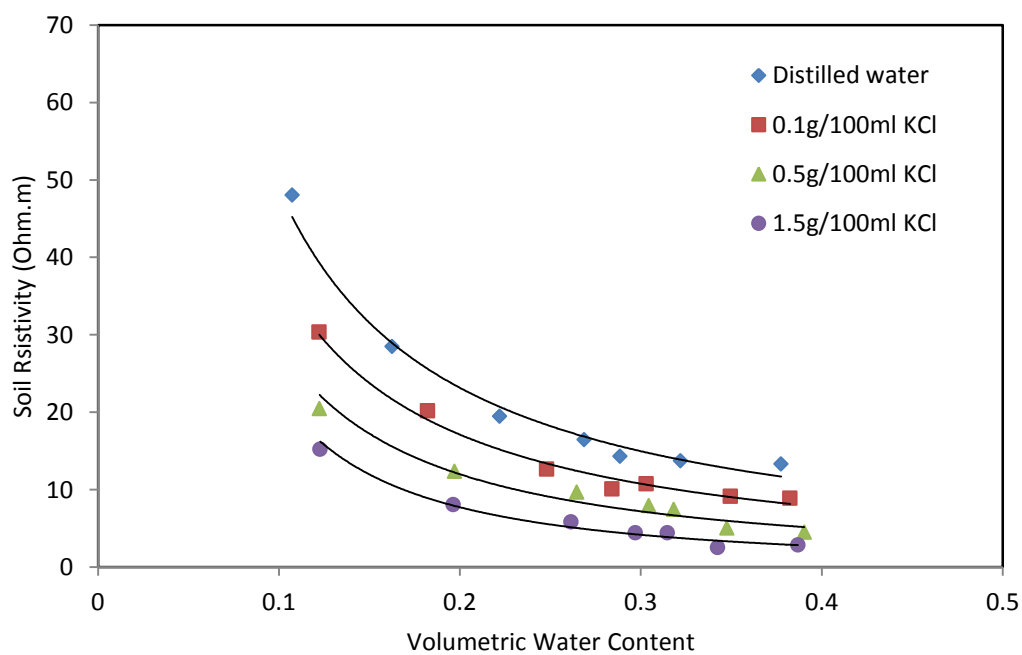


Figure 6.20. Resistivity- volumetric water content of specimens prepared using different KCl concentrations

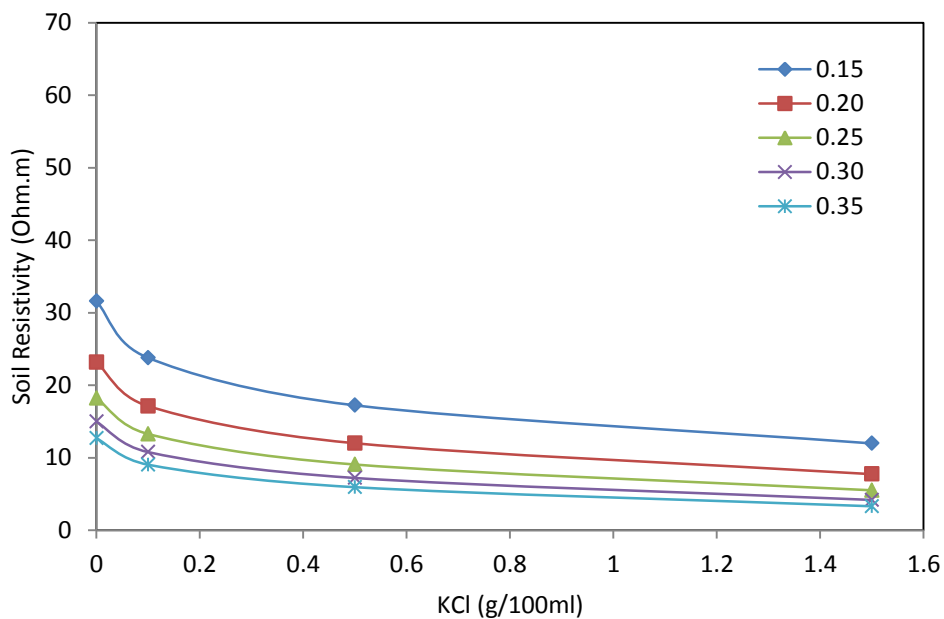


Figure 6.21. The influence of KCl concentration on resistivity at constant volumetric water content

The influence of salt composition on resistivity of soils of different water content

To explore the influence of the salt composition on the soil resistivity measured on specimens prepared at different water content, NaCl salts were added to KCl salts at different concentrations.

Figure 6.22 shows the resistivity-volumetric water content of specimens prepared using 0.1g/100ml KCl, 0.1g KCl and 0.1g NaCl/100ml and distilled water. Soil resistivity increases with decreasing the volumetric water. The resistivity increases from 6.47 to 25.19 Ohm.m for specimens prepared using 0.1g KCl and 0.1g NaCl/100m solution while the resistivity increases from 8.91 to 30.35 Ohm.m for specimens prepared using 0.1g/100ml KCl solution. Adding 0.1g NaCl to the KCl solution decreases the soil resistivity. Adding more salts to the solution increases the number of ions in the water, therefore, decreases the soil resistivity. However, this effect is relatively less significant at high water content.

Similarly, Figure 6.23 shows the resistivity-volumetric water content of specimens prepared using 0.5g/100ml KCl, 0.5g KCl and 0.5g NaCl/100 and distilled water. Soil resistivity increases with decreasing the volumetric water content. The resistivity increases from 3.64 to 15.19 Ohm.m for specimens prepared using 0.5g KCl and 0.5g NaCl/100m solution while the resistivity increases from 4.53 to 20.47 Ohm.m for specimens prepared using 0.1g/100ml KCl solution. Adding 0.5g NaCl to the KCl solution decreases the soil resistivity.

Figures 6.24 and 6.25 present the influence of electrolyte composition on soil resistivity at constant volumetric water content, based on the regressions of the relationships shown in Figure 6.22 and 6.23, respectively.

For a constant volumetric water content, adding more salts to the water decreases soil resistivity comparing to the resistivity of soil mixed with distilled water. Figure 6.24 shows that at 0.15 volumetric water content, the resistivity decreases from 31.58 Ohm.m for a specimen prepared with distilled water to 16.24 Ohm.m for a specimen prepared with 0.1g KCl and 0.1g NaCl/100 ml (the percentage decrease 94.46%). Similarly, Figure 6.25 shows that at 0.15 volumetric water content, the resistivity decreases from 31.58 Ohm.m for a specimen prepared with distilled water to 12.36 Ohm.m for a specimen prepared with 0.5g KCl and 0.5g NaCl/100 ml (the percentage decrease 155%). Again, adding more salts to the solution increases the pore water conductivity, therefore, decreases the soil resistivity.

Further research is needed to determine the pore water salinity changes in the field in order to determine the implication of salt type and concentration variations on soil resistivity.

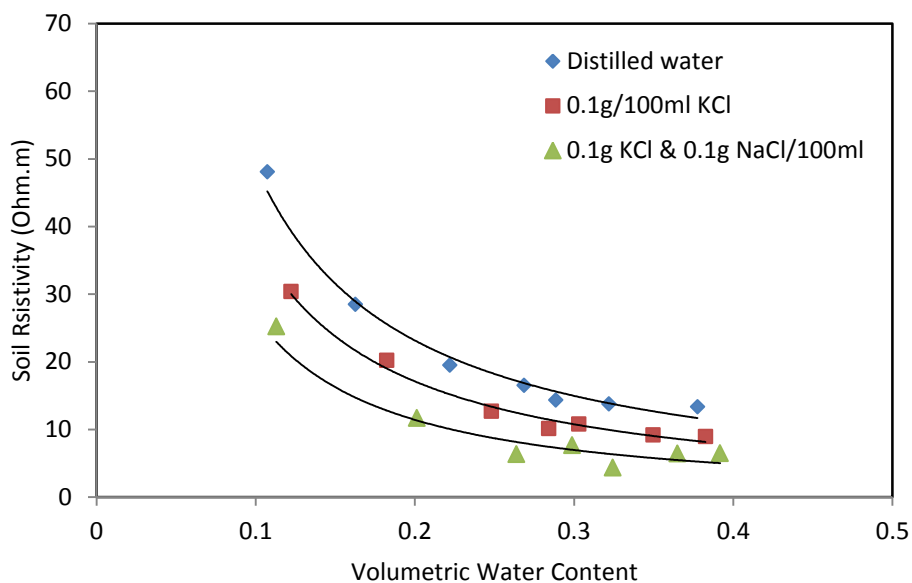


Figure 6.22. Resistivity-volumetric water content of specimens prepared using 0.1g/100ml KCl, 0.1g KCl and 0.1g NaCl/100ml and distilled water

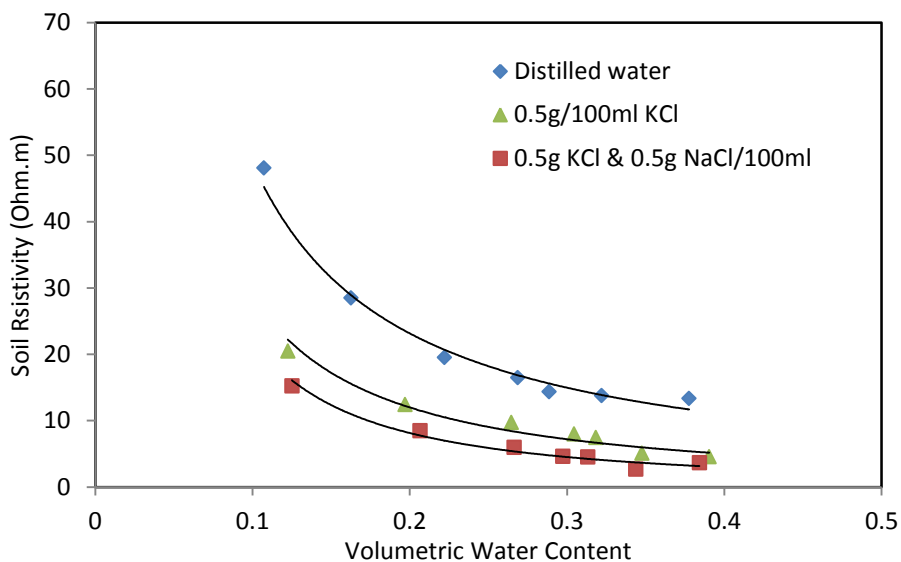


Figure 6.23. Resistivity-volumetric water content of specimens prepared using 0.5g/100ml KCl, 0.5g KCl and 0.5g NaCl/100 and distilled water

CHAPTER 6: THE ROLE OF TEMPERATURE AND PORE WATER CONDUCTIVITY ON RESISTIVITY OF CLAY SOIL

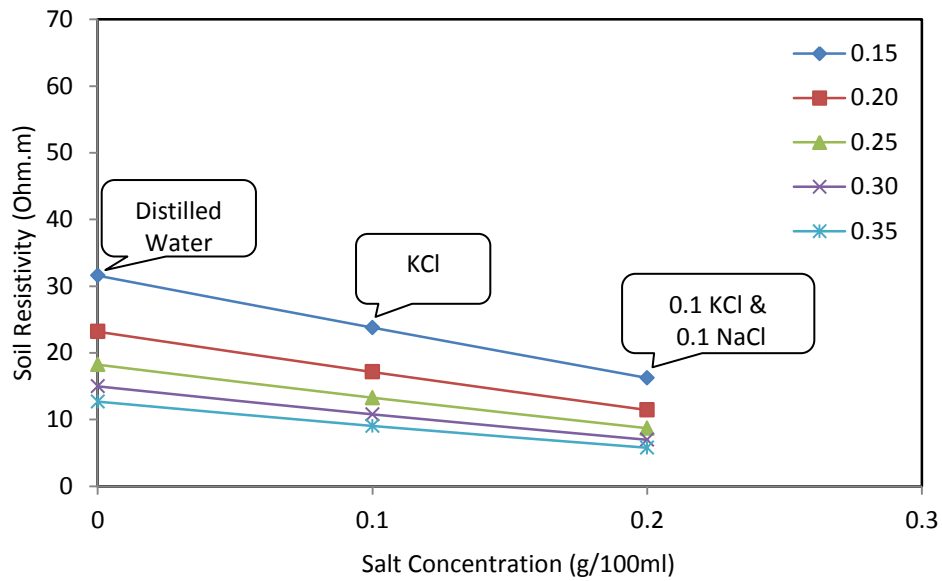


Figure 6.24. The influence of electrolyte composition on soil resistivity at constant volumetric water content (based on the regressions of the relationships in Figure 6.22)

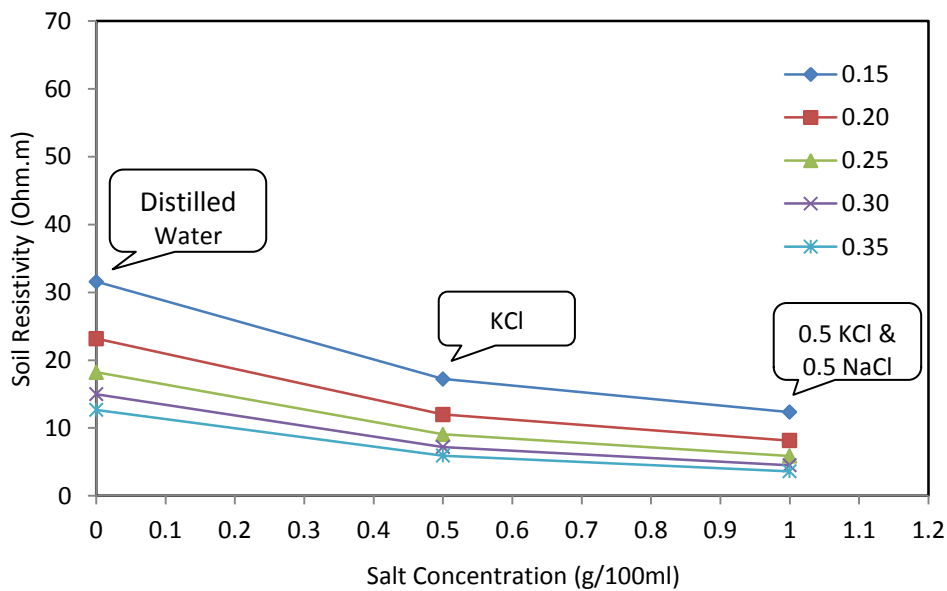


Figure 6.25. The influence of electrolyte composition on soil resistivity at constant volumetric water content (based on the regressions of the relationships in Figure 6.23)

6.4 Chapter summary

This chapter aimed to explore the role of temperature and pore water conductivity on resistivity of BIONICS clay. The influence of temperature was investigated over the temperature range -12 to 43°C. The resistivity of the soil decreases when the temperature increases. At temperatures above the freezing point, the resistivity is low and decreases with the temperature following the Campbell model. At temperatures below freezing, the resistivity is significantly higher and decreases non-linearly with the temperature. The developed relationship between the resistivity and temperature for the data above freezing is useful to correct the field data to a reference temperature.

The results showed that the pore water conductivity plays an important role on soil resistivity. As electrical conduction takes place via displacements of ions, changing the type and concentration of salts mixed with water changes the resistivity of the soil significantly. However, this influence is less significant at high water contents and at high concentrations, where the current paths are already achieved. In addition, since different ions have different ionic mobility, specimens mixed with different salts of the same concentration showed different resistivities. The results also showed that, for a given water content, increasing salt concentration (or decreasing pore water resistivity) causes a decrease in soil resistivity. This explains the differences in soil resistivity resulting from the variations of ionic concentration and composition in soils of the same water content.

Further research is needed to determine the pore water conductivity changes of BIONICS clay in the field in order to understand the implications of the pore water conductivity changes on resistivity of the soil measured at different seasons. For short term studies, pore water conductivity is relatively constant and hence its effect can be ignored compared to water content changes.

Chapter 7

Electrical resistivity for characterising drying and wetting of clay soils

Unsaturated clay soils are inevitably subjected to drying and wetting cycles linked to climate effects. In addition to negative pore pressures (suctions) induced by drying, water content and volume changes are essential controlling parameters that should be investigated further. Although numerous studies have been undertaken to consider the effect water content has on soil resistivity, the effects of drying and wetting of clay soil, and the volume changes associated have rarely been addressed. However, such tests are important to understand the long-term stability and serviceability of engineered earth structures such as road embankments.

Therefore, this chapter explores the potential of the resistivity method for characterising the drying and wetting of clay soils. The resistivity behaviour of BIONICS clay and other local clays (from Birtley, Co. Durham and Newcastle) and pure clays (Kaolinite and Bentonite) subjected to controlled drying and wetting procedures are studied. In addition to a discrete drying and wetting procedure, the resistivity, water content and volume changes are obtained automatically in a continuous procedure.

7.1 Introduction

Clay soil is subjected to progressive failure due to the swell and shrink behaviour of clay minerals. The soil absorbs the water during wet seasons and hence the volume increases, and dries out during the dry seasons and hence the volume decreases.

Geotechnical studies of unsaturated clay soils have shown that clay soils exhibit hydraulic hysteresis (i.e. drying and wetting paths of the soil water retention curve (SWRC) do not coincide; see the SWRC of BIONICS clay shown in Figure 2.10, Chapter 2). For BIONICS clay, this behaviour is mainly attributed to the pore network structure of ink-bottle shape, and the volume changes linked to the shrink-swell behaviour, as detailed by Lourenço (2008).

A number of authors have discussed the resistivity behaviour of clay soils in terms of soil microstructure. Fukue et al. (1999) showed that the continuity/discontinuity of pore water plays an important role in soil resistivity. At high water content, the continuity of the water phase provides pathways for current and, therefore, results in low resistivity. At low water content, the discontinuity of the water causes abrupt resistivity changes. Therefore, the resistivity-water content relationship can be divided into two segments of low and high resistivity. Robain et al. (2001) linked the low and high resistivity values, respectively to the macro and micro porosity, where low resistivity is related to macropores, as water can be more easily accessible to the electrical current compared to micro pores. Pozdnyakov et al. (2006) discussed soil resistivity in terms of the mobility of the ions that are highly influenced by the state of pore water molecules. At low water content (i.e. adsorbed, film and film-capillary water as will occur in micro-pores), the influence of water on resistivity is significant while, at high water content (capillary and gravitational water as will exist in macro-pores), the effect of water on the resistivity is less significant. Therefore, the resistivity decreases rapidly with increasing water content in the first range then decreases less rapidly in the second range. At water content close to saturation, the resistivity is almost independent of water content, as the electrical charges are not affected by the mobility of water molecules.

As reviewed in Chapter 2, a number of studies have demonstrated an explicit relationship between resistivity and water content. However, drying and wetting of clay soil

and the volume changes associated have rarely been considered. In a few studies, the soil resistivity has been measured in a discrete style (i.e. stage drying/wetting). According to the author's knowledge, no previous tests have conducted where resistivity, water content and volume changes are monitored continuously and simultaneously on soil specimens subjected to drying/wetting procedures. These tests are essential to explore the effects of water content and volume changes during drying and wetting of the soil. Such tests require automated and continuous data acquisition which add complexity to the measurement setup.

7.2 Experimental setup

7.2.1 Specimen preparation

For uncompacted specimens, following the work of Russell and Barker (2010), distilled water was added to the oven dried and sieved soil to achieve a malleable homogeneous texture. The soil samples were left to equilibrate in plastic containers (180mm length, 120mm width and 70mm depth). Four stainless steel electrodes with 15mm inter-electrode spacing were fixed on a perspex plate (See Figure 3.14a, Chapter 3), and used to measure the resistivity during drying and wetting of the soil. At each stage, ρ_α and ρ_β resistivity values were obtained and hence the mean of the two directional measurements was calculated. The resistivity and water content of BIONICS and other local and pure soils were obtained in a discrete style, provided one of the first studies of the electrical characteristics of clays during drying and wetting.

For compacted specimens, the soil was compacted following the procedure described in Chapter 5. The tests were performed in discrete and continuous procedures on BIONICS specimens. Resistivity measurements were obtained using the resistivity probe described in Chapter 3.

7.2.2 Drying and wetting procedures

Drying and wetting of the soil were performed using discrete and continuous styles (Lourenço, 2008). In the discrete method, the drying or wetting was performed in stages where the resistivity and mass (or water content) of the specimen were obtained at each stage after 24 hours of equalisation to allow water content homogenisation. In the continuous method, the resistivity, mass and volume changes of the specimen were collected continuously.

Although the discrete style offers the time needed for water content homogenisation, only the gravimetric water content can be obtained and compared with the measured resistivity. Volume changes measurement of the specimen is clearly beneficial to observe changes in the volumetric water content and the degree of saturation.

Drying was achieved by exposing the specimens to air in a temperature controlled laboratory. Wetting of specimens was achieved by carefully adding water to the surface of the samples using a syringe. To ensure water content homogeneity (Muñoz-Castelblanc et al., 2011) water drops were uniformly distributed over a filter paper placed on the top of the sample (the filter paper was used for uncompacted samples).

7.2.3 Automated data acquisition: Continuous procedure

The continuous procedure requires automated measurements of the resistivity, mass and volume changes (if included) of the specimen. Several factors affect the measurement setup. Lourenço (2008) pointed out factors that can contribute to the spread of the data collected such as heterogeneities in drying or wetting, evaporation rates, surface area exposed to the air and the influence of the equipment cables, hence, errors in mass readings.

Volume changes of the specimens were obtained using a modified apparatus designed by Guanshi Liu (unpublished) for continuous drying experiments. Five displacement transducers, installed in PVC beams, were used to measure the radial and vertical changes of specimen dimensions (Figure 7.1). The specimen (50mm Diameter, 20mm Height) was placed on a support plate, and the resistivity probe was attached on the top of the specimen (Figure 7.1). To minimize the effect of the cables on mass measurement (Lourenço, 2008), the cables were supported by stands. The apparatus was placed on an electronic balance for mass measurement logged via RS232 interface. The gravimetric water content of the specimen was calculated from the dry mass obtained at end of the test, and used for back calculation of the gravimetric water content throughout the test. The volume changes were used to calculate the volumetric water content and the degree of saturation.

The resistivity, mass, radial and axial displacements of the specimen, were all logged automatically by the data acquisition system developed in the current thesis. Figure 7.2 shows an example of the mass and the displacement measurements versus the elapsed time during a continuous drying test. Because of drying, the mass and volume of the specimen reduce with time. The displacement measurements indicate relatively high, linear changes to a particular point (below the shrinkage limit) then these changes become insignificant. This can be attributed to the microstructure changes during drying. At the beginning of the test where the water content is high, the water dries out from the macropores with high volume change. With the progressive drying, the water comes from the micropores with little overall volume change. Figure 7.2 shows that the decrease of the specimen mass was nearly linear with time.



Figure 7.1. The experimental setup of the continuous procedures tests

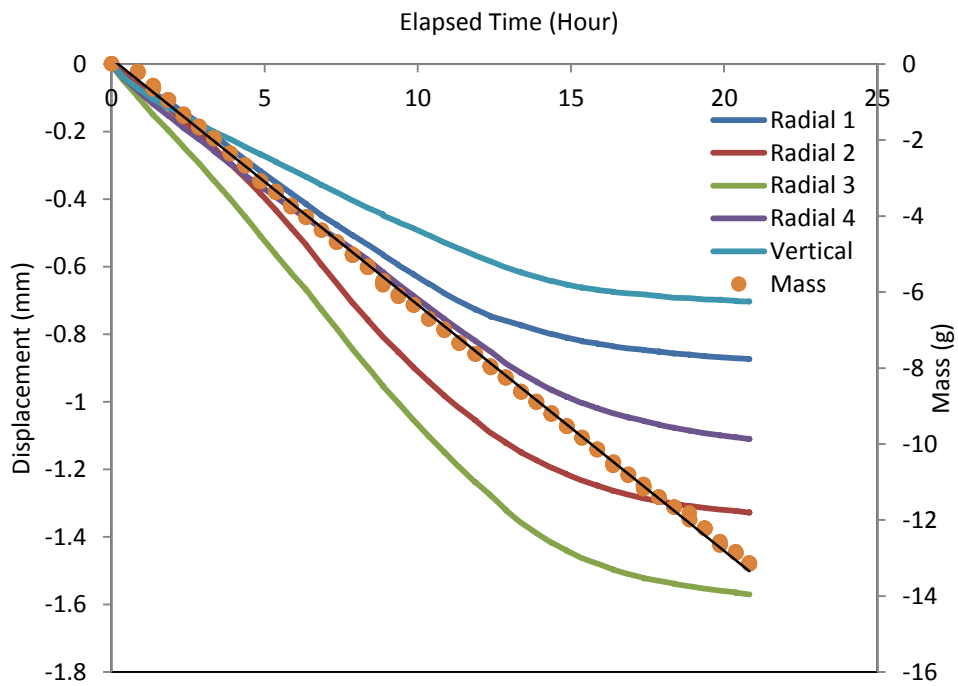


Figure 7.2. Volume and mass measurements of drying test

7.3 Results and discussion

7.3.1 Discrete drying and wetting: uncompacted specimens

Figures 7.3, 7.4 and 7.5 show the resistivity-gravimetric water content relationships of the uncompacted specimens, respectively, BIONICS, Birtley and a contaminated soil from Newcastle (Asquith, PhD thesis in preparation). The measurements were repeated daily in discrete drying and wetting styles with the samples being sealed between the measurements.

In general, the range of the measured resistivities is within the typical resistivity range of clay soils, and the resistivity-water content relationships illustrate the power law relationship reported in the literature for different types of clay soils (e.g. McCarter, 1984; Calamita et al., 2012).

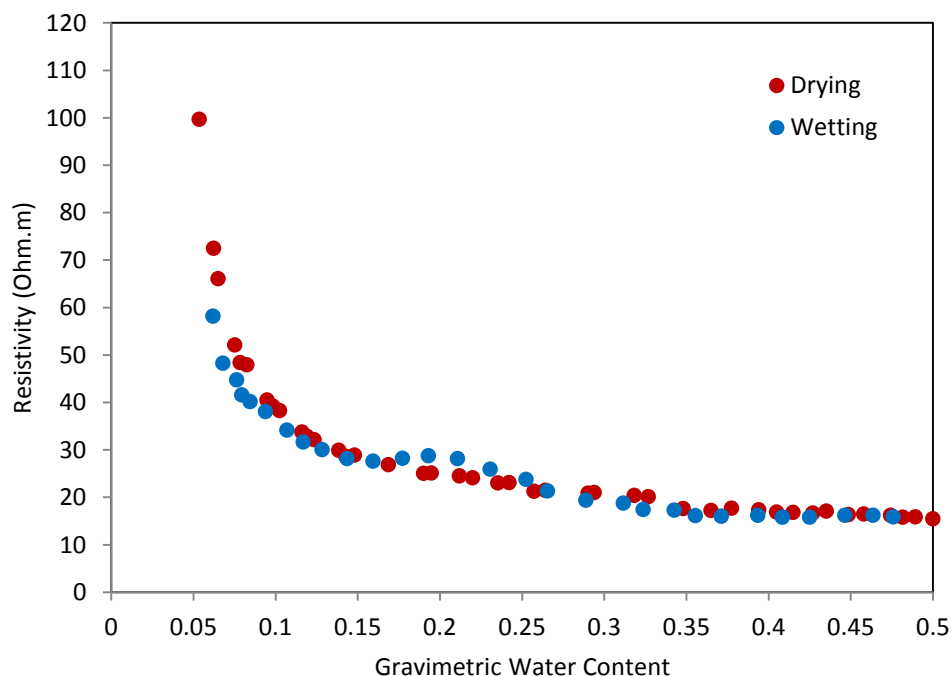


Figure 7.3. The resistivity-gravimetric water content relationship of BIONICS clay

CHAPTER 7: ELECTRICAL RESISTIVITY FOR CHARACTERISING DRYING AND WETTING OF CLAY SOILS

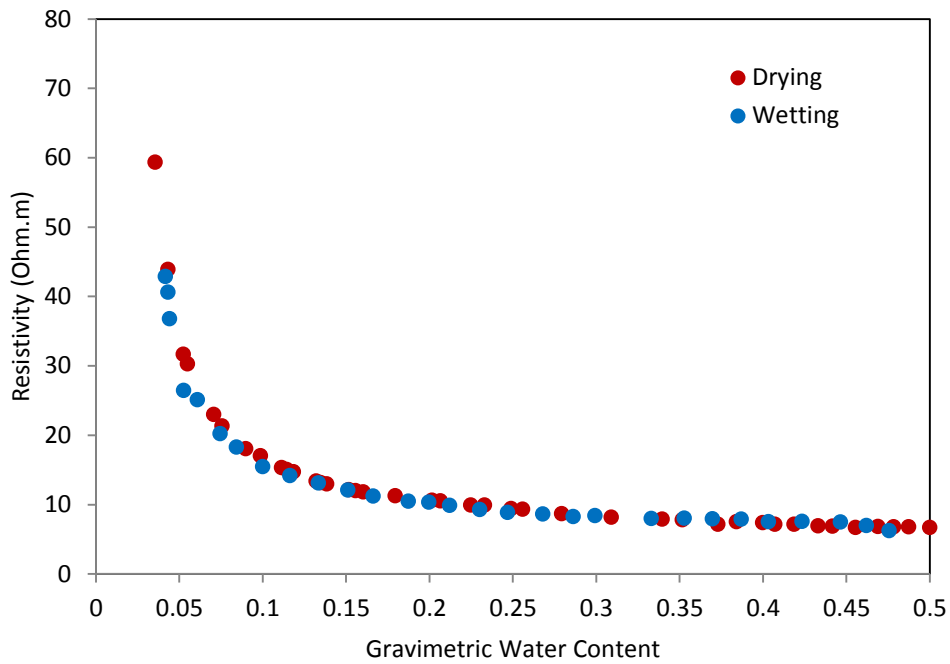


Figure 7.4. The resistivity-gravimetric water content relationship of Birtley Clay

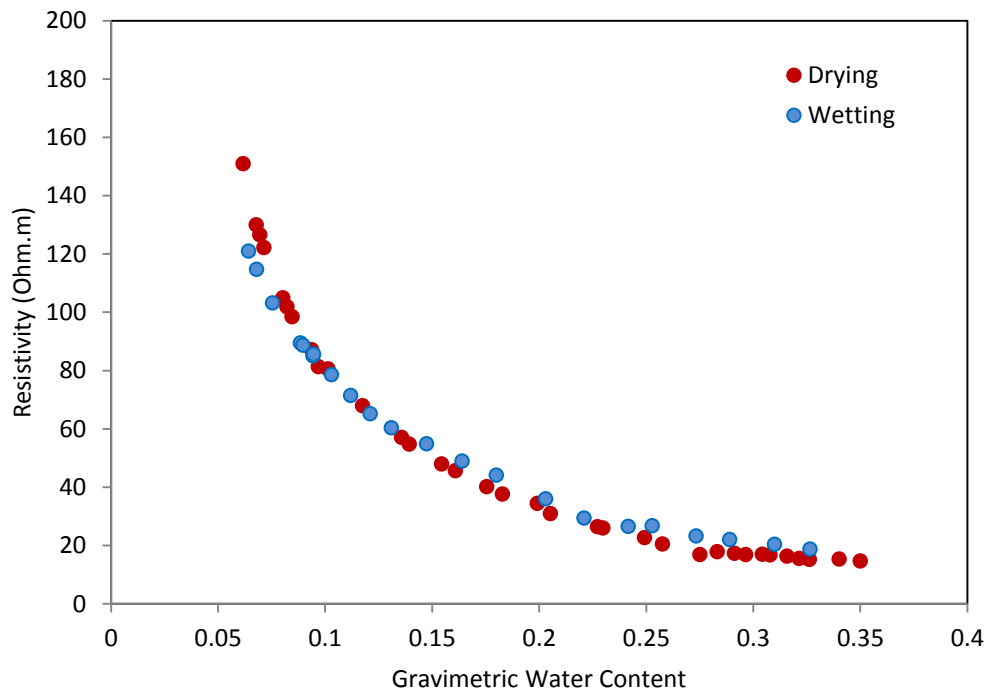


Figure 7.5. The resistivity- gravimetric water content relationship of the contaminated soil

As the electrical conduction takes place via the ions in the pore water, the resistivity increases with decreasing water content for the drying path and decreases with increasing the water content for the wetting path. This trend is consistent with other drying/wetting tests (e.g. Muñoz-Castelblanco et al., 2011; Hen-Jones et al., 2014). The resistivity of BIONICS clay increases from 15.51 to 99.70 Ohm.m for the drying path and decreases from 58.20 to 15.84 Ohm.m during the wetting path. For Birtley Clay, the resistivity increases from 6.66 to 59.34 Ohm.m during the drying path and decreases from 43.89 to 6.22 Ohm.m during the wetting path. The resistivity of the contaminated soil increases from 14.67 to 150.99 Ohm.m during the drying and decreases from 121.00 to 18.73 Ohm.m during the wetting.

It also can be noticed that the resistivity decreases abruptly at the beginning of the wetting path due to the water added, and then decreases gradually when water content increases. At the end of the wetting path, the resistivity returns to a value very close to the value measured at the beginning of drying test.

The BIONICS clay exhibits some "electrical" hysteresis (the resistivity of the wetting path does not coincide with the resistivity of drying path). The hysteresis can be explained by differences in the saturation history (i.e. differences in water geometries being setup during drying and wetting) (Knight, 1981). In other words, the water does not occupy the same pores during drying and wetting, hence, differences in the measured resistivities. According to Knight (1981), the hysteresis, although not repeatable, was noticed at mid saturation level, and the resistivity rapidly returns to the values measured during drying. The hysteresis in SWRC of BIONICS clay was reported by Lourenço (2008). Electrically, the drying and wetting curves have relatively comparable shapes which confirm that the resistivity is mainly dependent on the water content not the energy potential (i.e. the matric suction) (Muñoz-Castelblanc et al., 2011). The resistivity behaviour can be related to the microstructure and the pore water state changes during drying and wetting. In the drying

path, at high water content (the gravitational range), the pores are filled with water, hence, low resistivity and the influence of water content changes on the measured resistivity is insignificant. With progressive drying, the resistivity changes more abruptly due to the air replacement and the discontinuity of the water phase. In the wetting path, differences in the saturation history caused the hysteresis. At the end of the wetting path, the pores are filled again by water; hence, the resistivity returns to a value very close to the value measured at the beginning of drying test.

Figures 7.6 and 7.7 show the resistivity-gravimetric water content relationships of Speswhite Kaolinite and Wyoming Bentonite, respectively. The resistivity of Kaolinite increases from 10.91 to 121.81 Ohm.m for the drying path and decreases from 95.60 to 11.70 Ohm.m during the wetting path. The drying path shows that the resistivity increases gradually with decreasing water content, and an abrupt increase in the resistivity was seen at a relatively low water content. The Kaolinite is characterised by 1:1 structure which explains the gradual resistivity changes, as the resistivity changes mainly as a function of the water from the macropores (Russell and Barker, 2010). The wetting path exhibits considerable hysteresis. However, the resistivity returns to a value close to the value measured at the beginning of drying test.

For the Bentonite (known by 2:1 structure of high shrink-swell behaviour), the resistivity is very low and changes gradually for much longer. The resistivity increases from 1.49 to 23.61 Ohm.m. During drying, a sharp increase in the resistivity was seen at a relatively high water content (comparing to all other samples) due to the considerable shrinkage and cracks developed at the surface (Russell and Barker, 2010). Therefore, the wetting was not performed. The resistivity-gravimetric water content relationships of pure clays show a similar nonlinear trend to other natural clays.

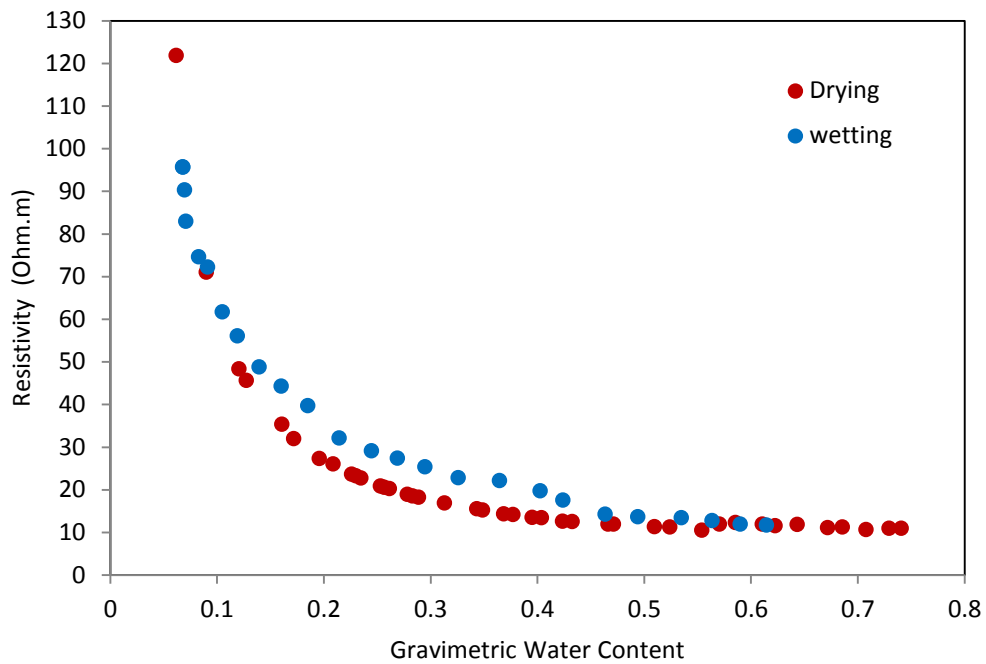


Figure 7.6. The resistivity-gravimetric water content relationship of Kaolinite

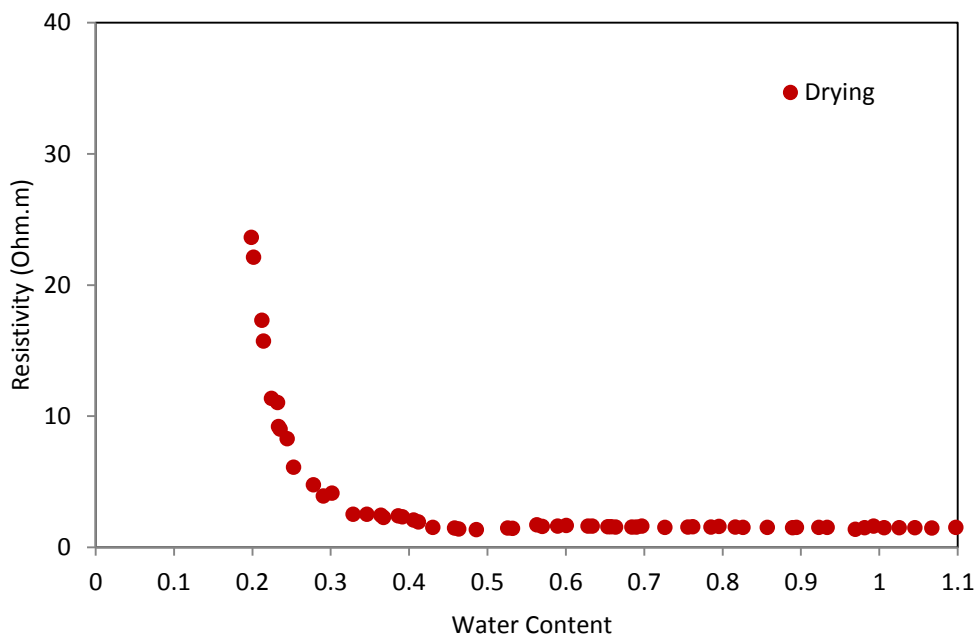


Figure 7.7. The resistivity-gravimetric water content relationship of Bentonite

7.3.2 Drying and wetting: Compacted specimens

Drying and wetting tests were performed on compacted specimens of BIONICS clay. The tests are outlined in Table 7.1.

Table 7.1 Tests performed on compacted samples

Test	Initial water content (%)	Test type	Volume change measurement
t1	24.90	Discrete drying	No
t2	24.72	Discrete drying	No
t3	25.18	Discrete drying and wetting	No
t4	24.56	Discrete drying and wetting	No
t5	29.96	Continuous drying	No
t6	24.75	Continuous drying	Yes
t7	25.00	Continuous drying	Yes
t8	24.66	Continuous drying	Yes
t9	24.72	Continuous drying	Yes
t10	19.92	Continuous drying	Yes
t11	19.90	Continuous drying	Yes
t12	19.97	Continuous drying	Yes
t13	20.21	Continuous drying	Yes

Discrete Drying

Figure 7.8a shows the discrete drying of tests t1 and t2. The tests t1 and t2 indicate a very comparable power law trend mentioned previously. The range of the measured resistivity (13.44 to 49.50 Ohm.m for t1 and 14.55 to 39.00 Ohm.m for t2) was relatively lower than the range measured for the uncompacted sample for the same range of water content, as shown in Figure 7.8b for comparison. This can be attributed to the influence of the compaction. Compaction reduces the voids and increases the degree of saturation, hence, lowers the soil resistivity (Abu-Hassanein et al., 1996; Seladji et al., 2010).

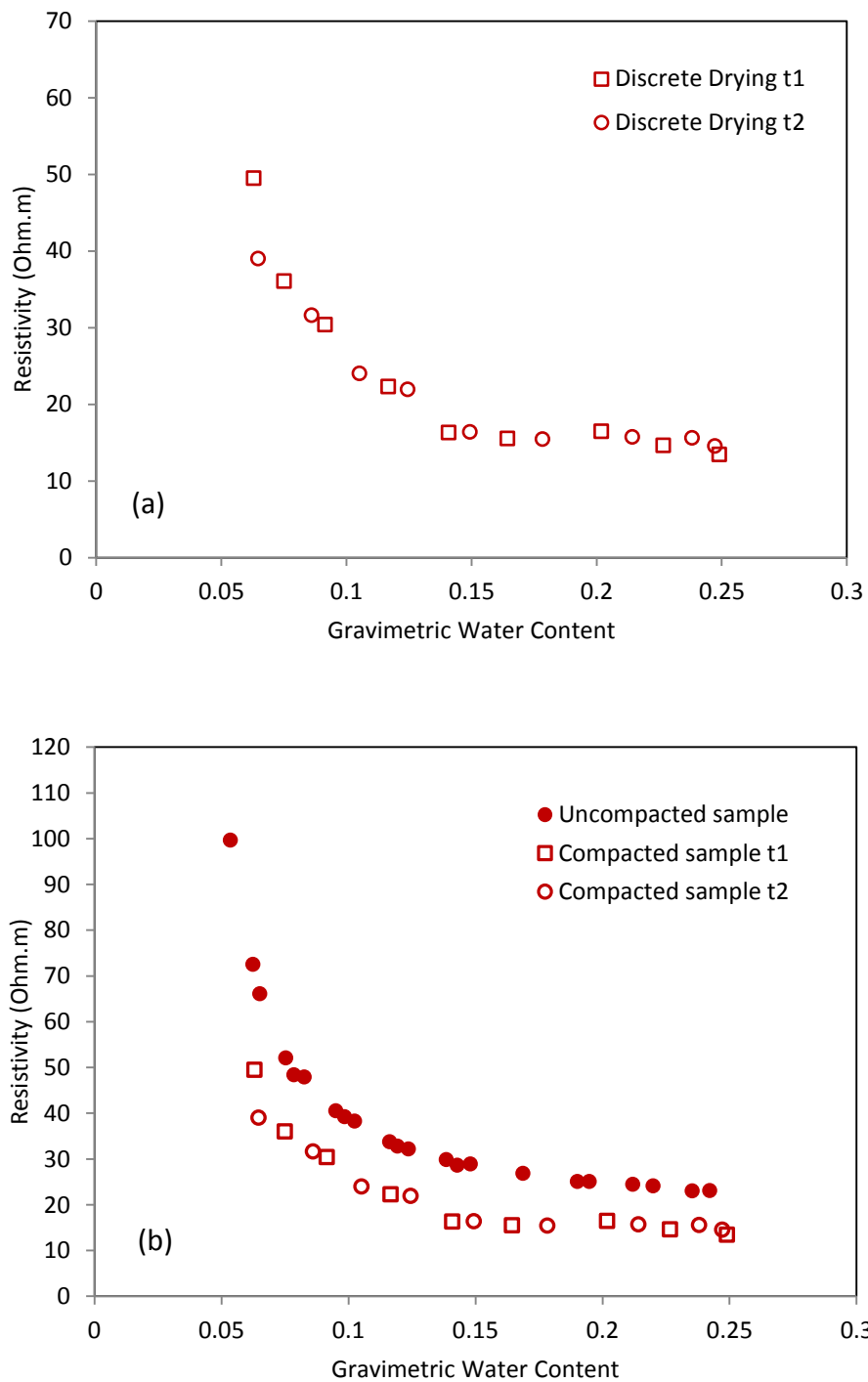


Figure 7.8 The resistivity-gravimetric water content of discrete drying (a) Compacted samples t1 and t2 (b) A comparison of t1 and t2 with the uncompact sample

Discrete drying and wetting

Discrete drying and wetting were conducted on BIONICS specimen t3 (Figure 7.9) and t4 (Figure 7.10). The resistivity of t3 increases from 13.79 to 49 Ohm.m for the drying path and decreases from 44.38 to 15.23 Ohm.m for the wetting path. For t4 test, the resistivity increases from 16.17 to 45.52 Ohm.m for the drying path and decreases from 33.76 to 17.42 Ohm.m for the wetting path. The resistivity-water content relationships exhibit hysteresis.

Figure 7.11 presents the data of t3 and t4 together. The drying paths of t3 and t4 show a relatively similar trend, and the hysteresis occurs in the middle part of the paths.

The resistivity of BIONICS clay exhibits hysteresis as has been confirmed by SWRC. The hysteresis can complicate the use of the resistivity data in unsaturated soil testing as the relationship between the resistivity and water content is dependent on the saturation history, therefore, the hysteresis of the resistivity has to be considered when using the resistivity to interpret cycles of drying and wetting.

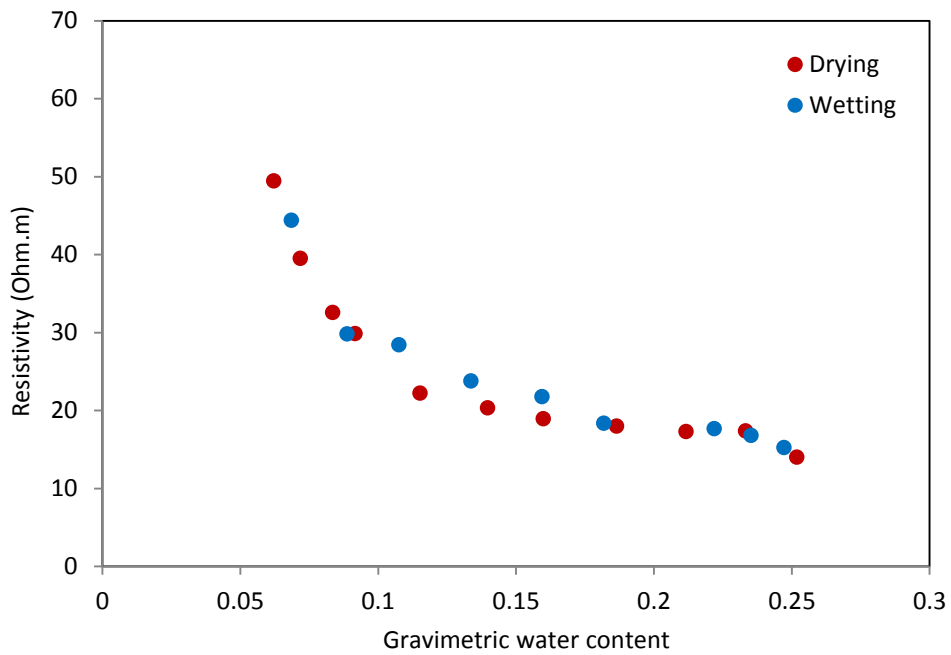


Figure 7.9. Discrete drying and wetting test t3

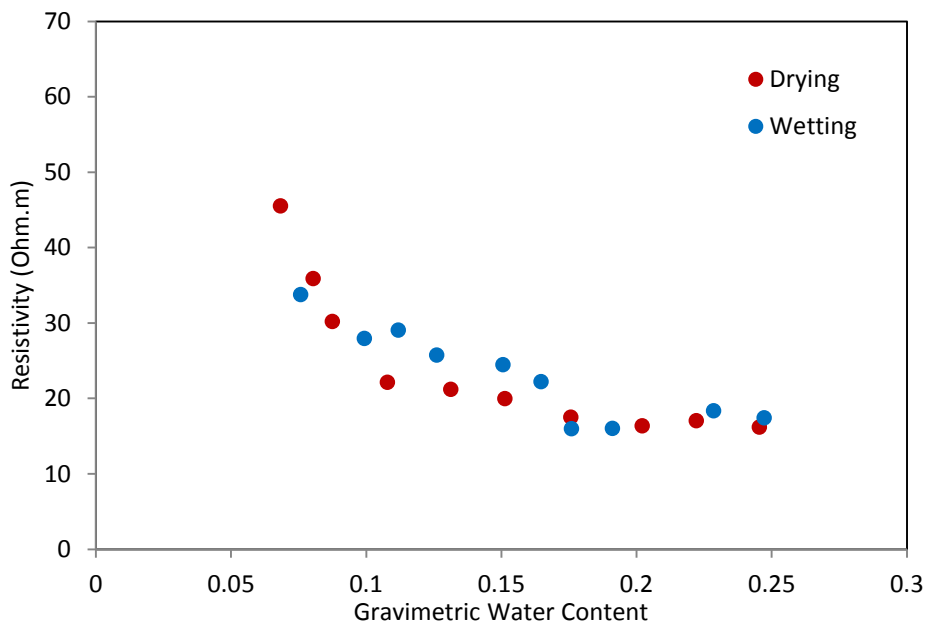


Figure 7.10. Discrete drying and wetting test t4

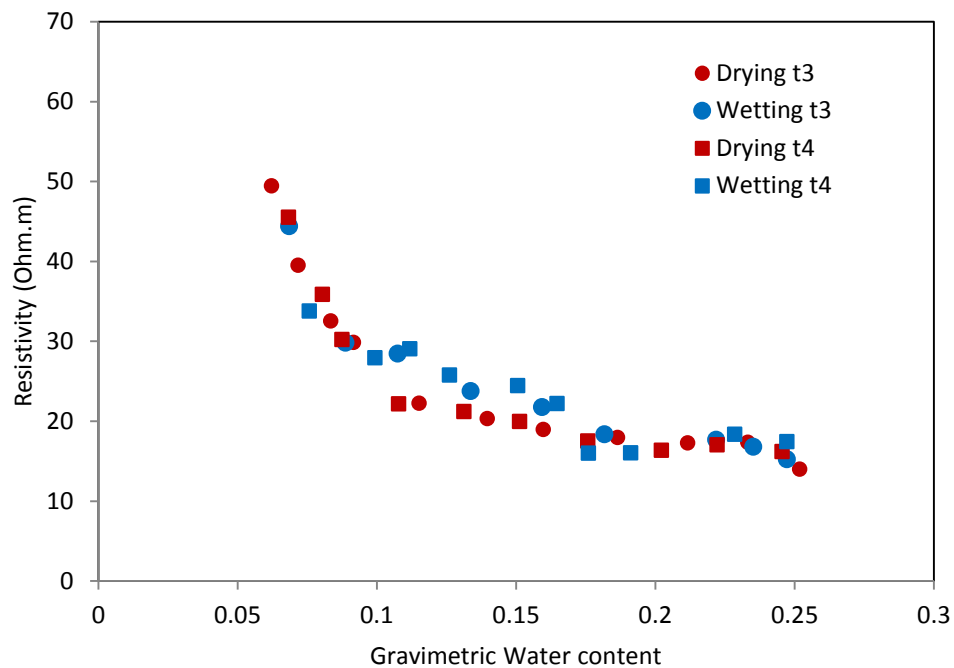


Figure 7.11. A comparison between t3 and t4

7.3.3 Continuous drying

Continuous drying without volume change measurement

A continuous drying test t5 (without volume changes measurement) was conducted on the specimen t5 ($w=30\%$). Figure 7.12 shows the resistivity and gravimetric water content versus the elapsed time. Inspection of Figure 7.12 shows that the gravimetric water content decreases linearly with respect to the time. The resistivity increases non-linearly with time. Figure 7.13 shows the resistivity-gravimetric water content of the test that indicates a typical power law relationship noticed in the discrete drying tests. The resistivity increases from 12.86 to 50.08 Ohm.m with decreasing water content from 0.30 to 0.08.

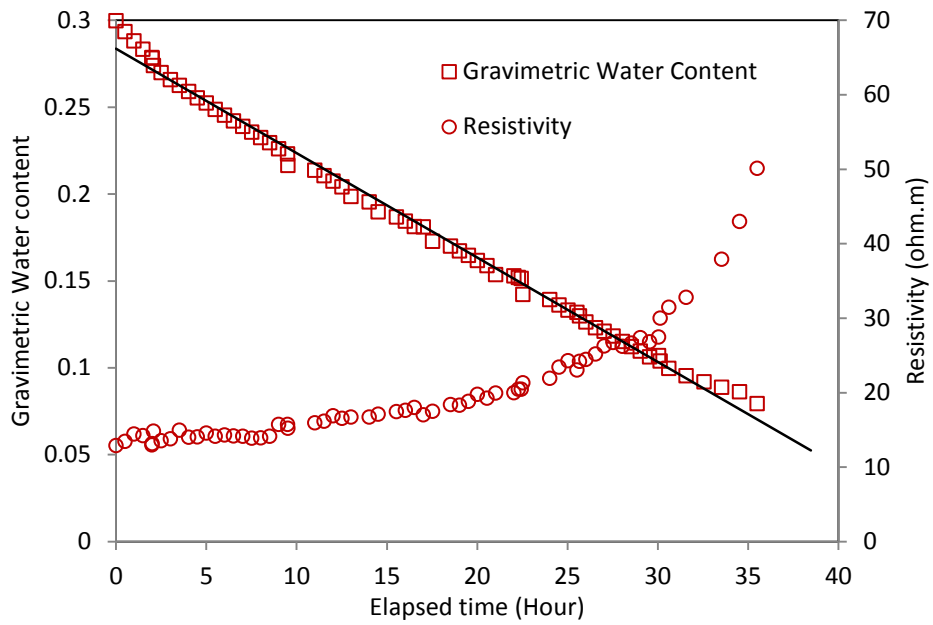


Figure 7.12 The resistivity and gravimetric water content versus the elapsed time of test t5

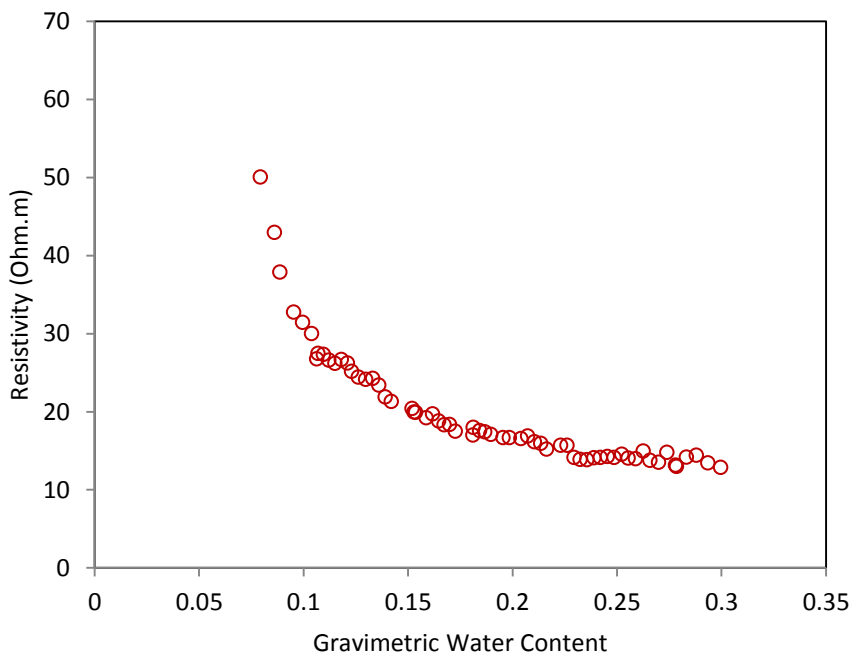


Figure 7.13. The resistivity-gravimetric water content relationship of drying test t5

Continuous drying: Volume changes measurement

In this section, volume changes of the specimens were added to correlate the resistivity with volumetric water content and degree of saturation.

Figures 7.14, 7.15 and 7.16 correlate the resistivity with, respectively, gravimetric water content, volumetric water content and degree of saturation of four specimens (t6 to t9) prepared at the same gravimetric water content (approximately 25%). Continuous drying test t5 ($w=30\%$) is included in Figure 7.14, but as no volume change measurements were performed, it cannot be included in the other plots.

The continuous drying tests all show a similar trend. At high water content levels, where the pores are filled with water, and electrical paths are continuous, the resistivity is low and changes gradually with water content. With progressive drying, the resistivity changes become quicker. At low water content, differences in the pore network microstructure are expected (the pore water geometries will have natural variations) and hence differences in the measured resistivities can be expected. Soil and water content heterogeneity are additional factors that can contribute to the spread of the data.

The resistivity behaviour can be explained according to the water retention properties of clay soil (Lourenço, 2008). For the drying from a saturated state ($S_r=1$), the suction initially increases while still maintaining S_r close to 1 (the pores at this stage are saturated with water). The suction at this stage is not enough to drain the pores. At a particular suction value (air entry value AEV), air enters the pores as the suction is sufficient to drain the pores.

An inspection of Figure 7.16 indicates that the resistivity is low and constant at high degree of saturation (S_r close to 1). At S_r close to 0.8, the resistivity starts to increase abruptly. This represents the transition from the capillary regime (where the air phase is discontinuous i.e. present as occluded bubbles) to the funicular regime (Likos and Lu, 2004) where the water phase remains continuous but is held in place by menisci, hence, higher resistivity. Difference in the pore geometries being setup can explain the spread of the data from one test to another.

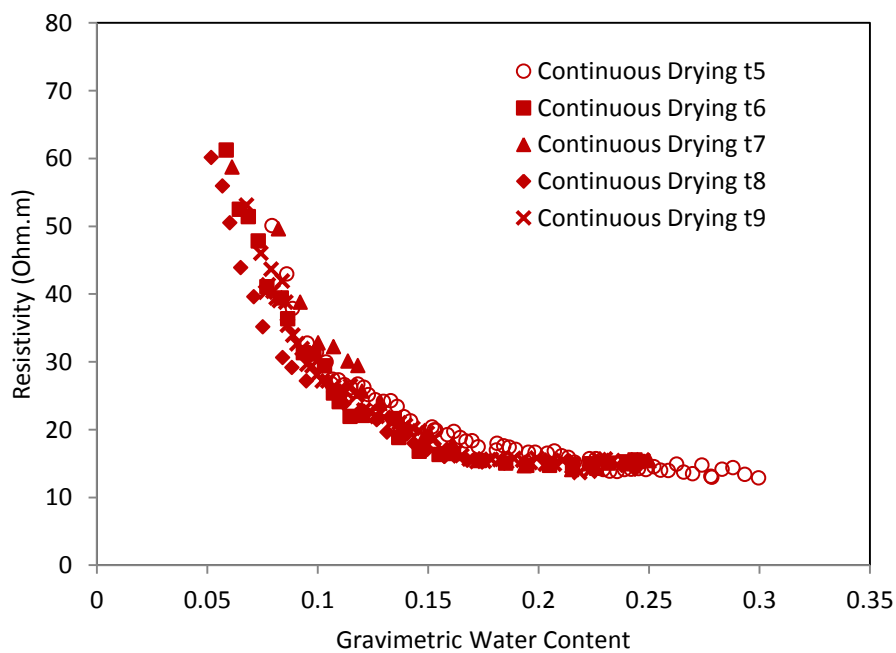


Figure 7.14. The resistivity-gravimetric water content of the continuous drying tests (t6 to t9) and t5

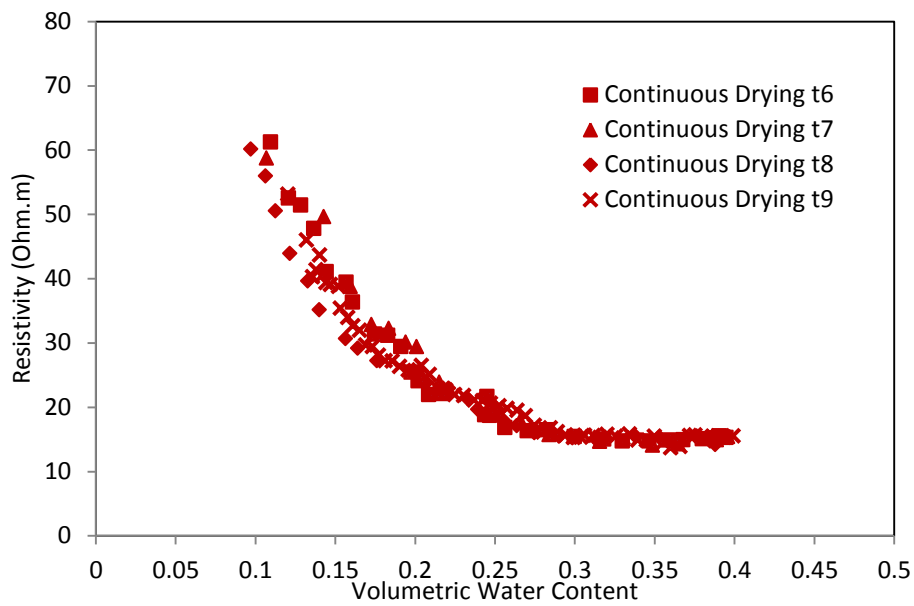


Figure 7.15. The resistivity-volumetric water content of the continuous drying tests (t6 to t9)

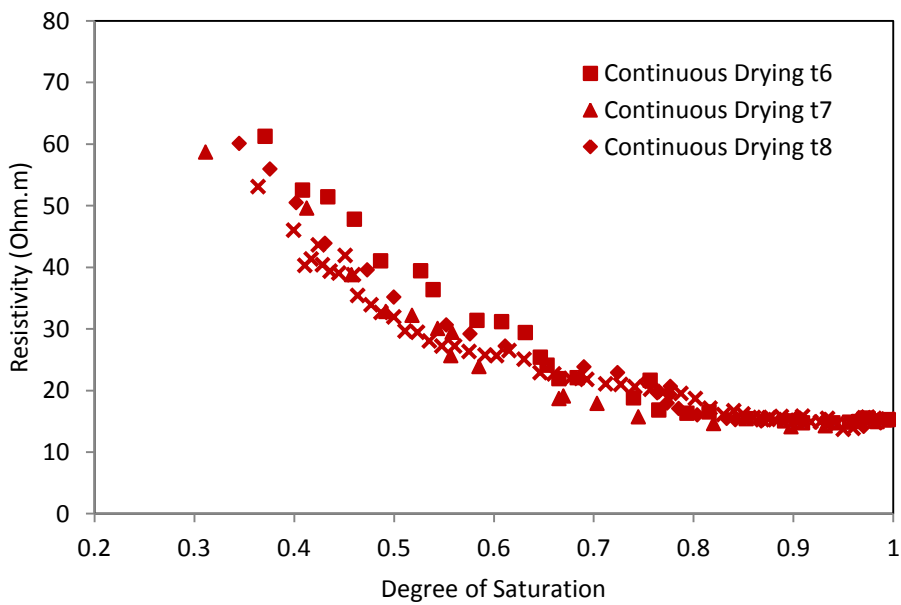


Figure 7.16. The resistivity- degree of saturation of the continuous drying tests (t6 to t9)

Additional tests were conducted on specimens prepared at approximately 20% gravimetric water content. Figures 7.17, 7.18 and 7.19 correlate the resistivity with, respectively, gravimetric water content, volumetric water content and degree of saturation for the continuous drying tests t10 to t13. Inspection of the drying curves indicates a similar nonlinear trend. From Figure 7.19, it can be seen that, the resistivity-degree of saturation can still be distinguished into two segments. The first segment of low, almost constant resistivity with a high degree of saturation. In the second segment, the resistivity starts to increase abruptly, due to air entry.

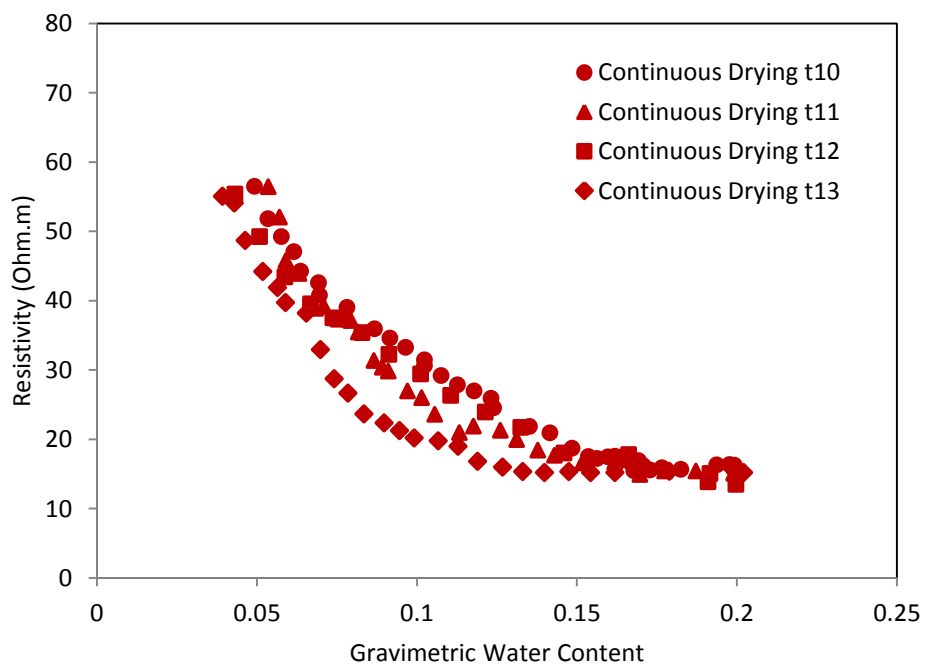


Figure 7.17. The resistivity-gravimetric water content of the continuous drying tests (t10 to t13)

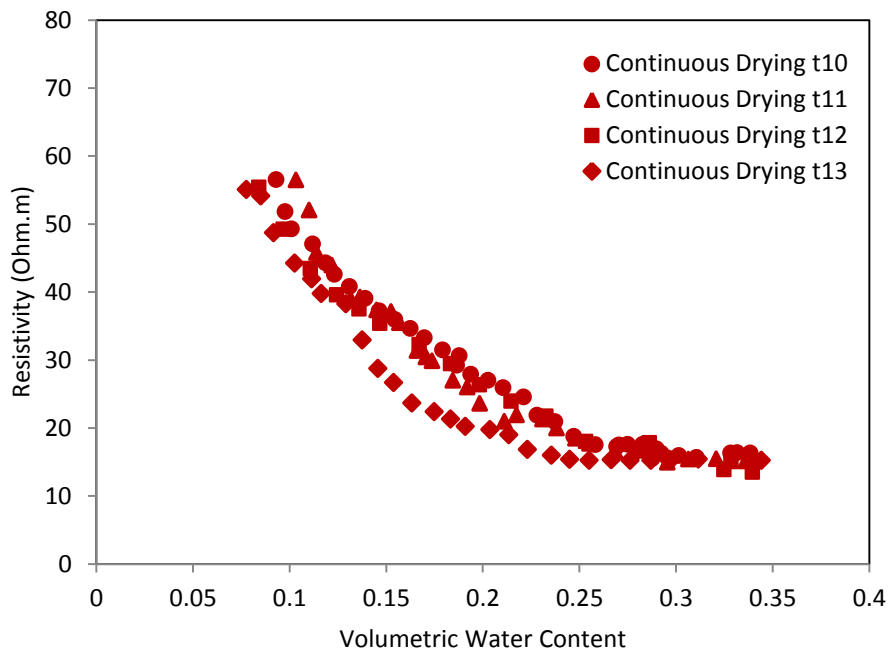


Figure 7.18. The resistivity-volumetric water content of the continuous drying tests (t10 to t13)

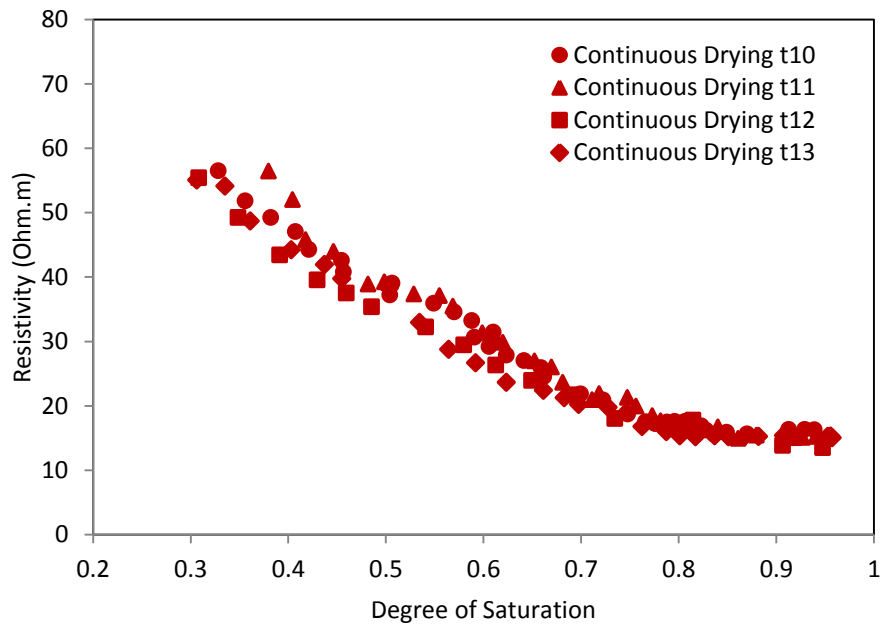


Figure 7.19. The resistivity-degree of saturation of the continuous drying tests (t10 to t13)

Finally, Figure 7.20 presents the resistivity-degree of saturation data for all continuous drying tests performed (t6 to t13). The drying curves show similar relationship independent of the initial water content, which supports the argument from Chapter 5 that S_r is the controlling variable of the resistivity measurements. Again, Figure 7.20 highlights the transition from the capillary regime to the funicular regime discussed earlier.

It is worth mentioning that factors such as soil heterogeneities, density variations and differences in the evaporation rates can contribute to the spread of the data collected. These factors need to be addressed carefully.

Continuous wetting of clay soils is experimentally challenging. It requires imposing a relative humidity to 100%. A new system that facilitates a continuous drying and wetting would be useful to carry out experiments on specimens subjected to continuous cycles of drying and wetting.

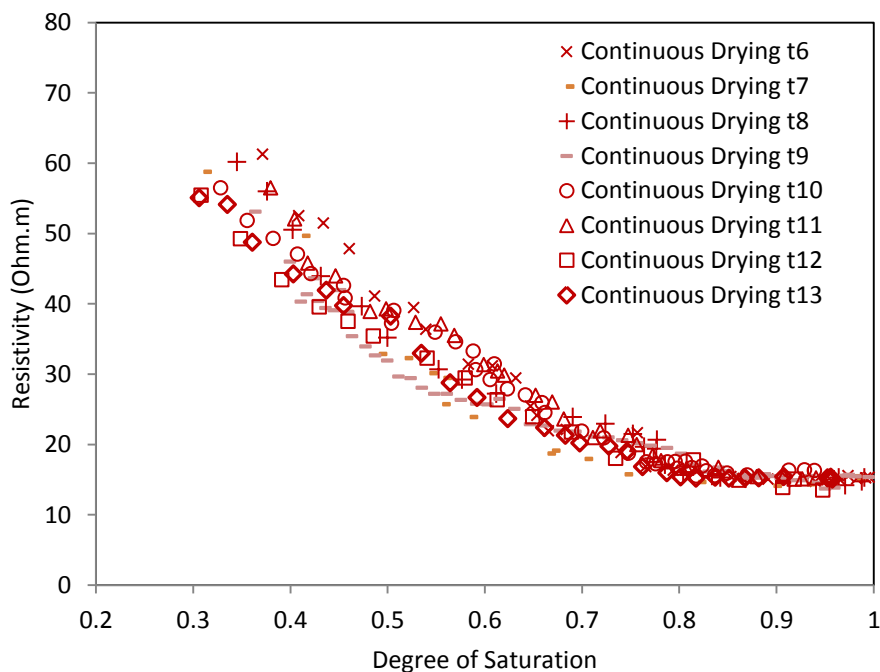


Figure 7.20. The resistivity-degree of saturation of all continuous drying tests (t6 to t13)

7.4 Chapter summary

This chapter has reported the resistivity-water content relationships of clay soils subjected to drying and wetting procedures.

The resistivity of BIONICS clay, other local clays (from Birtley, Co. Durham and Newcastle) and pure clays (Kaolinite and Bentonite) subjected to controlled drying and wetting procedures was discussed. In addition to the discrete drying and wetting procedures adopted in the literature, the resistivity, water content and volume changes were obtained automatically in a continuous procedure.

Correlations between the resistivity and water content of clay soils showed that the resistivity is mainly controlled by water content and the microstructure of the soil. The resistivity-water content relationships are nonlinear. At high water content, the resistivity is low and changes gradually due to the free water that fills the pores (in the capillary water regime). At low water content (in the funicular water regime), the resistivity is high and increases rapidly. The arrangement of the pore water phase linked to the microstructure of the clay controls the resistivity-water content behaviour.

The resistivity data showed that BIONICS clay exhibits hysteresis as confirmed by the SWRC from previous studies. The results also showed that the degree of saturation is the controlling variable of the resistivity behaviour. This argument agrees with the main argument of chapter 5. Again, this suggests that degree of saturation or volumetric water content is more reliable than gravimetric water content to correlate with the resistivity of clay soil.

It is suggested that the resistivity could be a useful indicator for monitoring water content changes in clay soils subjected to drying and wetting cycles.

Chapter 8

Electrical resistivity for characterising cracking of clay soils

Desiccation cracks which are commonly associated with shrinkage of clay soils change the geotechnical properties of soils, and are known to contribute to slope failures. Measurement of cracking patterns, however, has largely been limited to measuring crack geometries at the soil surface. Although soil cracks have complex patterns, their formation causes directional dependence of the electrical current flow, which makes the resistivity method promising for detecting cracking in clay soils. Therefore, in this chapter, numerical and experimental techniques are investigated to explore the potential of the resistivity method for characterising cracking of clay soils. Numerical modelling is used to simulate dry and wet clays with different cracking scenarios. Experimental techniques are adopted to investigate the directional dependence of soil resistivity in cracking clays and the influence of cracking depth, length, width and orientation on resistivity of clay soils.

8.1 Introduction

Water content changes in clay soils cause cyclic processes of swelling, shrinkage and cracking that adversely impacts the engineering properties and behaviour of soils. In particular, desiccation cracks alter the macro porosity, infiltration and runoff and create pathways for water that reduce soil strength and stability (e.g. Kodikara et al. 1999). However, cracks have complex patterns that are difficult to measure. Although surface crack networks can directly be described by measuring crack geometries (Ringrose-Voase and Sanidad, 1996), or imaging crack morphology using surface imaging analysis (Velde et al., 1996; Vogel et al., 2005), these methods are largely based on inadequate visual inspections. 2D laser scanning technique as adopted by Sánchez et al. (2013) can be used only for small scale samples under laboratory conditions. Field measurements of cracking dynamics are difficult and have largely been limited to soil pits (Bouma and Dekker, 1978), or pushing

a probe wire or measuring tape into the crack (Abedine and Robinson 1971; Kishne et al. 2009). Obviously, these techniques are destructive and prohibit repetitive measurements. In addition, as stresses vary with depth, crack geometry networks and their development cannot be characterised from surface geometrical analysis and 2D Imaging studies (Chen et al., 2007).

In a recent review paper, Dinka and Lascano (2012) concluded that, in the field, none of the available techniques can provide sufficient information on cracking dynamics continuously, non-destructively and with a reasonable certainty. Clearly, an accurate understanding of cracking dynamics requires a non-invasive technique that can offer in-situ continuous monitoring of cracking dynamics below the surface.

The electrical resistivity method offers non-invasive measurements that, in addition to providing water content estimation, can also identify the formation of soil cracks, as crack formation causes directional dependence of the electrical current flow (Feng et al., 2003; Kong et al., 2013; Hassan and Toll, 2013; 2014). The method has recently proven successful to map a cracking network forming in clay soil at lab scale (Sentenac and Zielinski, 2009; Jones et al., 2012) and field scale (Jones et al., 2014).

Numerical and experimental methods are adopted to characterise the cracking in clay soil. In cracking soils, resistivity of the linear array is strongly affected by the orientation of the electrodes (Habberjam and Watkins, 1967). Therefore, due to the unique characteristics of the square array (discussed in Chapter 3), this array was chosen. α -resistivity, β -resistivity, average resistivity $A\nu$ and anisotropy index AI are used to characterise the cracking in BIONICS clay.

8.2 Numerical modelling

8.2.1 Method

In ERT, the aim of the numerical modelling is to simulate real scenarios and to test the effectiveness of the method applied before carrying out costly actual laboratory and field measurements (Yang and Lagmanson, 2003). Numerical modelling has commonly been used to simulate, for instance; fractures (Seaton and Burbey, 2002), subsurface cavities (Satarugsa et al., 2004), landslides (Guo et al., 2005) and faults (Nguyen et al., 2005).

Numerical modelling is a two-step procedure (Olayinka and Yaramanci, 2000; Yang and Lagmanson, 2003; Giao et al., 2011); (i) a synthetic resistivity model is created based on the user prior information and assumptions (i.e. forward modelling), and (ii) the model is inverted to reconstruct the subsurface resistivity distribution (i.e. inverse modelling), see Figure 8.1.

To simulate cracking in clay soil, 3D forward modelling (RES3DMOD) and 3D inversion (RES3DINV) packages (Loke, 2014) were used. RES3DMOD is finite difference forward modelling software that determines the apparent resistivity values for a synthetic survey carried out with a user defined electrode arrangement and resistivity distribution using a rectangular grid of electrodes. The program is based on the finite different method which solves the 3D potential distribution due to point current source in a half space subsurface. A 3D subsurface model is created using rectangular blocks with a number of electrodes at the nodes. The user must supply the resistivity of each cell in addition to other parameters such as minimum electrode spacing, mesh size, and the number and thickness of the model layers. RES3DINV uses the smoothness-constrained least squares method to produce a 3D model of the subsurface resistivity distribution from the apparent resistivity data. The software attempts to determine the resistivity of the cells in the inversion model that will closely reproduce the observed apparent resistivity.

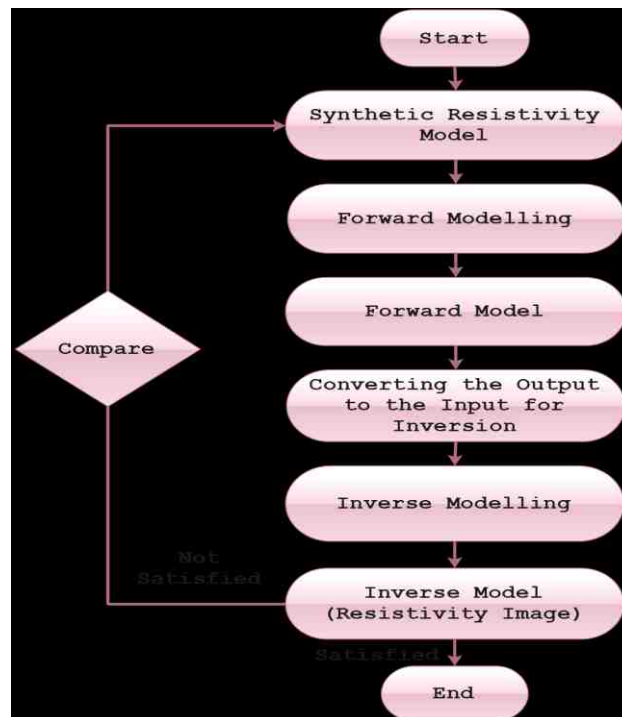


Figure 8.1. Flowchart shows resistivity modelling steps (Giao et al., 2011)

To explore the effectiveness of the resistivity method to detect small scale centimetric cracks, a model consisting of six layers with 8 by 8 electrodes (i.e. 14 by 14 grids) was generated. The minimum electrode spacing was set to be 5cm. Based on the literature (e.g. Telford et al., 1990; Reynolds, 1997; Loke, 2014), a 100 Ohm.m resistivity value for dry clay and 20 Ohm.m for wet clay were chosen. As the crack is filled with the air, that is infinitely resistant, model blocks containing a crack were simulated by setting their resistivity to 100000 Ohm.m (Greve et al., 2009). Once the model file is supplied, RES3DMOD is used to calculate the apparent resistivity at each node, and the results were saved to be used for input in RES3DINV software to produce subsurface resistivity distribution. For the 3D visualizations of the inverted models, 3D visualization program <http://www.slicerdicer.com> was used. To simulate real situations, adding 5% resistivity noise is a common practice in resistivity modelling (e.g. Miller et al., 2008). Therefore, a scattered 5% resistivity noise was added. Cracks (25mm width, 200mm length) of different depths were simulated.

8.2.2 Numerical modelling results and discussion

Figure 8.2 shows the XY slices of the simulated 70mm depth crack at different depths interval in dry soil. As the resistivity contrast between air and soil is large, the crack forms an object with high resistivity compared to the surrounding soil (Amidu and Dunbar, 2007; Sentenac and Zielinski, 2009). Therefore, cracks can be identified as a high resistivity isolated spots on the resistivity sections (Samouëlian et al., 2004). The crack is clearly detected in slice 1, 2 and 3 at depths (0.00-0.01m), (0.01-0.04m) and (0.04-0.07m), respectively. No clear trace for the crack is evident in the subsequent slices below a depth equal to 0.07m, the crack depth.

Figure 8.3 and Figure 8.4 show, respectively, the XZ and YZ slices of the model. The XZ slice 4 at Y distance (0.15-0.20m) in Figure 8.3 clearly indicates the crack position, and the length of the crack is estimated fairly well. The YZ slices 3, 4 and 5 in figure 8.4 which respectively intersect the crack at X distances, (0.10-0.15), (0.15-0.20) and (0.20-0.25m) show the extent of the crack. Although the slices show high resistivity values at the vicinity of the crack, the crack width is poorly estimated. This can be attributed to the smoothness-constrained nature of the inversion method. Moreover, Figures 8.3 and 8.4 show that higher resistivity anomaly is detected at the surface of the soil and this anomaly reduces with depth (Samouëlian et al., 2003a). The high resistivity anomaly indicates that the current is more blocked at the surface due to the presence of the crack. Although the actual resistivity of air filled crack can be assumed infinite, the calculated resistivity of the soil contained a crack in the model is far lower as it represents the average resistivity of the soil as confirmed in the cracked clay soil (Jones et al., 2012; 2014). Figure 8.5 shows the 3D visualization of the model. The XY cut in the figure indicates the depth of the crack and no clear trace for the crack below a depth equal to 0.07m, the crack depth.

CHAPTER 8: ELECTRICAL RESISTIVITY FOR CHARACTERISING CRACKING OF CLAY SOILS

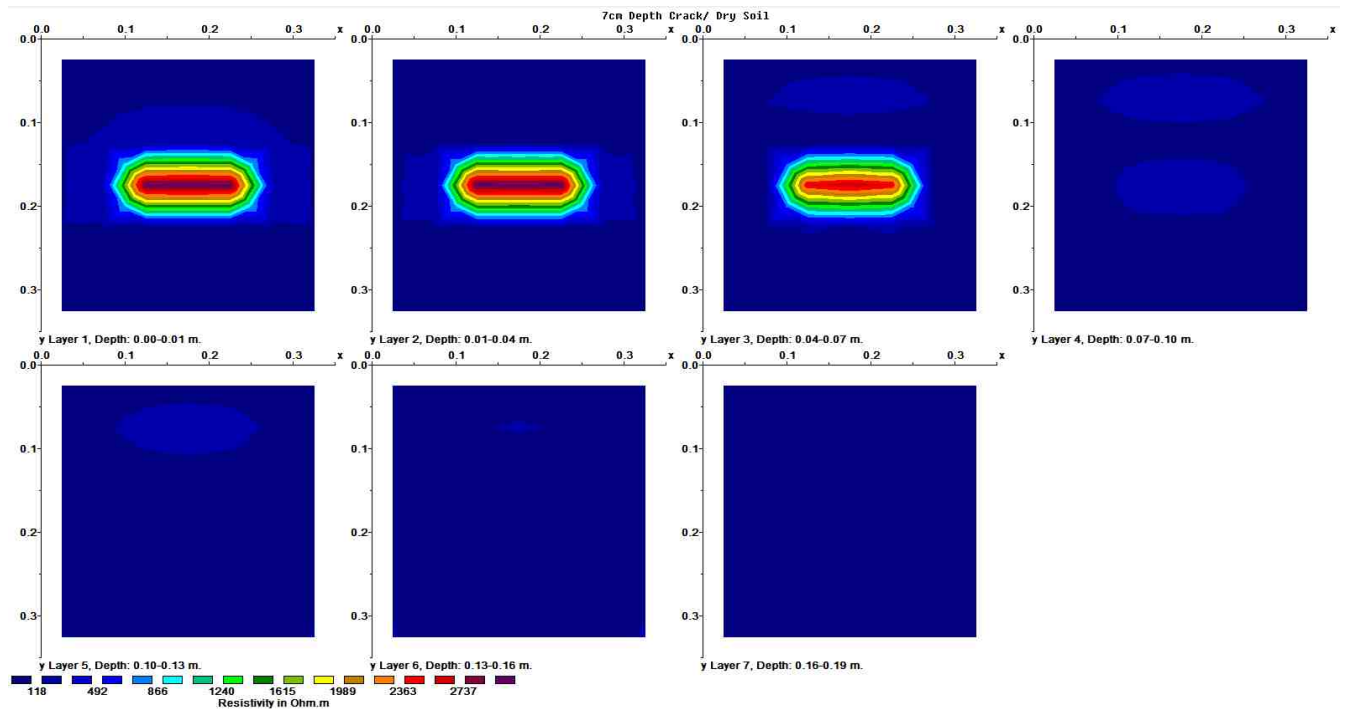


Figure 8.2. XY slices of the 70mm depth crack model in dry soil

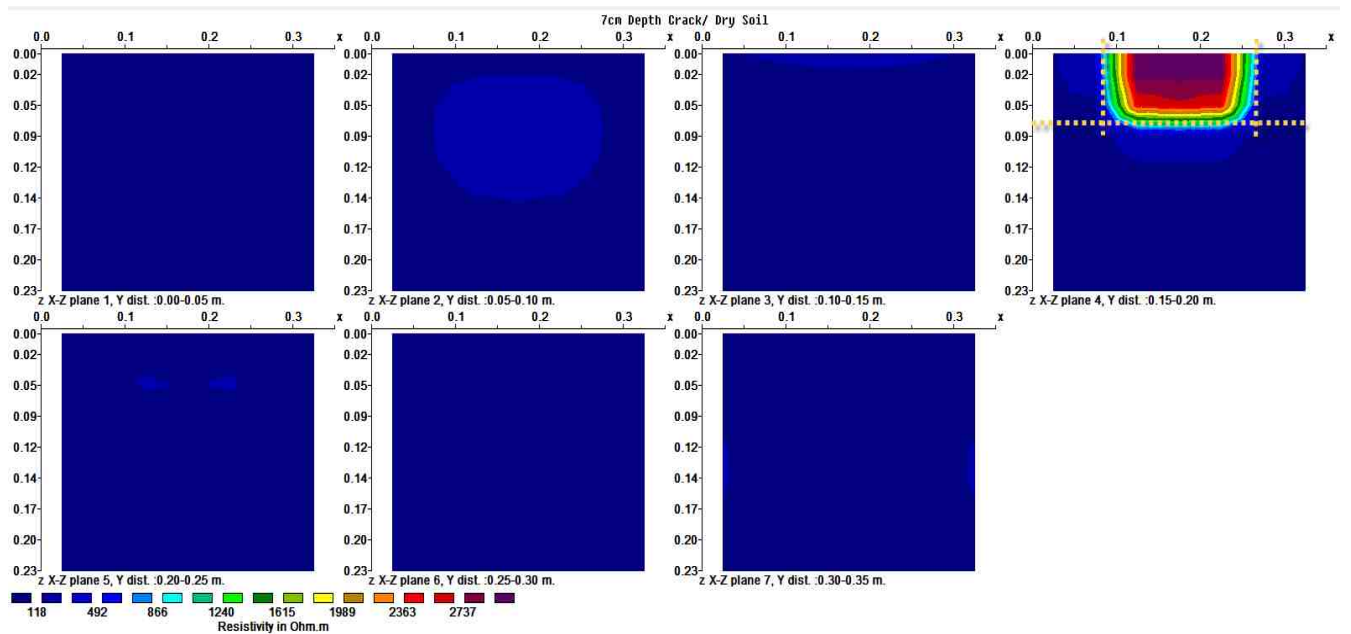


Figure 8.3. XZ slices of the 70mm depth crack model in dry soil

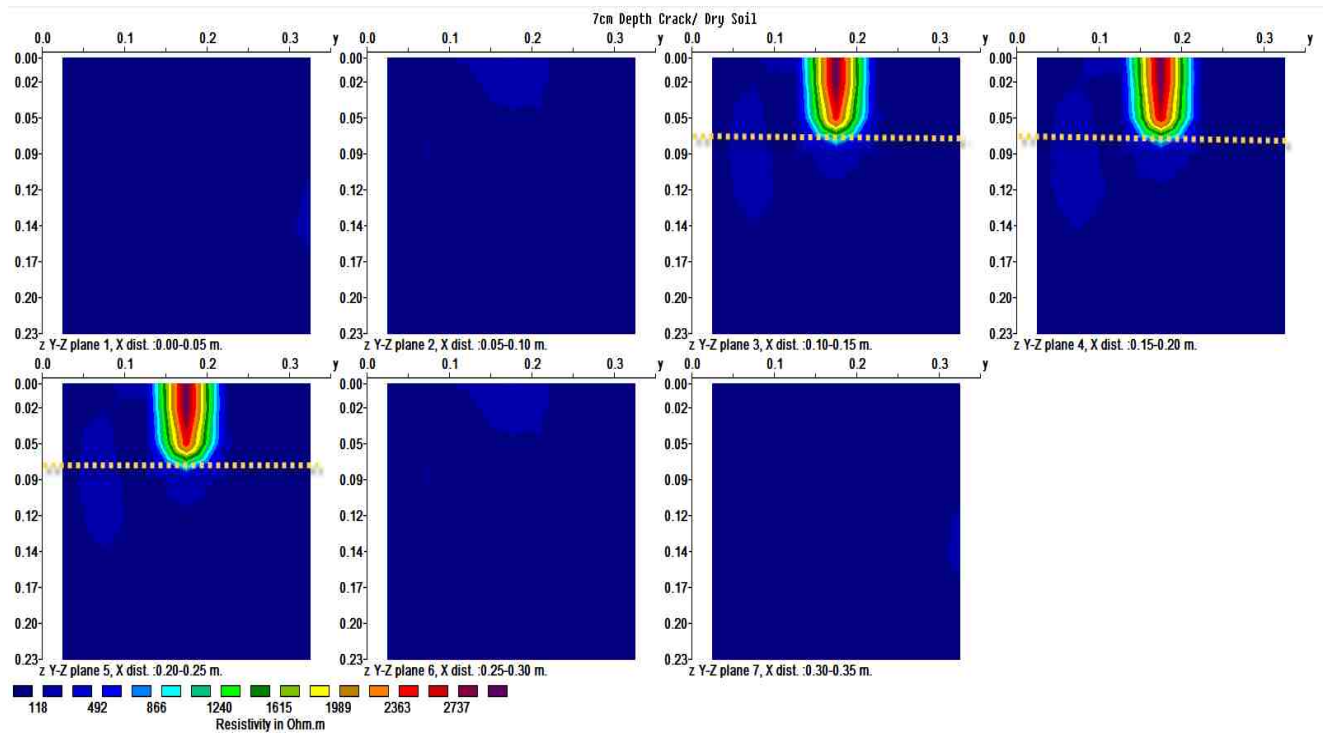
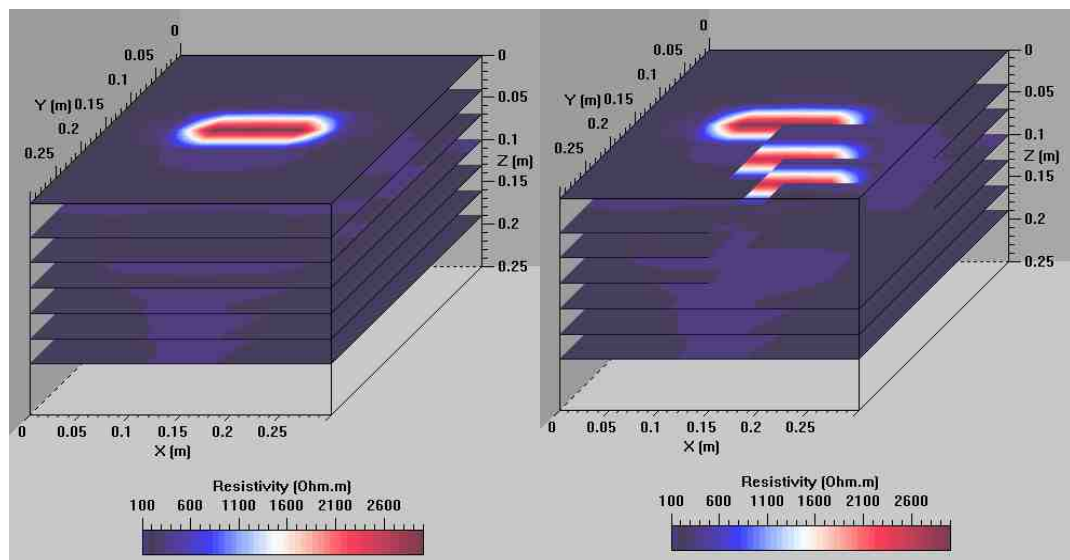


Figure 8.4. YZ slices of the 70mm depth crack model in dry soil



(a)

(b)

Figure 8.5. 3D visualization of the 70mm depth crack model in dry soil (a) the model (b) the model with XY cut

To simulate real situations, Figures 8.6, 8.7 and 8.8, respectively, show XY, XZ and YZ slices of the same model with 5% resistivity noise added. Figure 8.9 shows the 3D visualization of the model. As the resistivity of the crack is significantly higher than the surrounding soil, the geometry and extent of the crack can still be distinguished from the background even with 5% resistivity noise added.

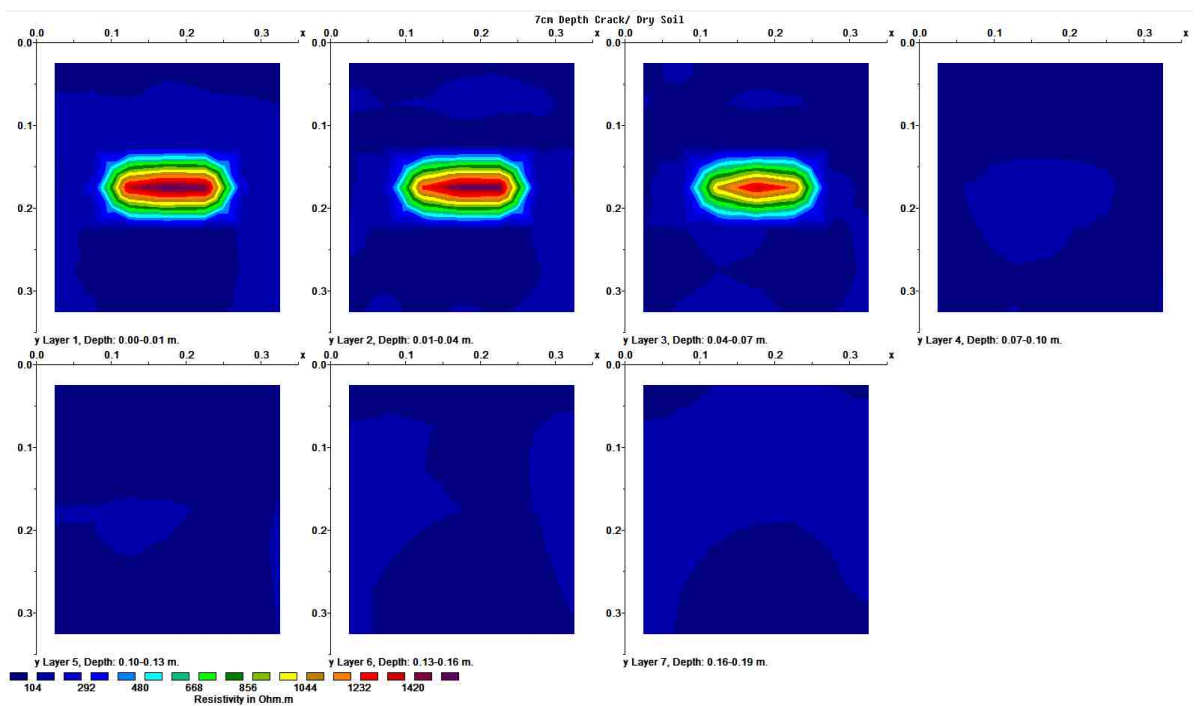


Figure 8.6. XY slices of the 70mm depth crack model in dry soil (5% added noise)

CHAPTER 8: ELECTRICAL RESISTIVITY FOR CHARACTERISING CRACKING OF CLAY SOILS

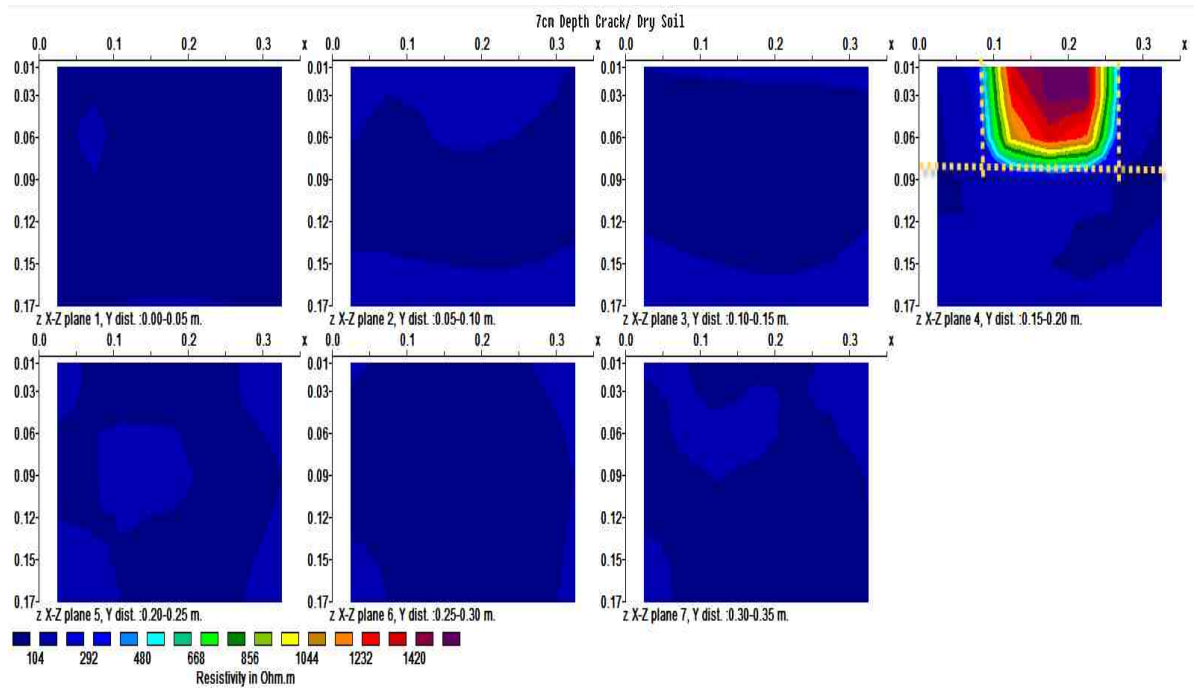


Figure 8.7. XZ slices of the 70mm depth crack model in dry soil (5% added noise)

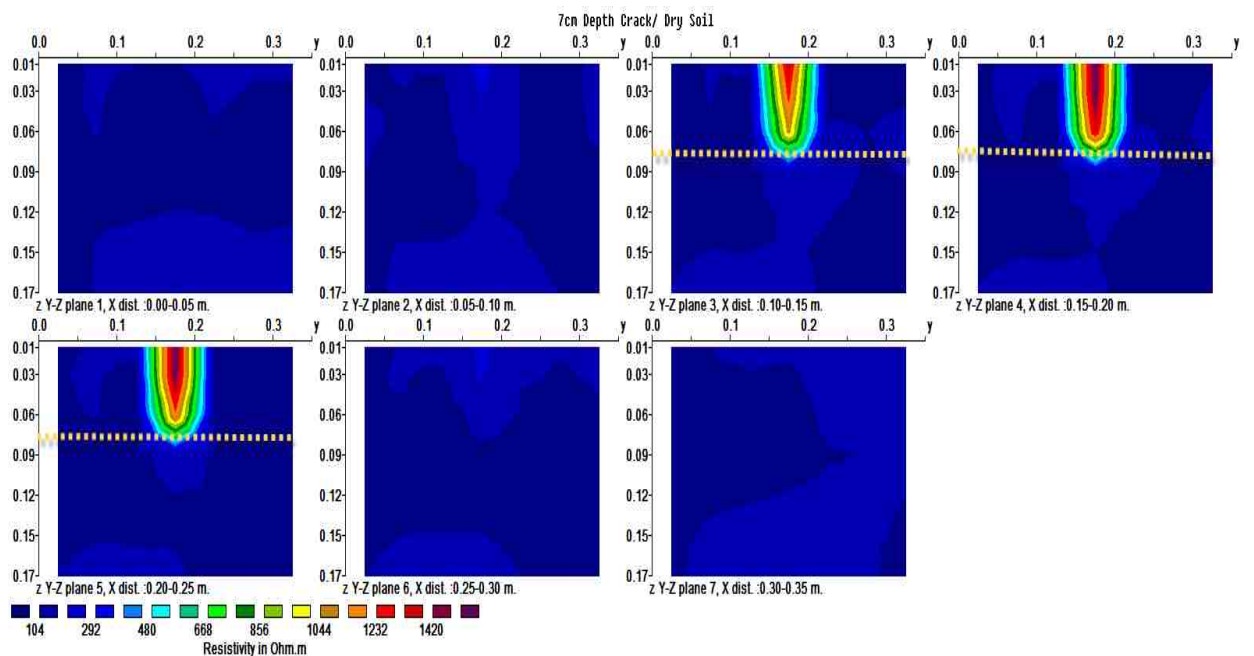
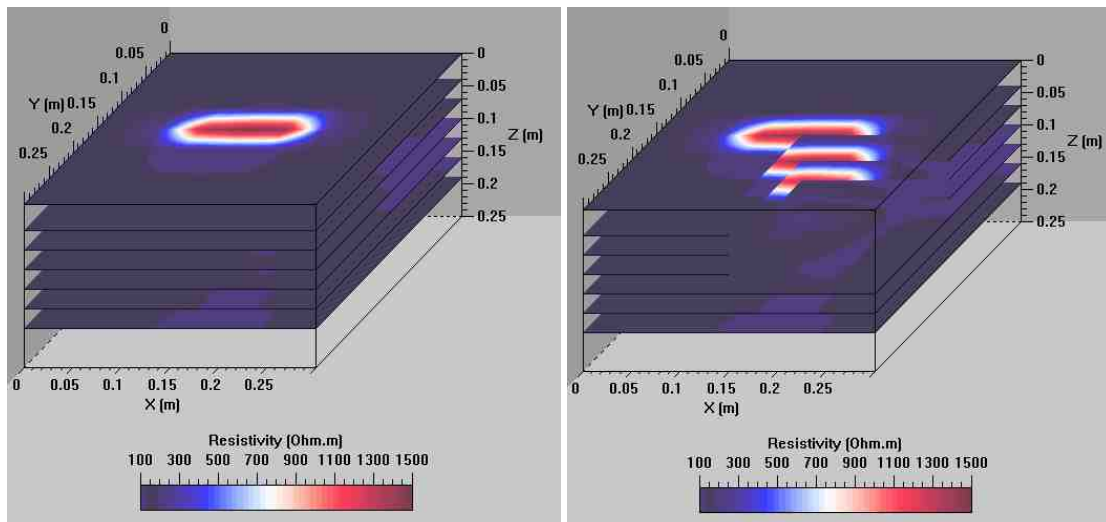


Figure 8.8. YZ slices of the 70mm depth crack model in dry soil (5% added noise)



(a)

(b)

Figure 8.9. 3D visualization of the 70mm depth crack model in dry soil (5% noise added) (a) the model (b) the model with XY cut

To simulate the 70mm depth crack in wet soil, Figures 8.10, 8.11 and 8.12 show, respectively, XY, XZ, YZ slices of the model. Figure 8.13 shows the 3D visualization of the model. Obviously, the same discussion provided for the dry model is valid here, as the crack can still be characterised in wet soil due to the high resistivity contrast.

Figures 8.14, 8.15 and 8.16 show, respectively, XY, XZ and YZ slices of the model with 5% added resistivity noise. Figure 8.17 shows the 3D visualization of the model. Again, the crack still has an anomalous high resistivity value that can be distinguished from the background even with 5% noise added. The resistivity distribution of the soil is severely affected by the presence of the crack, and at any situation, this effect is more significant than of the material variability (Lataste et al. 2003).

CHAPTER 8: ELECTRICAL RESISTIVITY FOR CHARACTERISING CRACKING OF CLAY SOILS

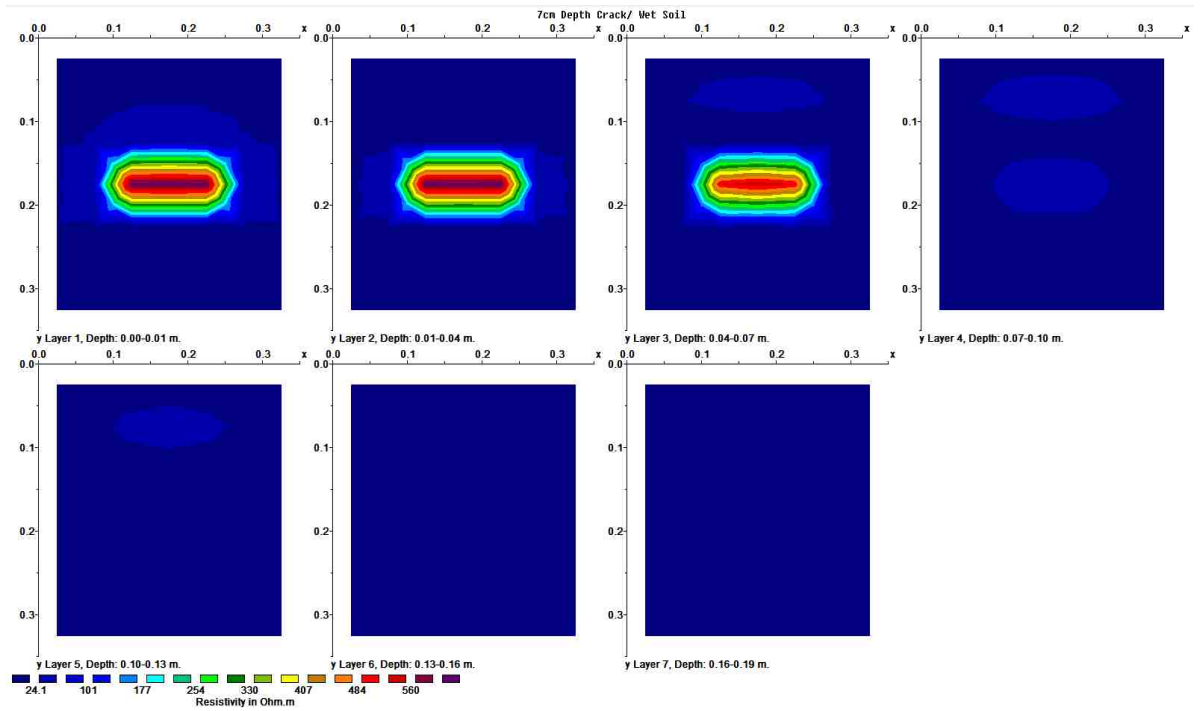


Figure 8.10. XY slices of the 70mm depth crack model in wet soil

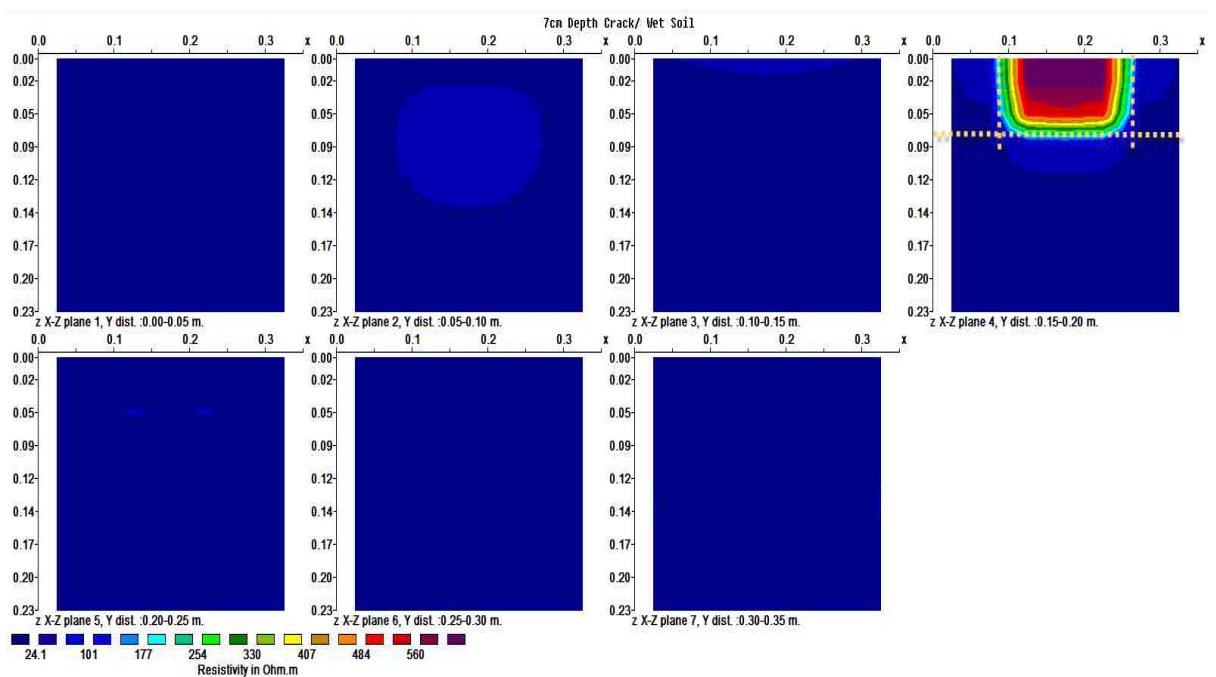


Figure 8.11. XZ slices of the 70mm depth crack model in wet soil

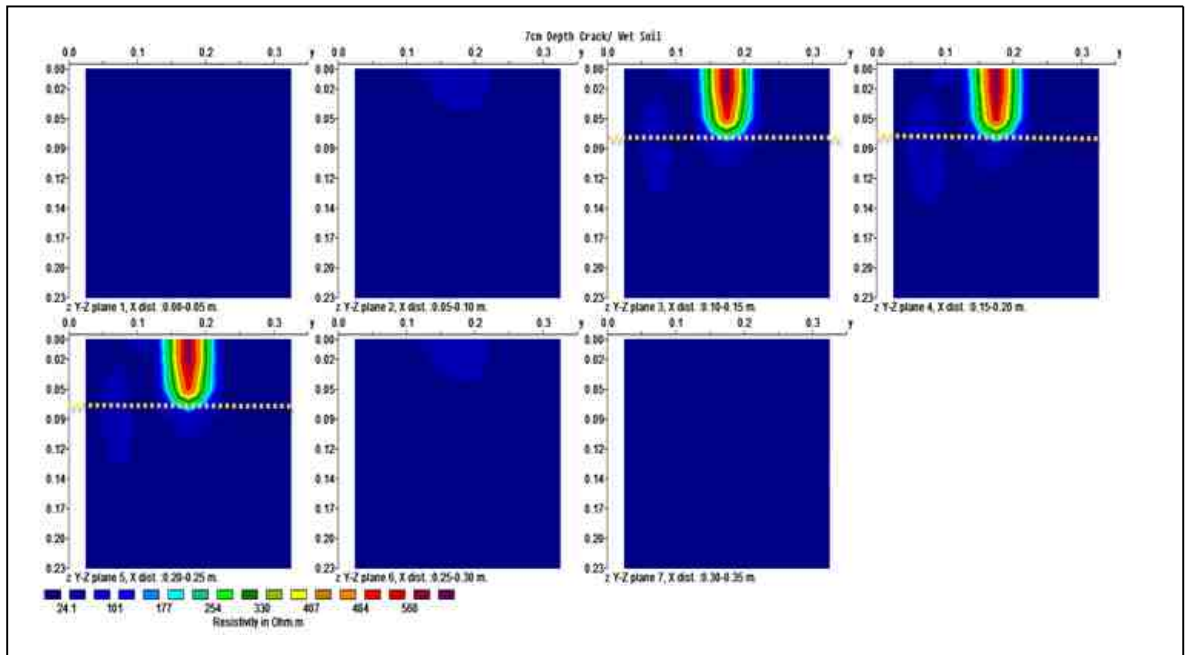
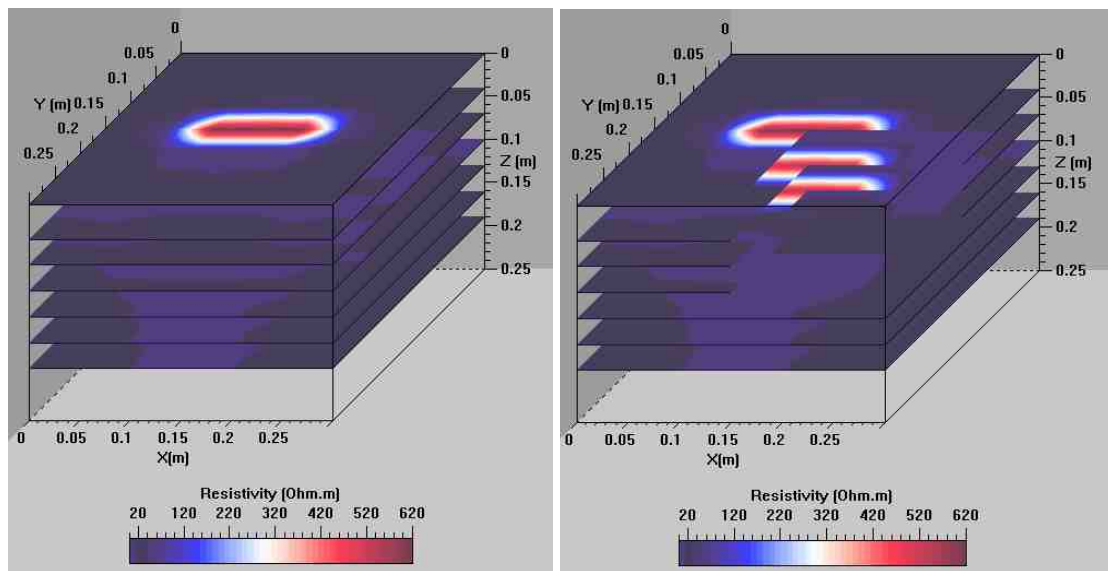


Figure 8.12. YZ slices of the 70mm depth crack model in wet soil



(a)

(b)

Figure 8.13. 3D visualization of the 70mm depth crack model in wet soil (a) the model (b) the model with XY cut

CHAPTER 8: ELECTRICAL RESISTIVITY FOR CHARACTERISING CRACKING OF CLAY SOILS

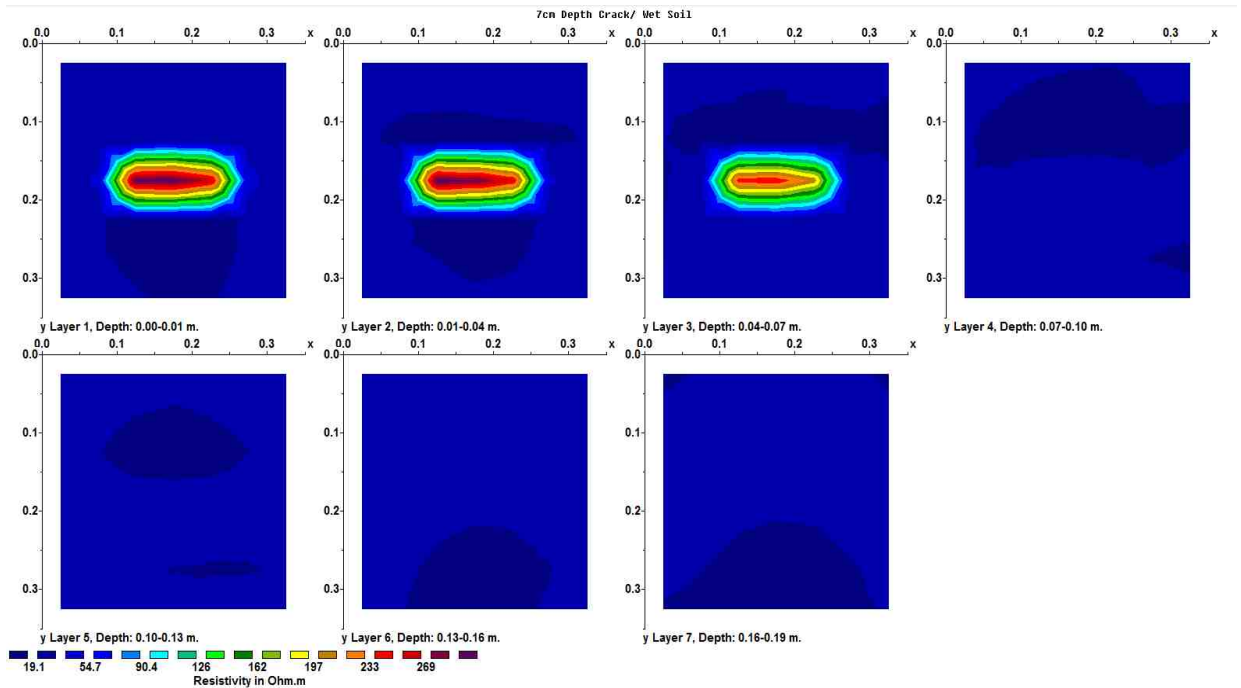


Figure 8.14. XY slices of the 70mm depth crack model in wet soil (5% noise added)

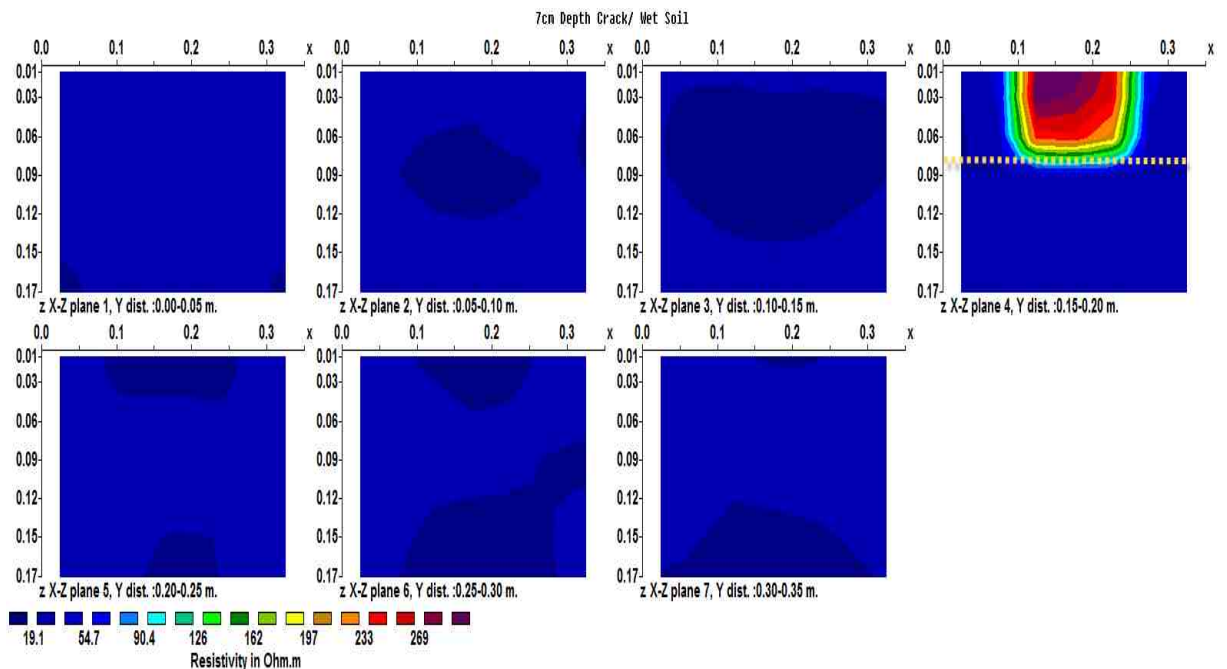


Figure 8.15. XZ slices of the 70mm depth crack model in wet soil (5% noise added)

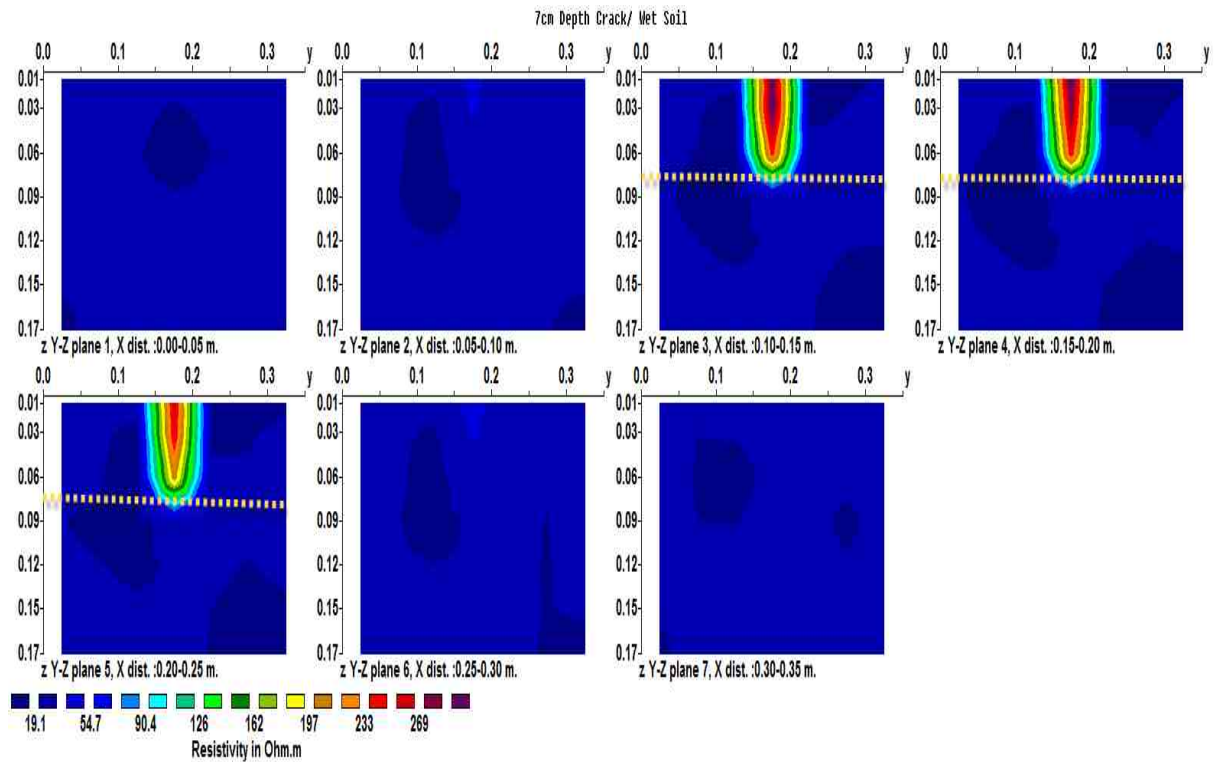


Figure 8.16. YZ slices of the 70mm depth crack model in wet soil (5% noise added)

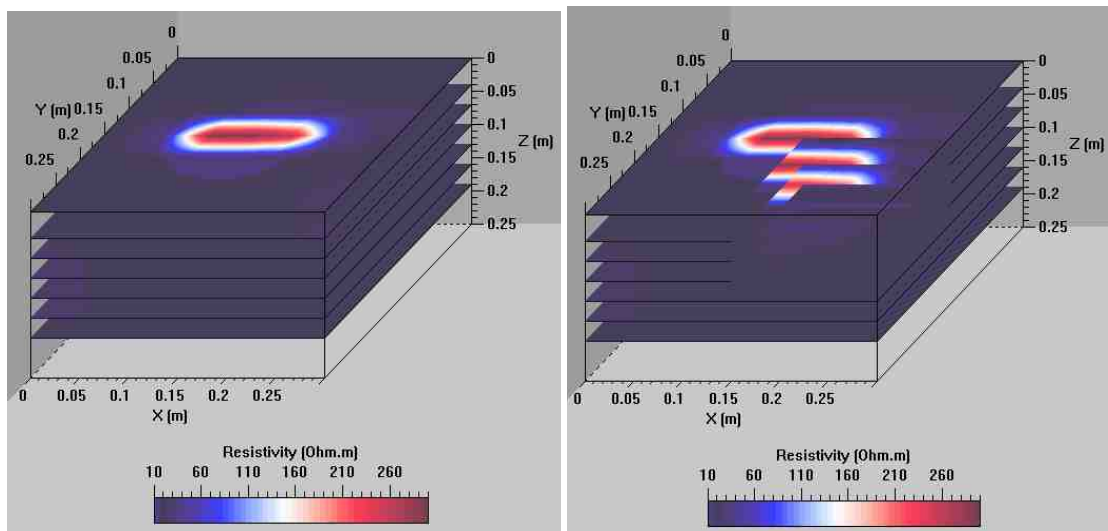
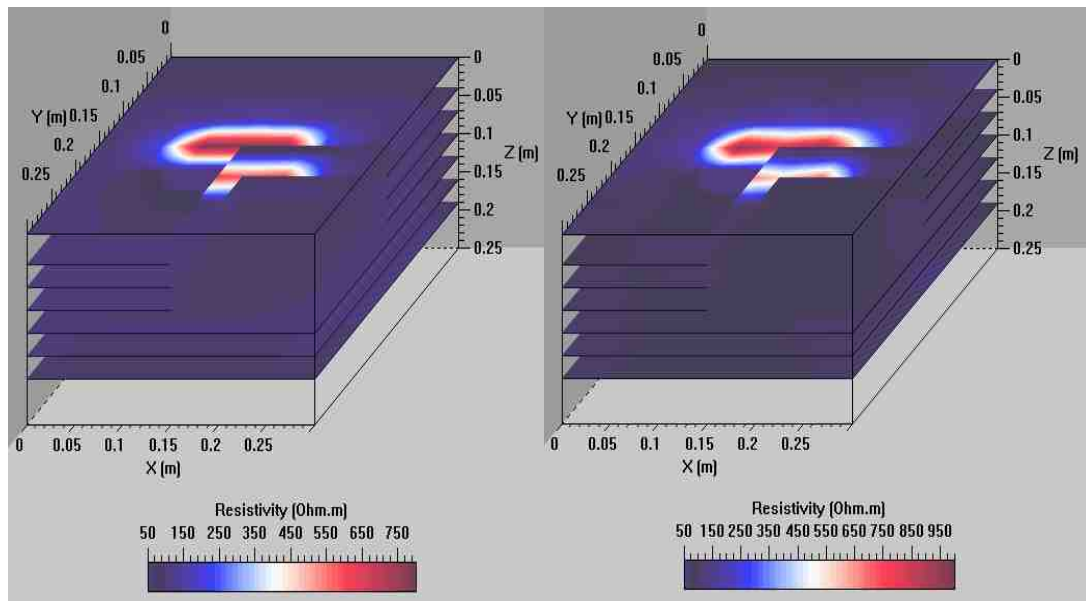


Figure 8.17. 3D visualization of the 70mm depth crack model in wet soil (5% noise added) (a) the model (b) the model with XY cut

Cracks of 10mm and 40mm depths were simulated to explore the ability to detect cracks of different depths. Only the 3D visualizations are presented here. Figures 8.18 and 8.19 show the 3D visualization of the 40mm depth crack in dry and wet soil, respectively. The XY cut in the figures indicates the depth of the cracks as no high resistivity trace is seen below 40mm depth, the depth of the crack, even with 5% noise added.

Similarly, Figures 8.20 and 8.21 show the 3D visualization of the 10mm depth crack in dry and wet soil, respectively. Although the electrical signature of the crack can be recognized in the section, the geometry of the crack is distorted when 5% noise is added. Comparing to the 10mm depth crack model, 40mm and 70mm depth crack models can better be characterised, as increasing the cracking depth causes more blockage to the current and hence a higher resistivity anomaly.

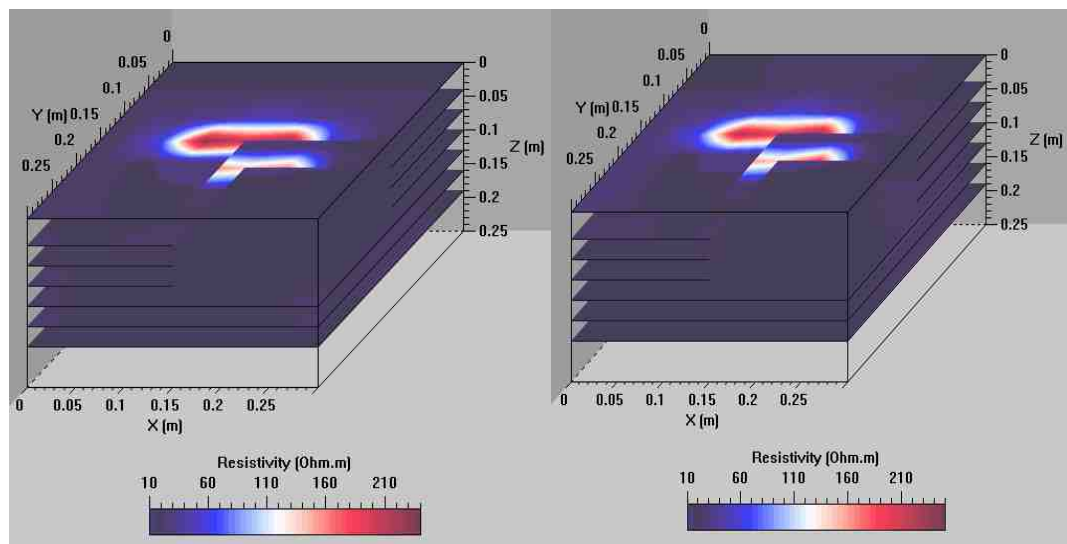
To conclude, in all tested cases, the crack has an anomalous high resistivity value that can be distinguished from the background even with 5% noise. Due to the presence of the crack, the higher resistivity anomaly is noticed at the surface of the soil, and this anomaly is reduced with depth. The 3D visualizations of the models show that the geometry and depth of the simulated cracks are clearly indicated. However, in the models tested, although the actual resistivity of air filled crack can be assumed infinite, the calculated resistivity of the soil contained cracks is far lower as it represents the average resistivity of the soil.



(a)

(b)

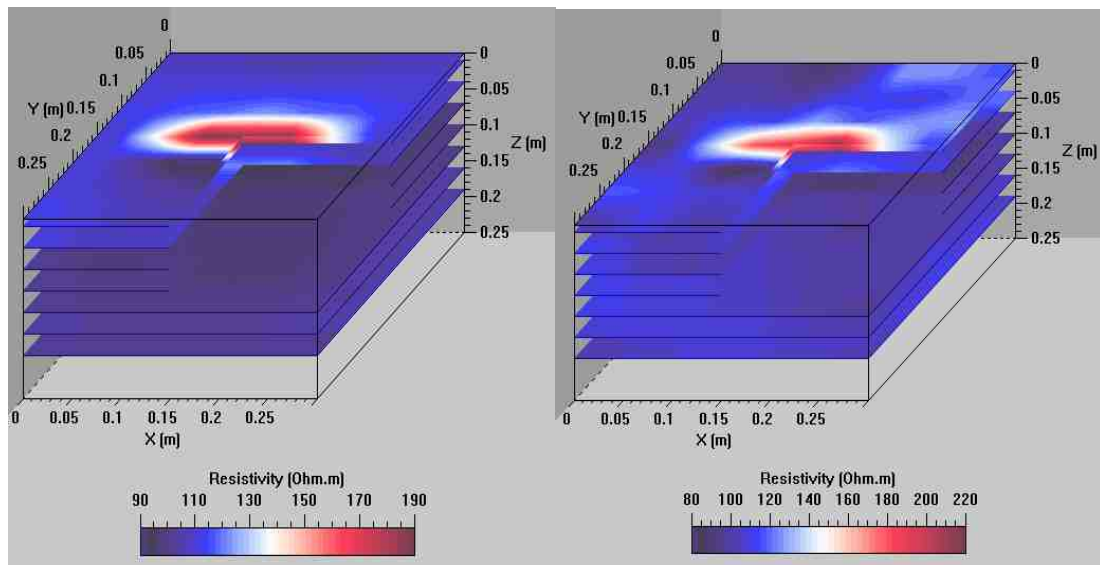
Figure 8.18. 3D visualization of the 40mm depth crack model in dry soil (a) the model with XY cut out (b) the model with 5% resistivity noise



(a)

(b)

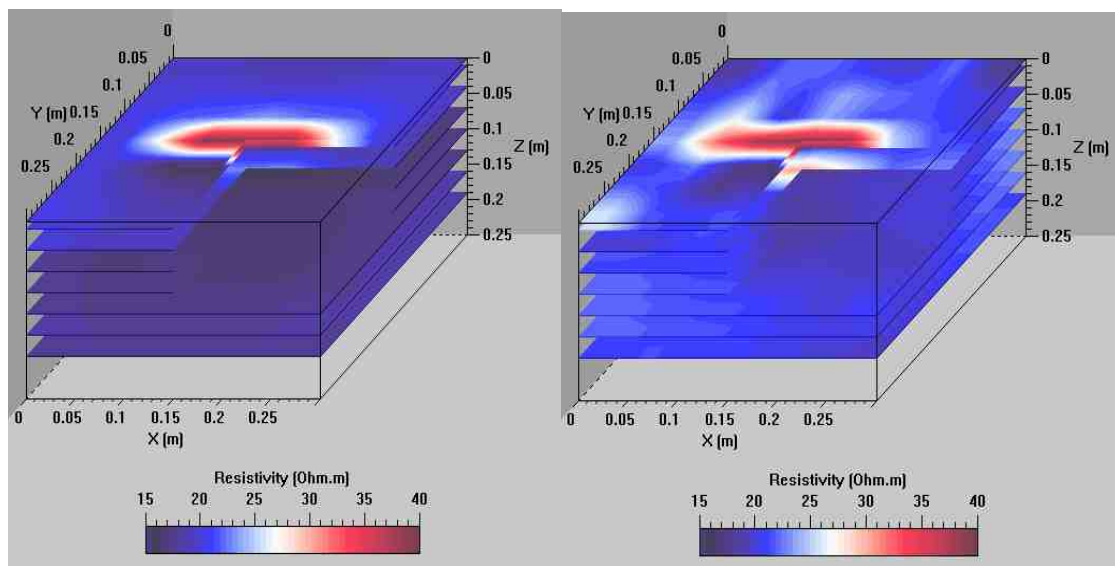
Figure 8.19. 3D visualization of the 40mm depth crack model in wet soil (a) the model with XY cut out (b) the model with 5% resistivity noise



(a)

(b)

Figure 8.20. 3D visualization of the 10mm depth crack model in dry soil (a) the model with XY cut out (b) the model with 5% resistivity noise



(a)

(b)

Figure 8.21. 3D visualization of the 10mm depth crack model in wet soil (a) the model with XY cut out (b) the model with 5% resistivity noise

8.3 Experimental methods

8.3.1 Methods

Square resistivity devices and the circular cell (described in Chapter 3) were used to investigate the influence of changing cracking parameters (i.e. depth, length, width and orientation) on resistivity of clay soils and the directional dependence in the resistivity measurements introduced by soil cracks.

The influence of cracking parameters on soil resistivity

Four stainless steel electrodes (50mm length and 4mm diameter) fixed at the corners of a square were used to serve as current and potential electrodes. α and β resistivity were collected to calculate: (i) The average resistivity A_v of α and β resistivity which averages out soil inhomogeneity and (ii) anisotropy index AI which highlights the directional dependence of the resistivity measurements introduced by soil cracks.

Artificial cracks of different dimensions were created in the soil using plastic sheets of different dimensions (as used by Kong et al., 2012). To consider the effect of cracking depth, cracks of 70mm length, 1.5mm width and depth range (10-70mm) were tested. With regards to the effect of crack length, cracks of 70mm depth, 1.5mm width and length range (10-70mm) were examined. To examine the influence of cracking width, cracks of 70mm length, 70mm depth and width range (1.5- 6mm) were tested. Finally, crack orientation (0-90°) was considered to examine the effect of orientation of a 70mm depth, 70mm length, and 1.5mm width crack. In a previous work, Kong et al. (2012) measured resistivity at a direction perpendicular to artificial cracks created in Laterite soil where the cracks intersect the current and potential lines. The measurements were carried out using fixed electrode spacing. In the current work, the current was injected at two perpendicular directions to highlight the directional dependence in the resistivity data and the resistivity measurements were performed using two inter-electrodes, 50mm and 100mm as shown in Figure 8.22.

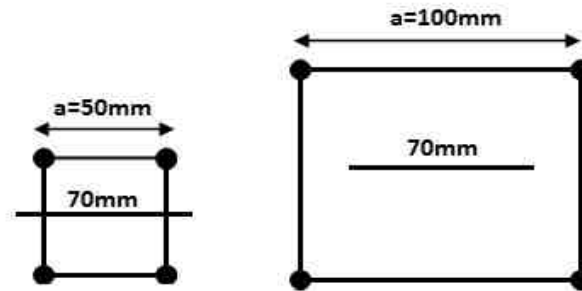


Figure 8.22. Square resistivity devices used with the crack positions tested

***AI*- depth profiles**

To generate *AI*-profiles, a surface square array can be used by increasing the electrode spacing progressively to investigate greater depths (Samouëlian et al. 2004). Recently, Greve et al. (2010a) introduced a novel technique that relates cracking depth to *AI* changes using a series of four vertically installed electrodes into the soil at regular depth intervals. In the current work, the electrodes were installed at the circumference of a perspex cylinder to minimize the disturbance of the soil. The cell was equipped with 56 stainless steel electrodes. Eight electrodes were installed at 10, 40, 70, 100, 130, 160, and 190 mm depth. *AI*-depth profiles were generated using four electrodes at the corner of the square at each depth, see Figure 8.23a. The profiles were obtained for soil with a manually introduced crack (70mm length, 1.5mm width) for depth range (10-70mm) in the direction shown in Figure 8.23b. This makes the proposed design suitable to carry out azimuthal measurements.

Azimuthal resistivity measurements

Azimuthal resistivity (Taylor and Fleming 1988) of the square arrangement was used to examine the directional dependence of resistivity measurements in cracking clay. The measurements were performed by rotating the array in the circular cell to determine the resistivity variations with orientation, see Figure 8.23b. α and β resistivity were obtained to calculate A_v resistivity and A_l . The measurements can be plotted as a function of azimuth in Cartesian coordinate, or on a polar diagram. Azimuthal resistivity data were collected for soil with manually created cracks and cracks developed during drying and wetting tests. Figure 8.24 shows the direction and measurement stages of the manually created cracks test. In the first stage, crack "a" (70mm length, 1.5mm width) was introduced for a range of depths (10-40mm) with 10mm increment. In the second stage, crack "b" (40mm length, 1.5mm width) was added for a range of depths (10-40mm) with 10mm increment. In the third stage, crack "c" (30mm length, 1.5mm width) was created for a range of depths (10-40mm) with 10mm increment. In these stages, α and β resistivity was obtained for eight positions shown in Figure 8.23b. Azimuthal measurements were also collected during drying and wetting cycles. Drying was achieved in the lab by exposing the soil to the air while wetting was performed by adding water to the soil.

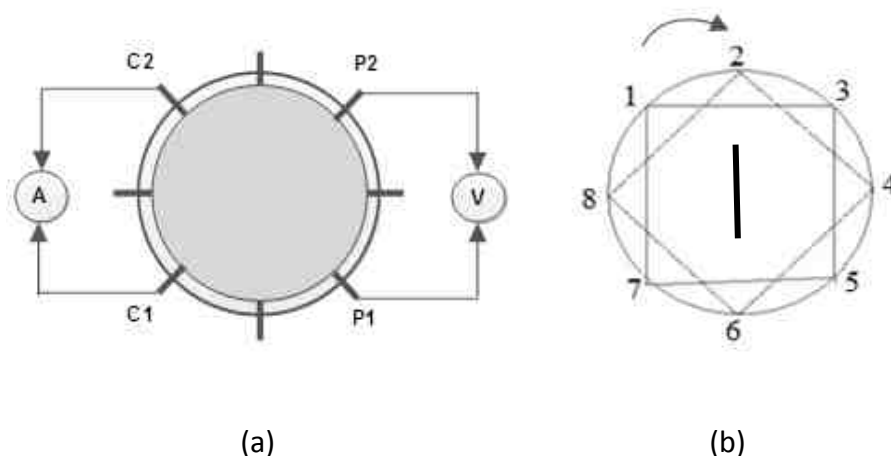


Figure 8.23. Square resistivity measurements (a) electrode arrangement (b) the measurement procedure

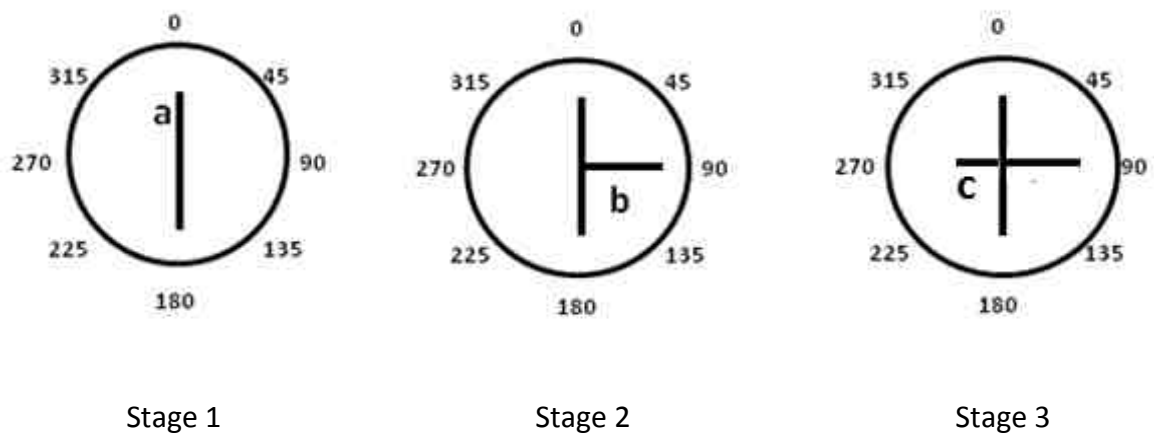


Figure 8.24. Azimuthal resistivity stages of the manually created cracks test

8.3.2 Experimental results and discussion

To assess the directional dependence of the resistivity measurements in cracking clay, a preliminary test was conducted using BIONICS soil ($w=15\%$) with a manually created crack of 70mm length, 50mm depth and 1.5mm width. The resistivity readings were collected at parallel and perpendicular directions to the crack using a square device of 15mm inter-electrode spacing as shown in Figure 8.25. It can be seen that, although the resistivity of the air filled crack is significantly high, the measured resistivity of the soil contained a crack is far lower (Jones et al., 2012; 2014) as also confirmed in the numerical simulation. In addition, the resistivity increases when the current is injected perpendicular (PP) to the crack axis, and decreases when the current is injected parallel (PL) to the crack axis. At PP and PL directions, resistivity is relatively constant away from the crack. Lataste et al. (2003) reported, through numerical and experimental tests, similar resistivity changes, the deeper the crack, the higher the changes and these changes are more significant than those of material variability. Thus, they found that the anisotropy index AI can be used as an indicator to detect the cracks. Therefore, an experimental program was adopted to investigate the directional dependence of resistivity measurement in cracking clay.

Preliminary results on the potential of the 2D ERT method to map cracks at the centimetre scale were discussed by Hassan and Toll (2013). The influence of cracking depth, width, length, and orientation on BIONICS clay ($w=15\%$) was reported by Hassan and Toll (2014).

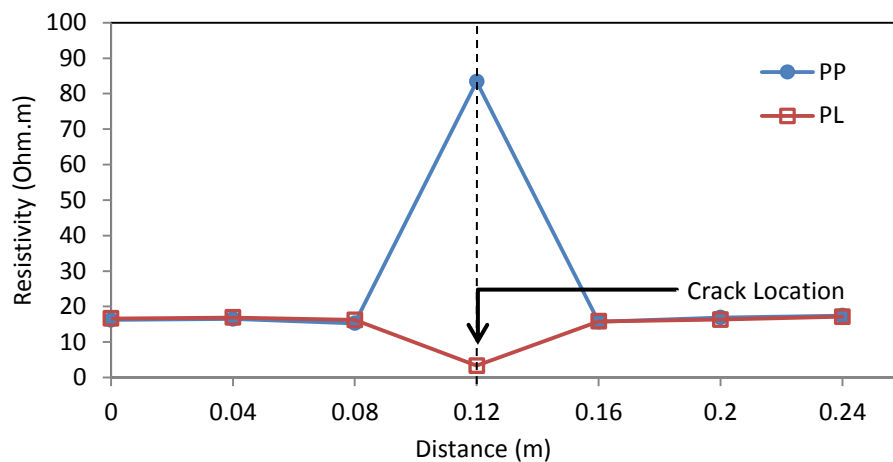


Figure 8.25. Resistivity profile of parallel (PP) and perpendicular (PL) measurements across a manually introduced crack (70mm length, 50 mm depth and 1.5mm width)

The influence of cracking parameters

The influence of the depth of the crack

Figure 8.26 shows the influence of increasing depth of an artificial crack (70mm length, 1.5mm width) created in BIONICS clay on the soil resistivity using electrode spacing $a=50\text{mm}$. To better embody the influence of cracks, resistivity readings were normalized by calculating resistivity ratio of each stage relative to the initial non-cracked state (Kong et al., 2012). The average resistivity increased by 4.70-63.80% relative to the initial state for a range of depths (10-70 mm).

As the crack is filled with air of high resistivity, increasing depth of the crack causes more blockage to the current flow and hence increases the resistivity. However, the resistivity increases in the direction perpendicular to the crack (i.e. α -resistivity) and decreases in the parallel direction (i.e. β -resistivity); the deeper the crack, the larger the influence (Lataste et al., 2003). In addition, the presence of the crack causes AI to deviate compared to the initial state. Increasing cracking depth causes a progressive increase in resistivity anisotropy, the deeper the crack, the higher the resistivity anisotropy (Greve et al., 2010a). The direct relation between cracking depth and AI downward deviations are consistent with the classical theory of increasing the depth of the crack downward during a drying period (Johnston and Hill, 1994).

Similarly, Figure 8.27 shows the influence of depth of the crack (70mm length, 1.5mm width) on the soil resistivity using electrode spacing $a=100\text{mm}$. The average resistivity increased by 2.5-4.6% relative to the initial state for a range of depths (10-70 mm). Using the larger electrode spacing, resistivity is less affected by the crack created as the crack does not intersect any side of the electrode square (i.e. the main current and voltage lines (Greve et al., 2010)). Nevertheless, the AI deviation is still evident compared to background anisotropy. Figure 8.28 shows a numerical simulation using a square device ($a=50\text{mm}$) by Lataste et al. (2003) normalized to the initial state along with experimental data from the current study. They show good agreement.

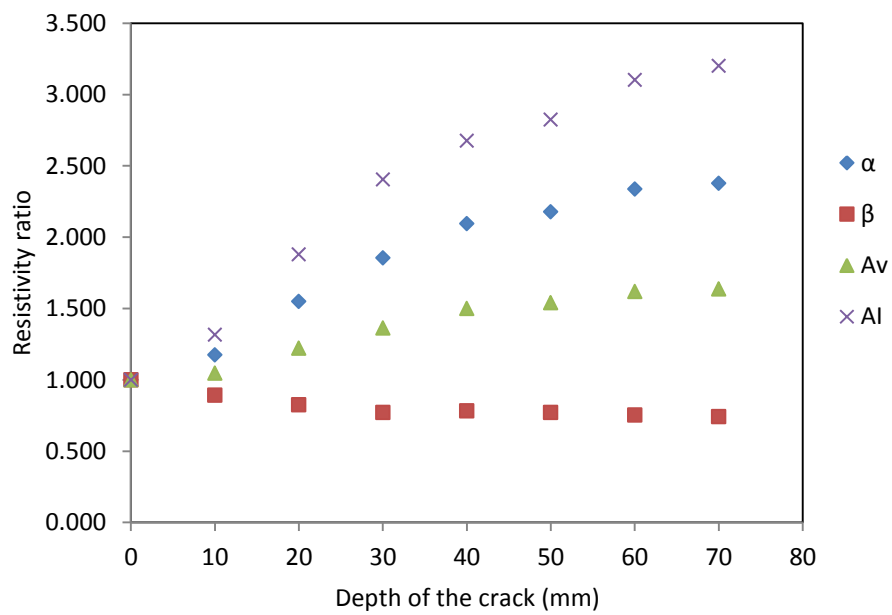


Figure 8.26. Influence of the depth of crack on soil resistivity ($a=50\text{mm}$)

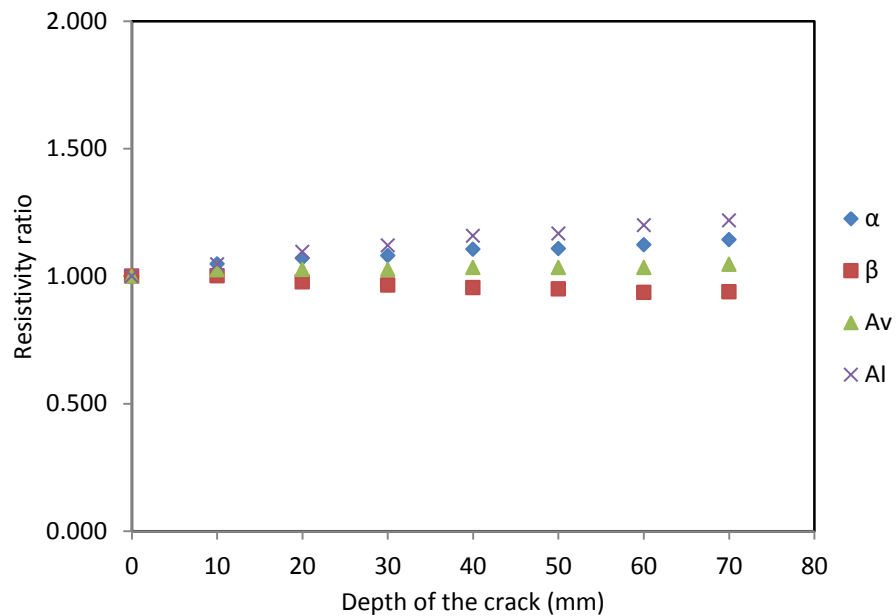


Figure 8.27. Influence of the depth of crack on soil resistivity ($a=100\text{mm}$)

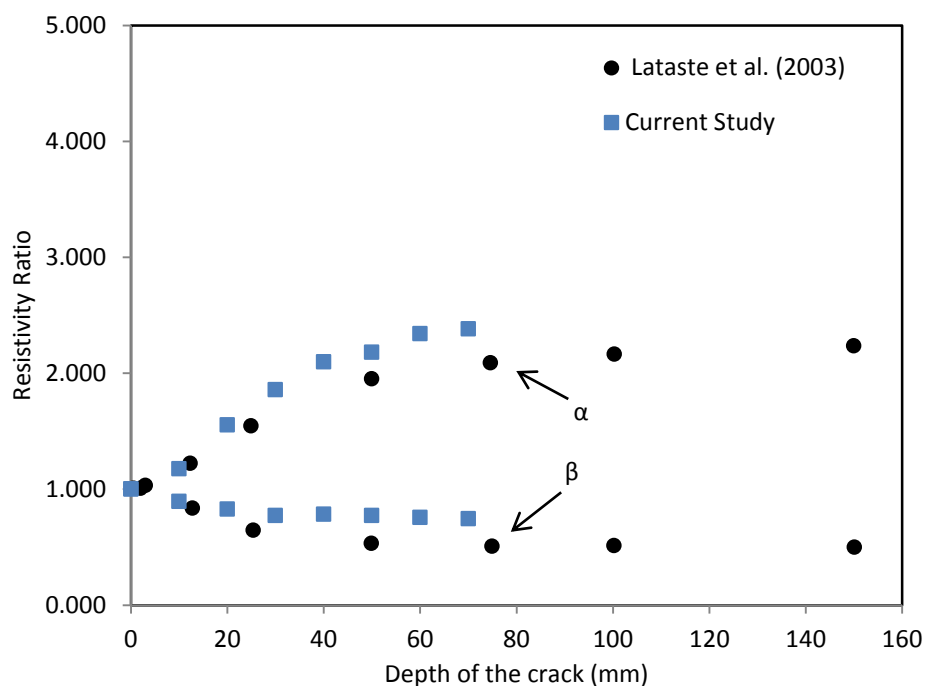


Figure 8.28. Resistivity as a function of the depth of the crack

The influence of the length of the crack

Figure 8.29 shows the influence of increasing the length of a crack (70mm depth, 1.5mm width) on soil resistivity of BIONICS clay using electrode spacing $a=50\text{mm}$. The average resistivity increased by 2.90-36.30% relative to the initial state for the range of crack lengths (20-70 mm). As increasing the length of the crack causes more blockages to the current, resistivity increase when length of the crack increases. However, this influence on resistivity is smaller than the influence of the depth of the crack, as observed by Kong et al. (2012). The presence of the crack deviates the A_I compared to the anisotropy background. Figure 8.30 shows the influence of increasing length of a crack (70mm depth, 1.5mm width) on soil resistivity using electrode spacing $a=100\text{mm}$. The average resistivity increased by 1.3-12.8% relative to the initial state for the range of crack lengths (20-70 mm). Using the larger electrode spacing, the influence of cracking length on the resistivity is less significant comparing to the same influence using an electrode spacing of $a=50\text{mm}$.

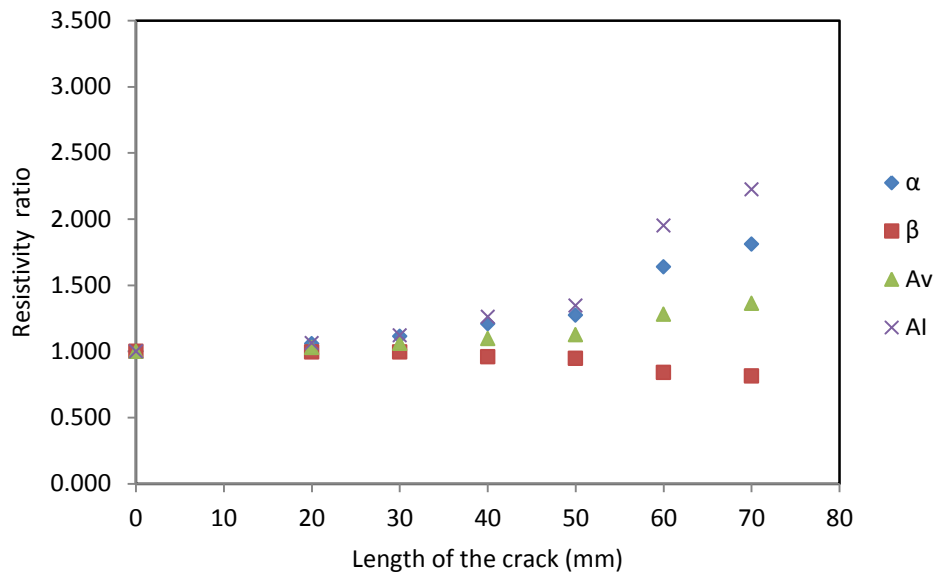


Figure 8.29. Influence of the length of the crack on soil resistivity ($a=50\text{mm}$)

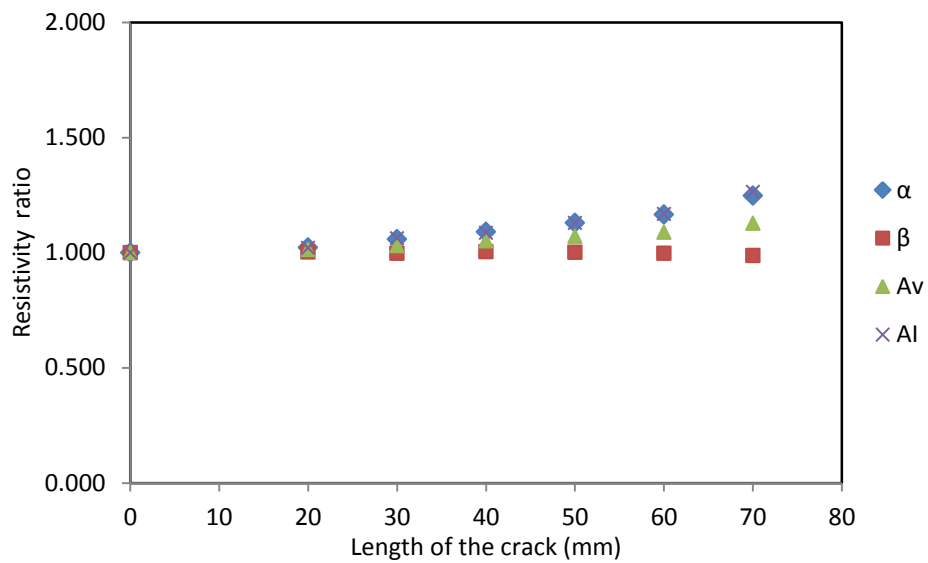


Figure 8.30. Influence of the length of the crack on soil resistivity ($a=100\text{mm}$)

The influence of the width of the crack

Figure 8.31 presents the influence of changing width of a crack (70mm length, 70mm depth) on soil resistivity using an electrode spacing $a=50\text{mm}$. The average resistivity increased by 17.4-35.8% relative to the initial state for a range of crack widths (1.5-6.0 mm). The first 1.5mm crack causes an increase in resistivity of 17.4%. However, for the subsequent stages, as the depth of the crack remains constant, increasing the width of the crack causes minor changes in resistivity. Numerically, Greve (2009) noticed that increasing cracking width caused only minor increase in AI deviations. Kong et al. (2012) experimentally demonstrated a similar result. For a constant cracking depth, increasing the width of the crack causes minor disturbance on the flow of the current within the soil body. This influence is less significant compared to the influence of the cracking depth or length.

Similarly, Figure 8.32 shows the influence of changing width of a crack (70mm length, 70mm depth) on soil resistivity using electrode spacing $a=50\text{mm}$. Using larger electrode spacing, increasing cracking width causes a minor effect on the resistivity as the average resistivity increased by 1.8-11.3% relative to the initial state for a range of crack widths (1.5-6.0 mm).

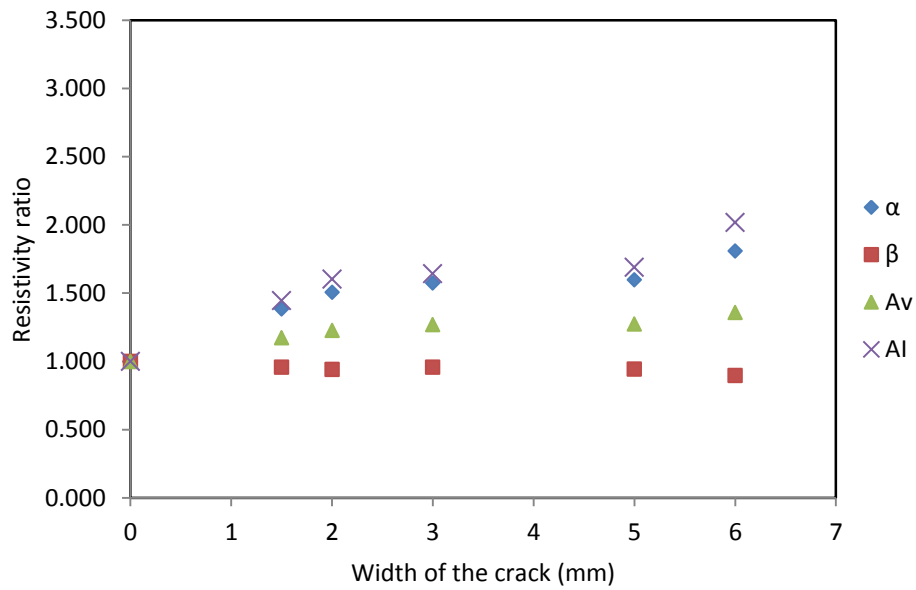


Figure 8.31. Influence of the width of the crack on soil resistivity (a=50mm)

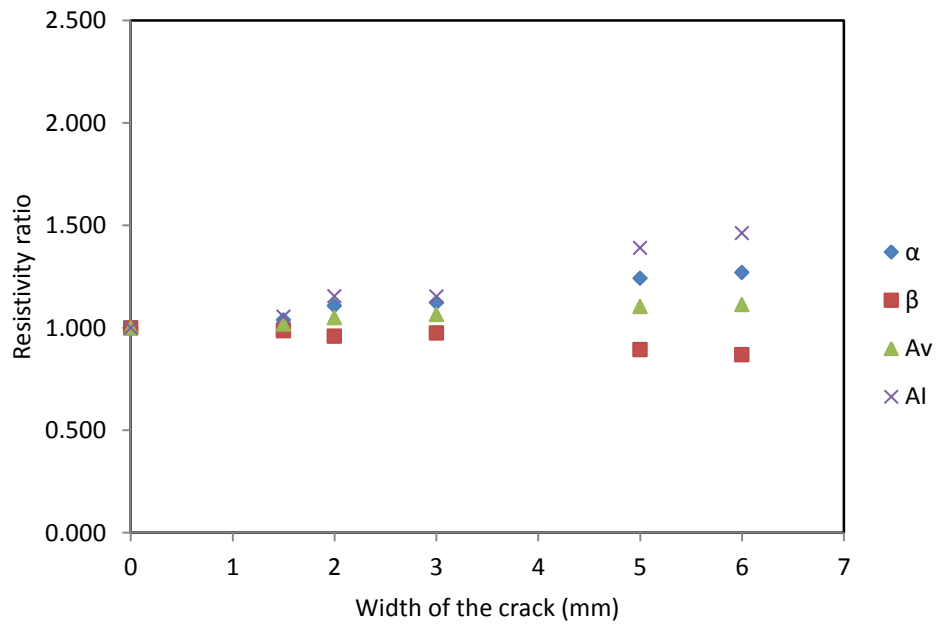


Figure 8.32. Influence of the width of the crack on soil resistivity (a=100mm)

The influence of the orientation the of crack

Figure 8.33 presents the effect of changing orientation of a crack (70mm length, 70mm depth and 1.5mm width) on soil resistivity using an electrode spacing $a=50\text{mm}$. Maximum resistivity is measured when the current is injected at a perpendicular direction to the crack while minimum resistivity is measured when the current is inserted parallel to the crack. Therefore, the AI data can better highlight the directional dependency of the measurements.

Figure 8.33 shows that AI is affected by the orientation of the crack, and at 45° no AI response is measured. Samouëlian et al. (2004) and Greve (2009) showed that cracks at 45° are difficult to capture as the AI value returns close to 1.0. This can be seen clearly in Figure 8.33 where the curve shows a turning point at 45° (as reported by Kong et al., 2012).

Similarly, Figure 8.34 shows the effect of changing orientation of a crack (70mm length, 70mm depth and 1.5mm width) on soil resistivity using $a=100\text{mm}$. Again, the figure indicates that the resistivity of the soil is less affected by the orientation of the created cracks.

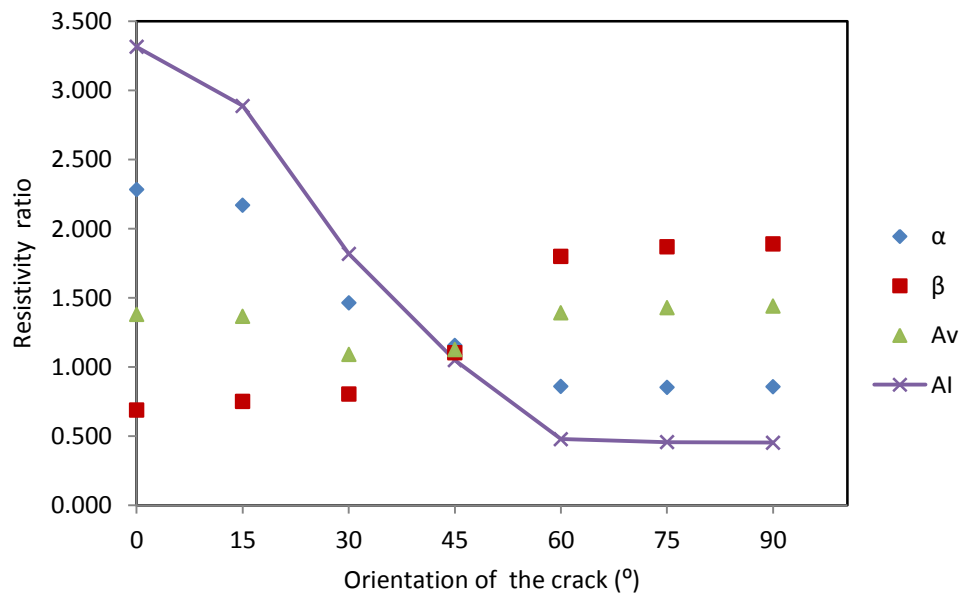


Figure 8.33. Influence of the orientation of the crack on soil resistivity (a=50mm)

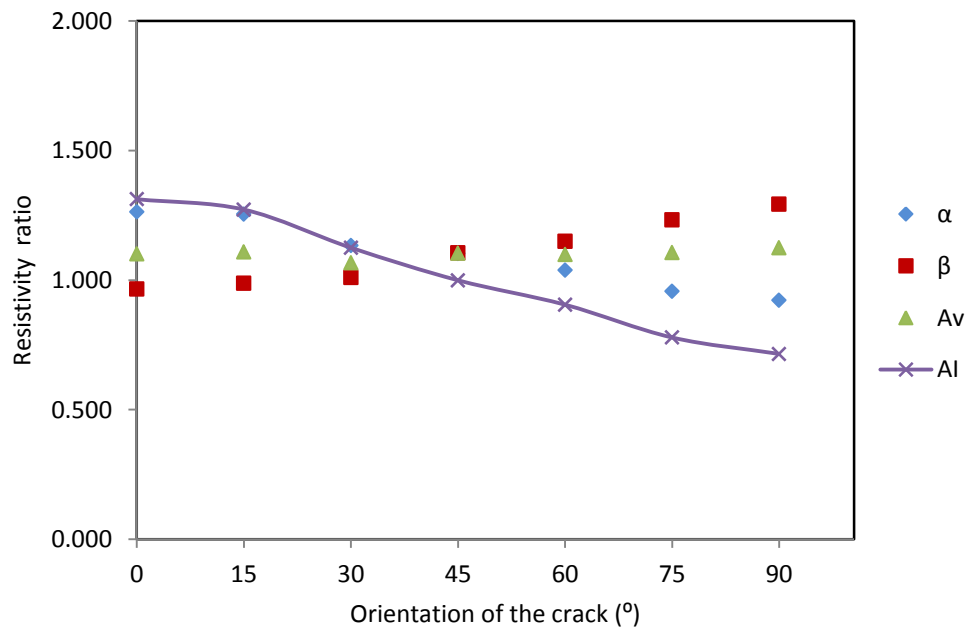


Figure 8.34. Influence of the orientation of the crack on soil resistivity (a=100mm)

***AI*-depth profiles**

As the cracking depth is of primary importance, its influence on soil resistivity was further investigated using *AI*-depth profiles. *AI*-depth profiles were generated for a soil with a manually introduced crack (70mm length, 1.5mm width) for a depth range (10-70mm), shown in Figure 8.35. For the initial stage (*AI* initial), *AI* is closed to 1.0 which indicates the homogenous resistivity distribution. However, the presence of the crack causes the *AI* to deviate significantly compared to the initial state. For crack depths of 10 and 20mm, there is an "apparent" change in *AI* at 40mm which indicates that the resistivity measurement is affected by the introduced cracks. Increasing cracking depth causes a progressive increase in resistivity anisotropy, the deeper the crack, the higher the resistivity anisotropy (Greve et al., 2010a). The direct relation between cracking depth and *AI* downward deviations agrees with the classical theory of increasing the depth of the crack downward during a drying period (Johnston and Hill, 1994). Therefore, time-lapses of *AI*-depth profiles can capture cracking depth development under the subsurface during drying.

Figure 8.36 shows *AI* changes calculated at depths 10-190mm. *AI* changes significantly at 10mm depth (close to the surface) and these changes are minor at 40 and 70mm depth. No changes are evident below 70mm (the maximum cracking depth). Electrically, Samouëlian et al., (2003a) found that the top layer of the soil is more sensitive to cracking of soil, as confirmed by the high resistivity anomaly at the top of the simulated models in the current study. Similarly, Greve et al., (2010a) showed that the largest *AI* changes are occurred at the top of the soil. At 10mm depth, more blockages to the current are expected and hence more *AI* deviations.

Figure 8.37 shows the polar diagram and *AI*-depth data at 10mm depth for the initial non-cracked stage and for the subsequent stages with cracks of 10, 40 and 70mm depth. *AI* is close to 1.0 in the initial stage. In the subsequent stages, *AI* increases when the current is injected perpendicular to the crack and the deeper the crack, the more *AI* deviation. Azimuthal measurements will be further analysed in the next section.

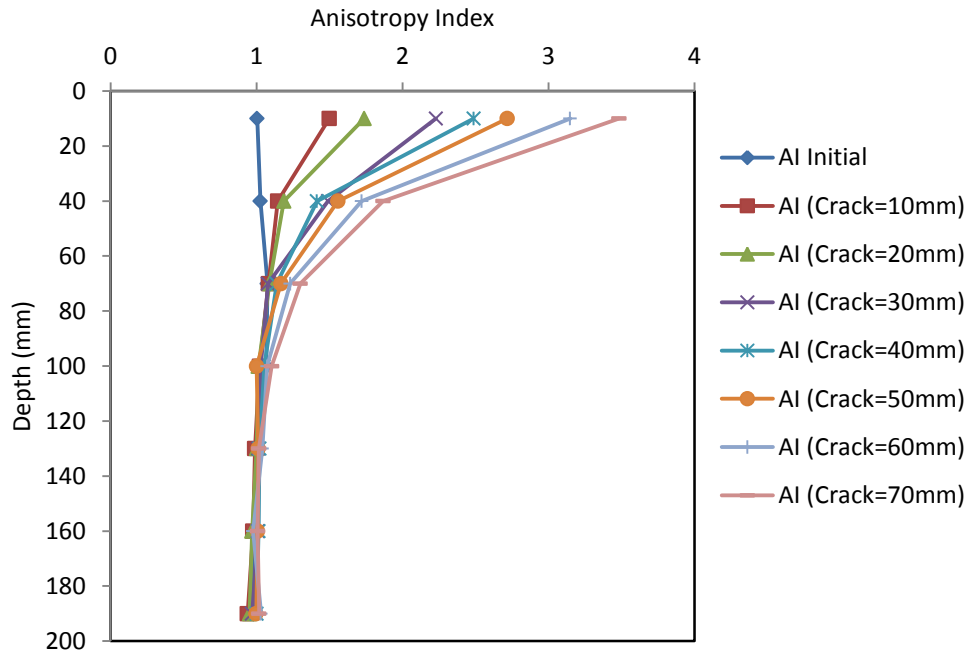


Figure 8.35 AI-depth profiles

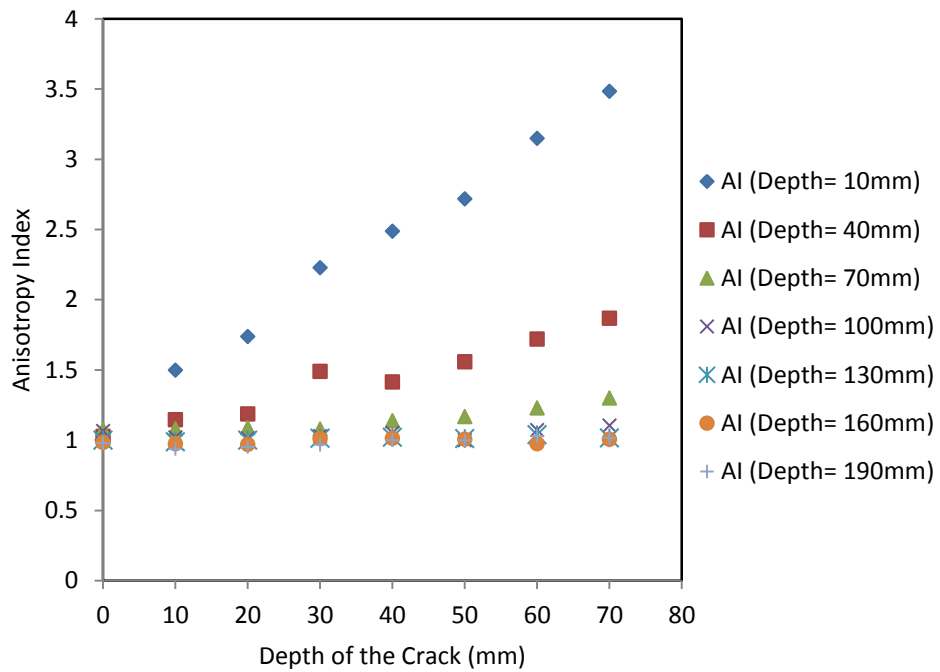
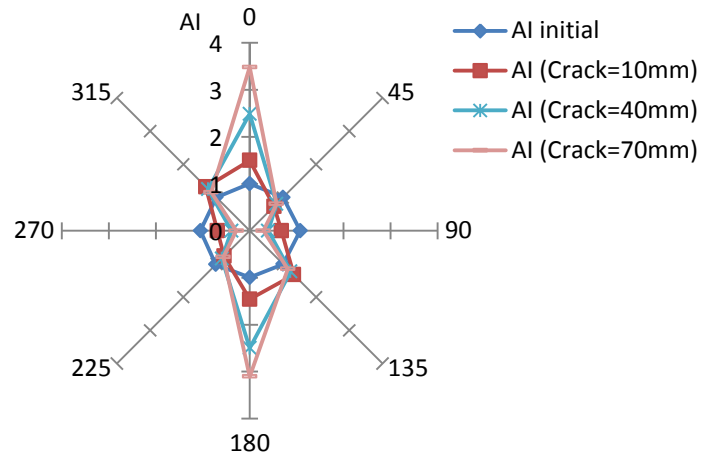
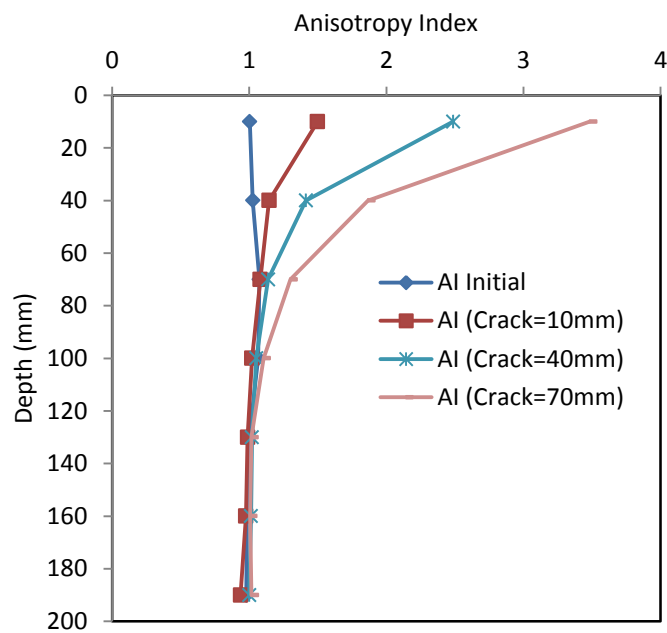


Figure 8.36. AI changes at different depths for the created cracks



(a)



(b)

Figure 8.37. Polar diagram and *AI*- depth data for the initial non-cracked stage and for the subsequent stages with cracks of 10, 40 and 70mm depth. (a) polar diagram at 10mm depth (b) *AI*-depth profiles

Azimuthal resistivity data

Azimuthal resistivity measurements were performed on BIONICS soil with manually created cracks in three stages as described in Figure 8.24. Figure 8.38 and 8.39 present the resistivity data of the original non-cracked soil as a function of azimuth in the Cartesian coordinate and the polar diagram, respectively. The measured resistivities of soil change from 14.24-14.41 Ohm.m (average 14.32 Ohm.m) with AI close to 1.0.

Figure 8.40 shows the AI polar diagrams for the three stages. In stage 1, a crack "a" of 70mm length and 1.5mm width was introduced. Increasing the depth of the crack from 10 to 40mm with 10mm increment causes significant changes in AI relative to the initial stage, the greater the depth of the crack, the greater the AI deviation. AI increases when the current is injected perpendicular to the crack and decreases in the opposite direction. In stage 2, a crack "b" of 40mm length and 1.5mm width was created for a range of depth (10-40mm) with 10mm increment. As the length of the crack is 40mm, adding this extra crack in a direction perpendicular to the crack introduced in stage 1 causes a minor deviation in AI as shown in Figure 8.40. Again, AI increases when the current is injected perpendicular to the crack and decreases in the opposite direction. Similarly, adding a crack "c" of 30mm length, 1.5mm width in the stage 3 for a range of depth (10-40mm) with 10mm increment causes similar deviations in AI .

Figure 8.41 shows the evolution of AI diagrams and AI profiles. A progressive increase in AI from 1.19 to 1.97 is noticed with increasing the cracking depth from 10 to 40mm in stage 1 comparing to initial non cracked state. In stage 2, AI decreased from 1.97 to 1.31. Further reduction in AI from 1.31 to 0.95 is measured in stage 3. The azimuthal resistivity data showed that changing cracking depth causes remarkable deviations in AI data, the more the depth of the crack, the more the deviation, and the main trend of the ellipse is affected by the direction of the crack.

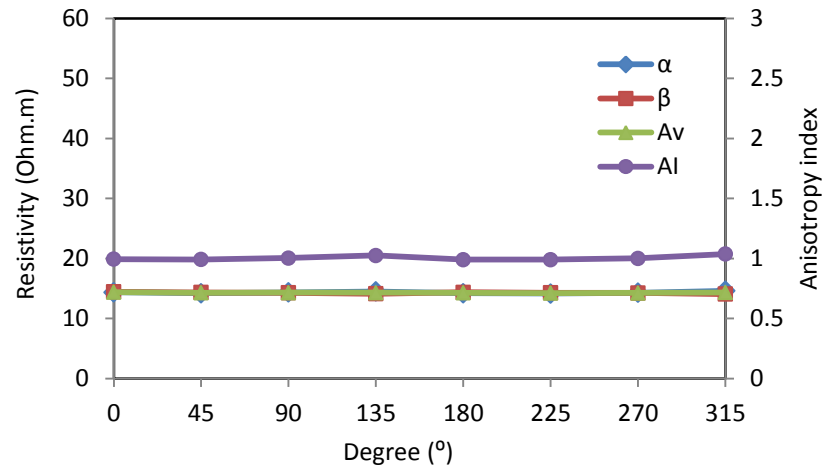
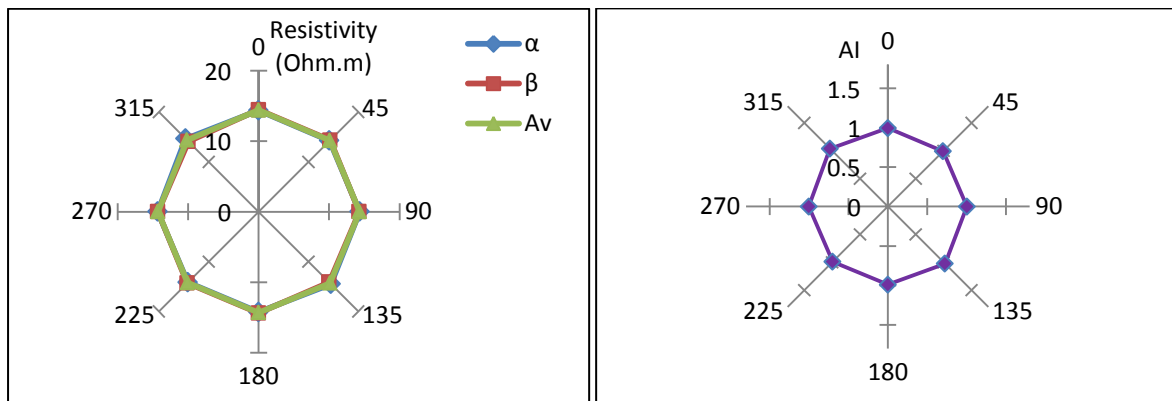


Figure 8.38. Resistivity data of the initial non-cracked stage as a function of the azimuth



(a)

(b)

Figure 8.39. Resistivity of the original non-cracked soil on polar diagram (a) α , β and A_v resistivity (b) AI data

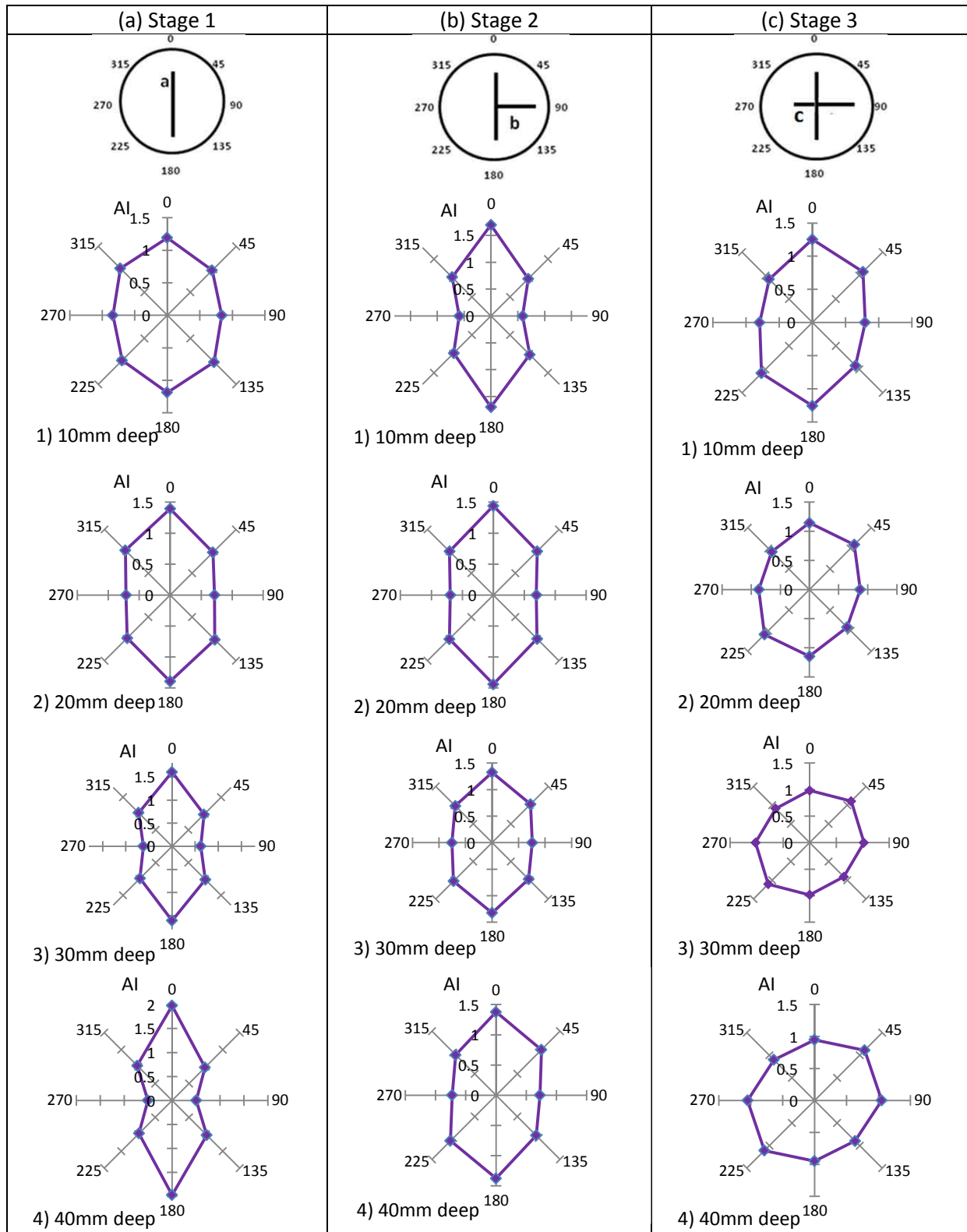
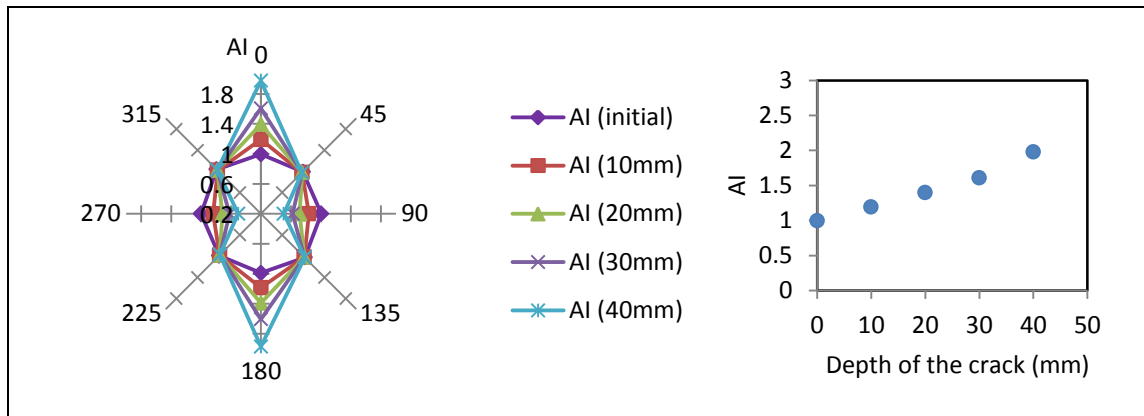
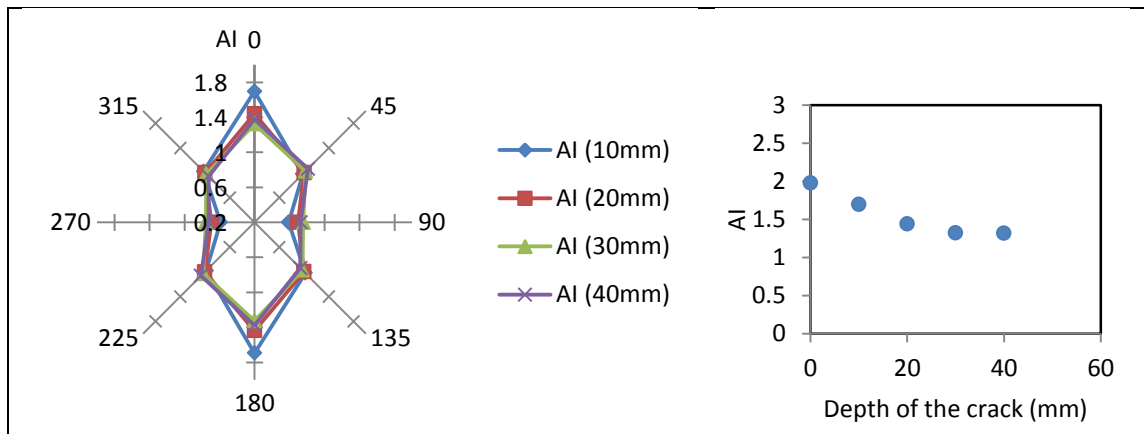


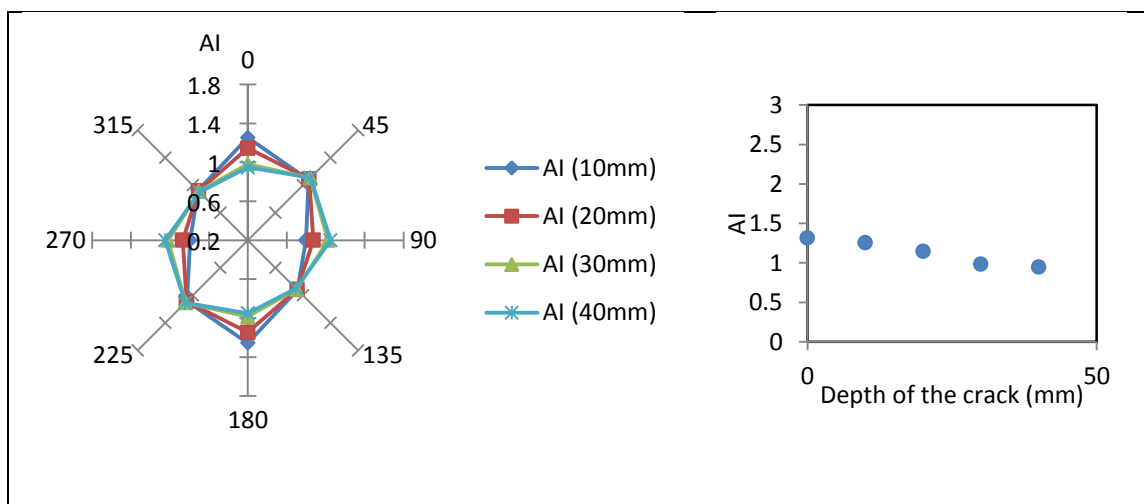
Figure 8.40. AI polar diagrams of the manually created cracks in stage 1, 2 and 3



(a) Stage 1



(b) Stage 2



(c) Stage 3

Figure 8.41. Evolution of AI polar diagrams profiles (a) Stage 1 (b) Stage 2 and (c) Stage 3

Drying and wetting cycles

Several studies have focused on characterising the influence of manually created cracks on the resistivity of the soil (e.g. Samouëlian et al., 2003a, b; Kong et al., 2012). Cracking of clay is more complicated than simple manually introduced crack scenarios. Further experiments are required to monitor cracking evolution during drying-wetting cycles. Therefore, Azimuthal resistivity measurements were performed during two drying and wetting cycles using BIONICS soil ($w=40\%$).

Figure 8.42 shows selected images of the first drying and wetting cycle and the corresponding AI data. Step 1 shows the initial non-cracked state of the soil with AI close to 1.0. With progressive drying, no obvious cracks can be seen at the surface of the soil and hence no major changes in AI data as can be seen in step 2. In step 3, two cracks "a" and "b" were developed which cause significant changes in AI data, as AI increases to 2.71 in the general trend of the cracks, when the current is injected at the perpendicular direction and decreases in the opposite direction to 0.37. In step 4, increasing the depth and length of "a" and "b" and the development of crack "c" causes an increase in AI in the diagonal direction to 7.59 and 8.56. In step 5, the depth of the crack "c" is further increased which changed AI to 6.44-11.76 in the diagonal direction and further decrease in the opposite direction to 0.11, however, the main trend of the polar diagram remains the same. In the first drying cycle, the development of the cracks causes significant changes in AI and the main trend of the polar diagram.

In the first wetting cycle, adding water to the soil causes a decrease in AI as can be seen in steps 6, 7, and 8, however, because of the presence of the cracks, the main direction of the polar diagram remains the same. This suggests that water content changes have a minor influence on the measured anisotropy of cracked clay (Greve et al., 2010a). With progressive wetting, the shape of the diagram is changed significantly in step 9, and became similar to the initial state in step 10 as the cracks are filled with water, and the electrical

conduction is achieved again through the cracks. The *AI* data of step 10 suggests that conductive water-filled cracks are difficult to characterise (LaBrecque et al., 2004).

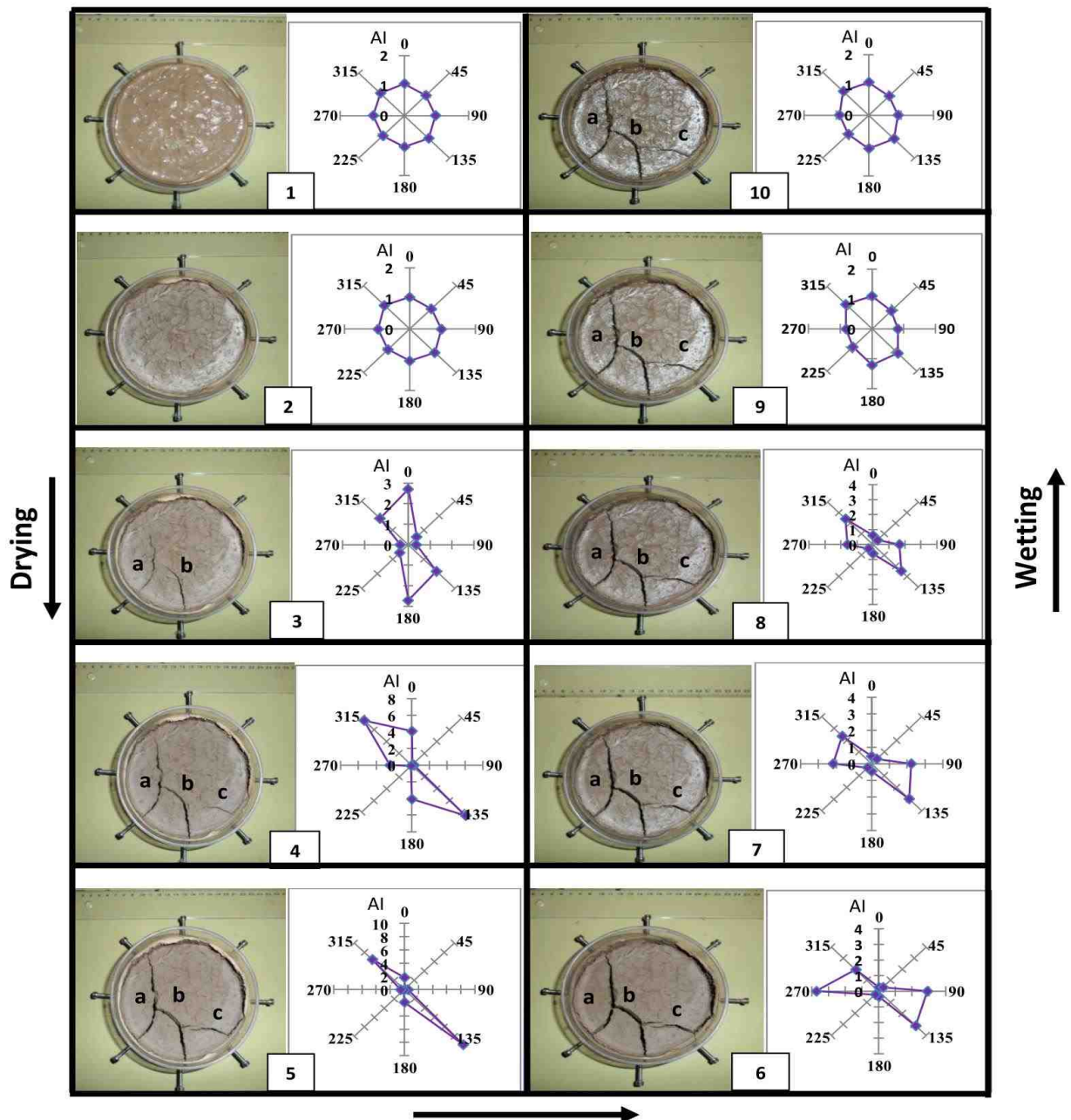


Figure 8.42. *AI* polar diagrams of the first drying and wetting test

The AI data of the second drying and wetting cycle is shown in Figure 8.43. In the second drying cycle, due to the water added and the closure of cracks in the first cycle, the AI diagram returns back to the circular shape with AI close to 1.0 as can be noticed in step 1. With progressive drying in the steps 2-5, the shape of AI polar diagram is changed in the same direction noticed in the first drying stage as the cracking network does not change significantly.

In the second wetting cycle, the main trend of AI diagram remains the same in step 6 and 7, due to the small amount of the water added which indicates that cracking has the significant impact on AI data. With the addition of more water, the cracks are filled with water which causes AI to return to the circular shape, where the electrical conduction is achieved again through the cracks as shown in step 8, 9 and 10. Again, this confirms the difficulties of detecting water-filled cracks reported in the literature. However, the steps 8, 9 and 10 also suggest that water content changes after the closure of the cracks have only a minor influence on AI data which indicates that the cracking dynamics, not the water content changes, dominates the AI variations (Greve et al., 2010a).

The cracks formed during drying and wetting produced significant changes in AI data. However, the influence of cracking developed was more complicated than the simple manually created cracks. Increasing the number of the electrodes at the boundary of the cell (e.g. 16 instead of 8 electrodes) can offer more resistivity readings and hence improve the AI data.

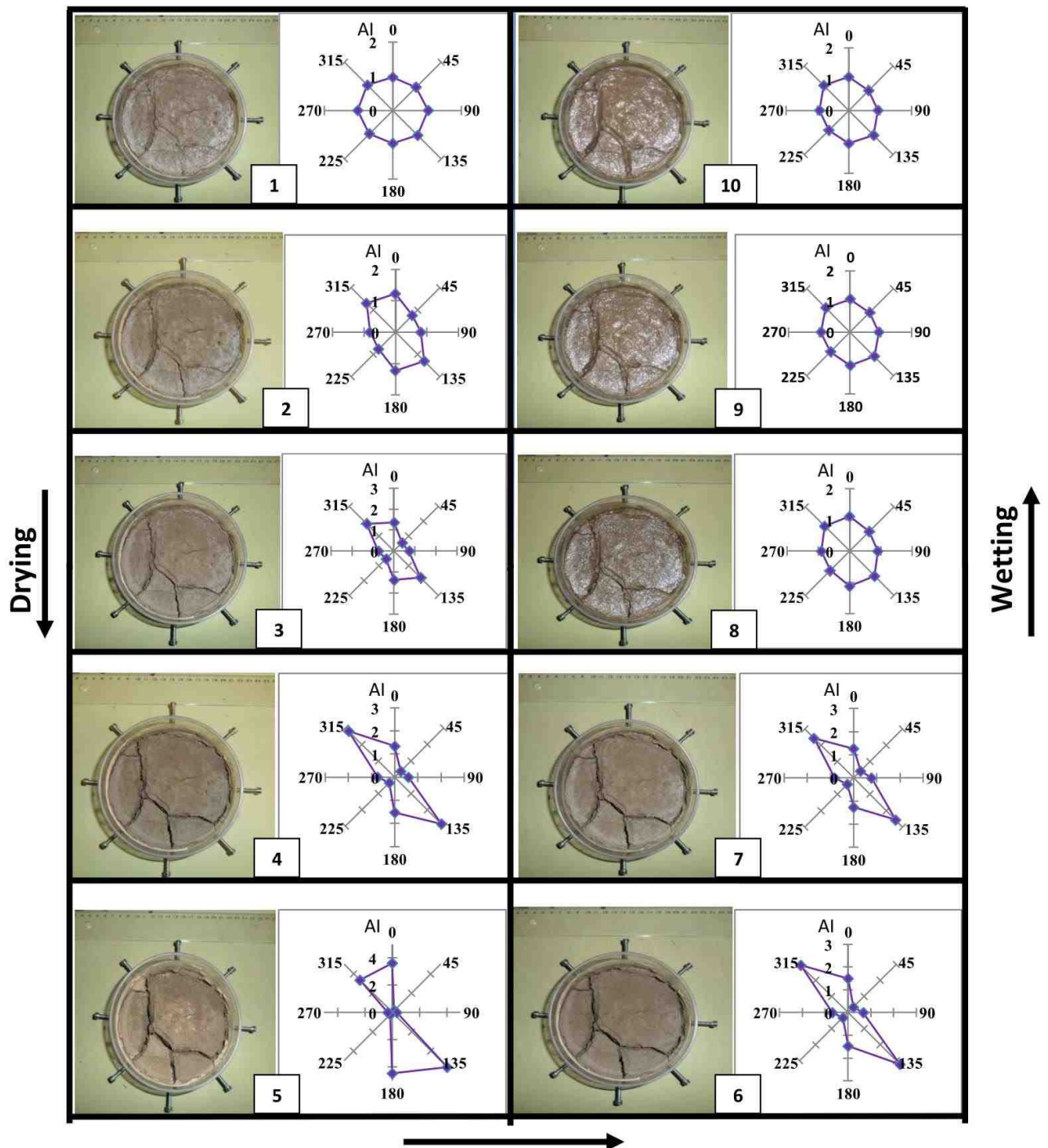


Figure 8.43. Al polar diagrams of the second drying and wetting test

8.4 Chapter summary

In this chapter, numerical and experimental techniques were used to explore the potential of the resistivity method for characterising cracking of clay soils. The directional dependence of resistivity measurements in cracking clays is investigated, and the influence of cracking depth, length, width and orientation on clay resistivity are addressed.

As the resistivity of the air filled cracks is significantly higher than the surrounding soil, the numerical simulations showed that cracks have an anomalous high resistivity that can be distinguished from the background. The geometry and depth extent of the simulated cracks can be estimated reasonably well. However, more work is needed to simulate water-filled cracks.

The experimental results showed that changing cracking depth, length, width and orientation causes significant changes in soil resistivity. As the cracks form barriers that disturb the flow of current, the depth and length of the crack have the major influence on soil resistivity.

In addition, air filled cracks cause a directional dependence in resistivity data. The directional dependence was investigated using *AI*-depth profiles and azimuthal resistivity measurements. Increasing the cracking depth causes a progressive increase in resistivity anisotropy, the deeper the crack, the higher the resistivity anisotropy. The experimental data showed that *AI* polar diagrams are significantly affected by cracking of clay soil. However, water-filled cracks are difficult to characterise. Although the cracking networks developed during drying and wetting cycles are significantly more complex than simple cracking scenarios, the cracks produced significant changes in *AI* data. The high resistivity contrast between the cracks and the surrounding soil can be used to characterise cracking in clay soil which is of a great importance in slope stability studies, which so far has been hampered by the lack of non-invasive technique than can monitor cracking dynamics.

Chapter 9

Conclusions and recommendations for future work

9.1 Conclusions

This thesis describes the design and construction of a new automated multi-electrode resistivity system and resistivity devices developed for water content characterisation of unsaturated clay soil, commonly being used as fills in engineered earth structures.

A broad spectrum of techniques are available to measure soil water content. However, reliable and efficient techniques that can measure soil water content need further investigation, particularly to consider of the influence of wetting, drying and cracking on soil properties. The main water content measurement techniques were reviewed in Chapter 2 to provide the background and basis for the work described in the current thesis and to identify the knowledge gaps. Among the options available, electrical resistivity offers quick, non-invasive and low cost estimates of soil water content at different scales.

One of the recent advances in the resistivity instrumentation is the development of automated multi-electrode systems and devices for water content determination. The design and construction of automated multi-electrode resistivity system and resistivity devices were presented in Chapter 3. A flexible data acquisition and control software package has been developed to acquire resistivity data using different resistivity arrays in a real-time procedure. The user can remotely set the current and voltage, switch 64 electrodes, read the output current and voltage difference and store the resistivity data for interpretation in a fully automated procedure. This advantage made the system relevant for characterising water content changes of unsaturated soil subjected to drying and wetting procedures, one of the main interests in the current thesis. A new resistivity probe based on the square electrode configuration was developed for localised water content

determination. The probe offers a quick and easy tool to monitor water content changes in unsaturated soil subjected to drying and wetting procedures.

As for all new equipment, calibration and validation of the system are crucial to check the data quality and performance of the system. Detailed experimental procedures were described in Chapter 4 and adopted to examine the system. The system was tested using a wide range of high precision reference resistors and different soils. The outputs were correlated with those acquired with commercial instruments at different situations. The system was examined using a wide range (2-3000 Ohm) of reference resistors to determine the measurement error. The measurement error was 0.19% (maximum 0.80%) in the four-electrode method and 0.21% in the automated data acquisition mode. This indicates the high accuracy of the measurements and the consistency of the data acquisition for long periods. The low standard deviation of the readings has indicated the high precision of the outputs. The experimental results have demonstrated the performance validity of the system for automated data acquisition which is one of the recent contributions in the resistivity instrumentation.

Validation of the data was achieved by comparing the outputs of the system with those acquired using standard conductivity and resistivity meter. Using chemical solutions of different concentrations, the measurements correlated well with the electrical conductivities measured using a HANNA conductivity meter. The system was also compared to a commercial resistivity system (Terrameter SAS 300 C) using a four-electrode, horizontal profiling and 2D ERT experiments. The results indicate a good comparison with an average percentage difference of 1.12%.

As reviewed in Chapter 2, a number of authors have reported the relevance of using resistivity for water content measurement. Numerous explicit relationships between the resistivity and water content have been presented and used to calibrate the resistivity against water content. However, the resistivity of clay soils is influenced, in addition to water content, by various parameters that should be considered. The water content

characteristics of compacted BIONICS clay were extensively investigated using a large number of specimens prepared at various water content and densities using different compaction efforts and methods. The influence of the compaction key variables such as water content, density and compaction effort was discussed in Chapter 5. The specimens were compacted using dynamic (standard Proctor and Modified), and static methods for a range of dry densities. Gravimetric water content, volumetric water content and degree of saturation were correlated with the measured resistivity. Development of laboratory correlations between soil resistivity and water content is practically useful, enabling field resistivity data to be used for mapping water content variations. The key findings can be listed as follow:

1. The resistivity of compacted clay soil is shown to be strongly influenced by water content, compaction and compaction effort. The resistivity is relatively low for soil compacted wet of the optimum, while the resistivity is relatively high for soil compacted dry of the optimum. Increasing the compaction effort reduces the soil resistivity. However, it was found that this influence is significant when the soil is compacted at low water content, or dry of the optimum; the more the compaction effort, the lower the soil resistivity. For the soil compacted at high water content, or wet of the optimum, this effect is insignificant. The resistivity behaviour was explained by changing of soil properties during compaction.
2. For a particular gravimetric water content, resistivity decreases with increasing dry density/decreasing the void ratio. As the dry density increases (the void ratio decreases), more pores are filled with water, hence, soil resistivity decreases. It is suggested, therefore, that using gravimetric water content as a criterion to calibrate resistivity against water content can be erroneous, as soils may be found at identical gravimetric water content but at different degrees of saturation.
3. Experimental relationships that relate soil resistivity with volumetric water content and the degree of saturation were developed. The high correlation coefficients of the experimental relationships achieved, for the wide range of water content covered, suggest

that these relationships can reasonably be used to calibrate in situ resistivity data against water content.

4. The resistivity behaviour of mechanically compacted clay soil is controlled by degree of saturation accompanied by changes in clay microstructure. At low degree of saturation, the discontinuity of pore water causes a relatively high resistivity, while, at high degree of saturation, where the pores are filled by water, the continuity of the water phase is improved, causing a decrease in the resistivity. At water content levels close to saturation, the influence of water content on resistivity is insignificant, as the electrical paths are already achieved for current conduction.

5. It is suggested that the degree of saturation or volumetric water content is more reliable than the gravimetric water content to calibrate in situ resistivity data against water content. The resistivity of mechanically compacted clay soil is influenced by several parameters that need to be considered, and resistivity investigation on remoulded soils must consider a range of specimens with various degrees of saturation for better water content estimates.

Recent work conducted by the British Geological Survey on the BIONICS embankment has reported resistivity variations across the embankment, mainly attributed, to water content changes; however, variations could also be due to variations in temperature and pore water salinity. It is, therefore, necessary to consider these effects on the measured resistivities. The influence of temperature and pore water chemistry was discussed in Chapter 6. The resistivity behaviour of BIONICS soil for a range of temperature (-12 to 43°C) and the effect of the salt type and concentration were addressed. The resistivity of the soil decreases when the temperature increases. This can be explained by increasing the mobility of the ions with increasing the temperature. At temperatures above the freezing point, the resistivity is low and decreases with the temperature following the Campbell model. At temperatures below freezing, the resistivity is significantly higher and decreases non-linearly with the temperature. The developed relationship between the

resistivity and temperature for the data above freezing can be used to correct field data to a reference temperature.

As electrical conduction takes place via displacements of ions in the pore water, changing the type and concentration of salts mixed with water changes the resistivity of the soil significantly. However, it was noticed that this influence is less significant for specimens prepared at high water contents or at high concentrations, where the current paths are well achieved. Since different ions have different ionic mobility, specimens mixed with different salts of the same concentration showed different resistivities. It was also noticed that, for a given water content, increasing salt concentration causes a decrease in soil resistivity. This explains the differences in soil resistivity resulted from the variations of ionic concentration and composition in soils of the same water content. The results showed that the impacts of temperature and pore water conductivity on the soil resistivity have to be considered particularly for long-term field studies.

Unsaturated clay soils are subjected to wetting, drying and cracking due to the shrink-swell behaviour and water content changes linked to the climate effects, hence progressive failures. Although numerous works have been published describing the resistivity and water content relationships, the effects of the drying and wetting and the accompanied volume changes have rarely been discussed. The resistivity-water content relationships of BIONICS clay and other local and pure clays subjected to drying and wetting procedures were presented in Chapter 7. Discrete drying and wetting were used. In addition, the resistivity, water content and volume changes were obtained continuously and simultaneously. The resistivity behaviour of clay soils subjected to drying and wetting is controlled by water content changes and the microstructure of these soils. The continuity/discontinuity of the pore water phase linked to the microstructure of the clay is a key controlling factor.

The results showed that BIONICS clay exhibits electrical hysteresis as could be expected as the soil water retention curve (SWRC) has been shown to be hysteretic from

previous studies. The resistivity of the drying path does not coincide with the resistivity of the wetting path. This behaviour was explained by difference in saturation history between drying and wetting. The hysteresis of the resistivity-water content relationship can complicate the use of the resistivity data in unsaturated soil testing, particularly when discussing the resistivity of clay soils subjected to drying and wetting cycles. However, the resistivity can be used as an indicator for monitoring water content changes in clay soils subjected to drying and wetting cycles.

Clay soils tend to crack when they lose moisture. Measuring cracking patterns has mainly been limited to inadequate visual inspections of cracking geometries. As cracks are normally filled with air that is infinitely resistive, cracks form barriers that disturb the flow of electricity. This makes the resistivity technique promising for detecting cracking in clay soils. Recent studies have focused on using the resistivity method, as a non-invasive tool, for mapping cracking networks forming in clay soils. Cracking in clay soil causes a directional dependence in the current flow which makes the method promising for characterising cracking in clay soils. Therefore, in Chapter 8, numerical and experimental techniques were adopted to address the directional dependence of resistivity measurements and the effects of crack depth, length, width and orientation on soil resistivity.

The numerical simulations showed that cracks have anomalous high resistivity values that can be distinguished from the background. The geometry and depth extent of cracks simulated can be estimated reasonably well. Although the resistivity of the air filled crack is significantly higher, the measured resistivity of the soil contained a crack is far lower. The directional dependence was investigated using anisotropy profiles and azimuthal resistivity measurements. The experimental results showed that the resistivity increases when the current is injected perpendicular to the crack axis and decreases when the current is injected parallel to the crack axis. The results also showed that changing cracking depth, length, width and orientation causes significant changes in soil resistivity. As the cracks form barriers that disturb the flow of current, the depth and length of the crack have the major

influence on soil resistivity. Increasing the cracking depth of air filled cracks causes a progressive increase in resistivity anisotropy, the deeper the crack, the higher the resistivity anisotropy. However, water-filled cracks are difficult to characterise due to the low resistivity contrast between the crack and the surrounding soil. Although the desiccation cracking networks are significantly more complex than simple cracking scenarios, the high resistivity contrast between the cracks and the surrounding soil can be used to characterise cracking in clay soil which is of a great importance in slope stability studies of engineered earth structures.

9.2 Future work

This thesis has described the design and construction of an automated multi-electrode resistivity system and resistivity devices developed for laboratory testing. The system could be developed further as a portable system for field measurements. This can be achieved by using a rechargeable current source powered by a renewable power energy that can provide the electrical current needed for the system. Since the system offers automated real time data acquisition, the system could be monitored and the data transferred using wireless telemetry and an IT infrastructure. Using permanently installed electrodes, an automated time lapse resistivity measurement can be collected to better understand the role of climate change on the engineered earth structure.

The laboratory work in this thesis has focused on the water content characteristics of unsaturated clay specimens of the BIONICS embankment. The research findings of the laboratory experimentation could feed back into improved ERT modelling of the BIONICS embankment field work. This can be achieved through use of experimental relationships developed between soil resistivity and water content to calibrate resistivity data from the field against water content. Using soil resistivity sections derived in the field, the water content can be estimated using the experimental relationships developed in the current study. This step is useful to convert the physical resistivity sections into water content sections in order to monitor water content changes across the embankment.

The experimental results have shown that temperature and pore water salinity play an important role in soil resistivity. The developed relationship between soil resistivity and temperature for the data above freezing can be used to correct field data to a reference temperature, particularly for resistivity measurements collected over a long period (i.e. time lapse field studies) where temperature correction due to seasonal temperature variations is essential to compare resistivity data collected at the same location but on different dates. The experimental findings have shown that changing the type and concentration of salts mixed with water changes the resistivity of the soil significantly. Further work is needed to monitor pore water salinity in the field to consider the implications of changing pore water salinity and concentration over a long period of field investigation. It is suggested that temperature and pore water salinity have to be considered for long term in situ studies.

The laboratory investigations have shown that soil resistivity is influenced by various parameters that have to be considered. More work can be conducted at laboratory and field levels. At laboratory level, a small scale embankment model compacted using different compaction specifications similar to that used in the field would be useful to monitor soil resistivity, water content, temperature and pore water salinity during drying and wetting cycles. At field level, it is essential to carry out long term field studies to monitor these factors during different seasons. The resistivity technique has been indicated as an effective tool for mapping the spatiotemporal variability of water content, and if linked with other moisture sensors can provide accurate information about soil water changes. It would be useful to carry out time lapse studies using an array of resistivity electrodes and moisture sensors to map 3D water content variations. Such a combined laboratory and field research approach would provide more detailed and accurate information on the impact of climate change on the embankment and improve the ERT physical modelling.

Most of the laboratory work discussed in this thesis has been conducted on compacted specimens. More research needs to be carried out on the poorly compacted panels of the BIONICS embankment. Such research would be useful to investigate the impact of water content changes on the poorly compacted engineered earth structures from Victorian times. It would also be interesting to investigate undisturbed samples taken from different panels of the BIONICS embankment, as the compaction conditions in the field might produce different soil fabrics to those in the laboratory.

Further research is needed on using the resistivity method for mapping desiccation cracks formed under natural drying and wetting conditions. At a laboratory level, the desiccation cracks can be monitored using a miniaturized electrode array of a small electrode spacing (e.g. 0.05m) using different electrode arrangements installed on small sections of the soil. Such a laboratory experiment would be useful to monitor the cracks developed under controlled laboratory conditions. At a field level, a high resolution (e.g. 0.5m) electrode spacing resistivity array can be used to map desiccation cracks developed under natural field conditions. Forward modelling can be used to aid the interpretation of laboratory and field studies.

The results have shown that the degree of saturation and clay microstructure controls the resistivity behaviour of unsaturated clay soil subjected to drying and wetting. It is suggested, therefore, that the degree of saturation or volumetric water content is a more reliable parameter than the gravimetric water content to calibrate soil resistivity against water content, and soil resistivity can be adopted as a useful indicator for monitoring water content changes in clay soils subjected to drying and wetting cycles. At a laboratory level, continuous wetting of clay soils is experimentally challenging. It requires imposing relative humidity at 100%. A new system that facilitates continuous drying and wetting would be useful to carry out experiments on specimens subjected to continuous cycles of drying and wetting. At a field level, monitoring the drying and wetting of soil through long term studies

is necessary to investigate the impact of shrink-swell behaviour on the engineering properties of the clay soil commonly used as fills in engineered earth structures.

Due to water content changes and shrink-swell behaviour, shear strength of clay soils reduces due to irreversible plastic strains accumulated within the soil. The earlier identification of water content changes along shear zones is crucial for monitoring slopes. The high water content level along slip surfaces can be monitored using the resistivity method. Although shear surfaces are very thin (<1-2mm) and cannot be detected by resistivity, the resistivity can be used as a useful indicator for identifying the wetting up of the soil mass.

The experimental results of the current thesis have shown that the electrical resistivity of clay soil is sensitive to soil density, compaction and compaction effort. It is suggested that the resistivity technique can be used as a useful tool for monitoring field compaction conditions. The experimental findings have also indicated that the resistivity method has the potential to provide relatively quick, non-invasive and low cost estimates of soil water content. It is suggested, therefore, to adopt the technique for monitoring water content changes in engineered earth structures such as road and rail embankments. However, electrical resistivity values of compacted clay soils are influenced by various interlinked parameters that all need to be considered to obtain reliable water content measurements.

References

- AASHTO T288-91. (2004). Standard method of test for determining minimum laboratory soil resistivity, American Association of State and Highway Transportation Officials, Washington.
- Abedine, A. and Robinson G. (1971). A study on cracking in some vertisols of the Sudan. *Geoderma*, 5, pp. 229-241.
- ABEM, Terrameter SAS 300 C, instruction Manual, [Online], <http://www.abem.se/files/upload/sas%20300%20manual.pdf>. Accessed 20/08/2014
- Abu-Hassanein, Z., Benson, C. and Blotz, L. (1996). Electrical resistivity of compacted clays. *J. Geotech. Eng.*, 122, pp. 397-406.
- Aizebeokhai, A. P. (2010). 2D and 3D geoelectrical resistivity imaging: Theory and field design. *Scientific Research and Essays*, Vol. 5 (23), pp. 3592-3605.
- Al Hagrey, S. A. (1994). Electric study of fracture anisotropy at Falkenberg, Germany. *Geophysics*, 59, pp. 881-888.
- Alonso, E. E., Vaunat, J. and Gens, A. (1999). Modelling the mechanical behaviour of expansive clays. *Eng. Geol.*, Vol. 54, No. 2, pp. 173-183.
- Amidu, S. A. and Dunbar, J. A. (2007). Geoelectric studies of seasonal wetting and drying of a Texas vertisol. *Vadose Zone J.* 6, pp. 511-523.
- Archie, G. E. (1942). The electric resistivity log as an aid in determining some reservoir characteristics. *Trans. Am. Inst. Min. Metall. Pet. Eng.*, 146, 54-62.
- ASTM G187. (2005). Standard test method for measurement of soil resistivity using the two-electrode soil box method, American Society for Testing and Materials. Pennsylvania, USA.
- ASTM G57. (2006). Standard test method for field measurement of soil resistivity using the Wenner four-electrode method, American Society for Testing and Materials. Pennsylvania, USA.
- Avants, B., Soodak, D. and Ruppiner G. (1999). Measuring the electrical conductivity of the earth. *Am. J. Phys.*, Vol. 67, No. 7, pp. 593-598.

REFERENCES

- Awotoye, K. S. and Selemo, A. O. I. (2006). Design and construction of a resistivity meter for shallow investigation. *Nigerian Journal of Physics*, Vol. 18 (2), pp. 261-270.
- Bai, W., Kong, L. and Guo, A. (2013). Effects of physical properties on electrical conductivity of compacted lateritic soil. *Journal of Rock Mechanics and Geotechnical Engineering*, 5 (5), pp. 406–411.
- Barker, R. D. (1997). Electrical imaging and its application in engineering investigations. *Geological Society, London, Engineering Geology Special Publications*, 12 (1), pp. 37-43.
- Barker, R. and Moore, J. (1998). The application of time lapse electrical tomography in ground water studies. *Leading Edge*, 17, pp.1454-1458.
- Beck, R. (1997). Earth resistivity meter, *Everyday with Practical Electronics*, Jan & Feb. pp. 1-9.
- Beck, Y. L., Lopes, S. P., Ferber, V. and Côte P. (2011). Microstructural Interpretation of water content and dry density influence on the DC-electrical resistivity of a fine-grained Soil. *Geotechnical Testing Journal*, Vol. 34, No. 6, pp. 1-14.
- Bell, J. P. and McCulloch, J. S. G. (1966). Soil moisture estimation by the neutron scattering method in Britain. *J. of Hydrology*, 4, pp. 259-263.
- Benson, C. H., and Daniel, D. E. (1990). Influence of clods on hydraulic conductivity of compacted clay. *J. of Geotech. Engrg.*, ASCE, 116(8), pp 1231-1248.
- Bera, T. K. and Nagaraju, J. (2011). Switching of the surface electrode array in a 16-electrode EIT system using 8-Bit parallel digital data. *World Congress on Information and Communication Technologies (WICT)*, pp. 1288-1293.
- Bery, A. A. and Saad, R. (2012). Tropical clayey sand soil's behaviour analysis and its empirical correlations via geophysics electrical resistivity method and engineering soil characterizations. *International Journal of Geosciences*, 3 (1), pp. 111-116.
- Besson, A., Cousin, I., Dorigny, A., Dabas, M. and King, D. (2008). The temperature correction for the electrical resistivity measurements in undisturbed soil samples: analysis of the existing conversion models and proposal of a new model. *Soil Science*, vol 173, pp. 707-720.
- BGS (2014a). Shrink-Swell map [Online] Available online at: http://www.bgs.ac.uk/products/geosure/shrink_swell.html, accessed 14/8/2014.

REFERENCES

- BGS (2014b). Landslide potential map. [Online] Available online at: <http://www.bgs.ac.uk/products/geosure/landslides.html>, accessed 14/08/2014.
- BGS (2014c). Rainfall and landslide data for the UK [Online] Available online at: <http://www.bgs.ac.uk/research/engineeringGeology/shallowGeohazardsAndRisks/landslides/LandslidesandRainfall.html>, accessed 14/08/2014.
- Binley, A., Cassiani, G., Middleton, R. and Winship, P. (2002). Vadose zone model parameterisation using cross-borehole radar and resistivity imaging. *Journal of Hydrology*, 267, pp. 147–159.
- Binley, A., Poulter, S. and Shaw, B. (1996a). Examination of solute transport in an undisturbed soil column using electrical resistance tomography, *Water Resour. Res.*, 32, pp. 763–769.
- Binley, A., Ramirez, A. and Daily, W. (1995). Regularised image reconstruction of noisy electrical resistance tomography data. *Proceedings of the 4th Workshop of the European Concerted Action on Process Tomography*, Bergen, pp. 401–410.
- Binley, A., Shaw, B. and Henry, P. S. (1996b). Flow pathways in porous media: electrical resistance tomography and dye staining image verification. *Meas. Sci. Technol.*, 7: pp. 384-390.
- Bittelli, M. (2011). Measuring soil water content: A review. *HortTechnology*, 21, pp. 293-300.
- Blonquist, J. M., Jones, S. B. and Robinson, D. A. (2005). Standardizing characterization of electromagnetic water content sensors. *Vadose Zone Journal*, 4 (4), pp. 1059-1069.
- Borsic, A., Comina, C., Foti, S., Lancellotta, R. and Musso, G. (2005). Imaging heterogeneities with electrical impedance tomography: laboratory results. *Geotechnique* 55 (7), pp. 539-547.
- Bouma, J. and Dekker, L. (1978). Case-study on infiltration into dry clay soil I. Morphological observations, *Geoderma*, 20, pp. 27-40.
- Brocca, L., Melone, F., Moramarco, T. and Morbidelli, R. (2010). Spatial-temporal variability of soil moisture and its estimation across scales, *Water Resour. Res.*, 46, W02516.
- Brunet, P., Clément R. and Bouvier, C. (2010). Monitoring soil water content and deficit using electrical resistivity tomography (ERT)- A case study in the Cevennes area, France. *J. of Hydrology*, 380, pp. 146-153.

REFERENCES

- Bryson, L. S. (2005). Evaluation of geotechnical parameters using electrical resistivity measurements. *Proc. Earthquake Engineering and Soil Dynamics*, GSP 133, Geo-Frontiers 2005, ASCE, Reston, VA. pp. 1-12.
- BS 1377-2 (1990). Soils for civil engineering properties. Part 2: Classification tests. British Standard Institution, London: BSI.
- BS 1377-4 (1990). Methods of test for Soils of civil engineering purposes Part 4: Compaction-related tests, British Standard Institution, London: BSI.
- BS 1377-3 (1990). Methods of test for soils for civil engineering purposes. Part 3: Chemical and electro-chemical. British Standard Institution, London: BSI.
- BS ISO 5725-1 (1994). Accuracy (trueness and precision) of measurement methods and results - Part 1: General principles and definitions. British Standard Institution, London: BSI.
- Budhu, M. (2011). Soil mechanics and foundations. 3rd ed. New York: Wiley.
- Busby, J. P. (2000). The effectiveness of azimuthal apparent resistivity measurements as a method for determining fracture strike orientations. *Geophysical Prospecting*, 48, pp. 677-695.
- Busby, J. P. and Jackson, P. (2006). The application of time-lapse azimuthal apparent resistivity measurements for the prediction of coastal cliff failure, *J. Appl. Geophys*, 59, pp. 261-272.
- Calamita, G., Brocca, L., Perrone, A., Piscitelli, S., Lapenna, V., Melone, F. and Moramarco, T. (2012). Electrical resistivity and TDR methods for soil moisture estimation in central Italy test-sites. *Journal of Hydrology*, 454-455, pp. 101-112.
- Campbell, R. B., Bower, C. A. and Richards, L. A. (1948). Change of electrical conductivity with temperature and the relation of osmotic pressure to electrical conductivity and ion concentration for soil extracts. *Soil Science Society of America Proceedings*, 13, pp. 66-69.
- Cassiani, G., Godio, A., Stocco, S., Villa, A., Deiana, R., Frattini, P. and Rossi, M. (2009). Monitoring the hydrologic behaviour of a mountain slope via time-lapse electrical resistivity tomography. *Near Surface Geophysics*, 7, pp. 475-486.

REFERENCES

- Celano, G., Palese, A. M., Ciucci, A., Martorella, E., Vignozzi, N. and Xiloyannis, C. (2011). Evaluation of soil water content in tilled and cover-cropped olive orchards by the geoelectrical technique, *Geoderma*, 163, Issues 3-4, pp. 163-170.
- Chambers, J. E., Gunn, D. A., Meldrum, P. I., Wilkinson, P. B., Ogilvy, R. D., Haslam, E., Holyoake, S. and Wragg, J. (2011a). Volumetric imaging of earth embankment internal structure and moisture movement as a tool for condition monitoring. *Railway Engineering 2009, 11th International Conference and Exhibition*, University of Westminster, London, UK, 29th-30th June.
- Chambers, J. E., Gunn, D. A., Wilkinson, P. B., Meldrum, P. I., Haslam, E., Holyoake, S., Kirkham, M., Kuras, O., Merritt, M. and Wragg, J. (2014). 4D electrical resistivity tomography monitoring of soil moisture dynamics in an operational railway embankment, *Near Surf. Geophys*, 12 (1), pp. 61-72.
- Chambers, J. E., Gunn, D. A., Wilkinson, P. B., Ogilvy, R. D., Ghataora, G. S., Burrow, M. P. N. and Smith, R. T. (2008). Non-invasive time-lapse imaging of moisture content changes in earth embankments using electrical resistivity tomography (ERT). E. Ellis, H.S. Yu, G. McDowell, A. Dawson, N. Thom (Eds.), *Advances in Transportation Geotechnics, 1st International Conference on Transportation Geotechnics Proceedings*, Nottingham, pp. 475-480.
- Chambers, J. E., Loke, M. H., Ogilvy, R. D. and Meldrum, P. I. (2004). Noninvasive monitoring of DNAPL migration through a saturated porous medium using electrical impedance tomography. *J. Contam. Hydrol.*, 68, pp. 1- 22.
- Chambers, J. E., Meldrum, P. I., Gunn, D. A., Wilkinson, P. B., Kuras, O., Weller, A. L., and Ogilvy, R.D. (2009). Hydrogeophysical monitoring of landslide processes using automated time-Lapse electrical resistivity tomography (ALERT), *15th European meeting of environmental and engineering geophysics*, Dublin, Ireland.
- Chambers, J. E., Wilkinson, P. B., Gunn, D. A., Ogilvy, R. D., Ghataora, G. S., Burrow, M.P.N. and Tilden Smith, R. (2007). Non-Invasive characterization and monitoring of earth embankments using electrical resistivity tomography (ERT). *Proc. 9th Int. Conf. Railway Engineering*, London.
- Chambers, J. E., Wilkinson, P.B., Kuras, O., Ford, J. R., Gunn, D. A., Meldrum, P.I., Pennington, C. V. L., Weller, A., L., Hobbs, P. R. N. and Ogilvy, R. D. (2011b). Three-dimensional geophysical anatomy of an active landslide in Lias Group mudrocks, Cleveland Basin, UK. *Geomorphology*, Vol. 125, pp. 472-484.

REFERENCES

- Chen, F., Liao, C. and An, J. (2003). Directional characteristic of resistivity changes in rock of original resistivity anisotropy, *Chinese Journal of Geophysics*, Vol. 46, no. 2, pp. 381-395.
- Chen, L., Yin, Z. and Zhang, P. (2007). Relationship of resistivity with water content and fissures of unsaturated expansive soils. *J. of China University of Mining and Technology*, 17 (4), pp. 537-540.
- Chrétien, M., Lataste, J. F., Fabre, R. and Denis, A. (2014). Electrical resistivity tomography to understand clay behavior during seasonal water content variations. *Engineering Geology*, 169, pp. 112-123.
- Christensen, N. B. and Sørensen, K. (2001). Pulled array continuous electrical sounding with an additional inductive source: an experimental design study. *Geophysical Prospecting*, 49: pp. 241-254.
- Corwin, D. L., Lesch, S.M. (2005). Apparent soil electrical conductivity measurements in agriculture, *Computers and Electronics in Agriculture*, 46, pp. 11-43.
- Cosentini, R. M., Della Vecchia G., Foti, S. and Musso G. (2011). Detecting water content changes in sand samples by means of Electrical Resistivity Tomography. *Unsaturated Soils* -Alonso & Gens (Eds.), Taylor and Francis Group, London.
- Dahlin, T. (1996). 2D resistivity surveying for environmental and engineering applications. *First Break*, 14, PP 275-284.
- Dahlin, T. (2000). Short note on electrode charge-up effects in DC resistivity data acquisition using multi-electrode arrays. *Geophysical Prospecting*, 48, pp. 181-187.
- Dahlin, T. (2001). The development of DC resistivity imaging techniques: *Computers and Geosciences*, 27, pp. 1019-1029.
- Dahlin, T. and Jonsson, P. (2011). A data acquisition system for geoelectric monitoring, in geoelectric monitoring current research and perspectives for the future, International Workshop within the frame of the FWF project TEMPEL (TRP 175-N21) and the 7th FP European project SafeL and November 30th-December 2nd, Vienna Berichte Geol. B.-A., 93, ISSN 1017- 8880, Instrumentation and Data Acquisition Technology.
- Damasceno V. M., Fratta D. and Bosscher P. J. (2009). Development and validation of a low-cost electrical resistivity tomographer for soil process monitoring. *Canadian Geotechnical Journal* 46, pp. 842-854.

REFERENCES

- Daniel, D. E. and Benson, C. H. (1990). Water content-density criteria for compacted soil liners, *J. of Geotech. Engrg.*, ASCE, 116(12), pp. 1811-1830.
- Dannovski, G. and Yaramanci, U. (1999). Estimation of water content and porosity using combined radar and geoelectrical measurements. *Eur. J. Environ. Eng. Geophys.*, Vol 4. pp. 71–85.
- Davis, J. L. and Annan, A. P. (1989). Ground penetrating radar for high resolution mapping of soil and rock stratigraphy, *Geophys. Prospect.*, 37, pp. 531-551.
- De Vita, P., Di Maio, R. and Piegari, E. (2012). A study of the correlation between electrical resistivity and matric suction for unsaturated ash-fall pyroclastic soils in the Campania region (southern Italy). *Environmental Earth Sciences*, 67(3). pp. 787-798.
- Department of Transport (2008). Rail Accident Report, Network Rail's management of Existing Earth-works, Report 25/ December 2008, Rail Accident Investigation Branch, Department for Transport.
- Devadasi, R. K., Naickb, P., Reddy, T. V. and Prasad, N. V. G. (2104). Automatic switching multi-electrode electrical resistivity profiling system. *International Journal of Electronics, Communication & Instrumentation Engineering Research and Development (IJECIERD)*, Vol. 4, Issue 1, pp. 47- 52.
- Di Maio, R. and Piegari, E. (2011). Water storage mapping of pyroclastic covers through electrical resistivity measurements. *J. Appl Geophys*, 75(2), pp. 196-202.
- Dickin, F. and Wang, M. (1996). Electrical resistance tomography for process tomography. *Meas Sci Tech*, 7 pp. 247-260.
- Dijkstra, T. A. and Dixon, N. (2010). Climate change and slope stability: Challenges and approaches. *Quarterly Journal of Engineering Geology and Hydrogeology*, 43, 4, pp. 371-385.
- Dinka, R. and Lascano, R. J. (2012). Challenges and limitations in studying the shrink-swell and crack dynamics of vertisol soils. *Open Journal of Soil Science* 2(2): pp. 82-90.
- Evelt, S. R. and Parkin, G. W. (2005). Advances in soil water content sensing: The continuing maturation of technology and theory, *Vadose Zone J.*, 4, pp. 986- 991.
- Farrell, D. M., Robbins, B. J., Stallings, J., Cardoso, S., and Bakker, W. (2008). Crack growth monitoring on industrial plant using established electrical resistance 'scanner' technology. *Insight*, 50(12), pp. 690- 694.

REFERENCES

- Franz, T. E., Nordbotten N. J., Caylor, J. M., Slater K. K. and Lee, D. (2011). Quantifying transient soil moisture dynamics using multipoint direct-current resistivity in homogeneous sand. *Vadose Zone J.*, 10, pp. 286-298.
- Fredlund, D. G. and Rahardjo, H. (1993). *Soil mechanics for unsaturated soils*, New York: John Wiley & Sons.
- Friedman, S. P. (2005). Soil properties influencing apparent electrical conductivity: A review, *Comput. Electron. Agric.*, 46, pp. 45-70.
- Fukue, M., Minatoa, T., Horibe, H., and Taya, N. (1999). The microstructure of clay given by resistivity measurements. *Eng. Geol.*, 54, pp. 43-53.
- Gardner, W. H. (1986). Water content. In: *Methods of soil analysis. Part 1. Physical and mineralogical methods* (Klute, A., ed). Agronomy Series No. 9. Am. Soc. Agronomy, 2nd edition, pp. 493-544.
- Garré, S., Javaux, M., Vanderborght, J., Pagès, L. and Vereecken, H. (2011). Three-dimensional electrical resistivity tomography to monitor root zone water dynamics. *Vadose Zone J.*, 10, pp. 412-424.
- Giao, P. H., Chung, S. G., Kim, D. Y. and Tanaka, H. (2003). Electric imaging and laboratory resistivity testing for geotechnical investigation of Pusan clay deposits. *J. Appl. Geophys.* 52, pp. 157-175.
- Giao, P., Nguyen Cuong, Q. and Loke, M. H. (2011). Monitoring the chemical grouting in sandy soil by electrical resistivity tomography (ERT), *Berichte Geol. B.-A.*, 93, *International Workshop on Geoelectric Monitoring*, pp. 168-178.
- Glendinning, S., Rouainia, M., Hughes, H. and Davies O. (2006). Biological and engineering impacts of climate on slopes (BIONICS): The first 18 months. In: *Engineering geology for tomorrow's cities. Procs. 10th IAEG International Congress*, United Kingdom.
- Godio A. and Naldi M. (2003). Two-dimensional electrical imaging for detection of hydrocarbon contaminants. *Near Surface Geophys.* 1(3), pp. 131-137.
- Goyal, V. C., Gupta, P. K., Seth, P. K. and Singh, V.N. (1996). Estimation of temporal changes in soil moisture using resistivity method. *Hydrol. Process.* 10, pp. 1147-1154.
- Grellier, S., Guerin, R., Robain, H., Bobachev, A., Vermeersch, F. and Tabbagh, A. (2008). Monitoring of leachate recirculation in a bioreactor landfill by 2-D electrical resistivity imaging. *J. of Environmental and Engineering Geophysics*, 13 (4), pp. 351–359.

REFERENCES

- Greve, A. K. (2009). Detection of subsurface cracking depth through electrical resistivity anisotropy. Ph.D. Thesis, The University of New South Wales, Sydney, Australia.
- Greve, A. K. (2011). Monitoring water migration processes in cracking clay soil with depth profiles of square array resistivity measurements, Near Surface 2011 - the 17th European Meeting of Environmental and Engineering Geophysics.
- Greve, A., Acworth, R. I. and Kelly, B. F. J. (2010a). Detection of subsurface soil cracks by vertical anisotropy profiles of apparent electrical resistivity. *Geophysics* 75, WA85-93.
- Greve, A., Andersen, M. S., Acworth, R. I. (2010b). Investigations of soil cracking and preferential flow in a weighing lysimeter filled with cracking clay soil. *Journal of Hydrology*, 393 (1-2), 105-113.
- Greve, A. K., Acworth, R. I. and Kelly, B. F. J. (2011). 3D Cross-hole resistivity tomography to monitor water percolation during irrigation on cracking soil. *Soil Research*, 49, pp. 661-669.
- Greve, A. K., Andersen, M. S. and Acworth, R. I. (2012). Monitoring the transition from preferential to matrix flow in cracking clay soil through changes in electrical anisotropy. *Geoderma*, 179-180, pp. 46-52.
- Griffiths, D. H. and Barker, R. D. (1993). Two dimensional resistivity imaging and modelling in areas of complex geology. *J. of Applied Geophysics*. 29, pp. 211-226.
- Griffiths, D. H., Turnbull, J. and Olayinka, A. I. (1990). Two-dimensional resistivity mapping with a computer-controlled array. *First Break*, Vol. 8, no. 4, pp. 121-129.
- Gunn, D. A., Chambers, J. E., Uhlemann, S., Wilkinson, P. B., Meldrum, P. I., Dijkstra, T. A., Haslam, E., Kirkham, M., Wragg, J., Holyoake, S., Hughes, P.N., Hen-Jones, R. and Glendinning, S. (2014). Moisture monitoring in clay embankments using electrical resistivity tomography. *Construction and Building Materials*, pp. 1-13.
- Gunn, D. A., Haslam, E., Kirkham, M, Chambers J. E., Lacinska, A., Milodowski A., Reeves, H., Ghataora, G., Burrow M., Weston, P., Thomas. A., Dixon, N., Sellers, R. and Dijkstra, T. (2009). Moisture measurements in an end-tipped embankment: Application for studying long term stability and ageing. *Proc. 10th Int. Conf. Railway Engineering*, London
- Gunn, D. A., Ogilvy, R., Chambers, J. and Meldrum, P. (2010a). ALERT-ME New technologies for embankment warning systems. *Rail Technology Magazine*, Oct/Nov 2010, pp 80-82.

REFERENCES

- Gunn, D. A., Ogilvy, R., Chambers, J., Meldrum, P. Haslam, E., Holyoake, S. and Wragg, J. (2010b). The first trials of the British Geological Survey's new ALERT-ME system for monitoring embankments using resistivity imaging have thrown up some fascinating results. *Ground Engineering*, Sept 2010, pp. 12-14.
- Gunn, D. A, Reeves, H., Chambers, J. E., Ghataora, G., Burrow, M, Weston, P., Lovell, J. M., Tilden Smith, R., Nelder, L. M. and Ward, D. (2008). New geophysical and geotechnical approaches to characterise under utilised earthworks. In: Ed. Ellis, E., Yu, H.S., McDowell, G., Dawson, A. & Thom, N. *Advances in Transportation Geotechnics. Proc. 1st Int. Conf. Transportation Geotechnics*, Nottingham, Aug 2008, pp. 299-305.
- Gunn, D. A, Reeves, H., Chambers, J. E., Pearson, S. G., Haslam, E., Raines, M. R., Tragheim, D., Ghataora, G., Burrow, M, Weston, P., Thomas, A., Lovell, J. M., Tilden Smith, R. and Nelder, L. M. (2007). Assessment of embankment condition using combined geophysical and geotechnical surveys. *Proc. 9th Int. Conf. Railway Engineering*, London.
- Guo, X. J., Huang, X. y. and Jia, Y. G. (2005). Forward modelling of different types of landslides with multielectrode electric method. *Applied Geophysics*, Vol 2, No.1, pp.14-20.
- Gupta, S. C. and Hanks, R. J. (1972). Influence of water content on electrical conductivity of the soil. *Soil Sci. Soc. Am. Proc.*,36, pp. 855-857.
- Habberjam, G. M. and Watkins, G. E. (1967). The use of square configurations in resistivity prospecting. *Geophysical Prospecting*, 15 (3), pp. 445-467.
- Hassan, A. A. and Toll, D. G. (2014). Investigation of the directional dependence of soil resistivity in cracking clays. *Unsaturated Soils: Research & Applications-* Khalili, Russell & Khoshghalb (Eds.) London: Taylor & Francis Group, pp. 137-142.
- Hassan, A. and Toll, D. G. (2013). Electrical resistivity tomography for characterizing cracking of soils. *Geo-Congress 2013: Stability and performance of Slopes and Embankments*, Meehan, C., Pradel, D., Pando, M. and Labuz, J. F. (Eds.), California, American Society of Civil Engineers ASCE, pp. 818-827.
- Hauck, C. (2002). Frozen ground monitoring using DC resistivity tomography. *Geophys. Res. Lett.*, 29(21), pp. 20-16.
- Hayashi, M. (2004). Temperature-electrical conductivity relation of water for environmental monitoring and geophysical data inversion, *Environmental Monitoring and Assessment*, Vol.96, pp. 119-128.

REFERENCES

- Heaney, B. M. (2003). Electrical Conductivity and resistivity, in *Electrical Measurement, Signal Processing, and Displays*, John. G. Webster, Ed., CRC, Press, Boca Raton, FL 2003, ch 7, pp. 1-14.
- Hen-Jones, R. M., Hughes P. N., Glendinning, S., Gunn, D. A., Chambers, J. C., Wilkinson, P. B. and Uhlemann, S. (2014). Determination of moisture content and soil suction in engineered fills using electrical resistivity. *Unsaturated Soils: Research and applications*- Khalili, Russell and Khoshghalb London: Taylor & Francis Group.
- Herman, R. (2001). An introduction to electrical resistivity in geophysics. *American Journal of Physics*, 69, pp. 943-952.
- Hughes, P., Glendinning, S. and Davies, O. (2008). Construction and monitoring of a test embankment for the evaluation of the impacts of climate change on UK transport infrastructure, Proceedings 1st International Conference Advances in Transportation Geotechnics. Nottingham. London: Taylor and Francis Group.
- Hughes, P. N., Glendinning, S., Mendes, J., Parkin, G., Toll, D. G., Gallipoli, D., and Miller, P. E. (2009). Full-scale testing to assess climate effects on embankments. *Proceedings of the Institution of Civil Engineers- Engineering Sustainability*, 162, pp 67-79.
- Huisman, J. A., Hubbard, S. S., Redman, J. D. and Annan, A. P. (2003). Measuring soil water content with ground penetrating radar: A review. *Vadose Zone J.* 2, pp. 476-491.
- Huisman, J.A., Lambot, S. and Vereecken, H. (2006). Determining soil water content variation along the TDR probe with inverse modelling: Theory, practice, and challenges, Proc.TDR, Purdue University, West Lafayette, USA, Sept. 2006, Paper ID 28, 10 p., <https://engineering.purdue.edu/TDR/Papers>.
- Hymer, D. C., Moran, M. S. and Keefer. T.O. (2000). Soil water evaluation using a hydrologic model and calibrated sensor network. *Soil Sci. Soc. Am. J.*, 64, pp.319-326.
- Igboama W. N. and Ugwu N. U. (2011) Fabrication of resistivity meter and its evaluation. *American, Am. J. Sci. Ind. Res.*, 2(5), pp. 713-717.
- Inci, G. (2008). Numerical modelling of desiccation cracking in compacted Soils. *Proceeding of the 12th International Conference of International Association for Computer Methods and Advances in Geomechanics (IACMAG)*, 1-6 October, Goa, India.
- IPCC (2007) Summary for policymakers. In: *Climate change (2007). The physical science basis. Contribution of working group I to the fourth assessment report of the intergovernmental panel on climate change*, Solomon, S., Qin, D., Manning, M., Chen,

REFERENCES

- Z., Marquis, M., Averyt, K.B., Tignor, M. and Miller, H.L. (eds.). Cambridge University Press, Cambridge, United Kingdom and New York, NY, USA.
- Jackson, P. D., Northmore, K. J., Meldrum, P. I., Gunn, D. A., Hallam, J. R., Wambura, J., Wangusi, B. and Ogutu, G. (2002). Non-invasive moisture monitoring within an earth embankment- a precursor to failure. *NDT and E Int.*, 35, pp. 107-115.
- JCGM 200 (2008). International vocabulary of metrology- Basic and general concepts and associated terms, Joint Committee for Guides in Metrology (JCGM/WG 2).
- Jinguuji, M. (2011). Development of multi-transmission high speed survey system and the application of geyser monitoring. International Workshop within the frame of the FWF project TEMPEL (TRP 175-N21) and the 7th FP European project SafeL and November 30th - December 2nd, Vienna Berichte Geol. B.-A., 93, ISSN 1017-8880 ,Instrumentation and Data Acquisition Technology.
- Johnston, J. and Hill. H. (1944). A study of the shrinking and swelling properties of Rendzina soils: *Soil Science Society of America Proceedings*, 9, pp. 24–29.
- Jones, S. B., Wraith, J. M. and Or, D. (2002). Time domain reflectometry measurement principles and applications. *Hydrol. Process.* 16, pp. 141–153.
- Jones, G., Sentenac, P. and Zielinski, M. (2014). Desiccation cracking detection using 2-D and 3-D Electrical Resistivity Tomography: Validation on a flood embankment. *Journal of Applied Geophysics* 106, pp. 196-211.
- Jones, G., Zielinski, M. and Sentenac, P. (2012). Mapping desiccation fissures using 3-D electrical resistivity tomography. *Journal of Applied Geophysics*, 84, pp. 39-51.
- Jones, S. B. and Or, D. (2004). Frequency domain analysis for extending time domain reflectometry water content measurement in highly saline soils. *Soil Sci. Soc. Am. J.*, 68, pp.1568-1577.
- Kalinski, M. E. and Vemuri, S. C. (2005). A geophysical approach to construction quality assurance testing of compacted soil using electrical conductivity measurements, earthquake engineering and soil dynamics (GSP 133), *Proceedings of the Sessions of the Geo-Frontiers Congress*, Jan 24–26, Austin, TX, USA.
- Kalinski, R. J. and Kelly, W. E. (1993). Estimating water content of soils from electrical resistivity, *Geotech. Test. J.*, (16), pp. 323-329.

REFERENCES

- Kalinski, R. and Kelly, W. (1994). Electrical-resistivity measurements for evaluating compacted-soil liners. *J. Geotech. Engrg.*, 120(2), pp. 451-457.
- Keller, G. V. and Frischknecht, F.C. (1966). Electrical methods in geophysical prospecting. New York: Pergamon Press.
- Kibria, G. and Hossain, M. (2012). Investigation of geotechnical parameters affecting electrical resistivity of compacted clays. *J. Geotech. Geoenviron. Eng.*, 138(12), pp. 1520-1529.
- Kim, J., Yoon, H. and Lee, J. (2011). Void ratio estimation of soft soils using electrical resistivity cone probe. *J. Geotech. Geoenviron. Eng.*, 137(1), pp. 86-93.
- Kishne, A., Morgan, C. and Miller, W. (2009). Vertisol crack extent associated with gilgai and soil moisture in the Texas Gulf Coast prairie: *Soil Science Society of America J.*, 73, pp. 1221–1230.
- Knight, R. (1991). Hysteresis in the electrical resistivity of partially saturated sandstones. *Geophysics*, Vol 56 (12), pp. 2139-2147.
- Kodikara, J., Barbour, S. L. and Fredlund, D. G. (1999). Changes in clay structure and behaviour due to wetting and drying. *In 8th Australian-New Zealand Conference on Geomechanics*, Australian Geomechanics, Hobart: Australia. pp. 179-186.
- Kodikara, J. K., Barbour, S. L. and Fredlund, D. G. (2000). Desiccation cracking of soil layers, *Proceedings of Asian Conference on Unsaturated Soils: From Theory to Practice*, Singapore, pp. 693-698.
- Kong, L. W, Bai, W. and Guo, A. G. (2012). Effects of cracks on the electrical conductivity of a fissured laterite: A combined experimental and statistical study. *Geotechnical Testing Journal*, 35(6), pp. 1-9.
- Konrad, R., Ayad, J. M. (1997). Dessication of a sensitive clay: field experimental observations. *Canadian Geotechnical Journal*, 34, pp. 929-942.
- Korteland, S. (2013). Quantitative characterization of solute transport processes in the laboratory using electrical resistivity tomography. Ph.D. dissertation, Technical University of Delft, Germany.
- Kuras, O., Pritchard, J. D., Meldrum, P. I., Chambers, J. E., Wilkinson, P. B., Ogilvy, R. D. and Wealthall, G. P. (2009). Monitoring hydraulic processes with automated time-lapse

REFERENCES

- electrical resistivity tomography (ALERT). *Comptes Rendus Geoscience*, 341 (10-11). pp. 868-885.
- LaBrecque, D. and Daily, W. (2008). Assessment of measurement errors for galvanic-resistivity electrodes of different composition. *Geophysics*, 73, F55 – F64.
- LaBrecque, D.J., Sharpe, R., Wood, T. and Heath, G. (2004). Small-scale electrical resistivity tomography of wet fractured rocks. *Ground Water*, 42(1), pp. 111-118.
- Lachhab, A. and Booterbaugh, A. P. (2011). A fabricated resistivity apparatus used with other geophysical methods to explore buried structure on the bench and in the field. *Fortimes*, Vol16, no., 4, Success with Geophysics: Integrated Geophysical Investigation.
- Lambe, T. W. and Whitman, R. V. (1969). *Soil Mechanics*. New York: John Wiley & Sons.
- Lane, J. W., Haeni, F. P. and Watson, W. M. (1995). Use of a square-array direct current resistivity, method to detect fractures in crystalline Bedrock in New Hampshire. *Ground Water*, 33, pp. 476-485.
- Lataste, J. F., Sirieix, C., Breyse, D. and Frappa, M. (2003). Electrical resistivity measurement applied to cracking assessment on reinforced concrete structures in civil engineering. *NDT & E International*, (36), pp. 383-394.
- Leontarakis, K. and Apostolopoulos, G. V. (2012). Laboratory study of the cross-hole resistivity tomography: The Model Stacking (MOST) Technique. *Journal of Applied Geophysics*, 80, pp. 67–82
- Likos, W. J. and Lu, N. (2004). Hysteresis of capillary stress in unsaturated granular soil, *J. Eng. Mech.* 130, 6, pp. 646-656
- Liu, S. and Yeh, T.–C. J. (2004). An integrative approach for monitoring water movement in the vadose zone: *Vadose Zone Journal*, 3, pp. 681-692.
- Loke, M. H. (2014). Tutorial: 2-D and 3-D electrical imaging surveys.
<http://www.geotomosoft.com/coursenotes.zip>
- Loke, M. H. and Barker, R. D. (1996a). Rapid least-squares inversion of apparent resistivity pseudosections by a quasi-Newton method. *Geophysical Prospecting*, 44, pp. 131-152.
- Loke, M. H. and Barker, R. D. (1996b). Practical techniques for 3D resistivity surveys and data inversion. *Geophysical Prospecting*, 44, pp. 499-524.

REFERENCES

- Loke, M. H., Chambers, J. E. and Kuras, O. (2011). Instrumentation, electrical resistivity, Solid Earth Geophysics Encyclopedia (2nd edition.), Electrical & Electromagnetic, H. Gupta (Ed.), Springer, Berlin, pp. 599-604.
- Loke, M. H., Chambers, J. E., Rucker, D. F., Kuras, O. and Wilkinson, P. B. (2013). Recent developments in the direct-current geoelectrical imaging method, *Journal of Applied Geophysics*, 95, pp. 135-156.
- Long, M., Donohue, S., L'Heureux, J. -S., Solberg, I. -L., Rønning, J. S., Limacher, R., O'Connor, P., Sauvin, G., Rømoen, M. and Lecomte, I. (2012). Relationship between electrical resistivity and basic geotechnical parameters for marine clays. *Canadian Geotechnical Journal* 49 (10), pp. 1158-1168.
- Lourenço, S. D .N. (2008). Suction measurements and water retention in unsaturated soils, PhD thesis, Durham University, Available online: <http://etheses.dur.ac.uk/1331/>
- Lunt, I. A., Hubbard, S. S. and Rubin, Y. (2005). Soil moisture content estimation using ground-penetrating radar reflection data. *Journal of Hydrology*, 307(1-4), pp. 254–269.
- Ma, R., McBratney, A., Whelan, B., Minasny, B. and Short, M. (2011). Comparing temperature correction models for soil electrical conductivity measurement. *Precision Agriculture*, 12, pp.55-66.
- Mansoor, N. and Slater, L. (2007). Aquatic electrical resistivity imaging of shallow-water wetlands. *Geophysics*, 72, F211-F221.
- Marescot, L. Rigobert, S., Palma Lopes, S., Lagabrielle, R. and Chapellier, D. (2006). A general approach for DC apparent resistivity evaluation on arbitrarily shaped 3D structures. *Journal of Applied Geophysics*, 60(1), pp. 55-67.
- Maryniak W. A., Uehara T. and Noras, M. A. (2003). Surface resistivity and surface resistance measurements using a concentric ring probe technique. TREK, INC. Trek Application Note Number 1005.
- Massoud, U., Qady, G. E., Metwaly, M. and Santos, F. (2009). Delineation of shallow subsurface structure by azimuthal resistivity sounding and joint inversion of VES-TEM data: case study near lake Quaroun, El Fayoum, Egypt. *Pure appl. geophys.* 166, pp. 701-719.
- McCarter, W. J. (1984). The electrical resistivity characteristics of compacted clays. *Geotechnique*, 34, pp. 263-267.

REFERENCES

- Meju, M. A. and Montague M. (1995). Basis for a flexible low-cost automated resistivity data acquisition and analysis system. *Comput. Geosci.*, Vol. 21, No. 8, pp. 993-999
- Mendes, J. (2011). Assessment of the impact of climate change on an instrumented embankment: an unsaturated soil mechanics approach, Ph.D. thesis, Durham University. Available online: <http://etheses.dur.ac.uk/612/>
- Michot, D., Benderitter, Y., Dorigny, A., Nicoullaud, B., King, D. and Tabbagh, A. (2003). Spatial and temporal monitoring of soil water content with an irrigated corn crop cover using surface electrical resistivity tomography, *Water Resour. Res.*, 39 (5), pp. 14-1-14-20.
- Miller, C. R., Routh, P. S., Brosten, T.R. and McNamare, J. P. (2008). Application of time-lapse ERT imaging to watershed characterization. *Geophysics*, 73, pp. G7-G17.
- Millero, F. J. (2001). The physical chemistry of natural waters, New York: Wiley-Interscience.
- Mitchell, J. K., Hooper, D. R. and Campanella, R. G. (1965). Permeability of compacted clay. *J. Soil Mech. and Found. Engrg. Div., ASCE*, 91(4), pp. 41-65.
- Mualem, Y. and Friedman, S. P. (1991). Theoretical prediction of electrical conductivity in saturated and unsaturated soil. *Water Resour. Res.* 27 (10), pp. 2771-2777.
- Muñoz-Carpena, R. (2002). Field devices for monitoring soil water content. Bulletin 343, Florida Cooperative Extension Service, Institute of Food and Agricultural Sciences, University of Florida, [Online], <http://edis.ifas.ufl.edu/pdf/FILES/AE/AE26600.pdf>, Accessed 15/08/2014.
- Muñoz-Carpena, R., Shukla, S. and Morgan, K. (2006). Field devices for monitoring soil water content. Regional Extension Bulletin no. SR-IWM-2. The Irrigation Water Management Program Team of the Southern Regional Water Program. USDA-CSREES.
- Muñoz-Castelblanco, J. A., Delage, P., Pereira, J. M. and Cui, Y.J., (2012). On-sample water content measurement for a complete local monitoring in triaxial testing of unsaturated soils. *Geotechnique*, 62(7): pp. 595-604.
- Muñoz-Castelblanco, J. A., Delage, P., Pereira, J. M. and Cui, Y. J. (2014). New triaxial device for unsaturated soils with local measurements. *Unsaturated Soils: Research and applications*- Khalili, Russell and Khoshghalb Taylor & Francis Group, London, pp.1617-1622.

REFERENCES

- Muñoz-Castelblanco, J. A., Pereira, J. M., Delage, P. and Cui, Y. J., (2011). The influence of changes in water content on the electrical resistivity of a natural unsaturated Loess. *Geotechnical Testing Journal*, 35 (1), pp. 11-17.
- Mwenifumbo, C. J. (1997). Electrical methods for ore body delineation, *Proceedings of Exploration 97: Fourth Decennial International Conference on Mineral Exploration*, A.G. Gubbins (edt.), pp. 667-676.
- Nguyen, F., Garambois, S., Jongmans, D., Pirard, E. and Loke, M. H. (2005). Image processing of 2D resistivity data for imaging faults. *J Appl. Geophys.* 57, pp. 260-277.
- Niininen, H. and Kehla, V. (1979). Construction of a wide-range specific resistivity meter with logarithmic output. *J.Phys. E: Sci. Instrum.*, 12, pp. 261-263.
- Nijland W., der Meijde, M. V., Addink, E. A. and de Jong, S. M. (2010). Detection of soil moisture and vegetation water abstraction in a Mediterranean natural area using electrical resistivity tomography. *Catena* 81, pp. 209-216.
- Nimmer, R. E., Osiensky, J. L., Binley, A. M., Sprenke, K. F. and Williams, B. C. (2007). Electrical resistivity imaging of conductive plume dilution in fractured rock, *Hydrogeology Journal*, Vol15, pp. 877-890.
- Noel, M. and Xu, B. (1991). Archaeological investigation by electrical resistivity tomography: A preliminary studies. *Geophys. J. Inter.*, 107, pp. 95-102.
- Ogilvy, R. D., Meldrum, P. I., Kuras, O., Wilkinson, P. B., Chambers, J. E., Sen, M., Pulido-Bosch, A., Gisbert, J., Jorreto, S., Frances, I. and Tsourlos, P. (2009). Automated monitoring of coastal aquifers with electrical resistivity tomography. *Near Surface Geophysics* 7 (5-6), pp. 367-375.
- Olayinka, A. and Yaramanci, U. (2000). Assessment of the reliability of 2D inversion of apparent resistivity data. *Geophysical Prospecting*, 48, pp. 293-316.
- Olowofela, J.A. Jolaosho, V.O. and Badmus, B.S. (2005). Measuring the electrical resistivity of the earth using a fabricated resistivity meter, *European Journal of Physics* 26, pp. 501-515.
- Overmeeren, R. A. and van Ritsema, I. L. (1988). Continuous vertical electrical sounding. *First Break*, 6 (10), pp. 313-324.

REFERENCES

- Ozcep, F., Tezel, O. and Asci, M. (2009). Correlation between electrical resistivity and soil water content: Istanbul and Golcuk. *International Journal of Physical Sciences*, Vol. 4 (6), pp. 362-365.
- Panissod, C., Dabas, M., Hesse, A., Joivet, A., Tabbagh, J. and Tabbagh, A. (1998). Recent developments in shallow depth electrical and electrostatic prospecting using mobile arrays. *Geophysics*, 63 (5), pp. 1542-1550.
- Parasnis, D.S. (1988). Reciprocity theorems in geoelectric and geoelectromagnetic work. *Geoexploration*, 25 (3), pp. 177-198.
- Peixoto, A. S. P., Pregolato, M. C., Silva, A. C. L., Yamasaki, M. T. and Conte Junior, F. (2010). Development of an electrical resistivity measure for geotechnical and geoenvironmental characterization. *Proceedings of CPT'10*. Huntington Beach, CA, USA, pp. 1-7.
- Pellerin, L. (2002). Applications of electrical and electromagnetic methods for environmental and geotechnical investigations. *Surveys in Geophysics*, 23, pp. 101-132.
- Petersen, T. and Al Hagry, S. A. (2009). Mapping root zones of small plants using surface and borehole resistivity tomography. *Leading Edge*, 28(10), pp. 1220-1224.
- Plooy, R. d., Palma Lopes, S., Villain, G. and De´robert, X. (2013). Development of a multi-ring resistivity cell and multi-electrode resistivity probe for investigation of cover concrete condition. *NDT&E International* 54, pp. 27-36.
- Polydorides, N. (2002). Image Reconstruction algorithms for soft-field tomography, Ph.D. dissertation, University of Manchester, Manchester, United Kingdom.
- Powrie, W. (2009). Soil Mechanics, concepts and applications, 2nd edition, Taylor & Francis e-Library.
- Pozdnyakov, A., Pozdnyakova, L. and Karpachevskii, L. (2006). Relationship between water tension and electrical resistivity in soils. *Eurasian Soil Sci.* 39 (1), pp. 78-83.
- Pozdnyakova, L. A. (1999), Electrical properties of soil. Ph.D. Dissertation. University of Wyoming, College of Agriculture, Laramie, WY.
- Raju N. J. and Reddy, T. V. K. (1998). Fracture pattern and electrical resistivity studies for groundwater exploration. *Environ Geol.* 34, pp. 175-182.
- Reynolds, J. M. (1997). An introduction to applied and environmental geophysics. Chichester: John Wiley & Sons.

REFERENCES

- Rhoades, J. D., Raats, P. A. C. and Prather, R. J. (1976). Effect of liquid phase electrical conductivity, water content, and surface conductivity on bulk soil electrical conductivity. *Soil Sci. Soci. Am.J.* 40, pp. 651-655
- Rinaldi, V.A. and Cuestas, G. A. (2002). Ohmic conductivity of a compacted silty clay. *J. Geotech. Geoenviron. Eng.*,128(10), pp. 824-835.
- Ringrose-Voase, A. and Sanidad, W. (1996). A method for measuring the development of surface cracks in soils: Application to crack development after lowland rice, *Geoderma*, 71, pp. 245-261.
- Robain H., Bellier G., Camerlynck C. and Vergnaut D. (2001). Relation between water content and resistivity, importance of particle size characteristics, mineralogical and rheological soil. *Proceedings of the Third Conference of GEOFCAN, Paris, France*, pp.101-105.
- Robert, T., Dassargues, A., Brouyère, S., Kaufmann, O., Hallet, V. and Nguyen, F. (2011). Assessing the contribution of electrical resistivity tomography (ERT) and self-potential (SP) methods for a water well drilling program in fractured/karstified limestones, *Journal of Applied Geophysics*, Vol 75, pp. 42-53.
- Robinson, D. A., Campbell, C. S., Hopmans, J. W., Hornbuckle, B. K., Jones, S. B., Knight, R., Ogden, F., Selker, J. and Wendroth, O. (2008), Soil moisture measurement for ecological and hydrological watershed scale observatories: A review, *Vadose Zone J.*, 7, pp. 358-389.
- Robinson, D. A., Jones, S. B., Wraith, J. A., Or, D. and Friedman, S. P. (2003). A review of advances in dielectric and electrical conductivity measurement in soils using time domain reflectometry. *Vadose Zone J.* 2, pp. 444-475.
- Robinson, D. A., Lebron, I., Kocar, B., Phan, K., Sampson, M., Crook, A. N. and Fendorf, S. (2009). Time-lapse geophysical imaging of soil moisture dynamics in tropical deltaic soils: An aid to interpreting hydrological and geochemical processes. *Water Resour. Res.* 45:W00D32.
- Romero, E. and Vaunat, J. (2000). Retention curves of deformable clays. *Proc. International Workshop On Unsaturated Soils: Experimental Evidence And Theoretical Approaches*, Balkema, PP. 91-106.
- Rugh, D. and Burbey, T. (2008). Using saline tracers to evaluate preferential recharge in fractured rocks, Floyd County, Virginia, USA. *Hydrogeology J.* 16(2), pp. 251-262.

REFERENCES

- Russell, E. J. F. and Barker R. D. (2010). Electrical properties of clay in relation to moisture loss, *Near Surface Geophysics*, 8, pp. 173-180.
- Samouëlian, A., Cousin, I., Richard, G., Tabbagh, A. and Bruand, A. (2003a). Electrical resistivity imaging for detecting soil cracking at the centimetric scale. *Soil Sci. Soc. J. Am.* 67, pp. 1319-1326.
- Samouëlian, A., Cousin, I., Tabbagh, A., Bruand, A. and Richard, G. (2005). Electrical resistivity survey in soil science: A review, *Soil Tillage Res.*,83, pp. 173- 193.
- Samouëlian, A., Richard, G., Cousin, I., Guérin, R., Bruand, A. and Tabbagh, A. (2004). Three-dimensional crack monitoring by electrical resistivity measurement. *Eur. J. Soil Sci.* 55, pp. 751–762.
- Samouëlian, A., Richard, G., Cousin, I., Tabbagh, A. and Bruand, A. (2003b). Can electrical resistivity tomography describe soil structure evolution?. *Presented at 16th Triennial Conference of the ISTRO*, Brisbane, AUS. <http://prodinra.inra.fr/record/252490>.
- Sánchez, M., Atique, A., Kim, S., Romero, E. and Zielinski, M. (2013). Study of desiccation cracks in soils using a 2D laser scanner, *Geo-Congress 2013*: pp. 804-807.
- Sass, O. (2005). Rock moisture measurements: Techniques, results, and implications for weathering, *Earth Surf. Processes Landforms*, 30, pp. 359-374.
- Sawazaki, M., Matsui, T. and Ueno, N. (2009). Laboratory investigation into control of soil compaction by resistivity. *The Nineteenth International Offshore and Polar Engineering Conference*, International Society of Offshore and Polar Engineers. June 21-26, pp 128-132.
- Schneider, G. W., De Ryck, S. M. and Ferre, P. A. (1993). The Application of automated high resolution DC resistivity in monitoring hydrogeological field experiments, *Proceedings of the symposium on the Application of Geophysics to Engineering and Environmental Problems (SAGEEP '93)* , San Diego, CA, pp. 145-162.
- Schwartz, B. F., Schreiber, M. E. and Yan T. (2008). Quantifying field-scale soil moisture using electrical resistivity imaging. *Journal of Hydrology* , 362, pp. 234-246.
- Seaton W. J., and Burbey T. J. (2002). Evaluation of two-dimensional resistivity methods in a fractured crystalline rock terrane. *Journal of Applied Geophysics*, 51, pp. 21-41.

REFERENCES

- Seladji, S., Cosenza, P., Tabbagh, A., Ranger, J. and Richard, G. (2010). The effect of compaction on soil electrical resistivity: a laboratory investigation. *European Journal of Soil Science*, 61, pp. 1043-1055.
- Sellers, R., Dixon, N., Dijkstra, T. A., Gunn, D. A., Chambers, J. E., Jackson, P. D. and Hughes, P. (2010). Electrical resistivity as a tool to identify areas of progressive failure within UK infrastructure embankments. In: *IAEG Congress 2010*, Auckland, New Zealand, 5-10 Sept 2010. EAGE.
- Sellers, R., Dixon, N., Dijkstra, T., Gunn, D., Chambers, J. and Jackson, P. (2012). Electrical resistivity tomography for earthwork condition appraisal. [poster]. Loughborough University- BGS.
- Sen, P. N., Godee, P. A. and Sibbit, A. (1988). Electrical conduction in clay bearing sandstones at low and high salinities. *J. Appl. Phys.*, 63 (10), pp. 4832-4840.
- Seneviratne, S. I., Corti, T., Edavin, . L., Hirschi, M., Jaeger, E. B., Lehner, I., Orlowsky, B. and Teuling, A. J. (2010). Investigating soil moisture climate interactions in a changing climate: A review. *Earth Sci. Rev.*, 99, pp. 125-161.
- Sentenac, P. and Zielinski, M. (2009). Clay fine fissuring monitoring using miniature geoelectrical resistivity arrays. *Environmental Geology*, 59, pp. 205-214
- Shah, P. H. and Singh, D. N. (2005). Generalized Archie's Law for estimation of soil electrical conductivity. *J. of ASTM Inter.*, 2 (5), pp. 1-20.
- Sharma, P. V. (1997). *Environmental and Engineering Geophysics*. Cambridge: Cambridge University Press.
- Shea, P. F. and Luthin, J. N. (1961). An investigation of the use of the four-electrode probe for measuring soil salinity in situ. *Soil Science*, 92(5), pp. 331-339.
- Sheffer, M. R., Reppert, P. M. and Howie, J. A. (2007). A laboratory apparatus for streaming potential and resistivity measurements on soil samples, *Review of Scientific Instruments* 78, 094502, pp.1-8.
- Sherrod, L., Sauck, W. and Werkema, D. D. (2012), A Low-Cost, in situ resistivity and temperature monitoring system. *Ground Water Monitoring & Remediation*, 32: pp. 31-39.

REFERENCES

- Sjödahl, P., Dahlin, T., Johansson, S. and Loke, M. H. (2008). Resistivity monitoring for leakage and internal erosion detection at Hällby embankment dam. *Journal of Applied Geophysics*, 65, pp. 155-164.
- Slater, L. D., Binley, A. and Brown, D. (1997). Electrical imaging of fractures using ground-water salinity change. *Ground Water*, 35, pp. 436-442.
- Slater, L., Binley, A. M., Daily, W. and Johnson, R. (2000). Cross-hole electrical imaging of a controlled saline tracer injection. *Journal of Applied Geophysics: Special Issue- Environmental Geophysics*, 44, pp. 85-102.
- Smethurst, J. A., Clarke, D. and Powrie, W. (2006). Seasonal changes in pore water pressure in a grass-covered cut slope in London Clay, *Géotechnique*, Vol. 56, No. 8, pp. 523-537.
- Sørensen, K. (1996). Pulled Array Continuous Profiling. *First Break*, 14 (3), pp. 85-90.
- Srayeddin, I. and Doussan, C. (2009). Estimation of the spatial variability of root water uptake of maize and sorghum at the field scale by electrical resistivity tomography. *Plant Soil* 319, pp. 185-207.
- Sreedeeep, S., Reshma, A. C. and Singh, D. N. (2005). Generalized relationship for determining soil electrical resistivity from its thermal resistivity. *Experimental Thermal and Fluid Science* 29, pp. 217-226.
- Sreedeeep, S., Reshma, A. C. and Singh, D.N. (2004). Measuring soil electrical resistivity using a resistivity box and a resistivity probe. *ASTM Geotechnical Testing Journal*, 27, pp. 411-415.
- Stacey, R. W, Li, K. and Horne, R. N. (2009). Investigation electrical impedance tomography as a technique for real-time saturation monitoring, *Society of Petroleum Engineers Journal*, 14, pp. 135-143.
- Stacey, R. W. (2006). Electrical impedance tomography; Technical Report SGP-TR-182; The Department of Petroleum Engineering, Stanford University: Stanford, CA, USA.
- Stummer, P., Maurer, H., Horstmeyer, H. and Green, A. G. (2002). Optimization of DC resistivity data acquisition: real-time experimental design and a new multielectrode system. *Geoscience and Remote Sensing*, Vol.40, No.12, pp. 2727-2735.
- Su, J. K., Yang, C. C., Wu, W. B. and Huang, R. (2002). Effect of moisture content on concrete resistivity measurement. *J. Chin Inst Eng*, 25(1), pp. 117-22.

REFERENCES

- Szalai, S. and Szarka, L. (2008). On the classification of surface geoelectric arrays. *Geophys. Prospect.* 56, pp. 159-175.
- Szalai, S., Kósa, I., Nagy, T. and Szarka, L. (2010). Geoelectric analogue modelling experiments to detect fissure directions in multidirectional fissure systems. *Acta Geodaetica et Geophysica Hungarica*. Vol 45. No. 2, pp. 137-147.
- Szczepanik, Z. and Rucki, Z. (2000). Frequency analysis of electrical impedance tomography system. *IEEE Trans. Instrum. Meas.*, Vol 49, No 4, pp. 844-51.
- Tabbagh, A., Dabas, M., Hesse, A. and Panissod, C. (2000). Soil resistivity: a non-invasive tool to map soil structure horizonation. *Geoderma* 97, pp. 393-404.
- Tang, C. -S, Shi, B., Liu, C., Suo, W. -B and Gao, L. (2011). Experimental characterization of shrinkage and desiccation cracking in thin clay layer. *Applied Clay Science*, Vol 52, Issue 1-2, pp.69-77.
- Taylor S. B. and Barker R. D. (2002). Resistivity of partially saturated Triassic Sandstone. *Geophysical Prospecting*, 50, pp. 603-613.
- Taylor, R. W. and Fleming, A.H. (1988). Characterizing jointed systems by azimuthal resistivity surveys. *Groundwater*, 26, pp. 464-474.
- Telford, W. M., Geldert., L. P. and Sheriff, R. E. (1990). Applied geophysics. Cambridge University Press., Cambridge, UK.
- Toll, D. G. (1999). A data acquisition and control system for geotechnical testing, Computing developments in civil and structural engineering (eds.B. Kumar and B.H.V. Topping), Edinburgh: Civil-Comp Press, pp. 237-242.
- Toll, D. G. and Hassan, A. (2014). Data acquisition and control software for automated resistivity measurements, 2nd International Conference on Information Technology in Geo-Engineering ICITG, D. G. Toll et al. (Eds.), IOS Press, pp. 170-176.
- Toll, D. G., Hassan A. A., King J. M. and Asquith, J. D. (2013). New devices for water content measurement. *Proceedings of the 18th International Conference on Soil Mechanics and Geotechnical Engineering*, Paris. France, pp. 1199-1202.
- Toll, D. G., Lourenço, S. D. N., Mendes, J., Gallipoli, D., Evans, F. D., Augarde, C. E., Cui, Y. J., Tang, A. M., Rojas, J. C., Pagano, L., Mancuso, C., Zingariello, C. and Tarantino, A. (2011) Soil suction monitoring for landslides and slopes. *Quarterly Journal of Engineering Geology and Hydrogeology* (44(1), pp. 23-33.

REFERENCES

- Toll, D. G., Mendes, J., Gallipoli, D., Glendinning, S. and Hughes, P. N. (2012a). Investigating the impacts of climate change on slopes: field measurements. Geological Society, London, *Engineering Geology Special Publications*, 26, pp. 151-161.
- Toll, D. G., Mendes, J., Hughes, P. N., Glendinning, S. and D. Gallipoli, D. (2012b). Climate change and the role of unsaturated soil mechanics. *Geotechnical Engineering - Journal of the SEAGS & AGSSEA*, Vol. 43 No.1, pp. 76-82.
- Toll, D. G., Mendes, J., Karthikeyan, M., Gallipoli, D., Augarde, C. E., Phoon, K. K. and Lin, K. Q. (2008). Effects of climate change on slopes for transportation infrastructure, *1st ISSMGE International Conference on Transportation Geotechnics*, Nottingham, UK, September 2008.
- Topp, G. C., Davis, J. L., and Annan, A. P. (1980). Electromagnetic determination of soil water content: Measurements in coaxial transmission lines. *Water Resour. Res.* 16, pp. 574–582.
- Tsourlos P. (1995). Modelling interpretation and inversion of multielectrode resistivity survey data, Ph.D. thesis, University of York.
- Tsourlos, P. (2004). Inversion of electrical resistivity tomography data deriving from 3D structures. *Proceedings of the 10th International Congress*, Thessaloniki, Greece, pp. 1289-1297.
- Turesson A. (2006). Water content and porosity estimated from ground-penetrating radar and resistivity. *Journal of Applied Geophysics*, 58, pp. 99-111.
- United States Corps of Engineers (1995). Engineering and design, geophysical exploration for engineering and environmental investigations. Engineering Manual, US Army Corps of Engineers, EM 1110-1-1802, Washington D.C.
- Van Weereld, J. J. A., Player M. A., Collie, D. A .L, Watkins, A. P. and Olsen, D. (2001). Flow imaging in core samples by electrical impedance tomography, SCA Society of Core Analysts.
- Velde, B., Moreau, E. and Terrible, F. (1996). Pore networks in an Italian Vertisol: Quantitative characterization by two dimensional image analysis. *Geoderma* 72: pp. 271-285.
- Vereecken, H., Huisman, J. A, Bogena, H., Vanderborght, J., Vrugt, J. A. and Hopmans J. W. (2008). On the value of soil moisture measurements in Vadose Zone hydrology: A review, *Water resources research*, vol. 44, W00D06.

REFERENCES

- VERTEK (2013) Geotechnical and Environmental products [Online], http://cdn2.hubspot.net/hub/295051/file-396518913-pdf/Vertek_Geotechnical_and_Environmental_Catalog.pdf?t=1407867417165, accessed 15/08/2014.
- Vogel, H. J., Hoffmann, H. and Roth, K. (2005). Studies of crack dynamics in clay soil, Experimental methods, results and morphological quantification, *Geoderma*, pp.125, 203-211.
- Walker, J. P. and Houser, P. R. (2002). Evaluation of the OhmMapper instrument for soil moisture measurement. *Soil Sci. Soc. Am. J.*, 66, pp. 728–734.
- Werban, U., Al Hagrey, S. and Rabbel, W. (2008). Monitoring of root-zone water content in the laboratory by 2D geoelectrical tomography. *J. of Plant Nutrition and Soil Science*, 171, pp. 927–935.
- Werkema, D. D. (2000). A generic automated and semi-automated digital multielectrode instrument for field resistivity measurements: *IEEE Transactions on Instrument and Measurement*, 49, pp. 1249-1253.
- Werkema, D. D., Atekwana, E. A., Sauck, W. A. and Asumadu, J. (1998). A versatile window based multi-electrode acquisition system for dc electrical methods surveys: *Environmental Geosciences*, 5, pp. 196-206.
- Western, A. W., Grayson, R. B. and Blöschl, G. (2002). Scaling of soil moisture: A hydrologic perspective, *Annu. Rev. Earth Planet. Sci.*, 30, pp. 149-180.
- Wilkinson, P. B., Loke, M. H., Meldrum, P. I., Chambers, J. E., Kuras, O., Gunn, D. A. and Ogilvy, R. D. (2012). Practical aspects of applied optimized survey design for electrical resistivity tomography, *Geophysical Journal International* 189 (1), pp. 428-440.
- Wiwattanachang, N. and Giao, P. H. (2012). Monitoring crack development in fiber concrete beam by using electrical resistivity imaging. *Journal of Applied Geophysics* 75 (2011) pp. 294-304.
- Xu, B. and Noel, M. (1993). On the completeness of data sets with multi-electrode systems for electrical resistivity survey. *Geophysical Prospecting*, 41, pp. 791-801.
- Yan, M., Miao, L. and Cui, Y. (2012). Electrical resistivity features of compacted expansive soils, *Marine Georesources and Geotechnology*, 30, pp. 167-179.

REFERENCES

- Yang, X. and Lagmanson, M. B. (2003). Planning resistivity surveys using numerical simulations. *Proceedings of the Annual Symposium for the Application of Geophysics to Environmental and Engineering Problems*, San Antonio, Texas: Environmental and Engineering Geophysical Society, pp. 488-501.
- Zha, F. S., Liu, S. Y. and Du, Y. J. (2006). Evaluation of swell- shrinkage properties of compacted expansive soils using electrical resistivity method. *Advances in Unsaturated Soil, Seepage, and Environmental Geotechnics*: pp. 143-151.
- Zha, F., Liu, S., Du, Y., Cui, K. and Xu, L. (2010). Characterization of compacted loess by electrical resistivity method. *Soil Behavior and Geo-Micromechanics, GeoShanghai 2010*, pp. 68-73.
- Zhang, D. W., Chen, L. and Liu, S. Y. (2012). Key parameters controlling electrical resistivity and strength of cement treated soils. *Journal of Central South University*, 19, pp. 2991-2998.
- Zhou, M., Wang, J. and Liu, F. (2013). Proposal of new temperature correction models for soil electrical resistivity. *11th IEEE International Conference on Solid Dielectrics* - June 30th - July 4th, Bologna, Italy.
- Zhou, Q. Y., Shimada, J. and Sato, A. (2001). Three-dimensional spatial and temporal monitoring of soil water content using electrical resistivity tomography. *Water Resour. Res.* 37, pp.273-285.
- Zhu, J. J., Kang, H. Z. and Gonda, Y. (2007). Application of Wenner configuration to estimate soil water content in pine plantations on sandy land. *Pedosphere*, 17(6): pp. 801-812.
- Zohdy A. A. R. (1989). A new method for the automatic interpretation of Schlumberger and Wenner sounding curves. *Geophysics*, Vol. 54, No 2, pp. 245-253.

Appendix A

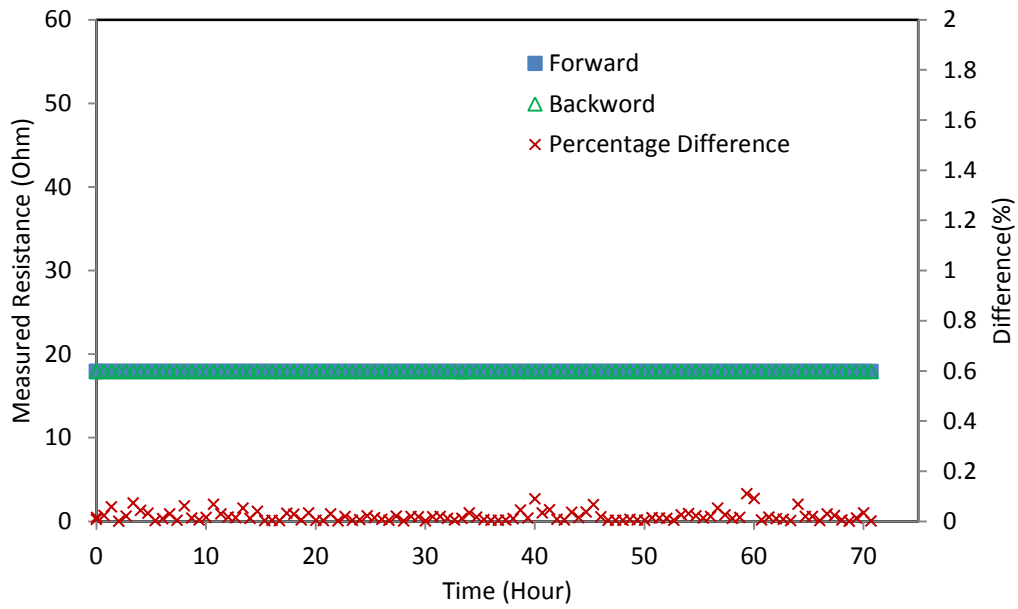


Figure A.1. The forward and backward readings of the 18 Ohm resistor test

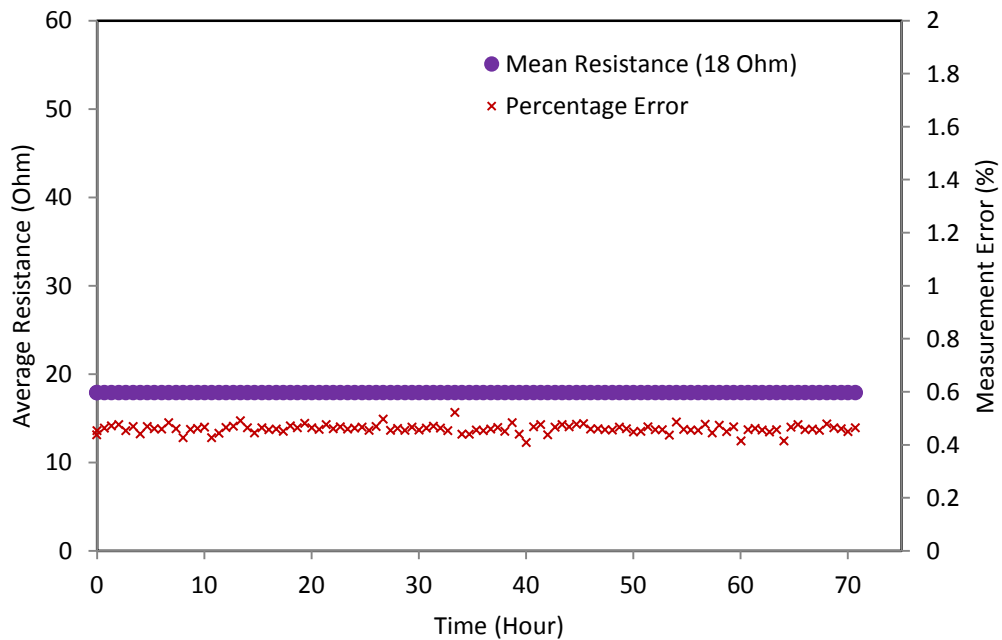


Figure A.2. The mean resistance and measurement error of 18 Ohm resistor test

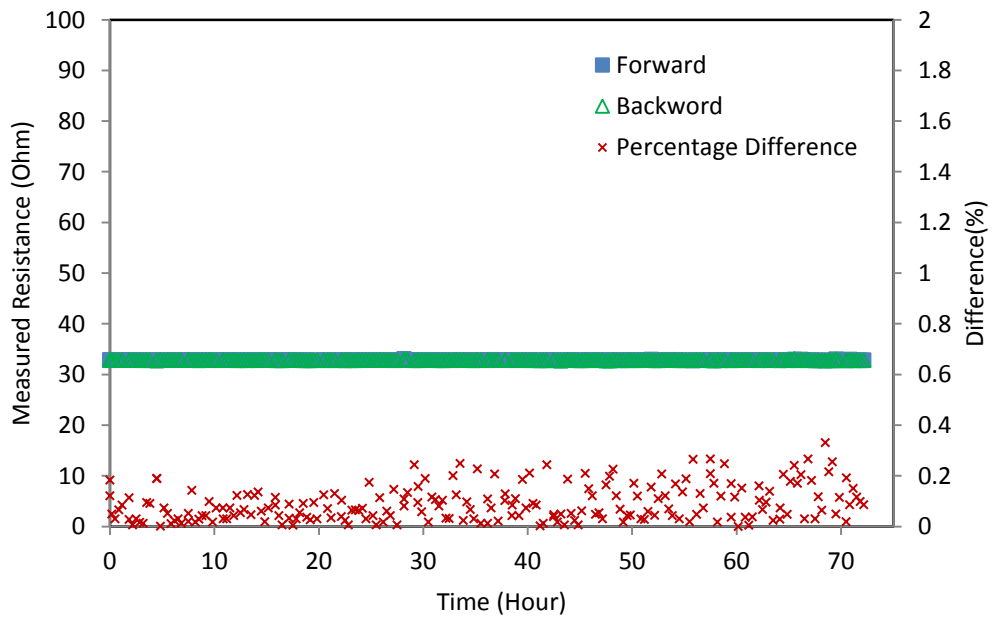


Figure A.3. The forward and backward readings of the 33 Ohm resistor test

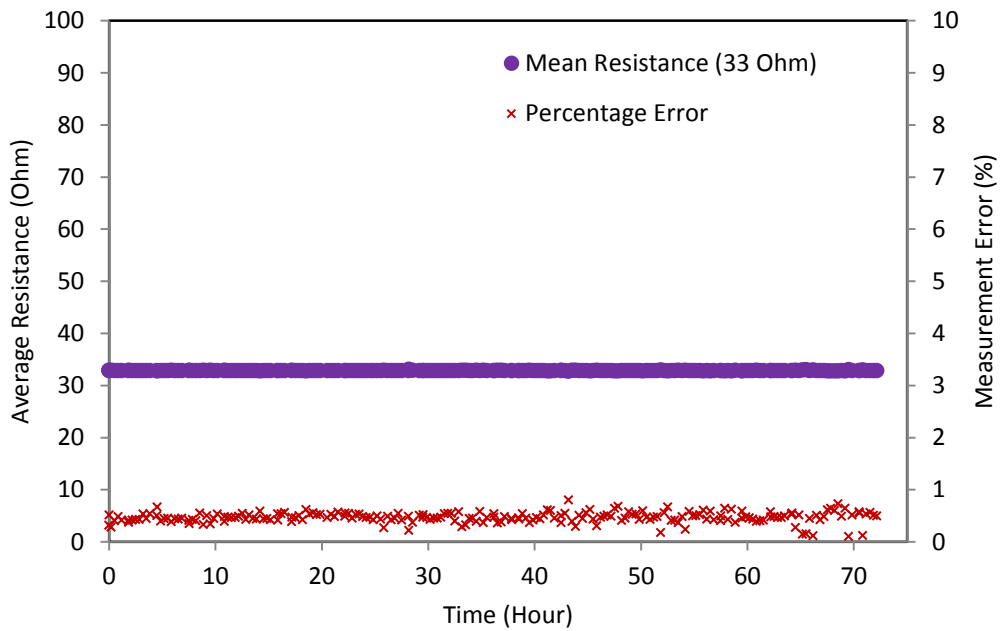


Figure A.4. The mean resistance and measurement error of the 33 Ohm resistor test

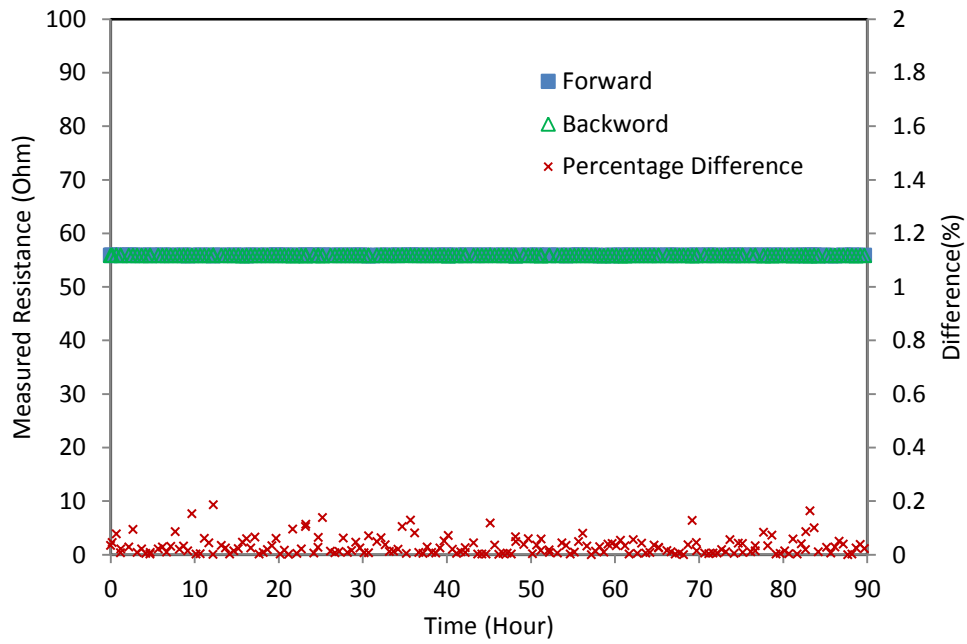


Figure A.5. The forward and backward readings of the 56 Ohm resistor test

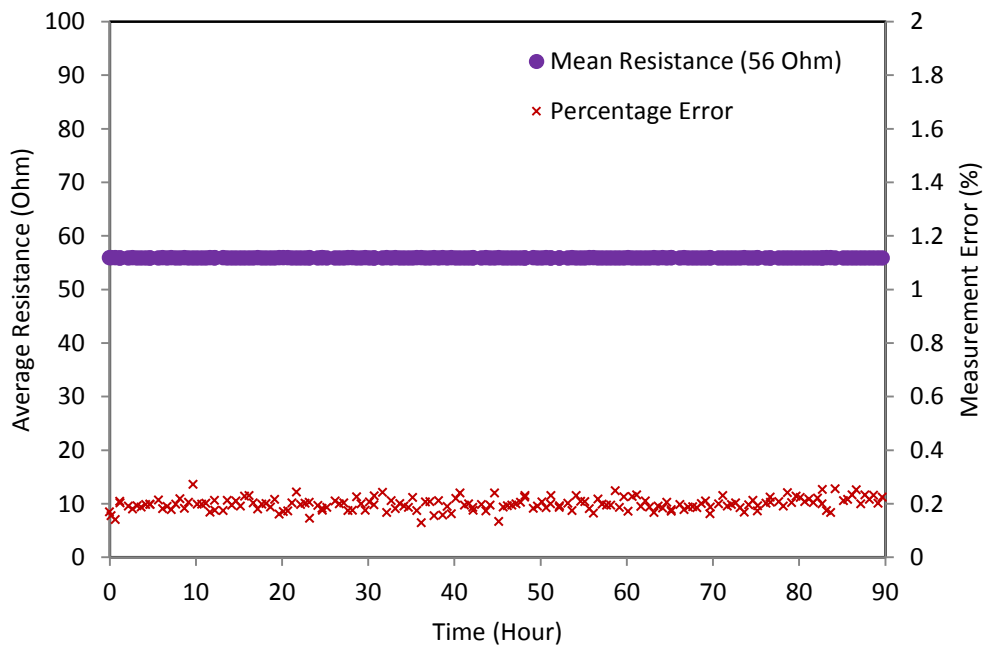


Figure A.6. The mean resistance and measurement error of the 56 Ohm resistor test

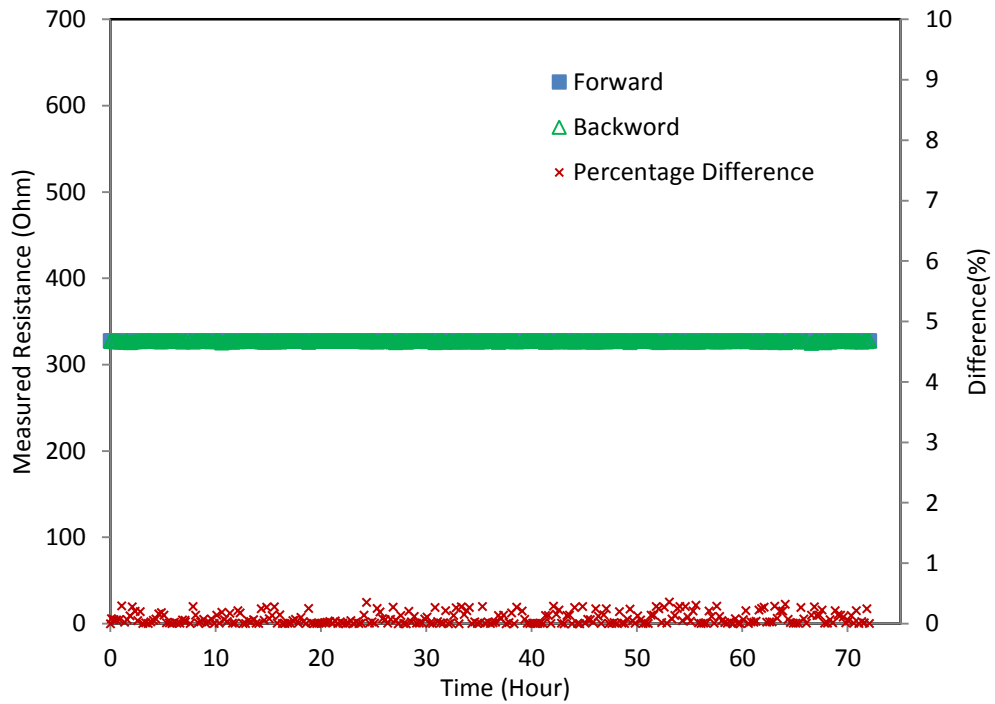


Figure A.7. The forward and backward readings of the 328 Ohm resistor test

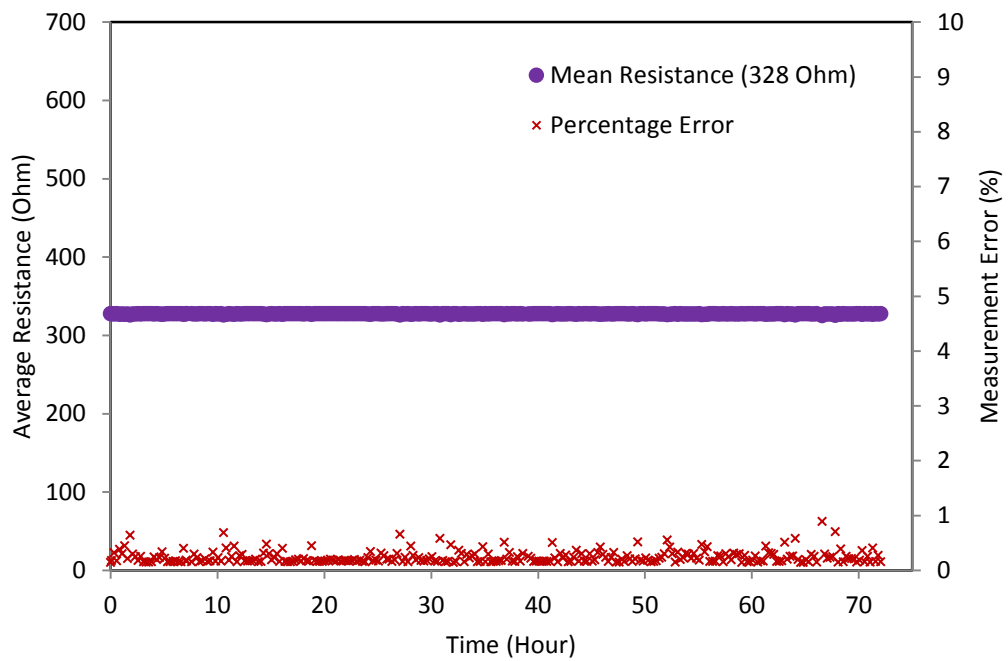


Figure A.8. The mean resistance and measurement error of the 328 Ohm resistor test

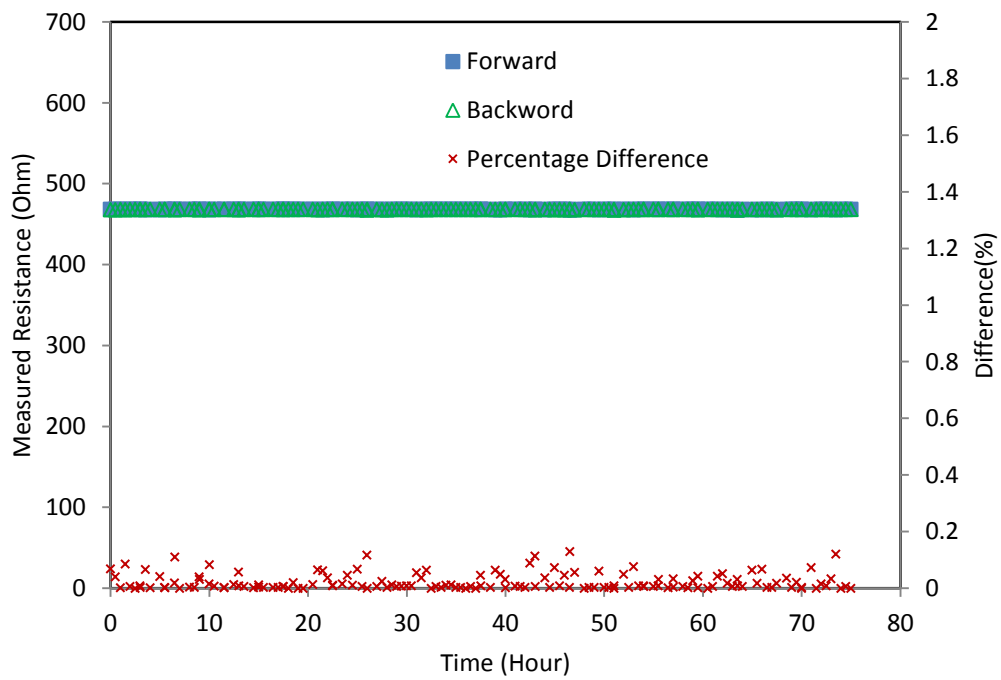


Figure A.9 The forward and backward readings of the 470 Ohm resistor test

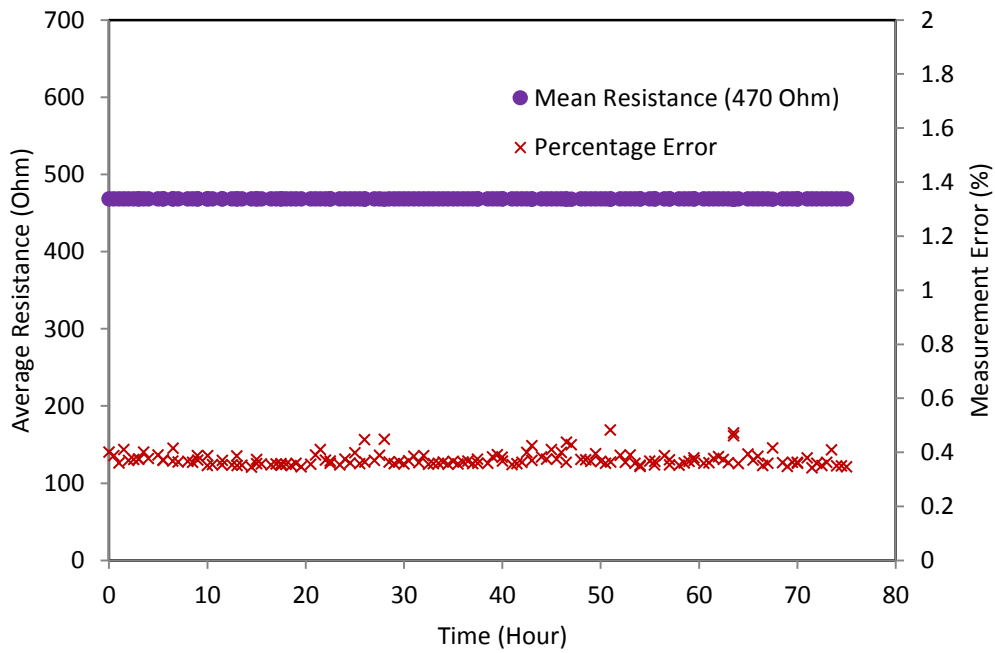


Figure A.10. The mean resistance and measurement error of the 470 Ohm resistor test

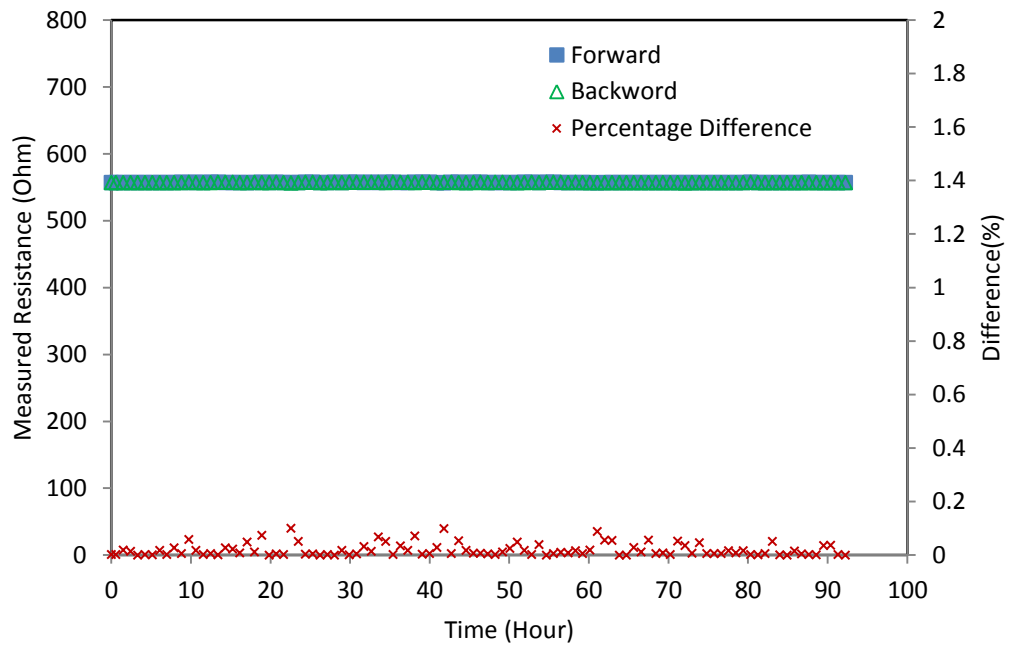


Figure A.11. The forward and backward readings of the 560 Ohm resistor test

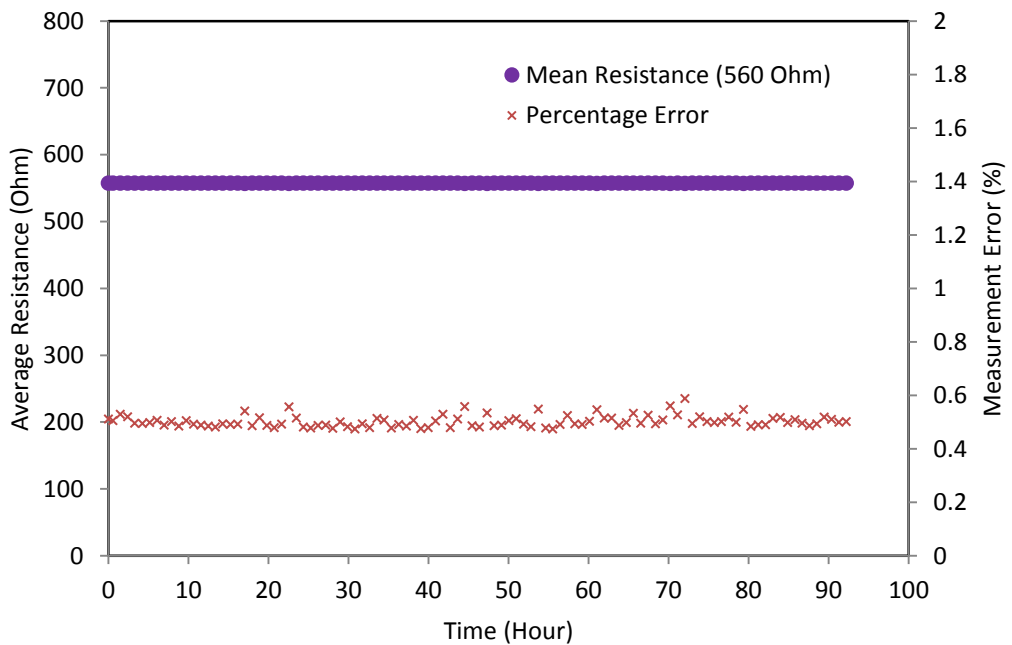


Figure A.12. The mean resistance and measurement error of the 560 Ohm resistor test

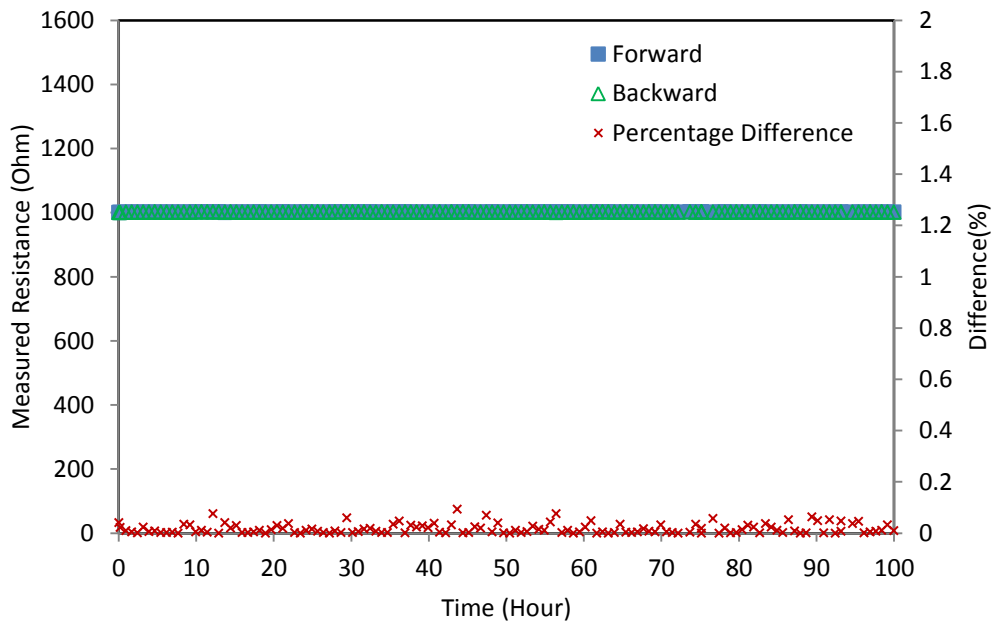


Figure A.13 The forward and backward readings of 1000 Ohm resistor test

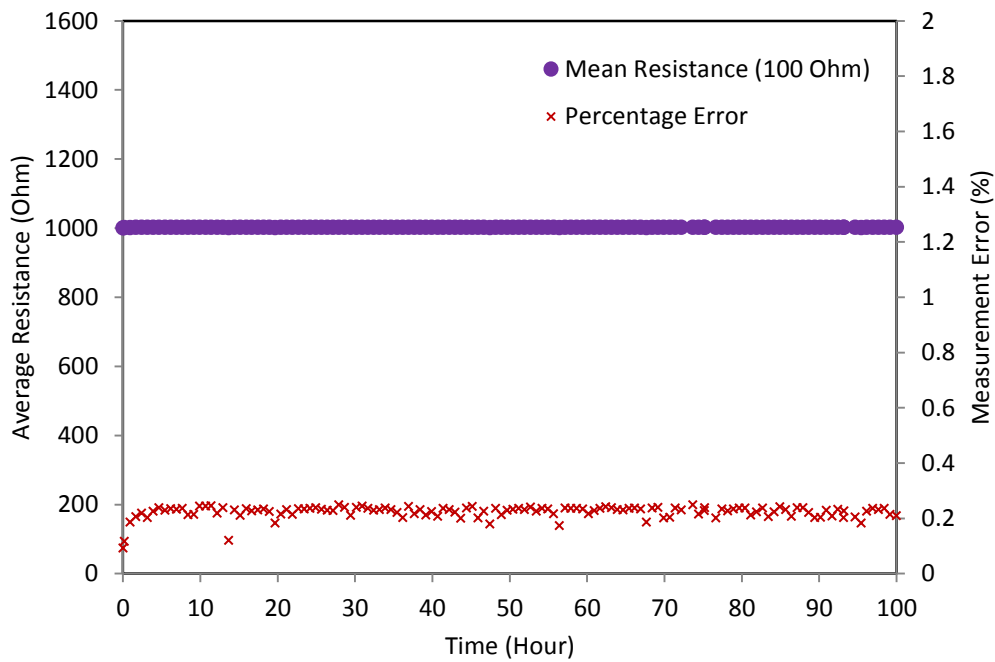


Figure A.14. The mean resistance and measurement error of the 1000 Ohm resistor test

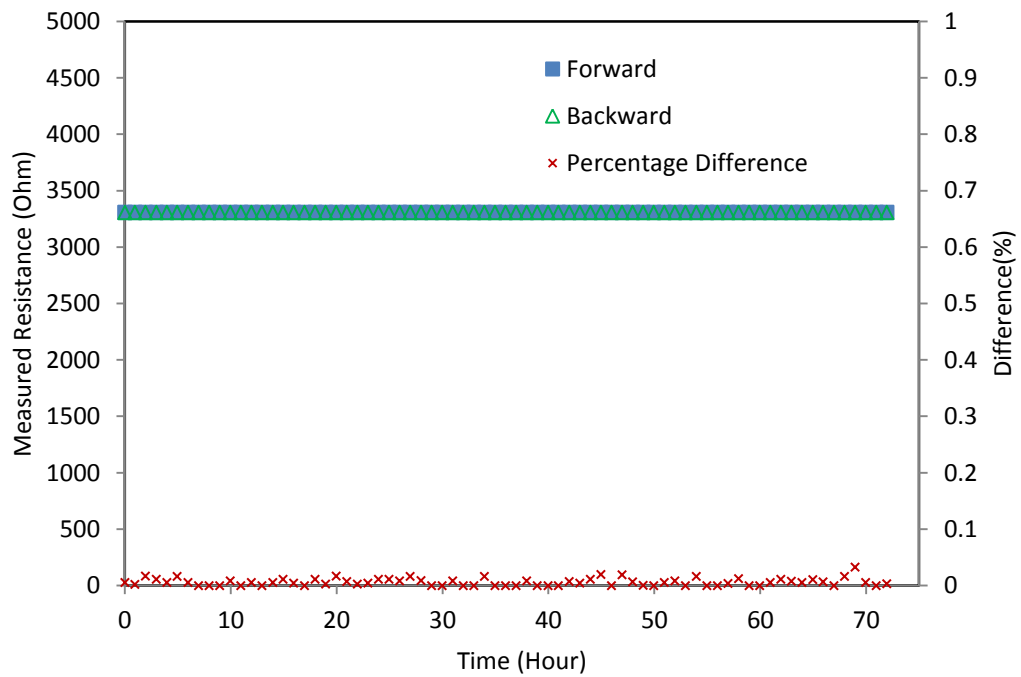


Figure A.15. The forward and backward readings of the 3300 Ohm resistor test

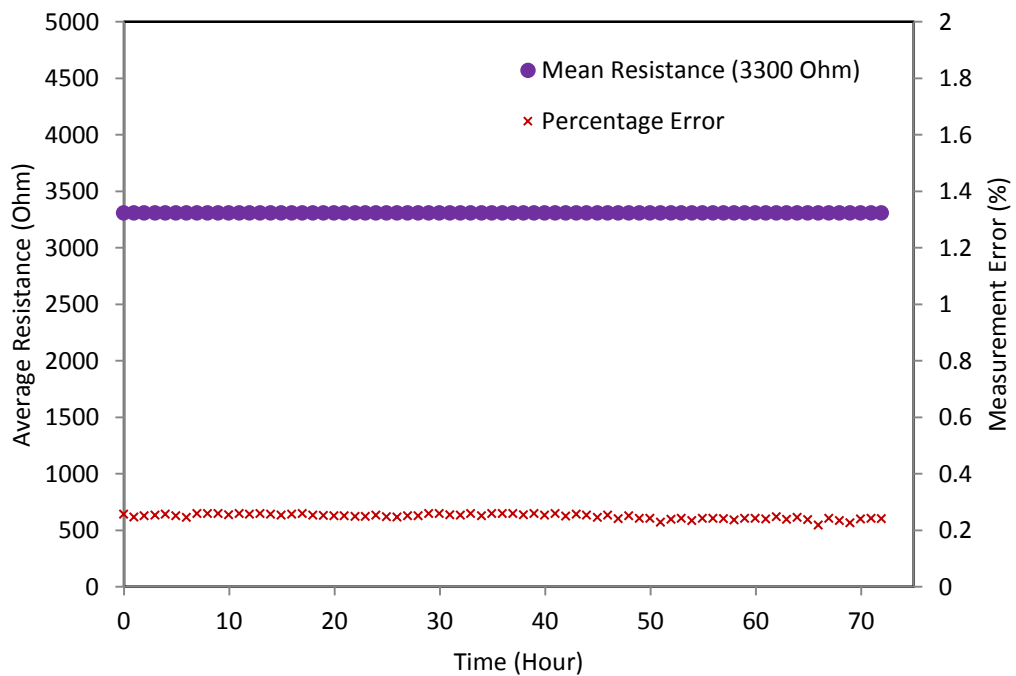


Figure A.16. The mean resistance and measurement error of the 3300 Ohm resistor test

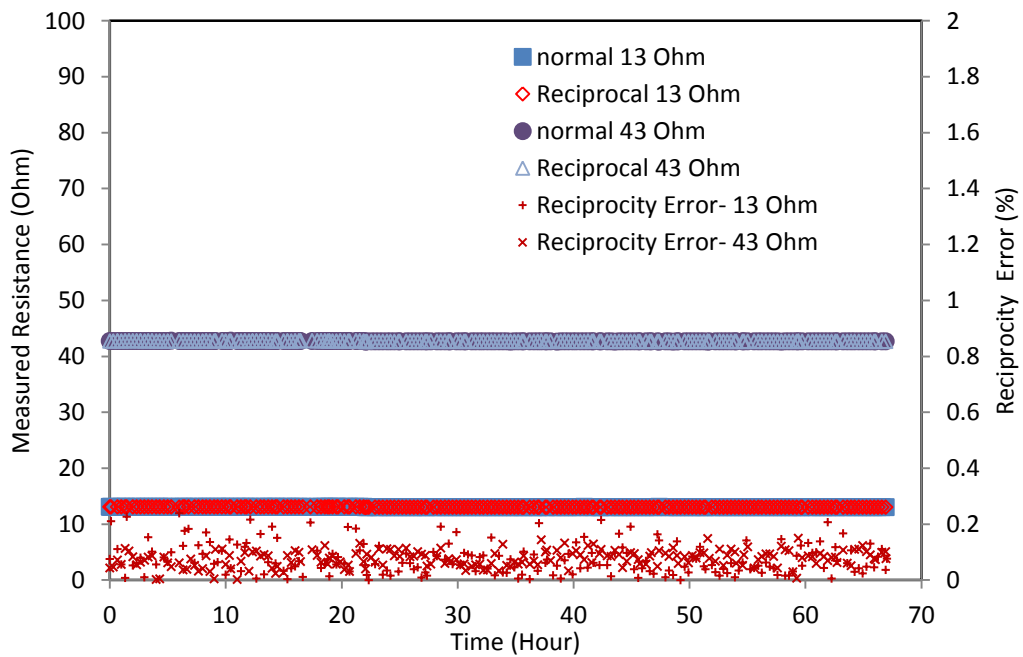


Figure A.17. Normal resistance, reciprocal resistance and reciprocity error of 13 and 43 Ohm resistor test

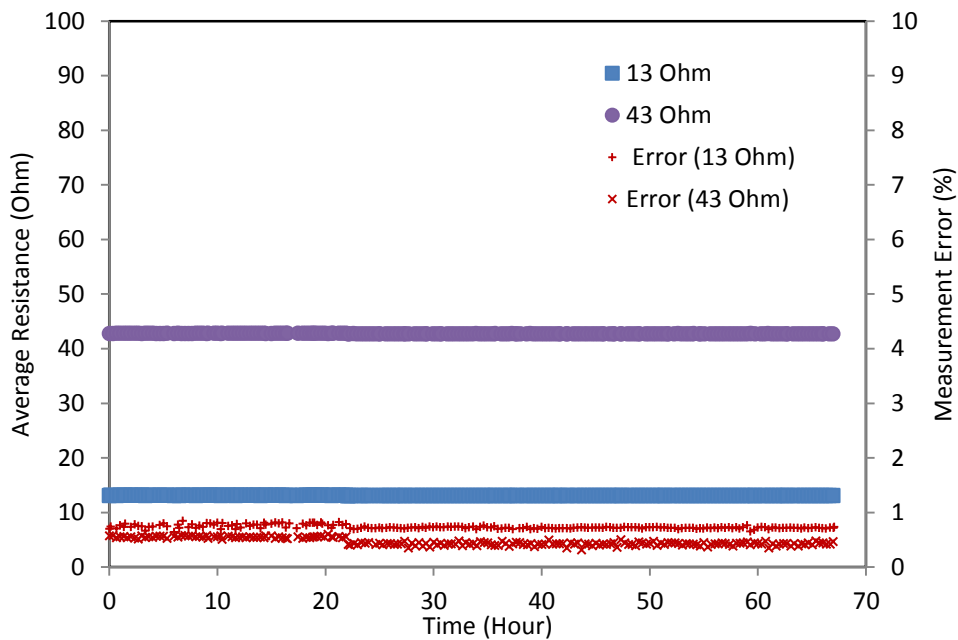


Figure A.18. Average resistance and measurement error of 56 and 68 Ohm resistor test

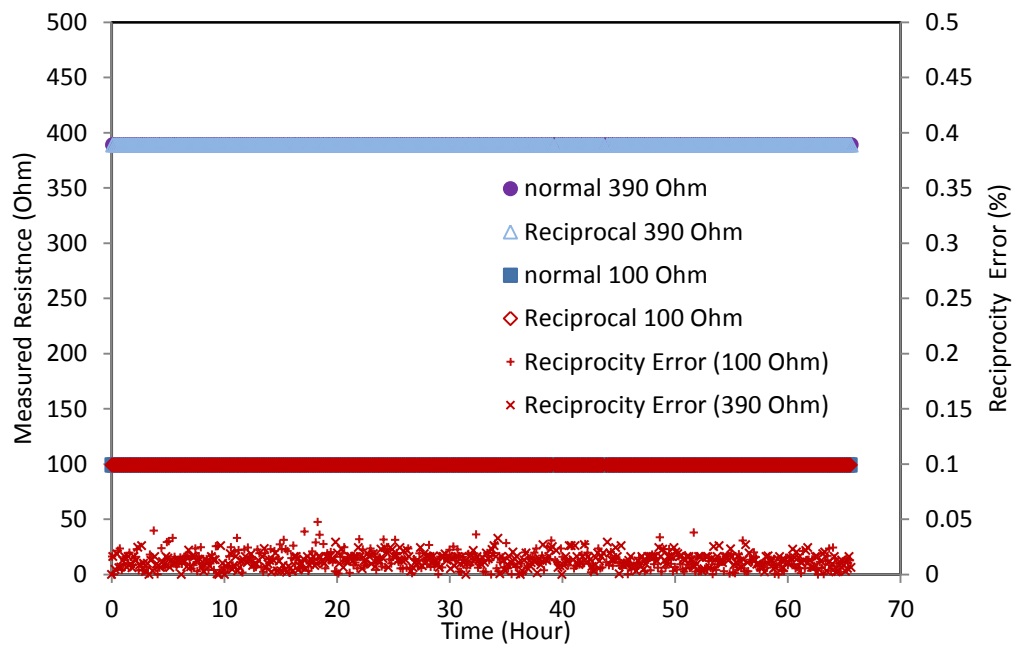


Figure A.19. Normal resistance, reciprocal resistance and reciprocity error of 100 and 390 Ohm resistor test

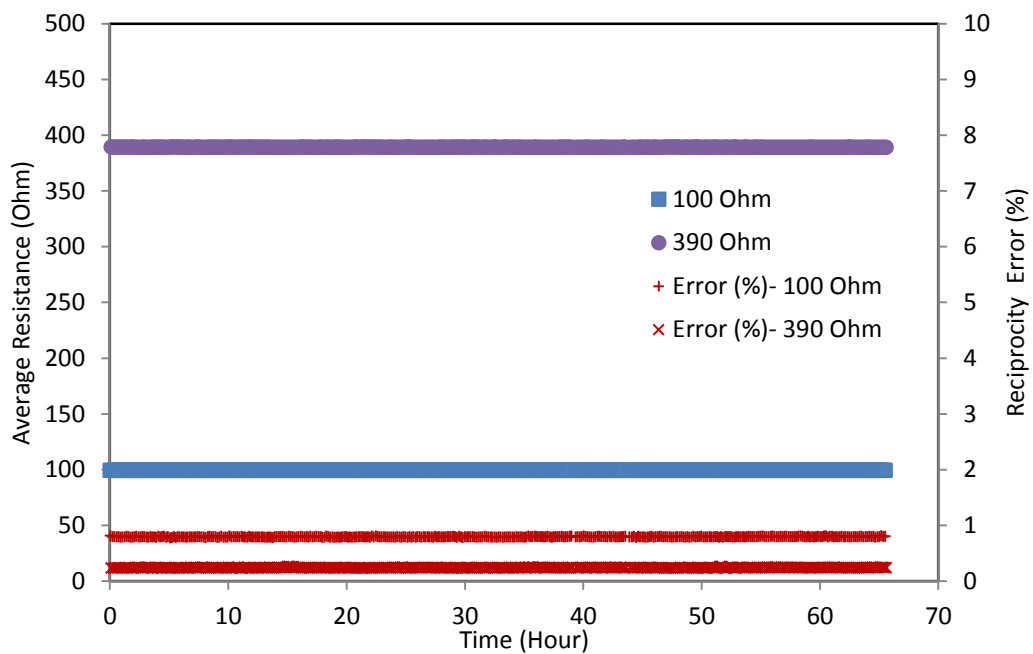


Figure A.20. Average resistance and measurement error of 100 and 390 Ohm resistor test

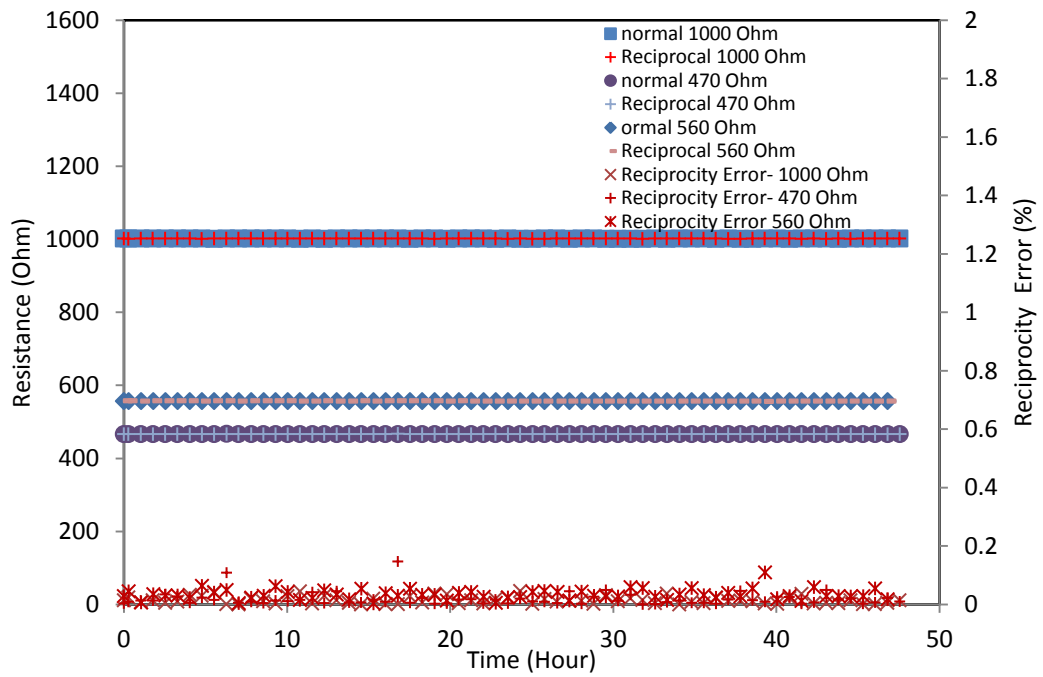


Figure A.21. Normal resistance, reciprocal resistance and reciprocity error of 1000, 470 and 560 Ohm resistor test

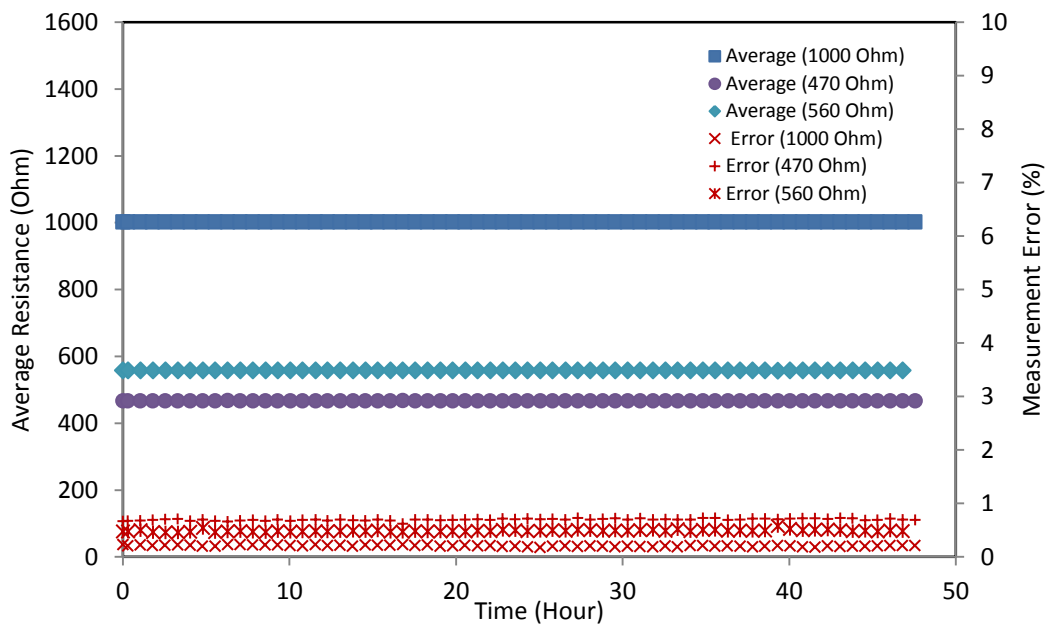


Figure A.22. Average resistance and measurement error of 1000, 470 and 560 Ohm resistor test

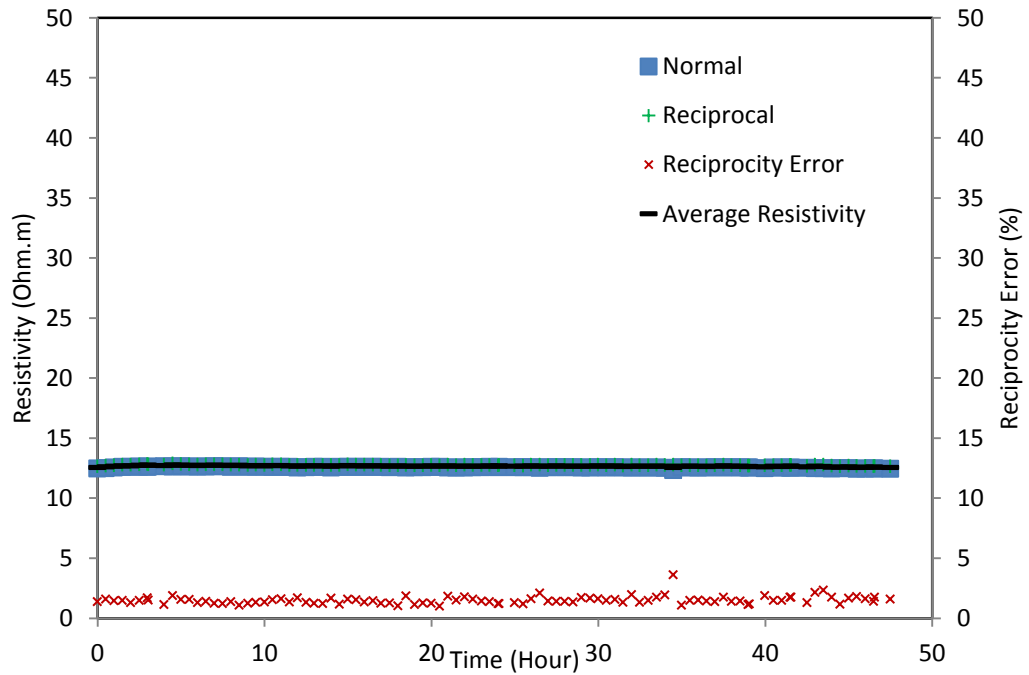


Figure A.23. Reciprocity test results of 20% water content of clay specimen

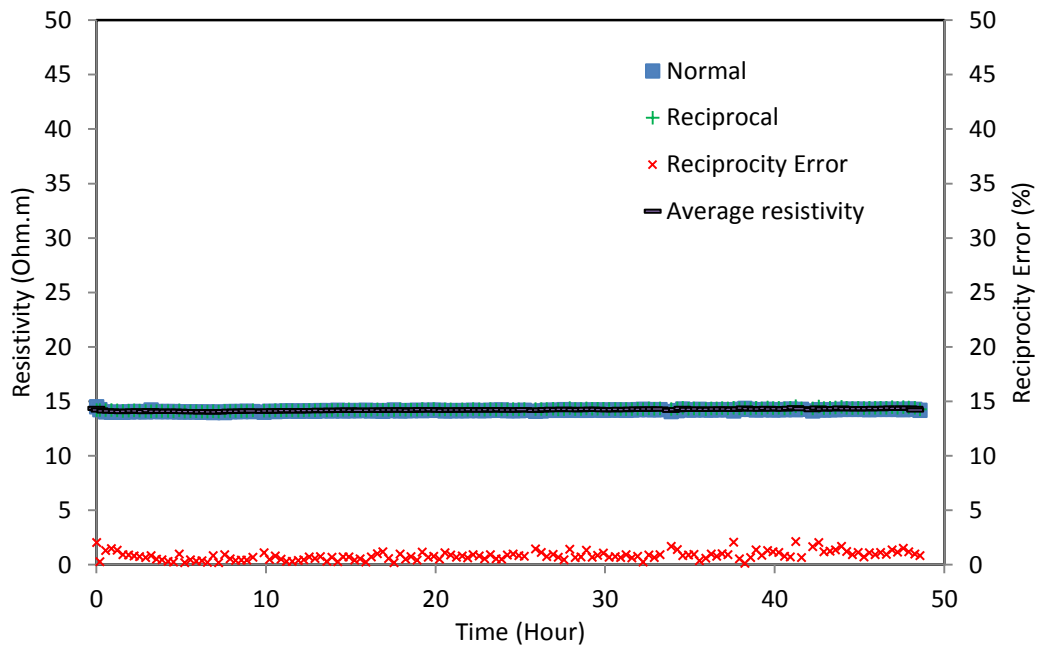


Figure A.24. Reciprocity test results of 15% water content clay specimen (1)

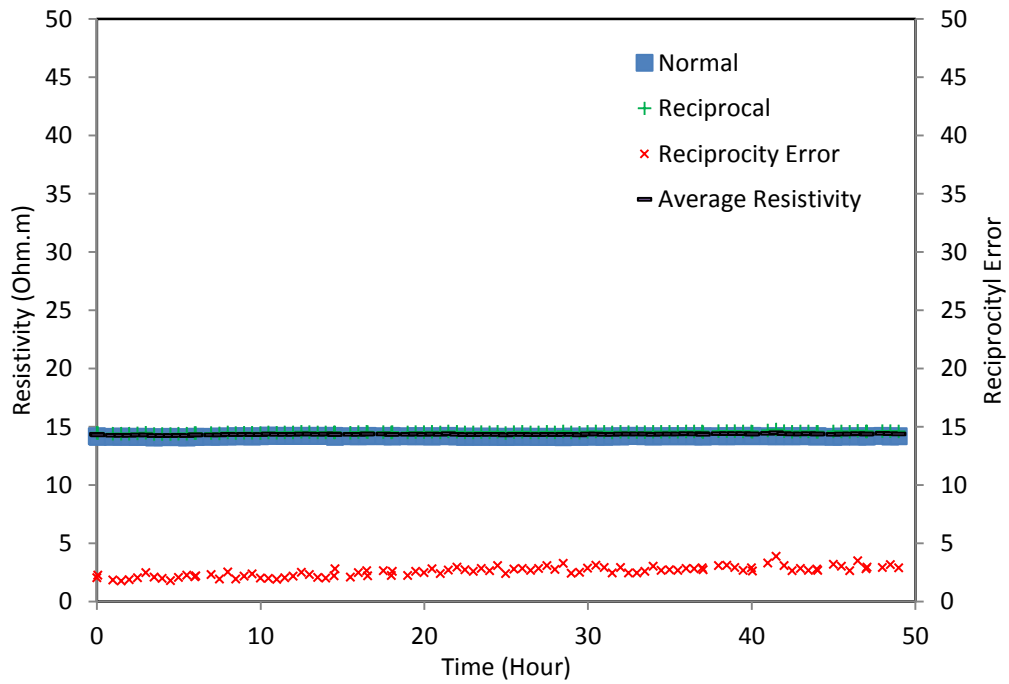


Figure A.25. Reciprocity test results of 15% water content clay specimen (2)

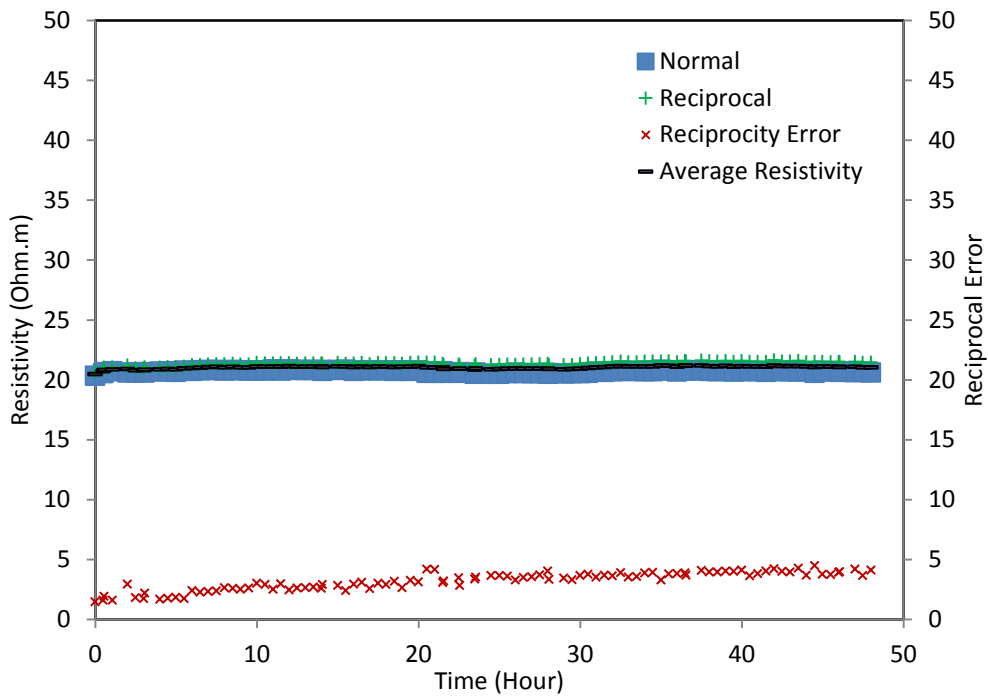


Figure A.26. Reciprocity test results of 12% water content clay specimen

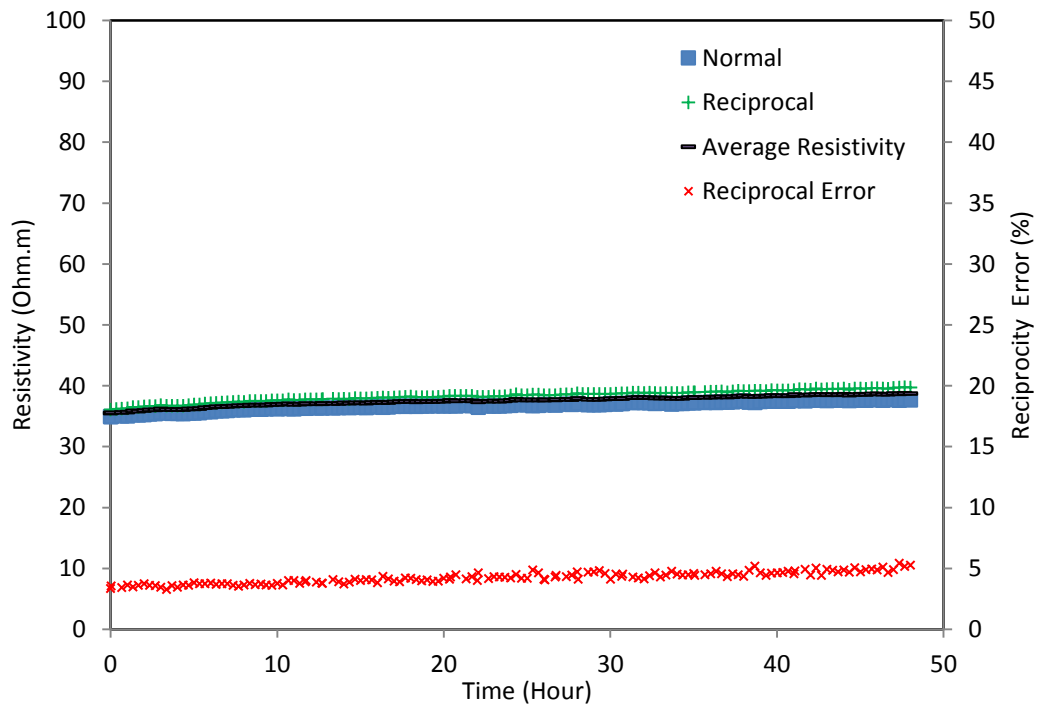


Figure A.27. Reciprocity test results of 10% water content clay specimen

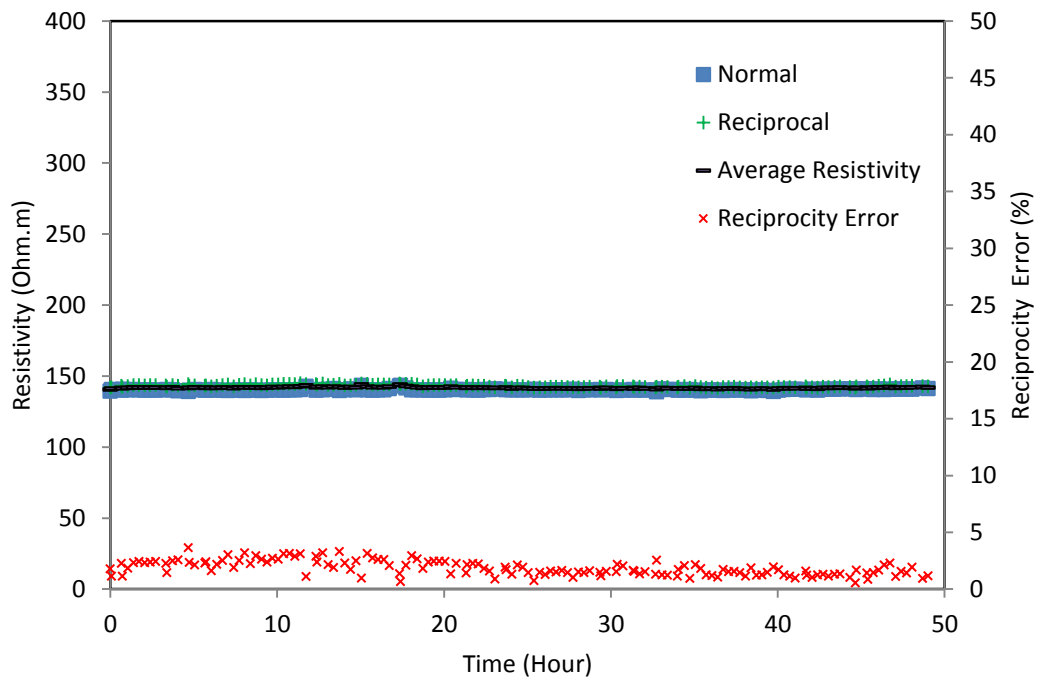


Figure A.28. Reciprocity test results of 30 % water content sand specimen

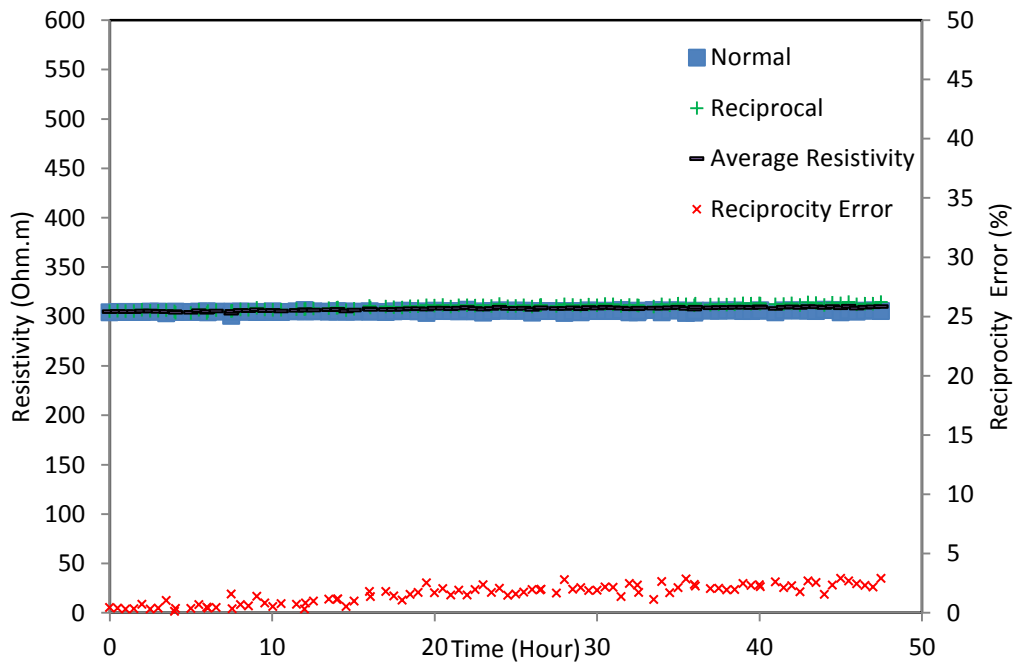


Figure A.29. Reciprocity test results of 15 % water content sand specimen